Investigation and development of a novel metrology standard for the measurement of relative intensity noise and frequency chirp of DFB lasers in optical networks

Michael Christopher Cox

BEng (Hons) MIET

A thesis submitted in partial fulfilment of the requirements of
London Metropolitan University
for the degree of
Doctor of Philosophy

May 2007

Communications Technology Group
Department of Computing, Communications Technology & Mathematics
London Metropolitan University
North London Campus

Abstract

Laser diode Relative Intensity Noise (RIN) metrology capabilities have been developed and demonstrated, providing significantly improved sensitivity and accuracy than existing methods. This is a key parameter for laser components used in telecommunication systems due to the drive to reduce inherent noise, improve overall signal-to-noise ratio and thus increasing achievable communication link length and reduce required component specification.

The novel use of the demonstrated reference noise source has shown significant advantages, achieving improved sensitivity, increase measurement accuracy as low as ±1dB and simplifying the system calibration methodology thus improving flexibility. Laser RIN of between 10 to 14dB below the Shot RIN have been shown (typically -170dB/Hz) which is a direct result of the improved system sensitivity

The developed system is based on an Neodinium Yag (Nd:Yg) 1319nm ring laser, essentially providing a 'cold' reference source, in a similar manner to that used in rf electrical metrology. High finesse Nd:Yag lasers inherently emit significantly small amounts of AM/FM noise being spectrally very pure. This is enforced further by the non-planar ring oscillator (NPRO) technology providing superior line width stability. The selection of a high output power version allows optical attenuation to be applied which provides a further 20dB attenuation of system spontaneous noise. Application of the 'flat' low noise optical rf noise source from 10MHz to 20GHz has been demonstrated for the first time in optical rf metrology, providing a calculable reference traceable via the incident optical power received. Due to the simplistic nature of this approach, system calibration can be measured for each RIN measurement performed, reducing measurement uncertainty associated with rf miss-match, system linearity and loss.

High specification components have been assessed individually and in the combined system indicating overall system noise figure of 2 to 3dB over the 10MHz to 20GHz frequency range (-171dBm to -172dBm), some 4 to 5dB better than previously reported. Good agreement has been shown comparing thermal noise subtraction and 3dB rise techniques confirming the theoretical dominance of the rf amplifiers noise figure.

Application of narrow band optical signals, by way of directly modulating a DFB laser and using an external optical modulator has confirmed the noise sensitivities found previously and also the theoretical 2dB wideband offset reported in literature.

Measurement methodology has been reported, describing the three stage approach and simple derivation of RIN. Extensive assessment of measurement uncertainty contributions are reported complying with UKAS standard guidelines for random and systematic terms. The overall uncertainty budget drawn from this is dynamically linked to the level of RIN under test. Application of the reference laser has additional benefits in allowing linearity contributions to be realised.

Intercomparisons with a commercially available RIN measurement system highlighted the sensitivity advantages of the reference technique. A number of short comings of the traditional approach in terms of systematic errors, such as the spontaneous loss over attenuation are reported.

Frequency excursion (chirp) metrology capabilities have been explored, developed and demonstrated. The final system is based on the gated delayed self homodyning interferometer. Inclusion of Faraday rotating mirrors has been reported showing favourable results, reducing systematic uncertainty by 7% at low modulation frequencies. These mirrors, one on each arm of the interferometer, effectively cancel out any fibre birefringence within the interferometer and also negate the need for a polariser to maximise the output signal.

Initial accuracies of ±10% have been achieved traceable to national standards. Intercomparisons with a commercially available interferometer show a 7 to 10dB more amplitude sensitivity thus improving the resolution capability, aiding line width and chirp determination. Analysis has been limited to low modulation frequencies due to equipment delivery limitations. The reference source has been utilised to provide modulation level calibration.

Concept for high modulation frequency testing has been reported based on tracking the relative ratio of two available Bessel peaks. This has been modelled via classic FM theory, knowing the line width, and modulation index to obtain a best fit. This technique has advantage in being able to operate without the need to meet a 'null'.

Contents

Acknowledgements

Dr S M Vaezi-Nejad (London Metropolitan University) – for his encouragement and academic support throughout this project

Dr Nigel Copner (Procen Ltd) – for the healthy discussions, interest in laser metrology and assistance in reviewing the theory of fibre interferometers, details in Appendix A

Prof C T Elliott (Qinetiq) – for his encouragement and professional support

Val McOmber (HP, Santa Rosa) – for the loan of their Lightwave analyser modules and swift technical assistance when requested

Greg Obarski (NIST, Colorado) – his input into the laser noise metrology development

Bernie Williams (Qinetiq) – technical support in RF noise metrology

Steve Harter (Qinetiq) – RF noise metrology

Gary Smith (Qinetiq) – Optical calibration

Dave Marshall (Qinetiq) – Test software support

Family support – and last by no means least the support of my family….many absent hours!

Published Papers & Patents

Development of a Novel Relative Intensity Noise Measurement techniques in Laser Diodes Transmitters in Optical Communication Networks, M Cox, S M Vaezi-Nejad and N J Copner, To be presented at the World Congress on Engineering WCE 2007: The 2007 International Conference of Electrical and Electronics Engineering (ICEE'07), 2-4 July, 2007, London, U.K

Measurement of noise in laser diodes for high data rate broadband telecommunication systems, S.M Vaezi-Nejad and M C Cox, Proceedings of the 8th Annual National Electrical & Electronic Engineering Conference (ISCEE) in Iran 2-5 Sep 2005

High Sensitivity Precision Relative Intensity Noise Calibration Standard Utilising A Low Noise Reference Laser Source, M C Cox, N J Copner, B Williams, Optical Fibre Measurement Conference, Sept 1997 & British Electro Magnetic Conference Nov 1997.

Accurate Optical Fibre Path Length Measurement based on Frequency Modulation of a Laser Diode, M C Cox, N J Copner, G F Smith, Optical Fibre Measurement Conference, Nov 1999.

Device Noise Measurement System (patent GB9622338.3), filed 26 October 1996

List of Figures

List of Tables

Abbreviations

AMPCOR	Amplitude Correction offset
ANF	Average-display Noise Floor
ASE	Amplified Spontaneous Emission
BER	Bit Error Rate
BII	Birefringence Insensitive Interferometer
DERA	Defence Evaluation Research Agency
DBR	Distributed Bragg Reflection
DFB	Distributed Feedback
DMM	Digital Multi Meter
DSH	Delayed Self Homodyning
DTI	Department of Trade and Industry
DUT	Device Under Test
DVM	Digital Volt Meter
EDFA	Erbium Doped Fibre Amplifier
EELED	Edge-Emitting Light-Emitting Diode
FP	Fabry Perot
FSK	Frequency Shift Keying
FSR	Free Spectral Range
GDSH	Gated Delayed Self Homodyning
GEC	General Electric Company
HP	Hewlett Packard
LD	Laser Diode
LED	Light-Emitting Diode
LO	Local Oscillator
LW	Line Width
MPN	Mode Partition Noise
NF	Noise Figure
NIST	National Institute of Standards and Technology
NMSPU	National Measurement System Policy Unit
NPL	National Physical Laboratory
NPRO	Non-Planar Ring Oscillator
OFMC	Optical Fiber Measurement Conference
OTC	Optical Test and Calibration
PDL	Polarisation Dependent Loss

PMT	Photo Multiplier Tube
RIN	Relative Intensity Noise
R&S	Rohde & Schwartz
SA	Spectrum Analyser
SAN	Storage Area Networks
SNR	Signal-to-Noise Ratio
Syscal	System calibration factor
SYSCOR	System Correction offset
UKAS	United Kingdom Accreditation Service
VSWR	Voltage Standing Wave Ratio

1 Introduction

In this introductory chapter a brief history of fibre optics communications is given along with a summary of its key advantages over traditional copper based links and its breadth of use in today's systems. Following this, emphasis is placed on the importance of 'clean' optical signals to allow expansion of optical telecommunications and discusses the resulting directive from National Measurement System Policy Unit to enhance metrology capability. Finally, thesis objectives are defined followed by a brief review of each chapter.

1.1 Optical Communication - General Systems

Visible optical communication has been in common use for years in the form of simple systems such as signal fires, reflecting mirrors and signalling lamps. As early as 1880 Alexander Graham Bell reported the transmission of speech using a light beam[1] known as the photophone. This modulated sunlight with a diaphragm giving speech transmission over a distance of 200m. But, for the early part of the twentieth century this was limited to mobile, low capacity links due to the lack of suitable light sources and the atmospheric restrictions due to rain, snow, fog, etc. Theoretical work on the electromagnetic field propagation in a round dielectric cylinder dates from 1910, by Hondros and Debye[2]. By the 1950's fibre bundles were being used for image reproduction in endoscopy[3].

The invention of the laser[4] in the 1960's provided a renewed interest in optical communications. The device provided a powerful coherent light source, together with the possibility of modulation at high frequency. In addition, the lasers low beam divergence improves free space optical transmission capabilities, but is ultimately constrained by atmospheric conditions as previously mentioned. Significant research was instigated in parallel, to develop optical components to achieve reliable information transfer using a lightwave carrier, formed via a dielectric waveguide or optical fibres fabricated from glass[5,6]. This was seen as the replacement for coaxial cables and within 10 years optical losses were reduced from 1000dB/km to <5dB/km and low loss jointing techniques were perfected.

Optical component developments lead to the semiconductor laser and photo-diode being of compatible size for optical fibre. Initially the semiconductor laser suffered very short life times of at best a few hours, but advances in device structure life times greater than 7000hr by 1977. These were originally fabricated from alloys of gallium arsenide, emitting in the

near infrared around 0.85um. Subsequently, wavelength range was extended to include the 1.1 to 1.6um region by the use of other semiconductor alloys to take advantage of the enhanced performance characteristics of optical fibres. Mean projected laser life times increased typically to greater than 25yrs at 10°C and greater than 100yrs at 70°C. Direct modulation to several giga bit s^{-1} became feasible at 1.3um for single mode fibre where intramodal dispersion is minimal. Later 1.5um dispersion shifted fibre was introduced to provide the best dispersion performance together with the lowest attenuation loss typically 0.2dB km^{-1}.

Many other optical components have been developed over the years to support this rapidly expanding technology field. These includes; fibre couplers, splitters, MUX/DEMUX, photodiodes, optical amplifiers, external optical modulators etc. The success of this field is down to the following key advantages over previous copper electrical links:

- Enormous potential bandwidth
- Small size and weight
- Electrical isolation
- Immunity to interference and cross talk
- Signal security
- Low transmission loss
- Ruggedness and flexibility
- System reliability and ease of maintenance
- Potential low cost

Today's telecomm links typically operate from Mb/s to 10Gb/s per channel with 40Gb/s now becoming available[7,8]. The significant technological advantages of optical links has lead to its introduction into all levels of communication from the long haul trunk telephony down to Metro and even local area networks, see Figure 1-1. Modulation formats include analog (for telephony and CATV applications) and digital (for telephony and data traffic) encoding. Digital has become the system of choice in recent years due to its greater efficiency thus less demand on signal to noise ratio at the receiver and also the reduced laser linearity requirement.

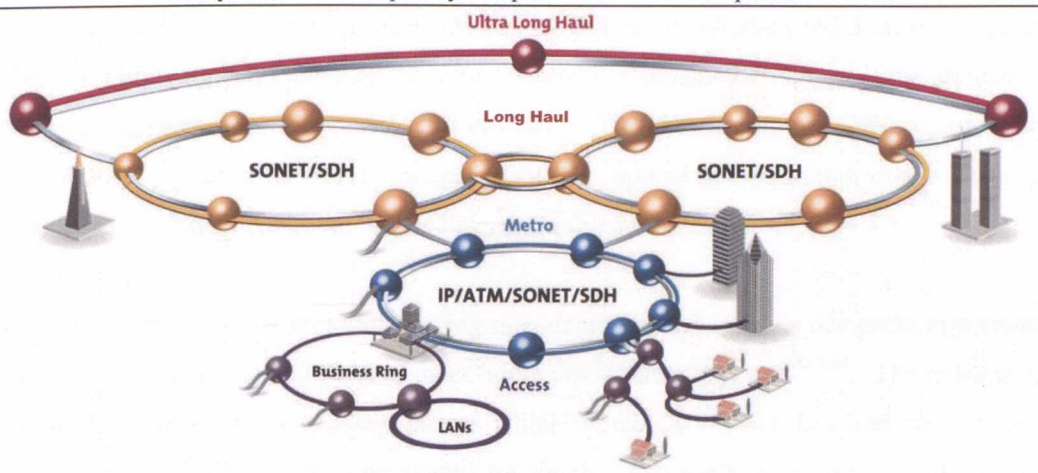

Figure 1-1: Overview of Optical Telecomm Link Structure[58].

Optical fibre technology has also spread into Local area networks (LANs) such as IEEE [9], storage area networks (SAN's)[10] and sensor applications to name but a few.

1.2 Technology Support

In today's world of rapid technical advances, businesses need to establish and maintain a competitive edge to survive. For manufacturers, quality control is an obvious target, to ensure product reliability, consistency and compatibility with the customer. This relies heavily on measuring conformance to customer specifications/contracts and/or national/international standards.

To aid and maintain UK industry's success the Department of Trade and Industry (DTI) operates a National Measurement System Policy Unit (NMSPU), set up to provide UK National Standard Measurements and harmonisation with other similar international organisations. This principally consists of maintaining and improving the measurement of the seven internationally accepted standard SI units; length, mass, time, electric current, temperature, luminous intensity and amount of substance. Further to this, additional derived units are also supported, for instance power and frequency.

A large amount of these UK scientific measurement standards are provided by organisations such as the National Physical Laboratory (NPL) and National Weights and Measures funded by the NMSPU. In recent years some new national standard proposals have been competitively tendered to other organisations to maximise technology exploitation and value

for money. One such tender has been secured by Defence Evaluation and Research Agency (DERA) which concerns developing a new national standard for temporal and frequency response measurements of optoelectrical devices[11]. This focuses on noise measurements of laser diodes primarily to serve the needs of the optical telecommunications industry, particularly long-haul communications links and cable television (CATV).

Market demands in these areas are forcing manufacturers and systems designers to increase data rate capacity of optical links to meet future communications use[12,13,14]. The noise level within a system is one of the key factors which ultimately restrict data rate capacity and hence *cleaner* optoelectronic components are sought. From simple estimations, increasing the bit rate from 10Gb/s to 40Gb/s requires a 6dB improvement in signal to noise ratio in order to maintain the same link spacing[15]. Future advances in system components needs to be met by an equivalent ability to measure their performance[16]. Key forms of transmitter noise concern AM and FM optical noise which are commonly expressed under the parameters Relative Intensity Noise (RIN) and Frequency Excursion (Chirp) respectively[17].

RIN is a kind of quality indicator which describes a laser's maximum available amplitude range for signal modulation and is derived from the ratio of the mean-squared-intensity-fluctuation spectral density of the optical output to the square of the average optical power. It can be thought of as a type of inverse carrier-to-noise ratio[12,18] indicating the maximum ratio obtainable in a lightwave transmission system, where the dominant noise source is the laser intensity noise, usually stated in dB/Hz.

Chirp characterises the change in lasing frequency when a laser is directly modulated with a signal, quoted in Hertz [19]. This consequently increases the laser's static linewidth which in conjunction with fibre chromatic dispersion can severely limit the transmission range of fibre optic links.

1.3 Investigation

This thesis details the theoretical and practical work I have undertaken researching laser diode rf noise metrology in support of the NMSPU proposal. Focus is primarily on developing capability to measure RIN and Chirp of laser diodes. The end objective is the creation of a measurement capability which advances the telecommunication metrology field in terms of performance and understanding. The advances made provide improved capability to assess and develop laser transmitters not only for today's transmitters but also

for tomorrow's and importantly forms the basis of a new UK National Standard. A break down of the thesis follows;

From the initial optical fibre technology overview chapter two identifies telecommunications systems which are highly susceptible to system noise contributions and the appraisal methods available, namely Bit Error Rate testing. The impact of the laser transmitter design is discussed leading to the definition of the Relative Intensity Noise and Frequency Chirp, critical parameters in fibre optical communications. A thorough understanding has been established relating these two parameters to system performance degradation and laser noise performance. Paper searches, reference books and communications with the industry have been utilised with this objective. The physical properties which affect a component's level of noise, such as resistive and capacitive parasitics, are discussed, helping form a clear picture of component designer's needs in terms of measurement sensitivity and scale as well as the requirements of customers.

Following this, existing measurement capabilities / approaches are reviewed in chapter three, gathered from research papers and commercial test equipment. Comparisons have been draw as to the merits and limitations of these approaches in terms of accuracy and sensitivity. Project objectives are then set in terms of specification level, dynamic range etc., with the intention of advancing current industry capabilities. From this an optimum measurement system approach is discussed and selected for the RIN and Chirp parameters. Performance expectations are defined along with calibration and traceability for each parameter. Subsequently, a number of interesting observations are made together with identification of novel techniques, most notably being a Shot Noise Limited Reference Laser and the Birefringence In-sensitive Interferometer. In summary, the reference laser potentially offers a calculable wide band noise source which can be used to derive laser spontaneous noise directly, provide a means of system calibration and provide traceability to National Standards at a higher echelon than is currently obtainable (patent filed). The Birefringence In-sensitive Interferometer essentially eliminates the need for polarisation adjustment and potentially will improve sensitivity (patent considered).

Chapter four details the build up of the general system with thorough assessments made at each stage focusing on noise figure and sensitivity level being of key importance to the overall aims of the project. The investigations compare traditional measurement methods with novel references techniques. Measurement procedure for RIN and Chirp is defined along with tabulated measurement uncertainties to form accurate budgets, in line with

national standard requirements. Reference is made for further analysis to advance overall system understanding.

Direct measurement intercomparisons are performed in Chapter five for both RIN and Chirp. This is essentially based upon commercially available RIN/Chirp measurement equipment, loaned specifically for these trials. Here in-depth analysis of measurement procedures and error terms are reported, together with the overall deviations between the techniques. Deficiencies in the commercial equipment are highlighted and key performance advantages of the selected system design become evident.

Finally, Chapter six initially draws conclusion upon the construction of the spectrum analyser-amplifier-detector combination confirming the performance expectations. Following this, results gained from various referencing and intercomparison approaches are discussed. This provides high confidence in system capability and highlights the key benefits of self calibration provided by the reference laser and the birefringent insensitive interferometer. Measurement limitations and system constraints are also included. The chapter closes with a summary of future incremental developments to purse and the wider spin-off application capabilities this research has offered the metrology field.

2 Lasers for Optical Communications

The fibre optic telecommunications fields which have particular interest in noise metrology are long and short haul coherent Gbit/s rate systems where there are likely to be a large number of interconnections. The problem that exists is how to characterise these systems, since real time testing and verification of such low Bit Error Rates (BER) is extremely difficult [20]. In real systems there are many sources of pulse distortion, causing the pulses to vary in shape, timing and amplitude. This in turn causes the BER to be determined by the performance of a few *bad bits*, not the performance of the typical, *well behaved* pulses.

We currently identify penalties, BER degradations and/or floor effects from: pure chirp (transient or adiabatic), chirp noise, mode partition noise (MPN), timing jitter, pattern effects. These effects are all similar in size and they may appear in almost any combination. It is not possible to single out any one effect beforehand, but we must instead take them all into account. Thus good BER performance is not achieved until the right combination of operating conditions are employed. Excellent system performance can then be achieved with standard laser diodes. However, good control over design, production and operating conditions needs to be enforced to utilise this performance.

This leads to the requirement to closely characterise noise contributions of associated components in coherent communication links. Coherent transmission systems are substantially formed by light generators whose radiation spectral width is smaller than 0.1nm. Particular laser structures have been developed to meet this goal such as distributed Bragg reflection (DBR) lasers[21] and predominately distributed feedback (DFB) lasers [22]. These feature narrow linewidths (less than a few MHz), reduced susceptibility to temperature and driving current variations and are robust, small in size and low cost. Non semiconductor devices, like the Nd:Yag laser can provide narrower linewidths than DFB's but are not often selected for systems because only low direct modulation can be supported, hence the need for external modulation and also optical pumps are required. This in turn significantly raises system costs.

Significant forms of system noise are generated by the laser source itself, concerning AM and FM optical noise, commonly expressed as Relative Intensity Noise (RIN) and Frequency Excursion (Chirp) respectively[17].

2.1 Relative Intensity Noise (RIN)

Spurious, random laser emissions cause intensity fluctuations in the laser's light output, often referred to as spontaneous emission. These fluctuations form the noise floor, the level of which is dependent on the frequency. The peak level is known as the relaxation resonance of the laser and is directly related to the laser's maximum modulation rate. Interaction between the optical field in the laser and the injected-electron density, due to the bias current, causes the relaxation resonance to vary as a function of the bias current. RIN is defined in terms of the ratio of the mean square power fluctuation spectral density of the optical output to the square of the average optical power, usually stated in dB/Hz.

$$RIN = \frac{<\Delta P_{opt}{}^{2}>}{P_{opt}{}^{2}} Hz^{-1} \qquad (2\text{-}1)$$

where; $<\Delta P_{opt}{}^{2}>$ is the mean-square optical intensity fluctuation (in a 1Hz bandwidth) at a specified frequency, and $P_{opt}{}^{2}$ is the average optical power squared.

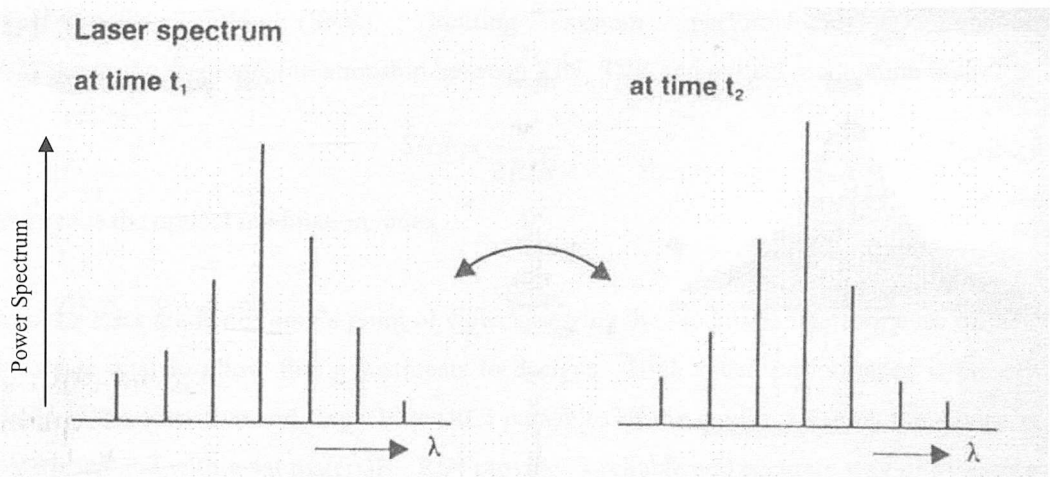

Figure 2-1: Mode Partition Noise[28].

Laser RIN measurements are important in digital systems via the mode partition noise (MPN). MPN is a phenomenon which occurs in multimode and even single mode (residual side modes) laser diodes when the modes are not well stabilized [23]. Intensity noise of the total light output of the laser is relatively low, however, the partition of the different lasing modes in the total light output fluctuates considerably, yielding mode partition noise. The mode partition noise is illustrated in figure 1 showing the laser spectrum at random times t_1 and t_2 . The total light output power remains essentially constant, but the relative portion of

the modal powers fluctuates. In a digital system the relative intensities of modes may vary considerably from one pulse to another. These fluctuations combined with the laser RIN and fibre dispersion produces random distortion of received pulses in a digital channel, causing an increased BER.

RIN measurements are also very important in analogue transmission where the DC optical power is generally lower than the digital case and therefore the effects of shot noise can be quite significant and the spontaneous emission from a laser can be even more significant. In addition, at wide bandwidths (>1GHz) the spontaneous level will increase as the relaxation resonance of the transmitting laser is reached. Ideally this level of laser noise should be below the system shot noise level to minimise system link penalties.

Laser RIN characteristics provide both systems designers and laser diode designers with valuable information[24]. From the systems designer's point of view even an ideal receiver generates quantum noise (shot) which yields a lower limit for detectable noise and signals. Hence any additional laser noise will add to the receiver RIN and therefore reduces the signal-to-noise ratio (SNR), limiting system performance. Equation (2-2) shows the theoretical relationship between RIN, SNR and optical modulation index [25],

$$SNR = \frac{m^2}{2RIN} \tag{2-2}$$

where m is the optical modulation index.

From the laser diode designer's point of view, assessing the modulation performance of their devices is vital to allow fine adjustments to designs. High speed performance is closely related to the Resistive and Capacitive (RC) parasitics of the device, i.e. how the device is constructed and with what materials. RIN provides a reliable and accurate way of assessing affects of device construction by determining the resonance frequency and the damping factor, derived from the peak frequency response. Combining these parameters with the intensity-current modulation transfer function, obtained via non-linear differential rate equations[24,25,26], the intrinsic modulation response can be gained. Designers ideally want a critically damped response, thus offering the highest modulation bandwidth. This is achieved by optimizing the parameters that determine the peak frequency, such as; increasing the gain coefficient; increase the photon density; increase the photon lifetime. But, this alone does not guarantee a wide modulation bandwidth as the device structure and package parasitics also play a part. Examples are: bondwire inductance, bonding pad capacitance, any device capacitance, and the resistance of the p-contact.

2.2 Frequency Chirp

The direct current modulation of a single longitudinal mode semiconductor laser can cause a significant dynamic shift of the peak wavelength emitted from the device[27]. This phenomenon, which results in dynamic linewidth broadening under the direct modulation of the injection current, is referred to as frequency chirping and can be seen in figure 2. It arises from gain-induced variations in the laser refractive index due to the strong coupling between the free carrier density and the index of refraction, which is present in any semiconductor structure. Hence, even small changes in carrier density, apart from producing relaxation oscillations in the devices output, will also result in a phase shift of the optical field. This consequently gives an associated change in the resonance frequency within both Fabry-Perot and DFB, DBR laser structures. Additionally to this carrier effect, a variation of temperature of the laser diode also causes a variation of the optical emission frequency of the device. Since the thermal time constant is rather large the thermal effect is important only for modulation frequencies less than approximately 10MHz[28].

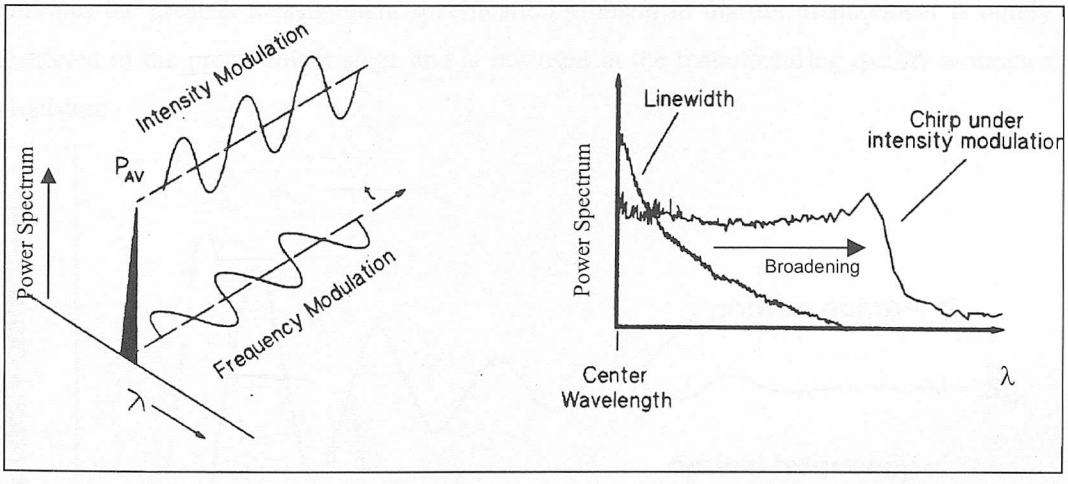

Figure 2-2: Incidental frequency (wavelength) modulation caused by intensity modulation[54].

The coupling between the real and imaginary components of the refractive index is quantified in laser diodes using the α coefficient [see 3.3.2.1]. This is quite high in laser diodes (≈6) and thus significant changes in frequency can be expected.

The laser linewidth broadening or chirping combined with the chromatic dispersion characteristics of single mode fibres can cause significant performance degradation within high transmission rate systems[29]. In particular it may result in a shift in operating

wavelength from the zero-dispersion wavelength of the fibre, which can ultimately limit the achievable system performance.

System designers quantify the effects of laser chirp on system performance by addressing the resultant dispersion over a defined length. Chirp is only one of several undesirable effects that contribute to dispersion penalties, and in 2.5Gbit/s systems it is not usually the most significant. Most laser diodes currently available have a chirp performance below the presently allowed 2dB of dispersion penalty over 60km. Coupled to this is the fact that chirp problems of laser diodes can be designed out, either by using measured lengths of dispersion shifted fibre or by avoiding direct modulation, i.e. the incorporation of external optical modulators. Apart from minimising chirp, frequency shift keying (FSK) designers actually desire a wide frequency chirp for FM discriminators.

The pulse response of laser diodes can be of interest to designers, particularly under digital modulation and is often referred to as Temporal Chirp, see Figure 2-3. This characteristic provides the greatest measurement specification problem in that the requirement is purely restricted to the procurement stage and is not used in the manufacturing quality assurance procedure.

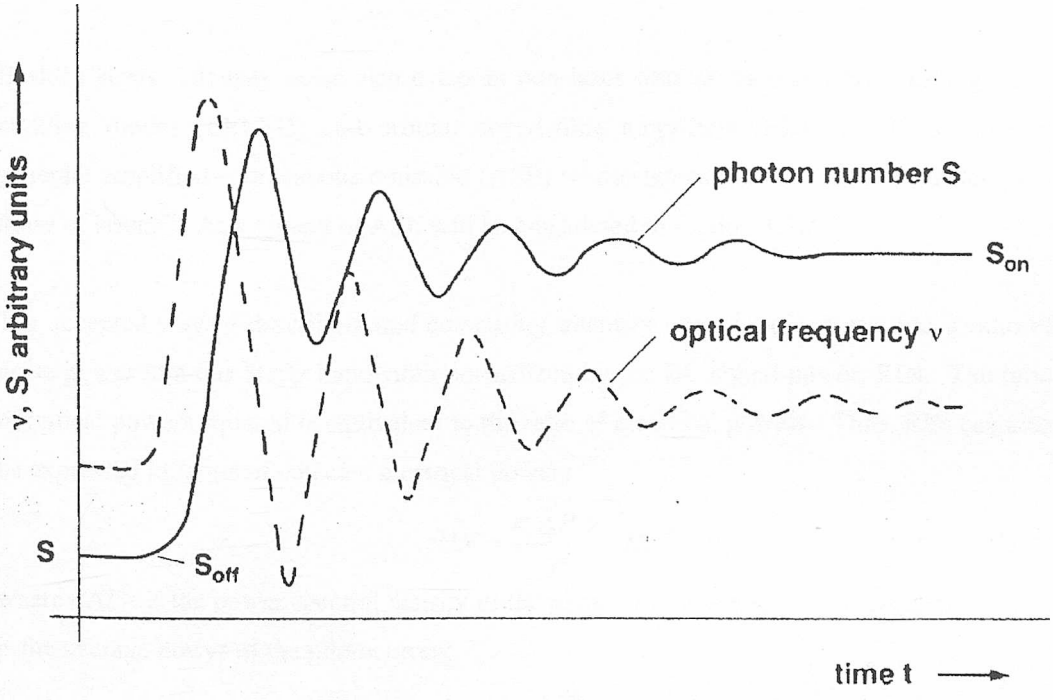

Figure 2-3: The temporal chirp for a step input to a laser diode[28].

3 Measurement of Laser Noise

3.1 Appraisal of Measurement Techniques

Searches for relevant laser noise characterisation papers provided an insight into techniques considered in the past and those currently used. An appraisal of each of these methods follows and has been used to identify any which may be a suitable basis for this project.

3.1.1 Relative Intensity Noise

3.1.1.1 Theory & Measurement

The fundamental origin of optical intensity noise, as mentioned previously in 2.1 occurs as a result of the optical interference between the stimulated laser signal and the spontaneous emission generated within the laser cavity. Laser sources such as DFB and Fabry-Perot laser diodes typically exhibit intensity noise whose value depends on pump levels and feedback conditions. Environmentally varying external feedback can affect the stability of a laser, resulting in large variations in its intensity noise.

Besides lasers, intensity noise also exists in non-laser sources such as edge-emitting light-emitting diodes (EELED) and erbium doped-fibre amplifiers (EDFA). These sources generate amplified spontaneous emission (ASE) whose intensity noise statistics differ from those of lasers[30]. Assessment of ASE will be considered in section 3.5.2.

The accepted way of describing and comparing intensity noise is to express it as a ratio of noise power in a one Hertz bandwidth normalized by the DC signal power, RIN. The ratio of optical powers squared is equivalent to the ratio of electrical powers. Thus, RIN can also be expressed in terms of detected electrical powers [18]

$$RIN = \frac{<\Delta P>}{P} \; Hz^{-1} \tag{3-1}$$

where $<\Delta P>$ is the power spectral density of the photocurrent at a specified frequency, and P is the average power of the photocurrent.

$$RIN = \frac{<\Delta i^2>}{I_{dc}^{\;2}} Hz^{-1} \tag{3-2}$$

This can be easily calculated using direct detection and an electrical spectrum analyser to measure the time averaged photocurrent noise power per unit bandwidth $<\Delta i^2>$, and a DC ammeter/voltmeter to determine the average DC photocurrent, I_{dc}.

For proper evaluation of laser RIN, other forms of noise need to be taken into consideration, especially when the laser noise is not the dominant one. These are known as detector shot noise (or photonic shot noise) and system thermal noise, which can be determined and subtracted from the total received noise, leaving the laser RIN. The total noise power $<P_T>(f)$ is the linear summation of these three noise sources.

$$< P_T > (f) =< \Delta P_L > (f) + P_q + < \Delta P_{th} > (f) \quad WHz^{-1} \tag{3-3}$$

where: $<\Delta P_L>(f)$ is the laser intensity noise power per Hz;

P_q is the photonic shot noise power per Hz;

$<\Delta P_{th}>(f)$ is the contribution of thermal noise power per Hz;

From Eqs. (3-1) and (3-3) RIN can be defined as the summation of the individual noise source ratios.

$$RIN_{system} = \frac{< P_T > (f)}{P} = \frac{< \Delta P_L > (f)}{P} + \frac{P_q}{P} + \frac{< \Delta P_{th} > (f)}{P} \quad Hz^{-1} \tag{3-4}$$

For simplicity, from this point on the noise power contributions will be referred to as

N_T – is the total noise power [$<P_T>(f)$];

N_L - is the laser intensity noise power per Hz [$<\Delta P_L>(f)$];

N_q - is the photonic shot noise power per Hz [P_q];

N_{th} - is the contribution of thermal noise power per Hz [$<\Delta P_{th}>(f)$];

The photodetector device converts optical energy, P_{opt} into an equivalent electrical signal, I_p, following the detector's responsivity relationship.[13,31]

$$I_P = \frac{\eta P_{opt} q}{hf} \quad Amps \tag{3-5}$$

where: η is the detector's quantum efficiency (electrons per photon);

q is electron charge constant (1.6×10^{-19} Coulomb);

h is Planck's constant;

f is the incident light frequency;

This electrical signal can then be evaluated using an electrical spectrum analyser. Any time-domain electrical phenomenon is made up of one or more sine waves of appropriate frequency, amplitude, and phase. Thus with proper filtering we can decompose the electrical signal into separate sine waves, or spectral components, that we can evaluate

independently[32]. The spectrum analyser will then provide amplitude verses frequency information.

From this information calculation of RIN can be performed. This consists of measuring the total system noise, N_T, and then accounting for the unwanted noise terms, i.e. the thermal noise and the shot noise.

A certain amount of noise power is generated at the input termination of a network, in this case by the photodetector, significantly being thermal noise. An impedance Z =R + jX at temperature T generates across its open circuit terminals a voltage resulting from the random motion of free electrons thermally agitated. This noise voltage, e_n, can be defined by [33]

$$e_n = 4kTBR \quad volts \tag{3-6}$$

where: k = Boltzmann's constant 1.374 x 10^{-23} joule/°K

T = absolute temperature °K

R = resistive component of impedance

B = Bandwidth

If the impedance Z = R + jX is connected to a matched load with input impedance Z = Z* as shown in Figure 3-1, maximum transfer of the noise power will occur. Noise power P_n will be dissipated in the load resistance R_L due to the noise voltage generated in the original resistance R. The noise power will be:

$$P_n = \frac{(e_n/2)^2}{R_L} = \frac{e_n^2}{4R_L} = \frac{4kTBR}{4R_L} \quad Watts \tag{3-7}$$

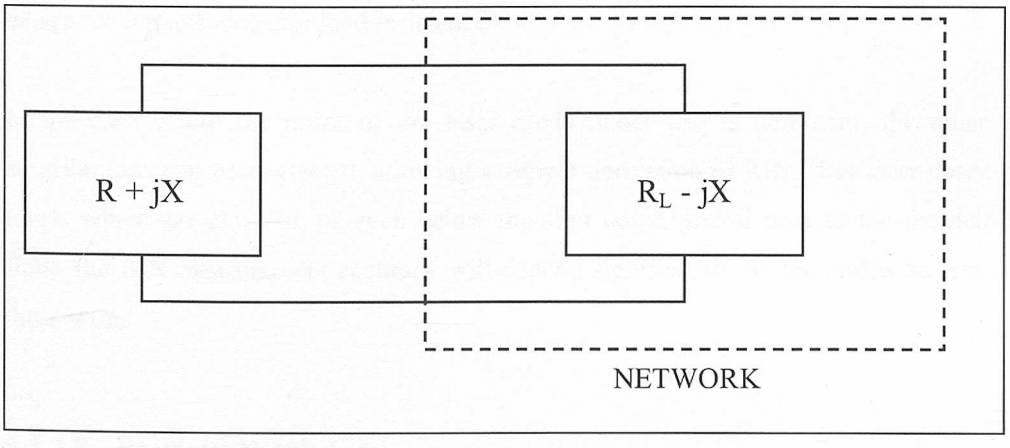

Figure 3-1: Available noise power P_n is equal to kTB.

Since there is equal noise voltage across source and load when R = R_L

$$P_n = kTB \quad Watts \tag{3-8}$$

Thus, for a 1 Hz bandwidth Pn = $1.374 \times 10^{-23} WK^{-1}Hz^{-1}$ or in dB's referenced to 1mW, Pn = -198.6dBm $K^{-1}Hz^{-1}$. With a typical laboratory temperature of 290K (20 ℃) the thermal noise power per Hz is therefore $-173.951 dBmHz^{-1}$.

Additional noise signals are referred to as background or dark noise, i.e. any leakage current found in the detector with no light applied.

This thermal and additional background information can be obtained either by taking a further measurement using the spectrum analyser with the photo-detector's optical input blocked, or by effectively eliminating it using a light chopper and a lock-in-amplifier (detailed in 3.1.1.2). Deriving the thermal noise from the operating temperature is not a practical approach as temperature will vary across the receiver system and also calibration will be tedious. Additionally to this, the background noise level would still need to be determined.

The average power and shot noise power terms can be derived from the dc photocurrent [16] typically using a high impedance digital voltmeter across the optical detector's 50Ω impedance. The mean-squared noise current from the photo-detector is:

$$\left\langle \Delta i^2 \right\rangle = 2qi_{dc}B \quad Amps \tag{3-9}$$

$$Shot\ Noise\ Power = N_q = 2qi_{dc}R \quad Watts \tag{3-10}$$

$$Average\ Power = P = i_{dc}{}^2 R \quad Watts \tag{3-11}$$

where: R = photo-detector load resistance

In the case where the noise of the laser diode under test is dominant, the other noise contributions can be neglected, allowing a simple derivation of RIN. For laser diode noise levels which are close to, or even below the shot noise, and/or near to the thermal noise floor, the RIN measurement accuracy will depend significantly on the ability to correct for these terms.

3.1.1.2 Previous Work

Technical papers have described the origins of RIN and have detailed suitable measurement systems to obtain the RIN response. All of these are based on the photo-

detector/amplifier/spectrum analyzer theme. An Italian telecommunications laboratory, CSELT, in 1989 [34], assembled an intensity noise set-up capable of assessing the frequency response up to 10GHz, using a wideband amplifier. Due to the relatively high noise figure of rf amplifiers, greater than 3dB, a synchronous detection system was employed. The laser light is chopped at a low frequency, and its fluctuations detected by a fast photodiode, then amplified and filtered at a given frequency by a SA. The demodulated output is in turn fed to a lock-in amplifier. The SA is used as a high sensitivity receiver whose output is related to the input noise powers, one being the optically originated noise (shot and laser), modulated by the chopper frequency and the other representing the receiver noise, uncorrelated to the chopper frequency. The lock in amplifier effectively allows measurement of the optical noise and rejects the receiver noise.

The relationship between the input optical noise of interest and the SA output level was calibrated by illuminating the detector with an incoherent light source, in this case a halogen lamp. This results in only shot noise, N_q, whose amplitude is easily evaluated by equation (3-10), being present at the output of the detector. By measuring noise at different optical power levels a calibration factor can be derived from the slope of the response. This has to be repeated across the complete frequency spectrum of interest. The objective of the experiment was to establish the effect of optical back reflections on laser RIN response. It was observed that reflections can cause the resonance frequency to increase in amplitude and also shift in frequency, which may have serious implications for high frequency applications.

A similar approach was also used by the French laboratory, CNET [26], incorporating a 0.8 to 10GHz rf amplifier. Receiver calibration was achieved using a surface emitting LED, providing a shot noise dominated signal, similar to the halogen lamp. Results obtained showed how RIN is dependent on laser structure, material properties and irregular behaviour, along with identifying back reflection effects.

Hewlett Packard have produced a number of papers/product notes centred round their lightwave signal analyser[18,19,25]. Again the system is based upon a SA coupled to a wideband amplifier and photo-detector giving a frequency response 10MHz to 22GHz. A number of calibration techniques are outlined and these are discussed latter. Synchronous detection is also mentioned if increased sensitivity is required. Also an alternative approach using a broadband detector with noise figure meters and power meters is mentioned, although this effectively integrates the noise and power over the bandwidth.

At lower frequencies, Hall and Carlsten of the Department of Physics, Montana State University [35] investigated intensity noise performance of Fabry Perot lasers from 1M to 100MHz. Laser noise contributors consist of spontaneous emission, mode partitioning (MPN) and injection current. It was demonstrated that the effect of noise, due to spontaneous emission generally can be reduced when the laser is operated at higher injection currents. If MPN exists then a high side mode suppression ratio is important, typically greater than 20dB to minimise contributions to intensity noise. Furthermore, noise can also be contributed from the injection supply more notably for high quantum efficient devices and thus effort should be made to use low noise drivers.

In summary, the best laser RIN sensitivity achieved as reported in these papers is estimated as -170dB/Hz with an uncertainty of 20%. But this could only be achieved either by taking a substantial number of repeat measurements (>200), or similarly by repeating measurements at different optical powers and applying line fitting and extrapolation. To minimise the affect of back reflection approximately 60dB isolation was found to be necessary.

3.1.2 Frequency Chirp

3.1.2.1 Theory & Measurement

Any variation of a laser diodes injection current yields a variation of the carrier density, which in turn yields a variation of the refractive index and hence changes the optical emission frequency. In the carrier effect regime, i.e. modulation frequencies greater than 10MHz the carrier density inside the laser diode controls both the optical intensity and the optical emission frequency. Thus it is often useful to relate intensity modulation and frequency modulation directly[36], referred to as the alpha coefficient (α).

For small sinusoidal modulation signals the frequency (FM) modulation is simply proportional to the intensity (IM) modulation and this proportionality is governed by the characteristic frequency ω_g. This holds for low modulation frequencies above 10MHz. Relating the FM-modulation index (M)

$$M = \left| \frac{2\pi \ \Delta v}{\omega_m} \right| \tag{3-12}$$

where ω_m is the modulation frequency and Δv is the static laser linewidth, to the IM-modulation index (m)

$$m = \left| \frac{\Delta S}{\langle S \rangle} \right| \tag{3-13}$$

where ΔS is the photon number fluctuation and <S> is the mean photon number, yields [28]

$$\frac{M}{m} = \frac{\alpha}{2} \sqrt{1 + \left(\frac{\omega_g}{\omega_m} \right)^2} \tag{3-14}$$

Typically a DFB-InGaAsP may exhibit an alpha coefficient (α) of around 6 and a characteristic frequency of 2GHz. The transfer characteristics between current modulation and optical frequency modulation can be expressed theoretically as

$$\frac{\Delta v}{\Delta I} = \frac{\Delta v}{\Delta S} \frac{\Delta S}{\Delta I} = \frac{\alpha \tau_{ph} \omega_g}{e 4\pi \langle S \rangle} \frac{1 + j(\omega_m / \omega_g)}{(j\omega_m / \omega_r)^2 + j\omega_m / \omega_d + 1} + \frac{C_{th}}{1 + j(\omega_m / \omega_{th})} \tag{3-15}$$

where τ_{ph} is the photon lifetime, ω_r is the resonance frequency and ω_d is the damping frequency. This includes the thermal effects, expressed as a low pass filter with a constant C_{th} and a thermal cut-off frequency ω_{th}. The emission frequency of a laser diode has a temperature sensitivity of about -20GHz/K [37]. C_{th} depends on the thermal resistance which is typically of the order of 20 to 100K/W yielding a negative C_{th} of several GHz/mA as in Figure 3-2.

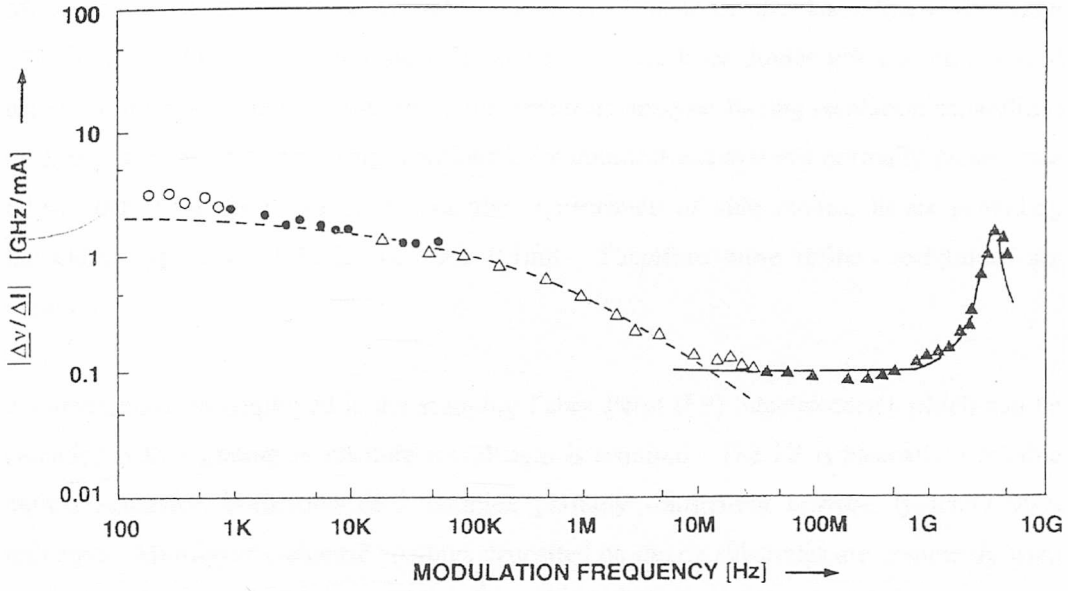

Figure 3-2: Current Frequency Transfer function, GHz/mA response[28].

The thermal cut-off frequency is typically in the order of $\omega_{th} / 2\pi \approx$ 100kHz to 1MHz. Since the characteristic frequencies ω_g, ω_r, ω_d are all in the GHz range, a nearly flat frequency response for frequencies 10MHz to 1GHz results. Thus, in frequency modulation applications lower modulation currents offer considerable frequency shift, i.e. good FM performance without significant intensity modulation.

The output of a well stabilised laser diode is affected in two ways by the presence of quantum noise[38]. Firstly, there are output amplitude intensity fluctuations as previously mentioned (RIN). This affect can be significantly reduced by biasing the laser well above threshold. The second effect is caused by the phase of the laser output to change with time in a random fashion. It is this random phase fluctuation which determines the theoretical minimum line width of the source. Thermal and carrier density variations, caused when direct modulation is applied, will increase this *static* linewidth[27].

An estimate of the magnitude of the spectral bandwidth is often obtained using sinusoidal frequency modulation and can be approximated from [28]

$$\Delta v_0 = 2(M+1) f_m \quad Hz \tag{3-16}$$

which holds for small modulation frequencies only, where f_m is the modulation frequency.

Measurement of frequency chirp relies upon assessment of the laser linewidth under modulated conditions. For normal LED and multimode laser diodes this can be assessed using a grating spectrum analyser or optical spectrum analyser having resolution capabilities of 0.05 to 0.1nm. As previously mentioned, communications systems normally incorporate DFB, DBR type lasers which reduce the significance of side modes, hence providing linewidths typically <50MHz, i.e.. sub 0.1nm. Therefore more refined techniques are required.

A common set-up employed is the scanning Fabry Perot (FP) interferometer which can be cascaded with a grating if absolute wavelength is required. The FP is basically a tunable optical resonator, consisting of 2 parallel, partially transparent mirrors, typically 99% reflective. Multilayer dielectric coatings deposited on quartz substrates are commonly used as high-performance mirrors. This arrangement forms a resonant cavity acting as a frequency filter with periodically spaced transmission peaks separated by $\Delta f = c / (2nL)$ often referred to as the Free Spectral Range (FSR) of the interferometer, where c is speed of light in a vacuum, n is the refractive index of the resonant cavity and L is the length of the resonant cavity.

The bandwidth of the individual resonance curves is usually defined as;

$$B = \frac{1-r}{\sqrt{r}} \cdot \frac{c}{2\pi nL} \quad Hz \tag{3-17}$$

where r is the mirror reflectance factor.

Relating the bandwidth B to the mode spacing FSR yields the finesse F;

$$\mathrm{F} = \frac{FSR}{B} = \frac{\pi\sqrt{r}}{1-r} \tag{3-18}$$

With practical resonators, both the 100% transmission and the ideal bandwidth / finesse cannot be achieved. This is due to losses in the optical system, finite mirror flatness, non-parallel mirrors and non-parallel beams. Even so FP's are capable of measuring the linewidth of individual modes, performed by changing the resonator length (scanning). The output power is measured for each L allowing the entire spectrum to be sampled. Tuning range should not exceed the FSR. A problem often encountered in this technique is the reflection back into the laser source. FP's strongly reflect when not in resonance, hence optical isolation is essential.

An alternative, higher resolution technique now used is the heterodyne method. It's commonly used for coherent fibre optic systems [39] and relies upon provision of a local oscillator (E_{LO}) field, having a very stable frequency close to that of the modulated signal (E_s) of interest. The two fields are superimposed onto a broadband detector taking care to preserve a good alignment. Since the detector responds to intensity, the output current is proportional to

$$i(t) \propto \left[E_s(t) + E_{LO}(t)\right]^2 \tag{3-19}$$

Expanding the quadratic term, we obtain a dc component and several oscillating components at frequencies $2\omega_s$, $2\omega_{LO}$, $(\omega_s + \omega_{LO})$, and $(\omega_s - \omega_{LO})$. The photodiode only responds to the dc and difference frequency terms, while the higher frequencies average to zero. Heterodyning preserves the amplitude or phase modulation contained in the original signal, but its frequency is down-converted from optical frequencies to the more easily measurable RF band. The linewidth of lasers can therefore be assessed by performing a fourier transform of the signal autocorrelation, providing a laser power spectrum. This can be observed using an RF spectrum analyser.

However, suitable laser local oscillator signals are often not available or at best expensive due to the very narrow linewidth required. To overcome this limitation, self heterodyne methods[40,41,42] can be employed. Basically the laser under test is also used as the local oscillator. The laser field is split in two, frequency shifted in one branch of a Mach-Zehnder interferometer and time delayed by a time τ_0 in the second branch. The beams are then recombined at the surface of a broadband detector. The frequency shift is provided by an optical modulator. The interferometer effectively converts the phase noise into intensity noise, the autocorrelation of which provides a dc term, a monochromatic term at frequency ω_m, and a modified Lorentzian component centred at the same frequency. By increasing the delay time τ_0, the weight of the monochromatic component becomes lower and lower until a strictly Lorentzian shape is obtained. The resulting power spectrum has a width which is twice that of the laser spectrum $\Delta\omega$, which is demonstrated in Figure 3-3, in terms of frequency, Δf. For gaussian broadening, the width of the heterodyne spectrum turns out to be $\sqrt{2}$ times the actual width.

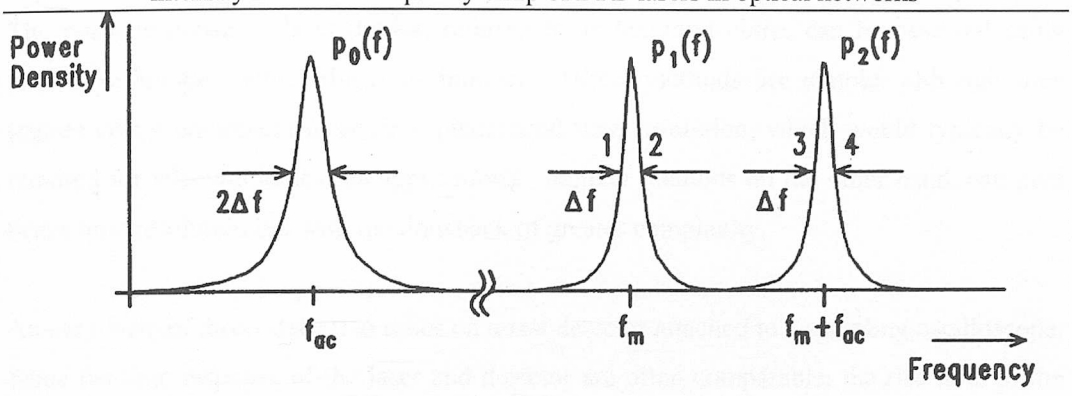

Figure 3-3: Low frequency spectrum obtained by self heterodyning[20].

Hence, a clear evaluation of laser linewidth can be achieved providing delays much longer than the coherence time of the laser are used, related by

$$\tau_{co} \geq \frac{2}{\Delta\omega} \tag{3-20}$$

for a Lorentzian line shape. The magnitude of this delay should be 5 to 6 times that of the laser coherence time [41].

A variation on this technique is to omit the frequency shift in one arm, usually an A/O modulator. In this case the centre frequency of the mixing product is zero and is termed self homodyning. The disadvantage of this variant is the lowest linewidth which can be measured is limited by the lowest frequency of the spectrum analyzer. Also, if modulating the laser the rf self beating of the two arms generates numerous cross products causing the observed spectral width to cycle as the modulation frequency is changed, i.e. the combined signals move in and out of phase with each other [43].

The latter phasing problem can be eliminated by gating the modulation frequency on and off with a period twice the delay time between the two arms, referred to as Gated Delay Self Homodyning[46] (GDSH). This way, the modulated signal is always mixed with an unmodulated signal. Hence the laser functions as both the local oscillator and the modulated laser under test. The result is that the spectral width observed will be the time-average of the chirp induced frequency-offset.

In summary, homodyning offers one important characteristic over heterodyning in that no thermal or current stabilization are required because of its wavelength self-tracking.

The pulse response of laser diodes, referred to as temporal chirp, can be assessed using several techniques, either direct or indirect. Direct methods are simpler although they require costly equipment to achieve picosecond time resolution, which would typically be required for telecommunication applications. Indirect methods on the other hand, can give better time resolution but with the drawback of greater complexity.

An easy form of direct detection relies on a fast detector attached to a sampling oscilloscope. Since the time response of the laser and detector are often comparable, the rise time of the detection circuit must be known to allow de-convolution. This time response may typically be as short as 30ps. Shorter optical pulses can be resolved using a streak camera, which is basically a special kind of image intensifier providing a 2D image of spatial (or spectral) variation verses time variation. Commercial devices can now offer time resolutions better than 10ps, but at high cost. Indirect techniques are based on obtaining the optical autocorrelation using a Michelson interferometer and a non-linear crystal. A high repetition rate pulse train generated by the device under test is sent to the interferometer while the length of one of the arms is continuously scanned within a range dependent on the pulse duration to be measured. The time between successive pulses must be much shorter than the scan time. Typically a high sensitivity photomultiplier tube (PMT) is employed since the signal level may be very low. This technique does somewhat rely on a reasonable estimate of the pulse shape, gaussian FWHM being 1.41 times the original.

3.1.2.2 Previous Work

As already mentioned, due to the poor resolution capabilities of grating spectrum analysers and the practical difficulties in constructing suitable FP interferometers and heterodyning systems, very little previous research has been found. Instead most research activities have concentrated on the self heterodyning/homodyning techniques and are discussed here.

The drive in this area has mainly been in assessing the rapid advancement in the spectral purity of single mode semiconductor devices, such as linewidth and frequency modulation efficiency. This started in the early 1980's when such organisations as the University of Tokyo[42] proposed self heterodyning using a fibre delay path and an acoustic-optic modulator. Here it was recognised that the time delay path defines the resolution, for example 1.5km providing 50kHz resolution at the 850nm band. AT&T Bell [43] also demonstrated the measurement of linewidth, here using a free space Mach-Zehnder, results subsequently being successfully cross referenced to an FP interferometer.

Following this and combined with the interest in Frequency Shift Keying (FSK) modulation schemes further papers looked at laser diodes frequency modulation efficiency, i.e. the lasers frequency deviation under differing modulation injection currents. KDD [44] set up a Delayed Self Homodyne (DSH) system to achieve this based on a 10km fibre delay path. Experimental results of FM efficiency versus modulation frequency confirmed the dipped response, predicted at low frequencies when crossing from the thermal to the carrier effect and also agreed with results gained using an FP interferometer. It highlighted that the frequency modulation index can be determined at low modulation frequencies by measuring the delay time and the sideband and at higher frequencies from the ratio of the carrier and the sideband.

Linewidth and linewidth enhancement factor measurements using a DSH variant were reported by Naval Research Laboratory[45] in 1988, based on the FWHM sideband approach. Modulation frequencies around 450MHz were assessed, and the importance of minimising intensity noise from back reflections was reported. Only small signal conditions were used, ensured by reducing the RF drive until the 2nd fm Bessel was at least 20dB down on the 1st fm amplitude level measured by the spectrum analyser. Low amplitude modulation index levels typically 0.2 to 0.8, were used.

In the late 80s Hewlett Packard[46] reported an enhancement to the DSH technique to assess frequency chirp of DFB laser diodes. This consisted of gating the applied modulation signal on and off at a set mark/space ratio matched to the long arm delay, thus preventing the modulated signal recombining with itself and causing multiple Bessel beating and cross products. This eliminated the minimum and maximum frequency excursion cycling under varying fm conditions. Low modulation frequencies, up to 100MHz were used and resulting frequency chirp spectrum measured similarly to the linewidth i.e. determining the half power frequency point. This spectrum consisted of numerous Bessel functions convoluted together and provided chirp's of up 13GHz. A linear relationship was reported between chirp and modulation index, and also a strong sensitivity to bias current and modulation frequency variations was observed.

A further paper by HP[47] looked at the behaviour of the Bessel functions under both low and high modulation frequencies. At higher frequencies (300MHz) individual Bessel functions become evident, thus preventing the half power point (3dB) from being easily distinguished. Instead it was proposed that by adjusting the laser injection current to null a specific Bessel

sideband, the frequency modulation index M could be determined. Then by knowing m, the alpha coefficient can be derived as well as the frequency chirp.

3.1.3 Commercial Test Equipment

Further to the paper search carried out, optical test equipment manufacturers were contacted to form a picture of commercial systems currently available. This concluded that HP were the only equipment manufacture's supporting RIN and chirp measurements. The system, known as the Lightwave Analyser, basically consists of an rf spectrum analyser (HP 71400C) coupled to a photo-receiver high speed PIN via an rf amplifier (HP70810B). The system, designed 8 to 10 years ago, is modular and hence various optional units can be inserted as desired. Although the spectrum analyser is a common HP module, the photo-receiver and amplifier module, known as HP70810, is very specific to the lightwave capabilities. It includes an optical attenuator to prevent optical overload and also a dc power monitor circuit to allow measurement of the average power as well as the modulated power. RIN can be measured directly with this equipment as well as other optical parameters such as modulation depth and power in the telecoms wavelength window of 1200 to 1600nm.

The system's noise figure is governed principally by the amplifier/receiver noise figure which is approximately 8 and 5dB respectively. Noise sensitivity is quoted as -166dBm, i.e. 8dB above the thermal noise floor (dominated by the amplifier noise figure). The photo-receiver has a maximum optical power limit of +3dBm and a bandwidth of 10MHz to 22GHz. To gain some picture of the units ability to measure RIN, if we take an example of incident laser noise being equal to the shot noise then to be within the system's sensitivity at least 0.9mW optical power is required. This corresponds to a laser RIN of -154dB/Hz which decreases as more optical power is applied. Figure 3-4 shows the operational range for measuring laser noise equal to the shot assuming a typical detector responsivity of 0.8 and thermal noise floor of -174dBm/Hz.

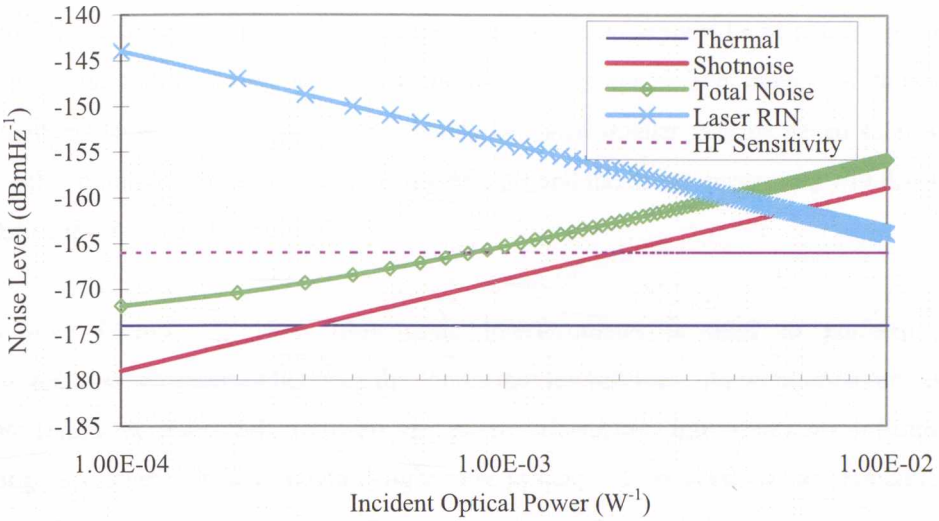

Note: RIN quoted in $dBHz^{-1}$ and noise in $dBmHz^{-1}$

Figure 3-4: System response when laser noise is equal to the shot noise.

Thus the HP instrument can potentially offer sub shot noise laser measurements but only at higher incident optical powers (>1.5mW) with uncertainties which will increase significantly, due to the dominant nature of the shot noise at high powers. At lower optical powers the shot noise becomes less dominant but, if the laser noise is low the total noise will tend towards the thermal noise floor. Although the laser noise may now be more evident compared to the shot noise, unfavourable measurement conditions still exist due to the thermal limit which now dominates.

Today's laser diodes now have RIN specifications beyond the scope of this system, some typically achieving (or claiming) -170dB/Hz at 1mW optical power.

A further observation concerns the shot noise derivation. In a similar way to the thermal noise discussed in 3.1.1.1, the shot noise power, Eq. (3-10) measured on the spectrum analyser will be:

$$N_q = \frac{qiR}{2} \; Watts \tag{3-21}$$

For perfect impedance matching the shot noise power measured by the spectrum analyser will be a factor of 4 (ie 6 dB) less than the standard noise power. It is unclear whether the HP system accounts for this as all the application notes refer to the standard shot noise power (2qiR). This essentially means that when subtraction of shot noise is undertaken the spontaneous noise values

will be much lower than their real values. Also, the spontaneous noise which passes through the circuitry will also see a similar effect and the spontaneous noise must be increased by 6 dB in order to relate to the actual noise incident on the detector. The impact of this is the measurements undertaken up to this time would be much smaller that the actual spontaneous noise with a minimum systematic uncertainty of 6 dB and the actual uncertainty will depend on the relative level of the Shot noise.

An additional unit, HP11980 fibre optic interferometer is used to perform chirp measurements when inserted between the source and the receiver. As mentioned previously, the interferometer effectively transfers the phase information into amplitude information, allowing assessment on the standard lightwave system. Two versions are available, the standard has a long path length of 730m, providing a delay of 3.5μs corresponding to a resolution of 225kHz. Option unit 005 has a delay of 25μs providing a resolution capability of 30kHz. No automatic chirp measurement is provided. Instead the effective line spread obtained has to be interpreted by the user.

HP's quoted measurement uncertainties are vague. A factory calibration is performed on the Lightwave Analyser coupled with the Lightwave section at 1300 and 1550nm in terms of modulated power over the bandwidth 100kHz to 22GHz stating an accuracy of ±1dB. A random uncertainty is mentioned for RIN, indicating levels up to ±2dB maybe encountered depending on the level of laser RIN being measured. For chirp measurements no details have been found in terms of an overall uncertainty. The only reference found regarded the systems over estimation of laser linewidth of around 10%.

3.1.4 Techniques Summary

From the techniques reviewed it is apparent that there is a short fall in sensitivity for RIN measurements of typical DFB lasers encountered today. Additionally the techniques are generally tedious in the number of measurements required and also in the test equipment required, especially when incorporating an optical chopper. There is also some ambiguity with the shot noise level when impedance matched, raised in section 3.1.3

Chirp measurement capabilities for typically narrow DFB sources are dominated by the interferometer methods. Homodyning offers the most simplistic approach but is limited to only observing half of the demodulated LW. Heterodyning provides the complete LW response but the stability of the additional laser source will no doubt add to the complexity and uncertainty of measurement. A further observation projects that these interferometer

methods may inherently contribute chirp through birefringence effects, see section 3.6.1. This will be investigated where possible.

Measurement uncertainty of any of the RIN or Chirp setups is unclear. In the commercial world this often leads to disagreements within industry and between suppliers/customers. It is vital, in forming a national standard that all uncertainty terms are thoroughly investigated and accounted for. Additionally, the highest confidence level should be targeted. To this end, system complexity needs to be minimised which would otherwise contribute to overall measurement uncertainty and test time.

3.2 Project Technical Aims

The predicted optical data capacity demands in the future will increase the need for lower noise components, such as Multi Quantum Well DFB laser devices[24] in current systems and for 10Gbit+ research purposes. Considering the immaturity of the telecommunications industry at the onset of this project, concerning higher data rates (>1Gbit/s) and the information gathered from companies, a versatile system specification was opted for. After an initial industry survey a project target specification was defined as follows.

The calibration standard must be able to measure laser noise down to the shot noise level for optical power levels which range between 100 μW to 5 mW. Laser RIN measurement sensitivities should be capable of measuring levels as low as -170 dB/Hz @1mW over a frequency range of 10MHz to 20 GHz to better than ±1dB uncertainty. The dynamic range of the RIN measurement should be at least 70 dB so that the versatility in the measurement can be achieved. The system must be able to measure frequency chirps as large as 50 GHz and as low as 100 KHz, over as wider modulation frequency range as possible to better than ±10%. Both parameters should focus on the two telecommunications windows at wavelengths of 1300nm and 1550nm (±50nm).

A wider range of optical power is desired since it allows for optical losses in telecommunication links and the measurement system, making it possible to accurately measure such parameters as backscatter. The proposed system is expected to be capable of performing a number of other parameters such as:

- back-scatter degradation
- linewidth of laser sources

- frequency response of detection systems
- noise figure of optical amplifiers
- gain of optical amplifiers

Temporal chirp was not pursued further after establishing little interest for this parameter in the telecommunications industry at this time. Additionally, the high equipment cost to perform this measurement would most likely have been beyond the budget of this project.

Finally, a requirement in forming this national standard is that all measurements attained should conform to United Kingdom Accreditation Service (UKAS) guidelines for the expression of uncertainty and confidence in measurement [M3003]. This will help ensure national standard recognition and also promote *good working practice* to industry on dissemination.

3.3 Measurement Approach Selection

Due to the low laser RIN specification and the national standard precedence, it is of prime importance that the shot and thermal noise terms are accurately measured along with the total noise. Hence high emphasis was placed on achieving optimum sensitivity and thoroughly assessing and minimising all measurement uncertainty contributions. Obviously costs and time scales play a significant *trade-off* role in this process.

From the RIN and chirp research papers discussed previously, it is clear that the more capable system approach for both parameters basically consisted of a photodetector, rf amplifier and spectrum analyser combination. Additional insertion of a fibre interferometer provides a suitable chirp measurement capability with the required resolution performance. However, the specification of the reviewed systems do not meet the project requirements here in terms of both sensitivity and uncertainty.

One of the critical elements in this project concerns measurement of such low noise signals associated with laser intensity noise to such high precision. To help visualise this problem Figure 3-5 demonstrates the influence of thermal noise, shot noise and system sensitivity on the laser signal under varying optical powers. A Thermal noise floor of –174dBm has been assumed for the example along with a detector efficiency of 0.8. We can see that when the laser noise dominates then a 1dB uncertainty in laser RIN correlates directly to being able to measure the system noise to 1dB. For the 1mW and 5mW responses this ratio reduces as the

influence of the shot noise becomes more evident at lower laser RIN's, sub -140dB/Hz and -150dB/Hz respectively. For lower optical powers, 100μW this effect is further degraded by the influence of the system thermal noise. When incident laser noise is equal to the shot noise we can see that to be able to derive laser RIN to within ±1dB, measurement of the system noise needs to be within ±0.51dB (5mW), ±0.5dB (1mW) and ±0.21dB (100μW).

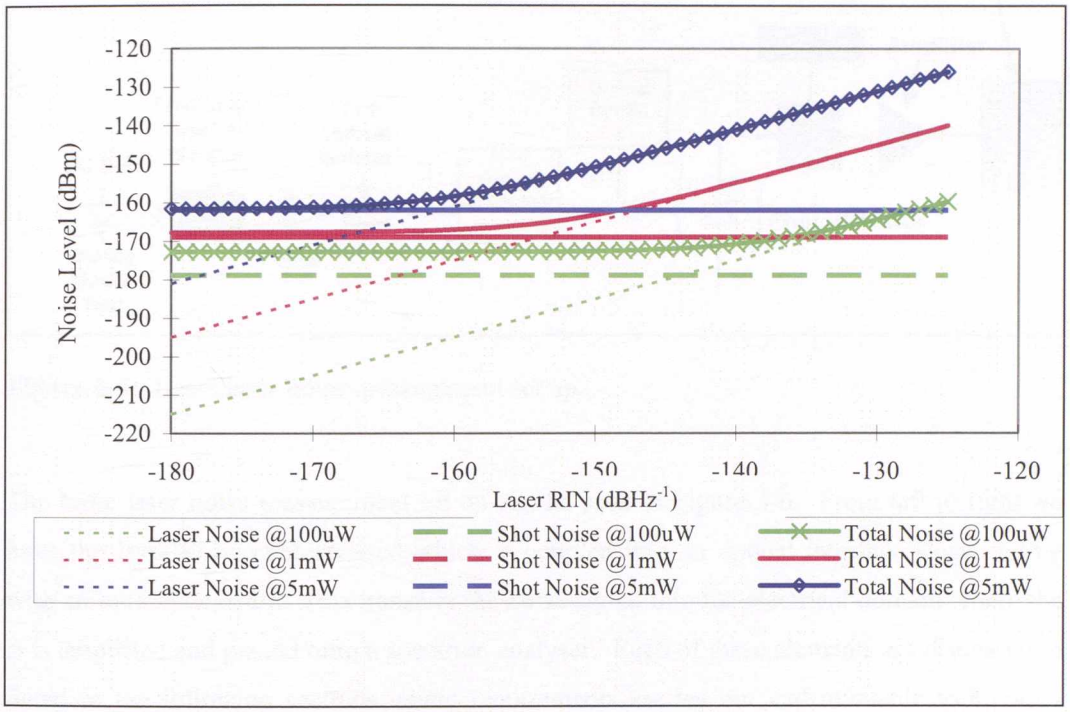

Figure 3-5: Simulated noise relationship at various optical powers.

For sub shot laser noise these uncertainties are further reduced, e.g. laser noise 10dB below the shot noise will necessitate system noise measurements to within ±0.1dB, ±0.08dB and ±0.03dB respectively. This level of measurement accuracy is clearly difficult to achieve when standard rf metrology is considered. Thus, technical proposals were identified to enhance the measurement system to meet the desired specification. This focused on two key aspects, a) gathering the very latest device/equipment technology to provide the utmost sensitivity and b) improving the measurement methodology and calibration process to provide the utmost precision measurements internationally.

3.4 Relative Intensity Noise System

Observations from past papers make it clear that sensitivity is severely governed by the system noise figure, predominately from the amplifier, but also the detector and analyser.

Thus, to start with a fighting chance of measuring low noise levels, the latest rf component technology was reviewed and engaged.

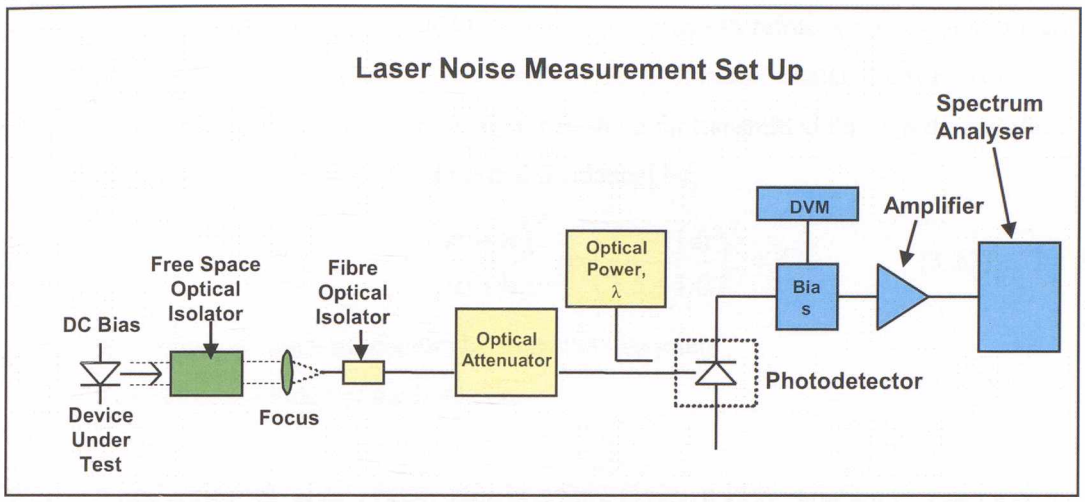

Figure 3-6: Basic laser noise measurement set up.

The basic laser noise measurement set up can be seen in Figure 3-6. From left to right we have the laser to be characterised which is coupled into an optical interface stage ending with an optical detector. This transfers the noise signal into the electrical domain where the rf is amplified and passed onto a spectrum analyser. Each of these elements are discussed in detail in the following sections where requirements are set out and available technology reviewed. Further on, assessments are made of their performance and contribution to the overall system.

3.4.1 Optical System

The main aim of this stage is to gather the optical signal of the laser to be characterised into fibre, if not already so and applied to the photodetector in a controlled manor. With communications lasers coming in various guises, such as; fibre coupled (various connector styles), free space (collimated or diverging beam), with built in driver or without etc, a flexible system has been built up. This includes the following items, mostly being commercially available:

fibre couplers; sourced from FOCI Fiber Optic Communications, Inc. Typical insertion loss 0.15dB, return loss <-65dB through use of anti-reflection coating. Optical working distance 2mm from the lens input

fibre connectors; data presented by some laboratories reviewed previously, it is clear that any optical reflections caused by fresnel reflections must be minimised. This phenomenon is associated with the step changes in refractive index at a jointed interface, such as a commonly used Fibre Connector Planar Convex (FC/PC) connection. Here a partial reflection, r of the light transmitted through the interface is typically estimated (light of normal incidence) by;

$$r = \left(\frac{n_1 - n}{n_1 + n}\right)^2 \Rightarrow \left(\frac{1.5 - 1.0}{1.5 + 1.0}\right)^2 = 4\% \qquad (3\text{-}22)$$

n = refractive index of medium between the two joints

n_1 = refractive index of the fibre core

Considering this level of reflection in a fibre cavity, a 15% variation in transmission can occur, hindering stable optical power measurements. An effective way of improving this situation is with the inclusion of angled FC/PC connectors (FC/APC). Here, a small angle is introduced at the connector interface of 8 or 9 degrees, with a radius of curvature between 5 and 12 mm (See Figure 3-7). By angle polishing the end of the fibre, the reflections at the fibre-air interface are not captured by the fibre core. This greatly reduces back reflection levels in fibre optic systems, and in turn reduces feedback problems and improves stability. Where ever possible these connectors will be selected.

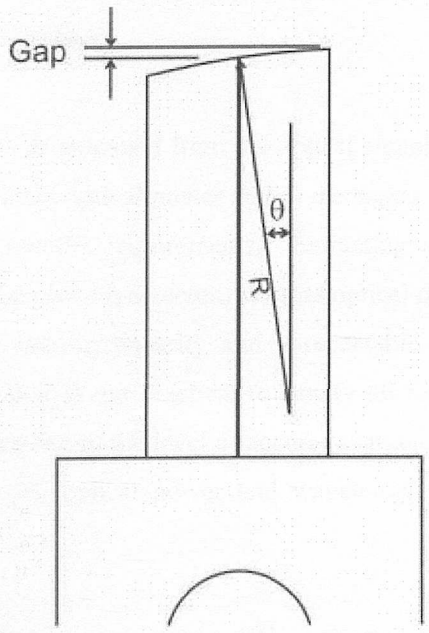

Figure 3-7: APC Ferrule Polish.

isolators; Similar to the fibre connectors just discussed it is desirable to minimise optical back reflections from entering the laser under test. To supplement the use of angled connectors optical isolators have been procured. Free space and in-fibre have been selected with quoted isolation of >40dB and return loss of >60dB. Insertion loss is typically 0.5dB.

attenuator; Control of the incident optical power on the photodetector is provided by an Hewlett Packard HP8156A optical attenuator. The attenuation is provided by a graduated disk in the optical path which can be rotated to provide varying attenuation up to 60dB with a resolution of 0.001dB and typical linearity of <0.05dB. The unit operates over the telecom wavelengths from 1200nm to 1650nm and has a low polarisation dependent loss typical of <0.02dB. With the inclusion of option 201 (APC angled connectors) a typical insertion loss of 2.5dB and return loss of 60dB can be achieved.

Miscellaneous hardware is provided such as fibre adapters, optical mounting clamps, laser diode mounts. Additionally, drive electronics is available for the laser to be tested in terms of forward current and thermal control when required.

3.4.2 Electro Optical Interface

Three key properties need to be extracted from the optical signal being analysed. These are 1) the rf noise signal, 2) incident optical power and 3) the signal wavelength. Each of these properties have their own specific requirements. Extracting an rf signal up to 20GHz requires an ultra fast / wide bandwidth detector, whereas optical power measurement is more dependent on having high stability/linearity and a repeatable optical interface. It was evident at an early stage that it is not practical to satisfy all these requirements with one detector especially when considering the level of accuracy targeted. Thus separate detectors were sourced to satisfy the rf, optical power and wavelength measurements. Each are discussed below.

Optical communications receivers use either PIN or avalanche photodiodes to convert optical power to electrical signals. PIN photodiodes are used for high bandwidth applications because of their fast response time and simple bias circuitry. The devices are operated under reverse bias where the intrinsic 'I' layer is depleted of charge and only the

small (pA or nA) reverse leakage current known as dark current flows in the absence of light. In the photodetection process, a photon of radiation enters through the transparent P-doped region and is absorbed in the I region, giving rise to an electron-hole pair. These carriers are swept out of the I region by the bias electric field and collected as photocurrent in the P and N regions. A desirable photodetector structure has the P and N regions of InP and the I region InGaAs which can be grown on a InP substrate.

There are basically three limiting factors to the speed of a photodetector; diffusion of carriers, drift transit time in the depletion region, and capacitance of the depletion region. The slowest of the three processes is the diffusion of carriers to the high electric field depletion region from outside that region. To minimise this slow effect, carriers should be generated near or in the depletion region. The second process, transit time, is the time required for the carriers to drift across the depletion region and get swept out of the device. With sufficient reverse bias, these carriers will drift at their saturation velocities. For GaAs this is in the order of $3x10^6$cm/s. Lastly, the capacitance of the device will determine its RC time constant; R being the load resistance (usually 50Ω). To maximise a photodiode response, the transit time is typically designed to be comparable to the RC time constant.

The Schottky photodiode improves on the performance of the PIN or APD photodiodes because of some special characteristics. Its parasitic resistance is lower since the N-type Schottky photodiode has only an N layer and no P layer. Moreover, the diffusion effect is minimised since the carriers are generated primarily at the metal semiconductor interface, where there exists a high electric field. In an N-type Schottky, the holes, which are the slow carriers, only have to travel a short distance to the metal.

Besides the high speed response required for this project, other important photodetector characteristics need to be considered. These include quantum efficiency and noise equivalent power (NEP). Quantum efficiency η is defined as the fraction of incident photons which are absorbed by the photodetector and generate electrons which are collected at the detector terminals. The absorption coefficient of the semiconductor material used within the photodetector significantly determines the quantum efficiency, which is generally less than 1 and is wavelength dependent. Responsivity R is often of more use when characterising a photodetector as it involves the photon energy, unlike quantum efficiency. This is defined as output photocurrent over the incident optical power i.e. Amps/Watt. The NEP, or the optical power required to have a signal-to-noise equal to 1, describes the weakest optical signal that could possibly be measured. Here we need to ensure there is sufficient sensitivity to cover the lower end of the power range, being 100μW.

Considering these important characteristics with regard to the targeted system specification a Schottky photodetector manufactured by New Focus was selected. The New Focus 1414 model is based on a 25μm diameter InGaAs photodiode, operating from 950 to 1650nm, thus covering both telecommunications bands. It provides a high responsivity for a high speed detector of typically 0.6A/W which in this application maximises the available noise signal available for analysis. The optical interface uses a fibre FC/PC connection. Saturation power is quoted as 2mW which falls some way short of the range set out for this project. Options here are limited as there are no other high speed detectors capable of higher saturation levels. From discussions with New Focus it was established that performance and reliability data for this relatively new detector was limited in terms of the saturation level and the 2mW quoted was considered pessimistic. This opened an avenue to explore capability beyond 2mW in liasion with New Focus in the interest of both parties. To cover any short fall in optical power range the optical attenuator can be employed to provide a number of RIN / Chirp measurements at varying power levels which can then be extrapolated to the desired optical power level.

The 1414's -3dB bandwidth of typically 25GHz extends well passed the targeted 20GHz with a rise time of 17ps. The photo detector has an output impedance of 50Ω, ideally suited for connection to rf instrumentation via a Wiltron K rf connector. Bias for the photodetector is provided by a 9V battery source (PP3) via an internal dc regulator. This isolated power source minimises any pick up of external noise sources which contributes to the units low noise equivalent power (NEP) of 30pW/√Hz The unit also offers a dc output port which could be coupled to a volt meter to gain the generated photocurrent for shot noise and responsivity derivation. From investigations, discussed in chapter 4 the dc port was found to be non linear. Additionally, the dc photocurrent is present on the rf port as well as the dc port. This would cause any following rf amplifier or spectrum analyser to saturate. Thus an additional dc block, discussed in section 3.4.3 is required after the detector to prevent the saturation.

Measurement of the incident optical power at the photodetector interface is of significant importance since it is a key parameter for the characterisation of RIN and is also an essential traceable link to National Standards. For a detector to act as transfer path it needs to have superior stability over time, good linearity and ability to measure at higher power levels (>5mW). Semiconductor materials, such as silicon and germanium generally fall into this category. Silicon has an indirect bandgap energy of 1.14eV giving a loss in response above 1.09μm, thus not covering the main two telecoms windows which we are targeting.

Germanium however, has an indirect bandgap energy of 0.67eV, providing a response over both windows, 1.3μm & 1.55μm. The disadvantage of Germanium is its relatively high dark current due to the narrow band gap in comparison to other semiconductor materials such as III-V alloys, especially at shorter wavelengths (below 1.1μm). In this application the bottom end optical power range of 100μW is considered to be significantly high compared to the dark level and thus would not prevent its use. Additionally, two such detectors complete with photocurrent amplifiers were readily available within the laboratory facilities which allowed project funds to be redistributed where necessary. The Ge photodiode is manufactured by EG&G and is mounted in a heatsink driven with peltiers and controlled by a thermoelectric cooler from Alpha Omega. The generated photocurrent is fed to a Vinculum amplifier which then displays the scaled photocurrent. This amplifier also provides the bias for the photodetector. Characterisation and traceability of this Ge photodetector is provided by the Optical Radiation Department of the National Physical Laboratories. This will include responsivity over wavelength and optical power linearity where ever possible using the fibre optic FC/PC adapter.

Wavelength measurement of the source laser is required so as to select the correct calibration factor to derive the incident optical power. Accuracy here need only be ±1nm. An ILX lightwave optical multimeter OMH6810 was selected coupled to an OMH-6725B optical head. The remote optical head consisting of an integrating sphere and an InGaAs detector. Wavelength is obtained via an incorporated coloured filter glass, which has a transmission verses wavelength response. This setup provides ±1nm accuracy and 0.1nm resolution. Optical power can also be measured, with a quoted uncertainty of ±3.5%.

3.4.3 Bias T Network / Digital Volt Meter

Following the detector the dc component of the electrical signal needs to be filtered from the noise signal. The primary reason for this is to prevent the next stage, the rf amplification input, from becoming saturated which would hinder its high frequency performance and in some instances even result in permanent damage. This is often referred to as AC coupling or a DC block and is found in all semiconductor based audio and rf amplification circuits. The secondary and more useful reason for this filtering is it provides a means to monitor the dc level present, which is essential to directly derive the shot noise present Eq. (3-10).

Figure 3-8 shows the bias T filter allowing the RF component (typically frequencies > 10MHz) to pass through to the amplifier / spectrum analyser and the DC component coupled out to a digital volt meter (DVM). Since, the DC component is coupled out at this stage, the voltage

measured by the meter will represent the voltage across the input termination resistor only (since no influence of the spectrum analyser impedance is seen by the DVM). Whereas the RF voltage passing through the bias T will be influenced in the way discussed in 3.1.1.1 and 3.1.3 such that the RF voltage measured by the spectrum analyser is halved (noise power is reduced by a factor of 4). Thus, the Shot noise can be calculated easily from the DC voltage measured on the meter via the bias T connection.

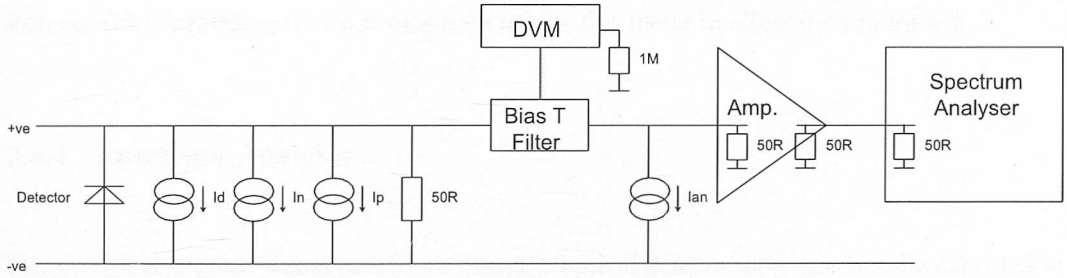

Figure 3-8: Block diagram of the Shot noise, bias T, amplifier and the spectrum analyser.

Id - Dark Current

In - Detector Current Noise

Ip - Photocurrent

Ian - Amplifier Noise Current

A wide selection of bias T's are available in the commercial market. The bias T for this project demands suitable cut off frequencies to satisfy the 10MHz to 20GHz range and critically to minimise insertion loss which would directly impact the systems sensitivity level. The component showing the best suitability was the 5541A produced by Picosecond Pulse Labs Inc., Boulder, CO. This unit has a frequency bandwidth (-3dB) of 80kHz to 26GHz and rise time of 8ps, 12ps maximum. The insertion loss is typically 0.4dB rising to 1.5dB at the high frequency end with an impedance of 50Ω. Other simple dc blocking capacitors can offer lower insertion loss across the frequency band but obviously not the capability to tap off the dc photocurrent. Within the rf laboratories on site a number of these capacitors, such as the Agilent 11742A were available and used for system verification. Connection to the rf and dc port of this unit is by standard 3.5mm SMA jack connections.

The dc port of this bias T provides a means to monitor the generated photocurrent from the detector. As stated earlier this is achieved by measuring the voltage drop across a known resistor. In this case, to minimise any external loading in parallel with the detectors 50Ω

impedance a high impedance digital voltmeter was sourced. The Keithley 2000 DMM unit has 10GΩ impedance and a voltage resolution of 100nV and a 6.5 digit display. Resultant external loading would be 0.25μΩ thus considered negligible. The high end optical detector range (<5mW) will provide a maximum voltage across the detectors 50Ω load of <150mV, after accounting for detector responsivity. At the low end of the optical range (100μW) the meter provides a resolution capability of better than 0.005%. This is considered more than adequate for determining the photocurrent.

Remote IEEE control option was also selected for this meter to allow for automation.

3.4.4 Spectrum Analyser

The electrical rf noise signal passed on from the optical detector now needs to be analysed in respect of amplitude over its frequency content. Obtaining this information is commonly gained through the use of a superheterodyne spectrum analyser. Heterodyne means to mix, i.e. to translate frequency and super refers to super-audio frequencies, or frequencies above the audio range. Referring to the block diagram in Figure 3-9 the basic elements forming a spectrum anaylser are; a) input attenuator to provide some input power control, b) low pass filter with cut off below the local oscillator c) a swept local oscillator signal with the same range as the input signal offset by the intermediate frequency (IF) filter, d) mixer which combines the input signal with a swept local oscillator signal, e) IF filter set at a frequency above the input signal range, f) envelope detector to provide a signal level suitable to drive a Cathode Ray Tube (CRT) or similar display being proportional to the signal amplitude of interest.

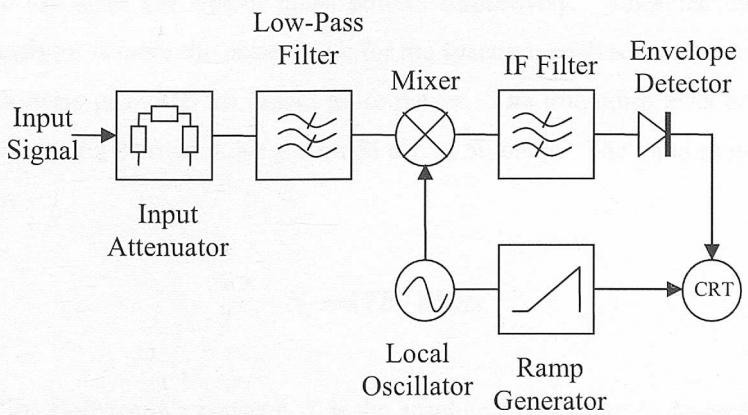

Figure 3-9: Simple Superheterodyne Spectrum Analyser.

The spectrum analyser forms an essential part of this laser noise measurement capability and as such attracts a significant proportion of the project budget. The key feature here is the analyser's sensitivity which needs to be as high as possible over the wide frequency range up to 20GHz to maximise the measurement sensitivity of laser noise. The sensitivity of the system is defined as the point at which the signal can be just observed and is taken as the point at which the RF signal is equal to the noise power. In practice this will occur when 3dB rise has been observed in the noise floor.

The ultimate limitation in these measurements is the random noise generated by the spectrum analyser. This noise, generated by the random electron motion throughout the various circuit elements, is amplified by the various gain stages in the analyser and ultimately appears on the display as a noise signal below which measurements cannot be made. In practice the noise of the spectrum analyser will be dominated by the front end of the system. An indication of the sensitivity of the spectrum analyser can be ascertained by measuring the displayed average noise floor with a 50 Ohm load placed on its output. However, this will only be an indication since the actual noise level of the spectrum analyser will depend on the type of signal being measured.

Noise figure is often quoted for the spectrum analyser instead of its sensitivity. The noise figure can be defined as the degradation of signal-to-noise ratio as a signal passes through a device i.e.,

$$F = \frac{S_i / N_i}{S_o / N_o} \tag{3-23}$$

where F is the noise figure, S_i and S_o are the input and output signal powers respectively and N_i and N_o are the input and output noise powers respectively. Since the overall gain of the spectrum analyser is unity the noise figure for the spectrum analyser can be reduced to the ratio of the input noise power to the output noise power. The true noise level at the input will be given simply by the thermal noise generated across 50 ohms. The input noise power will then be given by:

$$N_i = kTB \quad Watts \tag{3-24}$$

where k is the Boltzmann's constant, T is the absolute temperature in degrees Kelvin, and B is the effective bandwidth. At room temperature and a 1 Hz bandwidth the thermal noise will be given by -174 dBm. Thus the noise figure effectively indicates the additional noise of the

spectrum analyser above the thermal noise floor above ie a 20 dB noise figure would give rise to a measured noise floor of -154 dBm/Hz. Clearly, the displayed level of noise on the analyser will change with bandwidth i.e. a 10 Hz resolution bandwidth will increase the noise level by 10 dB. Thus if the actual effective bandwidth of the system is known it is possible to calculate the noise level in any resolution bandwidth. From the above it is clear that the noise figure is independent of the bandwidth

The selected spectrum analyser is manufactured by Rohde & Schwartz (R&S), Germany. The unit (FSEM30) boasts the lowest noise figure in its class of approximately 23dB for an operating range of 20Hz to 26.5GHz. Frequency resolution is 0.01Hz and resolution bandwidths of 1Hz to 10MHz are available. In terms of the rf power range this is commonly referenced as the 1dB compression point and in this case occurs at +10dBm. Maximum input signal level is +30dBm. A prototype unit was initially made available to allow system construction and characterisation whilst R&S finalised their analyser design and subsequently supply a fully specified unit. R&S suggested that the loan unit's noise figure was approximately 0.5dB away from that targeted and thus was noted in subsequent characterisations performed in chapter 4.

3.4.5 Spectrum Analyser + Pre Amplifier

As shown previously in Figure 3-4 the total system noise expected could be as low as -171dBm for a laser noise equal to the shot noise at low optical powers. Obviously the spectrum analyser just described is not capable of measuring signals this small. Hence the inclusion of the rf amplifier.

Placing a preamplifier before the spectrum analyser can improve the overall noise figure of the system [33]. Essentially, the input signal is amplified even further above the overall noise floor of the spectrum analyser and hence provides a reduction in the overall noise figure of the spectrum analyser. In a practical situation, however, the amplifier will provide a small component of noise which will need to be considered during the amplification. The overall noise figure of the system will be given by:

$$F_r = F_1 + \frac{F_2 - 1}{G_1} \tag{3-25}$$

where F_1 is the noise figure of the amplifier, F_2 is the noise figure of the spectrum analyser and G_1 is the gain of the preamplifier. For extremely high amplifier gains (with respect to the noise figure of the spectrum analyser) the noise figure of the overall system will tend to the noise figure of the preamplifier.

Thus, the main issues here were to select a preamplifier such that the overall noise of the system is dominated by the amplifier. If this situation could be achieved by choosing a low noise preamplifier, the noise of the system would be low as well. In order for the preamplifier to dominate the noise floor on the spectrum analyser, the noise floor would need to rise by at least 10 dB, ie the influence of the noise floor of the spectrum analyser would influence the overall noise of the system by less than 10%. A 20 dB rise in the noise floor would reduce the influence of the spectrum analyser noise to below 1% of the noise of the front end. This is expressed below:

$$(NF_{ampl} + 10\log G - 174) - (NF_{SA} - 174) > 10dB \qquad (3\text{-}26)$$

where NF_{ampl} is the noise figure of the preamplifier, G is the gain of the preamplifier and NF_{SA} is the noise figure of the spectrum analyser.

Clearly this above expression is dominated by the gain of the preamplifier and indicates that typically amplifier gains 15 dB larger than the noise figure of the spectrum analyser should be used. The Rohde and Schwarz spectrum analyser has a noise figure of ~ 23 dB and therefore gains in excess of 33 dB should be used. If the nearest equivalent HP71400 series spectrum analyser (noise figure ~ 30 dB) were to be used gains in excess of 40 dB would be necessary.

Two very high gain preamplifiers were sourced from Miteq Inc. in order to reduce the risk of project failure if the 'under development' spectrum analyser from Rohde and Schwarz fell outside specification. Two gain levels were selected being 35dB and 45dB. It is not feasible to increase the gain indefinitely since the dynamic range of the spectrum analyser is decreased. If the targeted spectrum analyser noise figure is achieved then a lower gain preamplifier maybe used to reduce any degradation in dynamic range. Both preamplifiers noise figures are quoted as <2.5dB which when coupled to the spectrum analyser will create an effective overall system noise figure of around 3dB. Thus, front end system sensitivity is anticipated to be around -171dBm, close to system requirements. The preamplifiers have a frequency bandwidth from 100MHz to 20GHz with a gain flatness of 1.8dB.

Connections to these rf components is through 3.5mm SMA connectors and the mating of each has be carefully selected to prevent the use of adapters/cables which would otherwise introduce more rf loss.

3.4.6 Broadband Noise Smoothing

From some initial experiments (chapter 4) used to assess the overall system sensitivity it was found there was a ~ 2 dB error in the results. On consultation with Rohde and Schwarz this error was related to the way that RF and broadband signals propagate through the spectrum analyser [32]. These various effects are discussed below.

By random noise, it is meant that a signal whose instantaneous amplitudes has a gaussian distribution versus time. At any instant the amplitude could be anything, however the average level will tend to zero. Thus in order to express the noise level averaged over time is to refer to the power or the RMS voltage. The RMS value of a gaussian distribution equals its standard deviation (σ). In the linear display mode the gaussian noise is band limited as it passes through the IF chain and its envelope becomes a Rayleigh distribution. The mean value of the Rayleigh distribution is 1.253σ.

However, the analyser is a peak-responding voltmeter calibrated to indicate the RMS value of a sine wave. Thus a scaling factor of 0.707 must be used in order to convert from peak to rms. The Rayleigh-distributed noise is scaled by the same amount giving a reading of 0.886σ (1.05dB below σ). This represents a constant error that can be corrected for by adding 1.05 dB to the displayed value.

Also, there is an error due to the log display mode. The gain of a log amplifier is a function of signal amplitude, so the higher noise values are not amplified as much as the lower values. As a result, the output of the envelope detector is a skewed Rayleigh distribution, and the mean value from the video filtering or averaging is another 1.45 dB lower. In the log mode, then, the mean or average noise is displayed 2.5 dB too low.

The shape of the resolution filter also plays a role. For comparison, if we define a standard noise-power bandwidth: the width of a rectangular filter that passes the same noise power as the analyser's filter, being near gaussian. The equivalent noise power bandwidth is about 1.05 to 1.13 times the 3dB bandwidth, depending on bandwidth selectivity. For example a 10kHz resolution bandwidth filter has a noise power bandwidth in the range of 10.5 to 11.3kHz. To

account for this, the bandwidth adjustment involves subtracting typically between 0.21 and 0.53 dB from the indicated noise level. Thus, the total correction given above will typically be 2.0 dB instead of 2.5 dB.

Rayleigh distribution (linear mode):	1.05 dB
Log amplifier (log mode):	1.45 dB
3dB/noise power bandwidths:	-0.5 dB
total smoothing :	**2.0 dB**

Thus, as the broadband noise and the RF signal passes through the spectrum analyser, the broadband noise is reduced by 2 dB whereas the RF signal observes no correction. Thus, the effective sensitivity of the system is increased by 2 dB. The quoted noise figures from the SA & preamplifier manufacturers, includes this smoothing factor and provides a means for better sensitivities. Interestingly, the thermal noise floor including this correction factor will be -176 dBm/Hz.

3.4.7 Sensitivity Correction for Responsivity/Gain

The responsivity/gain of a rf component varies with frequency due to many internal electrical mechanisms, e.g. mismatch etc. However, in order to assess the sensitivity of the system, when considering only its noise floor, these responsivity/gain changes can introduce errors i.e. if the responsivity of the spectrum analyser falls off then the noise figure of the spectrum analyser will follow. Thus, there may be an overall error associated with the effects of the responsivity/gain of such a system. Consider the following system:

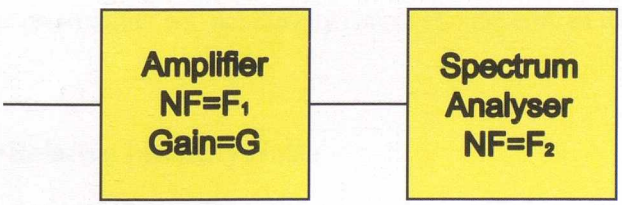

Figure 3-10: Block diagram of the preamplifier coupled into the spectrum analyser.

Now, on passing a known RF level through the system, the gain of the overall system can be assessed from the spectral readout. Usually a variation of the gain is observed. However, these gain variations cannot be directly subtracted or added to the noise floor of the system. From Section 3.4.5, the overall noise figure of such a system is given by;

$$F_r = F_1 + \frac{(F_2 - 1)}{G} \tag{3-27}$$

where F_T is the resultant noise figure, F_1 is the noise figure of the preamplifier, F_2 is the noise figure of the spectrum analyser and G is the gain of the preamplifier. Differentiating the above expression with respect to the gain variations ΔG one obtains:

$$\Delta F = -\frac{(F_2 - 1)}{G(G + \Delta G)} \Delta G \tag{3-28}$$

where ΔF is the change in the noise figure as a result of the gain variations. Thus, the correction factor will be given by:

$$Correction = 10 \log \left[\frac{F_r}{F_r + \Delta F} \right] \tag{3-29}$$

On substituting for F_T and ΔF the final expression is obtained:

$$Correction = -10 \log \left[1 - \frac{(F_2 - 1)\Delta G}{\left[G(G + \Delta G)F_1 + (F_2 - 1)(G + \Delta G) \right]} \right] \tag{3-30}$$

Now from the above expression if the Gain is set to 1 and the variation in the gain is 1 (3 dB variations) the correction factor in the noise floor would be 3 dB. These values have been set so as to mimic the spectrum analyser without a preamplifier and for low gain systems (such as this) the gain variations are directly coupled into the noise floor error.

When a preamplifier with high gains is used the overall correction factor tends to zero for reasonable gain variations (5 dB variations in a gain of 45 dB). Thus, in this high gain system, gain variations of the preamplifier will not directly couple into the error of the noise floor.

3.5 Extracting Relative Intensity Noise

From this outlined system we now look at the measurement in more detail. In order to derive a lasers RIN level a number of noise contributions need to be determined, being thermal noise, shot noise and total noise. Further to this, a means to determine the systems responsivity is essential.

Previous research investigated improvements to this configuration such as synchronous detection employing an optical chopper and lock in amplifier. This arrangement effectively eliminates the receiver noise leaving the laser and shot noise components, thus improving receiver sensitivity. The spectrum analyser would be set up at zero span (or to a desired bandwidth) and the subsequent proportional voltage output from the amplifier will represent the input noise level. Calibration of this response would be performed first, typically using a wide band noise source, such as an LED. A number of measurements at different input power levels would then be plotted and a straight line fitted to the data points, the slope of which represents the system responsivity.

This is a time consuming process especially if measurements were required over a large bandwidth (as in this project ≈20GHz) and may introduce higher uncertainties from system noise level non linearity and optical chopper duty cycle variations. System set up is more complex, with chopper monitor circuitry, lock-in amplifier etc., and its performance is still dependent on having a low noise figure amplifier.

An alternative method to improve sensitivity may be to cool the receiver head by say 300°K, from laboratory temperature to approximately 30°K. From Eq. (3-8) this would result in reducing the thermal noise level by ≈10dB thus increasing system sensitivity. This approach may prove to be impractical or at best costly in operation.

Due to these limitations this project will centre on maintaining the flexibility of the amplifier/spectrum analyser combination. This will rely on sourcing improved specification components, as outlined in the previous section coupled with developing an alternative calibration approach.

Key areas of measurement methodology concern a) how to separate the additional noise terms from the laser noise and b) how can calibration be performed to meet the strict traceability required of a national standard.

3.5.1 Linear Fitting

Laser noise contributions essentially consist of spontanteous noise, dependent on the quality of the laser and shot noise, dependent on the quantum limit. From standard theory, outlined in the background studies, section 3.1.1.1, it is clear that shot noise depends on the current generated whereas the spontaneous noise (similar to a signal) depends on the square of the current.

Consider the situation where light of optical power P_{opt} is incident on a photodetector of responsivity β the various noise terms will be given as:

(a) The Shot noise current will be given by $\sqrt{2q\beta P_{opt}}$,

(b) laser noise current will be given by $\beta.N_L$ and

(c) the thermal noise current will be given by Δi_{th}.

The total noise power will then be given by:

$$N_T = [2q\beta P_{opt} + \beta^2 N_L^2 + \Delta i_{th}^{\ 2}]R \quad Watts \tag{3-31}$$

Now consider the case where we use optical amplification (optical gain of A). The total noise power will now be given by:

$$N_T = [2q\beta\, A\, P_{opt} + \beta^2 A^2 N_L^2 + \Delta i_{th}^2]R + \{A^2 \Delta i_q^2\}R \quad Watts \tag{3-32}$$

the last term is included because the original Shot noise will be amplified as well.
One finds from above that:

$$(A^2 \Delta i_q^2)R > 2q\beta A P_{opt} R \tag{3-33}$$

Thus curve fitting cannot be used in this example since the Shot noise sees the same amplification as the laser noise and dominates.

Now on optical attenuation (/D) we find the following situation:

$$N_T = [\frac{2q\beta P_{opt}}{D} + \frac{\beta^2 N_L^2}{D^2} + \Delta i_{th}^2]R + (\frac{\Delta i_q^2}{D^2})R \quad Watts \tag{3-34}$$

This time on optical attenuation we find that:

$$\frac{2q\beta P_{opt} R}{D} > (\frac{\Delta i_q^2}{D^2})R \tag{3-35}$$

The newly derived shot noise dominates over the laser spontaneous noise by the square of the attenuation. Thus, if say a factor of 10 optical attenuation is applied externally to the optical laser cavity then the optical light and shot noise power will reduce by a factor of 10 but the spontaneous noise power will reduce by a factor of 100. Figure 3-11 illustrates the

effect. This attenuation concept should allow shot and spontaneous noise levels be measured at a range of attenuation levels and curve fitting techniques used to determine the noise contributions at a specified optical power.

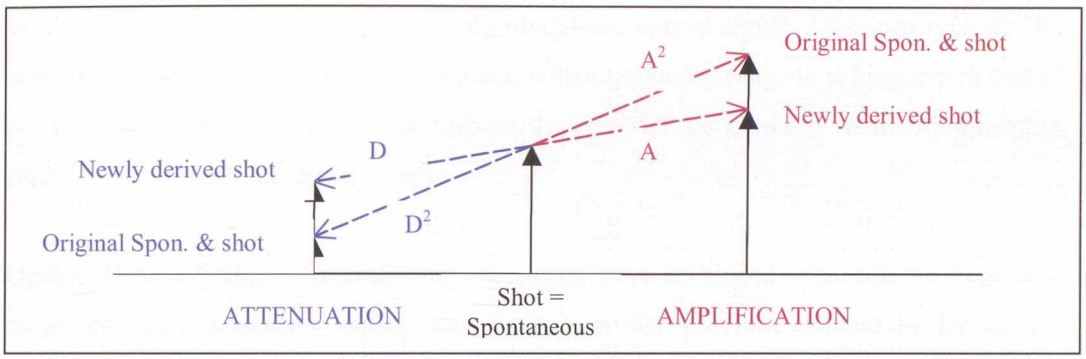

Figure 3-11: Attenuation and amplification on shot and spontaneous noise contributions.

3.5.2 System Responsivity Calibration

Various frequency responsivity calibration techniques have been applied to RIN measurement systems in the past. Each offer benefits and shortfalls over each other. A summary of each follows:

Component Level – Separate characterisation of each component within the system can be performed with relative ease but the interpretation of the combined systematic effect will be tedious and time consuming. The approach would necessitate the need for additional parameters such as input/output impedances, and reflection co-efficients be characterised to determine mismatch losses between components. The resulting large number of measurements performed would degrade overall system calibration accuracy. Subsequently, due to the calibration complexity, characterisations will be less frequent and hence degradation of accuracy will be further compounded by environmental variations such as temperature and by component variations.

Pulse Response – The frequency response of a receiver system is related to its pulse response. By sending a train of ultra-short laser pulses to the system the resultant pulse output signal can be monitored by a fast digital oscilloscope and Fourier analysis used to determine the frequency response. A laser diode or a mode locked laser can be used as the pulse source, which in the first case provides pulse duration in the region of 100ps and the later down to a few picoseconds. The pulse sources themselves would need to be fully characterised and can become costly when wide frequency bandwidths are required, such as

in this project. Additional calibration would be required in respect of the frequency response of the spectrum analyser itself.

External Modulation – A direct measurement of the frequency response of a receiver can be obtained by applying a high-frequency modulated optical signal. This can typically be achieved using a LiNbO3 external modulator with a frequency range to at least match that of the receiver. Commercial systems such as the HP8703 are currently available operating from 130MHz to 20GHz but are costly.

Optical Heterodyning - Heterodyning techniques were developed to extend the frequency range of characterisations which was limited in the previous techniques by device technology. Typically frequencies out to 50GHz have been achieved through heterodyning using Nd-Yag lasers at wavelengths around 1300nm. Basically the beams from two identical lasers are optically mixed, using a fibre optic coupler, to produce a beat signal at the frequencies required for a wide band measurement. The frequency of one laser is swept by varying the temperature of the device with a Peltier cooler. This technique produces a fairly stable oscillating signal spanning a range of several tens of GHz. The concern here is that the peak optical powers measured will be considerably higher than the DUT levels expected in this project thus non linearities may creep in. Also the beat frequency would need to be scanned through the frequency range, increasing the calibration time, and the set up is not known for its ruggedness.

All the techniques mentioned so far involve specific trade-offs among frequency coverage, complexity and sensitivity, none being completely satisfactory. This lead to further investigations[30] to develop a broadband frequency response capability which would be simple and robust.

Intensity Noise Sources - Broadband noise sources such as light emitting diodes (LEDs) and halogen lamps have been demonstrated[26,34] in relative intensity noise measurement systems discussed in section 3.1.1.2. This technique is of particular interest because the noise exists at all frequencies simultaneously, permitting rapid optical receiver characterisations. Intensity noise sources such as these take advantage of the beating between various optical spectral components of a broad bandwidth spontaneous emission source. Any two spectral lines will beat, or mix, to create an intensity fluctuation with a frequency equal to the frequency difference between the two lines. Optical bandwidths of spontaneous emission sources can easily exceed thousands of gigahertz, hence the intensity beat noise will have a similar frequency content.

More recently, erbium doped fibre amplifiers (EDFA's) have been used as spontaneous emission sources[30]. These have an advantage in providing higher power densities than LEDs which benefits characterisation of receivers with low quantum efficiency or measurement systems with poor sensitivities. Power densities of greater than 1mW/nm can be achieved.

In considering the use of a broadband source such as an EDFA for this project the following observations were made.

- The Intensity noise or RIN from an EDFA is only considered to be constant when the optical bandwidth is significantly larger than the electrical detection bandwidth. Thus care needs to be taken in selecting a suitable optical filter, which also determines the level of RIN obtained.
- Typically RIN levels of –120 to –110dB/Hz will be generated by an EDFA which is significantly greater than that of DFB type laser which are predicted to be measured using this system, thus non-linearities will need to be assessed and accounted for.
- Use of this calibration source is limited to determining the frequency response, thus it is an expensive option.

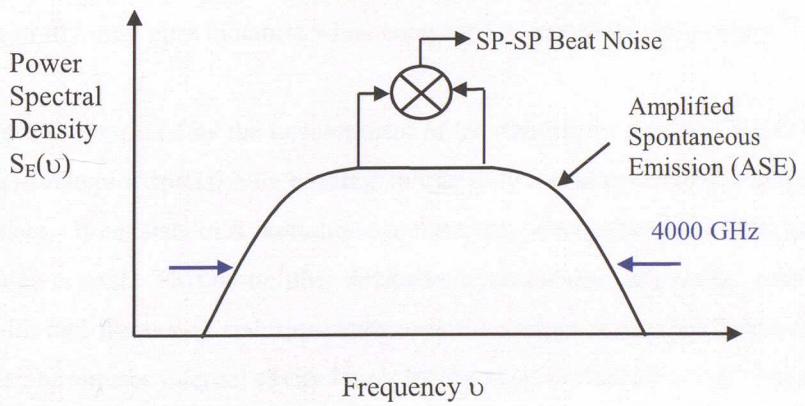

Figure 3-12: Spontaneous-spontaneous beat noise arising from spectral mixing[30].

Consideration has been given in this project to determine if a more ideal, calculable reference source can be found to improve measurement capabilities as well as absolute accuracy. Across the wider field of metrology ratio-metric techniques are commonplace, such as in rf measurements, offering a simplistic and often traceable reference source. Observation suggests a suitable source would consist of minimal spontaneous noise content

(*shot noise limited*) potentially offering the following advantages over all the other methods mentioned without detriment to system performance.

a) A wideband noise source offers a better match signal to the device under test (such as an EDFA) but at a level more appropriate to low noise devices which are likely to be encountered in the future
b) The means to determine and subtract accurately thermal and shot noise terms
c) A Simplified measurement process
d) Provides an accurate means to determine the system frequency response, which is calculable and therefore traceable to International Standard (SI) units. This absolute measurement would eliminate the need to take numerous data points and perform line fitting for every frequency point referenced. Also, if the reference source can be adjusted in amplitude then noise level nonlinearities will be minimised.
e) System calibration will be performed at every measurement, reducing drift uncertainties

A potential source which may fit the requirements is currently used in various applications such as optical radar where high reliability, robustness and efficiency are important. The device is a diode pumped solid state laser manufactured by Lightwave Electronics Inc. These high finesse Nd-Yag lasers inherently emit significantly small amounts of am/fm noise, being spectrally very pure in nature when compared to a semiconductor laser [48].

This has been further improved by the development of the non-planer ring oscillator (NPRO) to eliminate the problem of spatial hole burning so that only a single, dominant longitudinal mode will oscillate. It consists of a monolithic architecture where the entire laser cavity is within the Nd-Yag crystal. This monolithic device is mechanically very stable, resulting in superior linewidth and frequency stability characteristics compared to other laser resonator structures. It also minimises internal cavity losses by avoiding additional cavity elements, so that it has high efficiency. The NRPO design is illustrated in Figure 3-13. The diode pump light is focused into the Nd-Yag crystal at point A. This face of the crystal is coated to be highly transmissive at the pump wavelength, and partially transmissive at the lasing wavelength to act as an output coupler. Total internal reflection is used at points B, C & D to obtain a ring laser mode that closes back upon itself at point A, where the output beam is emitted.

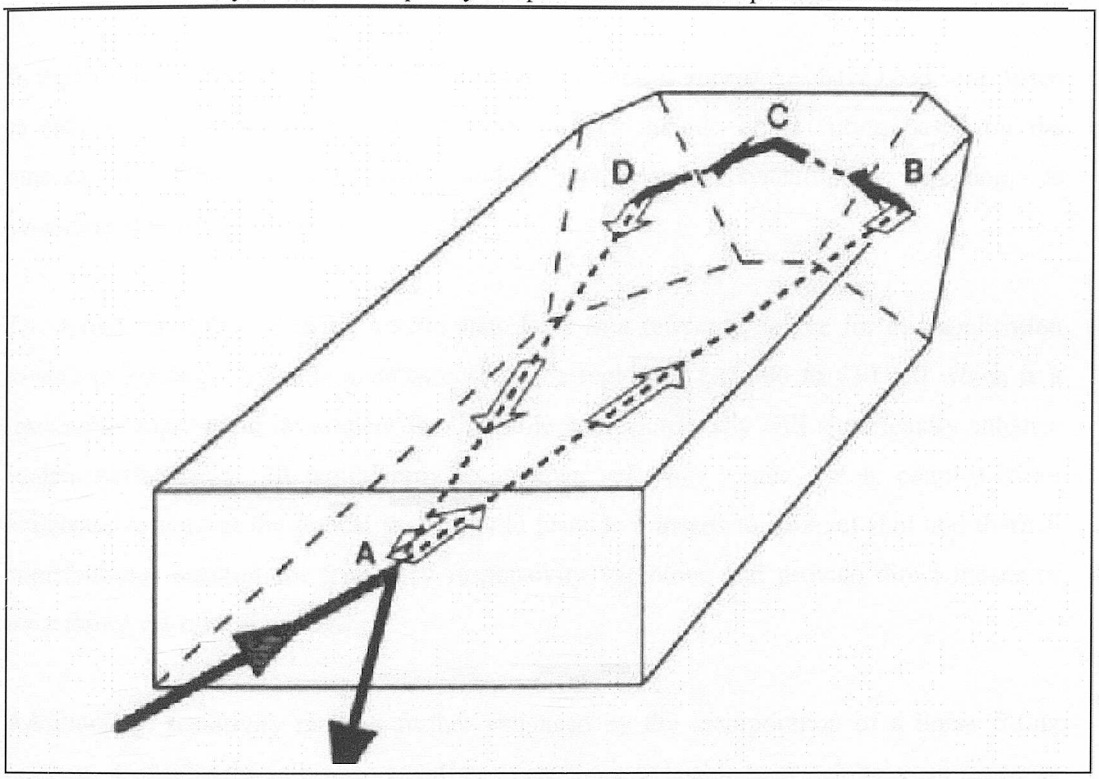

Figure 3-13: The non-planar ring oscillator design [48].

Linewidth of less than 1kHz are typically achievable along with frequency jitter of less than 10MHz per hour due to the diode laser power supply designed to minimise current fluctuations. This results in producing ultra low intensity noise, which above 20MHz has been reported to be below the shot noise limit of most photodiodes. Nd-Yag versions are available with emission at 1319nm which would be suitably within one of the telecom windows required for this project.

Confidence in this reference source will need to be paramount for this measurement capability. System calibration will be derived using this source and may also provide a means of noise term subtraction, thus thorough assessment needs to be performed to insure confidence. With the knowledge of the attenuation relationship between shot and spontaneous contributions, procurement of a substantially high power reference laser will allow the use of an optical attenuator to control the optical power. This would in turn provide further assurance that the reference source is shot noise limited. For instance, by optically attenuating a 100mW laser to 1mW, shot noise will decrease by factor of 100 but spontaneous noise will decrease by a factor of 100^2, thus providing an extra safety margin of 20dB. This indicates that spontaneous noise contributions equal to the shot noise could be determined to an accuracy of 1%.

In the interest of the project customer, alternative technical approaches have been short listed to reduce risk of project delivery failure. These include linear fitting based on the attenuation effect outlined earlier and/or incorporating synchronous detection, as investigated in previous papers.

The initial feasibility of using a solid state laser as a reference source for this application looked promising. Suitable sources cost in the region of £25,000 to £30,000 which is a reasonably high value investment for the project but potentially will significantly enhance system performance. It would provide an *ideal* reference source which, coupled to an attenuator to control the optical power could provide a means to subtract shot and thermal contributions, account for frequency responsivity variations and provide direct means of traceability via optical power.

Additionally, sensitivity may be further enhanced by the incorporation of a linear fitting concept. Consider the following situation where the user is able to switch between the noise created by the DUT and the reference laser. These two measurements would therefore be governed by the following equations:

$$N_{ref} = N_q + N_{th} + \Delta N_{\text{det}} \quad Watts \tag{3-36}$$

and

$$N_{dut} = N_q + N_{sp} + N_{th} + \Delta N_{\text{det}} \quad Watts \tag{3-37}$$

where N_{ref} is the total noise power of the reference laser, N_q is the shot noise, N_{th} is the thermal noise, N_{dut} is the noise power of the device under test, N_{sp} is the spontaneous noise contribution and ΔN_{det} is the error due to the detection system. The shot noise of the two lasers will be matched. Thus, at this particular DC optical power we can subtract the two measurements and obtain:

$$N_{ref} - N_{dut} = N_{sp} \quad Watts \tag{3-38}$$

In this technique, noise contributions due to shot, thermal and fluctuations in the responsivity of the detections are all removed. Also, with an increase in the attenuation factor the P_{spont} would vary in a linear fashion. Least squares techniques can be used to enhance the accuracy of the measurements. This technique relies on the accuracy with which user is able to match the two DC optical powers on the detector. However, an error of less than 1% in the optical power matching should be achievable. Performing this type of measurement will be time consuming and hence may fall outside a marketable calibration facility.

3.6 Chirp System

As discussed earlier 3.1.2, the self homodyning concept offers the best combination of performance verses cost when combined with the low noise optical receiver, proposed for RIN measurement. A suitable FP interferometer would require an exceptional finesse level, which if not impractical would exceed this project budget. Heterodyning offers a more complete picture of linewidth broadening offering both +ve and –ve excursions to be observed. This does necessitate either obtaining a stable laser reference close to the laser frequency under test, or incorporating an additional path, frequency shifted by a Mach-Zender interferometer forming a local oscillator. Both options are expensive and also introduce additional uncertainty terms likely to limit accuracy.

A useful feature of self-homodyning is the local oscillator is self tracking. Any changes in the device under test would be compensated proportionally by the local oscillator. Costs for such a system will be minimal, basically consisting of two fibre optic paths with a delta delay between them of greater than the coherence time of the laser under test. This delay also sets the system resolution capability which, as defined in the technical objectives needs to be better than 100kHz.

A typical configuration would be similar to the HP 11980 fibre optic interferometer as shown in Figure 3-14.

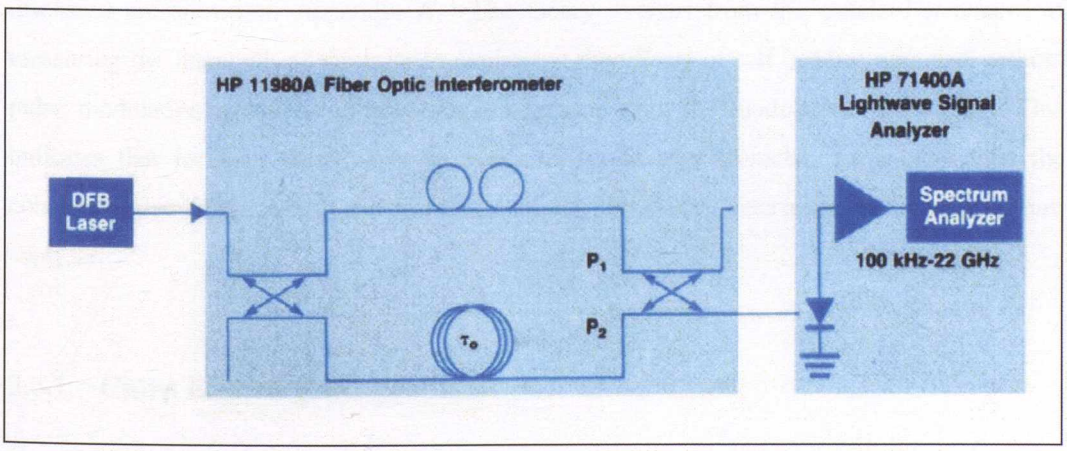

Figure 3-14: Delayed Self-homodyne system, HP11980A and HP71400A[19].

Self-homodyning does have limitations though. The minimum chirp excursion which can be measured will be governed by the lower bandwidth of the receiver system and/or flicker

noise. Flicker noise is an excess noise additional to shot and thermal noise, typically occurring at frequencies below 10^5Hz. As the frequency decreases, the power spectrum increases in many cases being inversely proportional to the frequency. The exact frequency at which the flicker noise equals the white noise varies from device to device as does the magnitude of the excess noise (factor of 3 or more). In semiconductors flicker noise is associated mainly with the effects of generation and recombination process which either produce or eliminate minority carriers. Under optimum conditions, some semiconductors can be as low as 1Hz.

Contributors of flicker noise applicable to the system will likely be from all components such as the detector, rf amplifier, spectrum analyser and any associated power supplies. An appreciation of the flicker noise can be observed by blocking any signal to the detector and observing the response on the SA, then comparing the resultant noise at low frequencies against higher frequencies which will be dominated by white noise.

Typically, DFB telecom lasers to be measured will have inherent linewidths in MHz. This is beyond flicker noise and thus should not cause specification issues. Lower bandwidth limitations will more likely be governed by components within the measurement system. Thus the receiver system will need to have a suitable specification to measure chirp as well as RIN. Essentially this will consist of the photo detector and rf spectrum analyser.

The theoretical power spectrum expectations for the delayed homodyne interferometers discussed are shown in Appendix A. The theory evolves from the standard treatment of measuring the linewidth of the laser to explaining the effects of self beating with and without pulse modulation and the corresponding relationship with the modulation index (M). This indicates that for long delay times in one arm of the interferometer, i.e. greater than the coherence time of the laser under test then its linewidth can be determined from the spectrum analyser.

3.6.1 Chirp Birefringence problems

A problem may exist in the long path interferometer system if polarisation induced intensity changes exist during the measuring time. It is clear that the effects of birefringence in determining the state of polarisation depends on the optical wavelength. Thus, as the optical wavelength changes (due to the chirp) the state of polarisation of the light may change. Since there is also an optical delay between the two polarisations. This effect could be used to provide

the temporal delay for the temporal interferometer. Long optical fibre delays and temporal chirp estimates could then be easily measured when the optical output is passed through a polarising element. If temporal chirps were to be required in the future this would be a novel approach which may be worth considering. However, in the present set up these polarisation effects could upset the intensity changes which are to be measured.

When laser light is passed down the fibre the two orthogonal polarisations will travel at different group velocities. The phase difference between the two will be given by:

$$\phi(x) = \frac{2\pi l}{(n_x - n_y)} \tag{3-39}$$

With a change in lasing wavelength the change in this phase will be given by:

$$\frac{\Delta\varphi}{\varphi} = -\frac{\Delta\lambda}{\lambda} \tag{3-40}$$

Relating this to Malus's law will give rise to an intensity change given by:

$$\frac{\Delta T}{T} \approx 2\varphi\Delta\varphi \tag{3-41}$$

Now if we restrict ourselves to polarisation maintaining fibre we have it that the phase difference between the two perpendicular axis will be given by:

$$\varphi \approx (\beta_x - \beta_y)L \quad rad \tag{3-42}$$

where β_x and β_y are the propagation constants along the x and y axis respectively and L is the length of the fibre. Now if the polarisation of the return beams are aligned to within one degree of each other the change in intensity expected over 4 km would be around 32% for single mode fibre when a chirp of 10 GHz is encountered. This represents a substantial change in intensity which has not been created by the interferometric action.

A method that is proposed for the chirp set up is based on a new technique used in sensor applications. In these systems random fluctuations in the state of polarisation (SOP) of the interfering beams give rise to variations in the interferometric output. Work by Martinelli[49] demonstrated a technique for the compensation of birefringence effects in a length of fibre which is retraced by an optical beam. The basic operation of the technique is the use of a "Faraday rotator mirror" to reflect the optical signal back along the fibre path. Using such an element with a single pass rotation of 45 degrees, the polarisation evolution in the fibre in one

direction is essentially "unwound" in the reverse direction, producing a returned state of polarisation which is stable in time irrespective of the birefringence properties of the fibre link.

In sensor applications the effect which has been neutralised originated from external sources such as mechanical disturbances of the fibre. In this case the technique will be used to remove the chirp birefringence properties and, is believed to be the first interferometer system to achieve this. This technique will work effectively, providing that the mechanical birefringence properties change at a rate much lower than the round trip transit time of the light in the fibre.

3.6.2 Proposed System

As explained in the previous section 3.6.1, the Faraday mirror approach has been used for the first time in order to eliminate the effects of the change in the birefringence with the frequency excursion of the laser source.

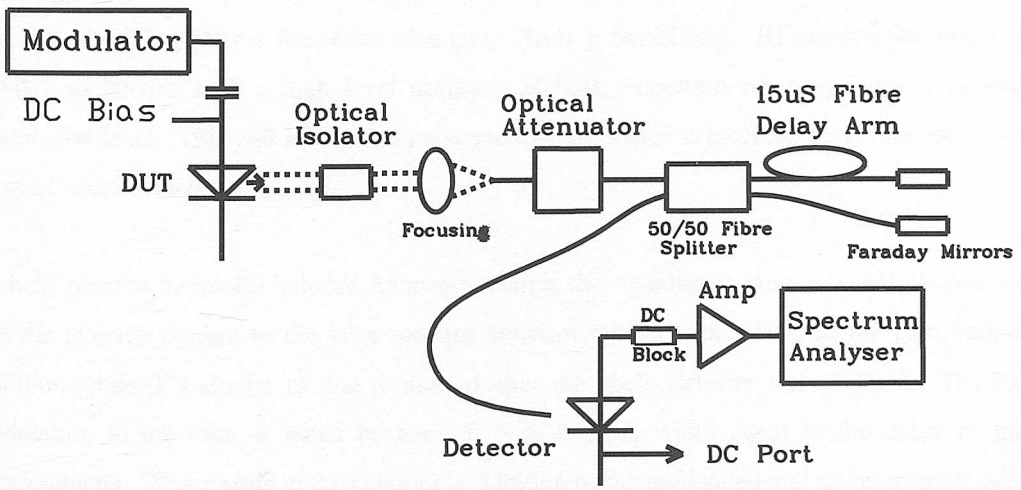

Figure 3-15: Faraday mirror long path interferometer set-up (with 15μS fibre delay).

The function of any interferometer system is to convert optical phase or frequency deviation into intensity variations which can then be detected using a square law photodetector (i.e. the high speed device used in the RIN set up). The interferometer consists of an input directional coupler which splits the incoming optical signal into two equal parts. The two signals then travel along separate fiber paths where they experience a differential delay, τ_o.

Each signal is then reflected off two Faraday mirrors, sourced from Isowave Inc. providing a 90° ±2° rotation, back reflection of >55dB and insertion loss of typically 0.5dB. The signals are then recombined using the original directional coupler. During the reflection the polarisation of the light is rotated through 90 degrees from its incident polarisation. This technique has the additional advantage that no polarisation controller is required. The total delay in the fibre is 3km which provides an overall spectral resolution of less than 100 KHz when used with a sufficiently narrow linewidth laser source. In most cases it does not make sense to measure chirps less than the linewidth of the laser source. The output is then coupled into the photo detector where the spectrum can be displayed on a spectrum analyser.

One or more optical isolators will be included to prevent laser diode instabilities induced by optical feedback from light scattering in the fibre and reflections from connectors and coupling optics.

An IEEE controlled current source and a Rohde and Schwarz modulation source (SMP22) has been selected to drive the laser. The SMP22 uses modern frequency synthesis concept with direct digital synthesis (DDS) ensuring a) stable output frequency, b) 0.1Hz frequency resolution and c) fast settling after a frequency change (<11mS + 5mS/GHz). RF modulation range is 10MHz to 20GHz with a high level accuracy ±0.9dB, important when applying a desired modulation level. This unit also offers pulse modulation which is essential to operate the gated delayed interferometer.

To help prevent thermally-induced frequency chirps, the modulation source is AC coupled so that the average current to the laser remains constant during both halves of the gate period. Additional bias T's similar to that connected after the photo detector was selected. The RF modulation to the laser is gated on and off with a pulse width equal to the delay of the interferometer. This results in the continuous addition of the modulated and un-modulated laser states. This arrangement effectively acts as an optical homodyne system, where a modulated laser is mixed with a CW local oscillator but without the constraint of requiring two separate lasers. The rotating mirrors concept provides an improved efficiency for the interferometer as the recombined signals will be well balanced.

Also, for comparison a standard interferometer (similar to Hewlett Packard) has been set up as shown Figure 3-16.

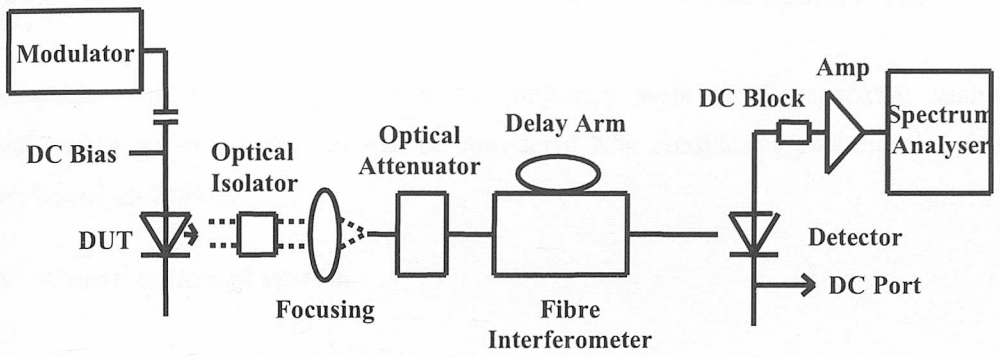

Figure 3-16: Standard interferometer system.

3.7 Extracting Chirp

Obtaining the level of frequency chirp will fall into one of three categories depending on the level of frequency modulation:

Low fm: Bessel's will be convolved together thus measure frequency excursion in similar manner to linewidth, i.e. 3dB bandwidth point (Direct Measurement)

Medium fm: Bessels unconvolved, measure relative height and fit to Bessel expression to derive chirp.

High fm: May only have one Bessel resolvable on spectrum analyser, track Bessel magnitude relative to amplitude modulation level to obtain a null. Chirp can then be derived from derived Bessel expression.

For completeness when stating chirp measurements, the intensity modulation m or modulation level should be stated. This can be obtained by measuring the optical signal directly without the interferometer.

The accuracy of this measurement will be dominated by the relative amplitude of the spectrum analyser to measure the E-field spectrum Bessel amplitudes and the intensity modulation index. Initial estimates suggest that measurement of the modulation index may be as much as ±10%, but this may be improved if calibration utilises the shot noise limited reference source, described previously. Other contributions will consist of establishing the

influence of the interferometer. Comparison chirp measurements will be taken between the proposed set up and the standard interferometer to identify any birefringence effects.

Traceability will be directly through the frequency scale of the spectrum analyser. Combined uncertainty reduction will be considered later considering potential line fitting from Bessel modelling.

3.8 Construction of system

The Electro & Visual Optics Laboratories of Qinetiq, formally Defence Evaluation Research Agency (DERA) operates a number of measurement laboratories suitable for standards/calibration and evaluation measurements of optical systems. This includes such items as; theodolites, photometers, image intensifiers, thermal imagers and laser systems. The laboratories, located in Bromley, South East London also host a wider spectrum of standards laboratories from dc through to rf. The facilities maintain a close link to National Physical Laboratory in maintaining and moving standards forward and are represented on many international boards. Historically the facilities solely served the defence industry but of the last +10 years have been allowed to expand into the commercial world. The RIN/chirp measurement system described here definitely fits into this latter category and thus, these laboratories form an ideal base for the proposed measurement system.

The measurement system is located on a large steel optical table within a controlled laboratory environment (21±0.25°C, stability <0.1°C/hr). Suitable laser safety features are incorporated including interlocks, where necessary and access to laser safety training. With the potential high risk of electro-static damage to laser systems under test and to the measurement system itself, a number of electro-static discharge points have been incorporated, inline with guidelines[50].

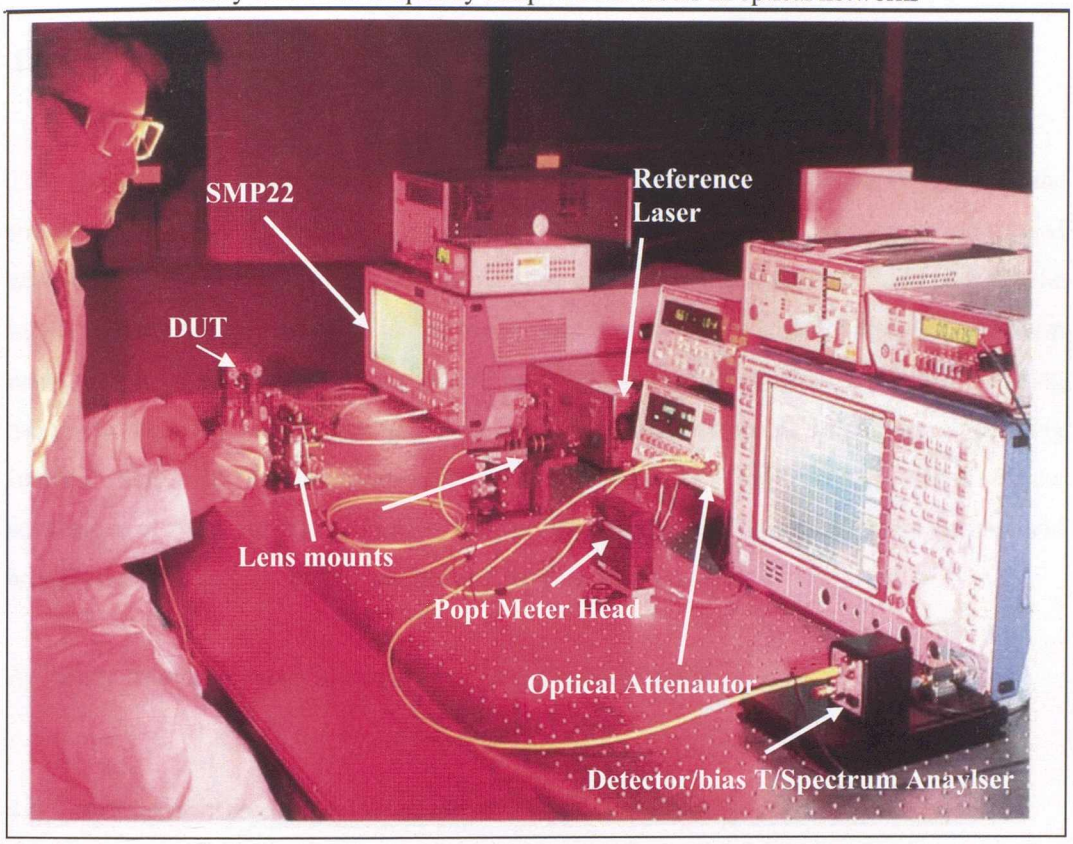

Figure 3-17: RIN/chirp measurement laboratory set-up.

Figure **3-17** shows the physical layout of the system components. The optical lenses are mounted onto '3 axis' micrometer stages which are, themselves bolted to the optical bench. This allows for stable and fine control when coupling free space lasers into fibre. Care has been taken in mounting the reference laser to ensure high thermal stability. This has also been seen as a priority for the high speed detector and subsequent rf amplifier which have been mounted together on a thermal heat sink along with the bias T circuit. Stability assessments are discussed in later sections. It can be seen that the physical rf path has been minimised by the correct selection of mating connectors and styles. This will improve the overall system loss and thus contribute to greater sensitivity level. The following chapter now looks at the experimental measurements gained for each stage of the construction.

4 Experimental Results

This chapter demonstrates the various experimental approaches undertaken to highlight the overall sensitivity of the RIN/chirp measurement system. Initially, the RIN set up was assessed without subtraction and later with the various subtraction techniques applied. Following this the insertion of the self-homodyne fibre into the system was assessed in terms of linewidth and chirp measurement capability. Comparisons are made to evaluate the addition of faraday rotating mirrors to eliminate fibre birefringence and also gating and non gating technique. Supporting sections define the measurement procedures selected and where necessary detail of the advantages of these methods. Finally, the overall measurement uncertainties are defined and brought together to form uncertainty budgets for each measurement.

All results were undertaken in temperature controlled conditions.

4.1 Performance of Preamplifier and Spectrum Analyser

The overall sensitivity of the system is an extremely important parameter for measuring the latest low noise laser diodes intended for use in the telecommunication industry. To this end extremely low noise components have been assembled in order to maximise the sensitivities obtained. This section discusses and presents the results on the individual components used in the RIN system.

4.1.1 Specification of Low Noise Preamplifier

The specification of the preamplifier was selected so that its gain was high enough to enable the noise of the system to be dominated at the front end (gain ~45 dB) and its noise figure was made as low as possible. The Miteq preamplifiers procured early on in this project represented the best preamplifiers of their type. To assess their individual performance the preamplifiers were tested in the rf calibration laboratory, located within the same building. The following figures show gain and noise figure of preamplifier JS42-00102000-25-8P-42 serial No 39482.

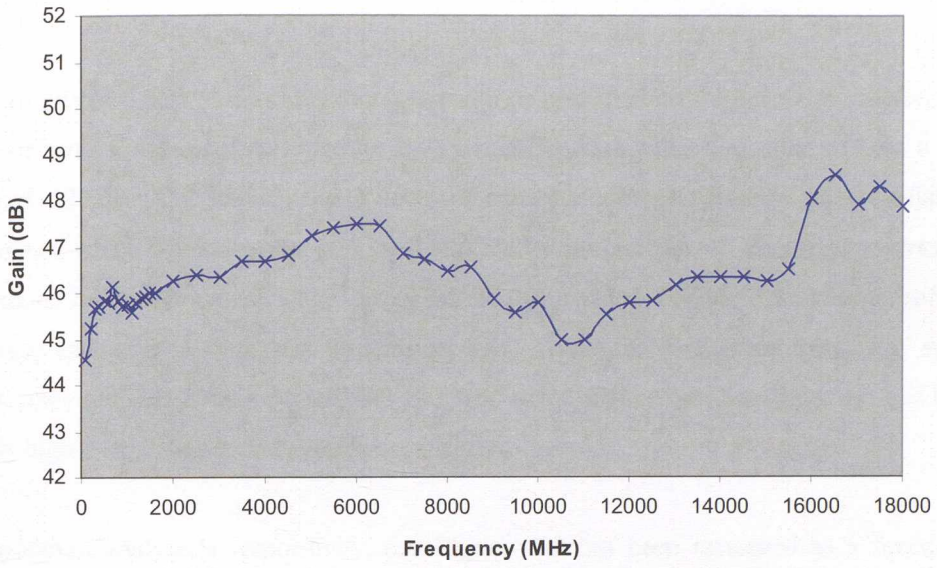

Figure 4-1: Gain of the preamplifier *(JS42-00102000-25-8P-42 Serial No 39482).*

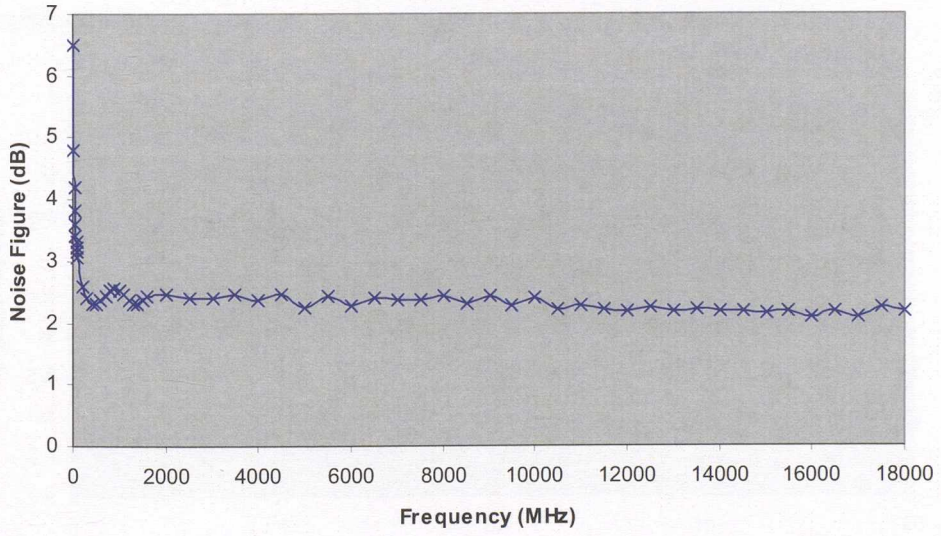

Figure 4-2: Noise figure of preamplifier (JS42-00102000-25-8P-42 Serial No 39482).

From Figure 4-1 the measured gain level is nominally around 46dB with the gain flatness over frequency being approximately 2.5dB rather than the manufacturers quoted < 1.8dB. The noise figure, Figure 4-2 comes in at < 2.5dB from 100MHz to 20GHz which is a significant feature for the overall system sensitivity and confirms the manufacturers claims.

4.1.2 Specification of the Low Noise Spectrum Analyser

The next essential part of the calibration system to be assessed was the spectrum analyser. This unit represents a new product range for Rohde and Schwarz which is quoted to have a noise figure of ~ 23 dB. Due to the stage of development a prototype was initially made available to this project, which was suggested may be 0.5dB higher in noise figure. This analyser was used throughout the development stage discussed in this chapter due to delays from software problems encountered with the preselected SA. With this being the case, the system performance outlined is thus degraded slightly (up to 0.5 dB increase in sensitivity) due to the slightly higher noise figure of the spectrum analyser.

The spectrum analyser's responsivity, see **Figure 4-3** has been measured as a function of frequency by using a calibrated signal generator (SMP22) and observing the signal level on the spectrum analyser as a function of frequency. The spectrum analyser consistently measured lower than the -10dBm applied RF level and a maximum error of 3.5dB was observed at the higher frequencies.

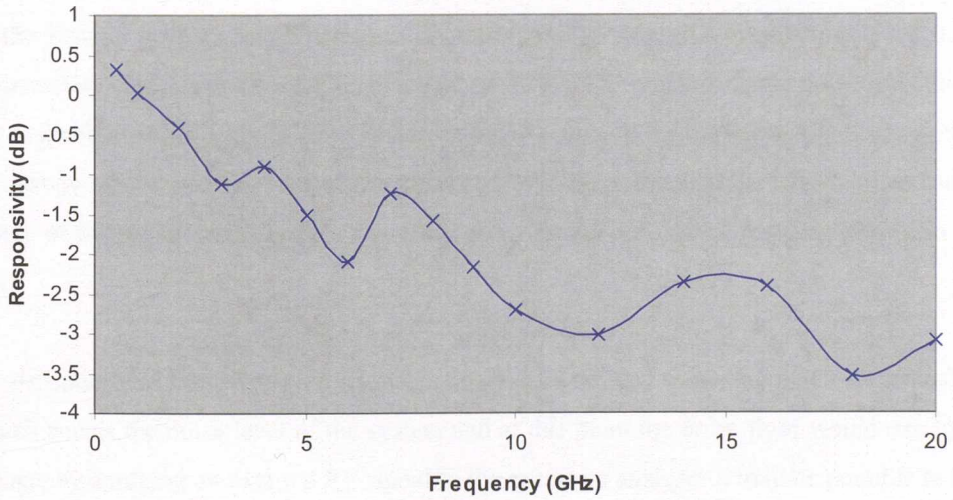

Figure 4-3: Measured responsivity of the spectrum analyser.

The displayed average noise level of the spectrum analyser has also been measured and this can be used to assess the noise figure of the spectrum analyser using:

$$NF_{SA} = ANF - 10\log(RB) + 174 \quad dB \tag{4-1}$$

where NF_{SA} is the noise figure of the spectrum analyser, ANF is the average displayed noise floor and RB is the resolution bandwidth of the spectrum analyser.

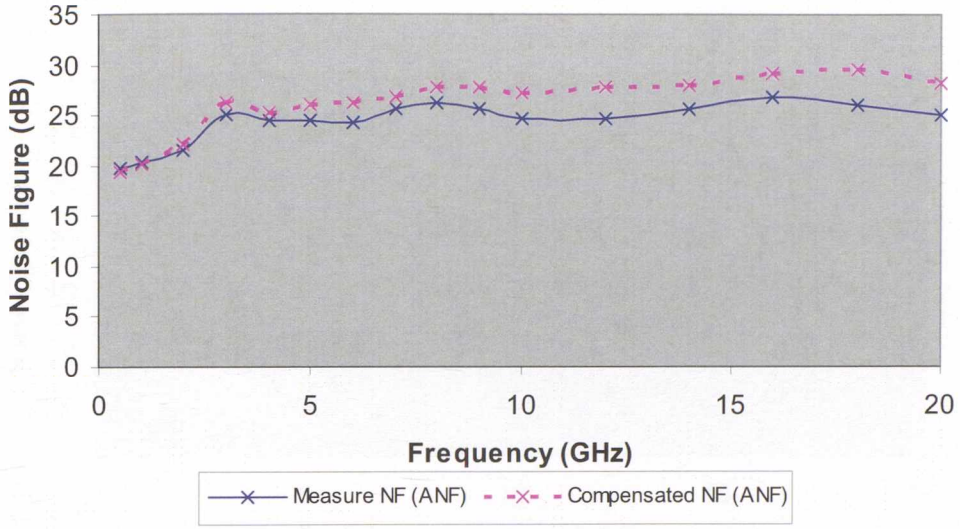

Figure 4-4: Measured and corrected noise figure of the SA as a function of frequency.

From Figure 4-4, the direct noise figure derived from the average displayed noise floor, normalised to 1Hz bandwidth varies between 19 to 28 dB (blue solid response). In most systems the noise observed on the spectrum analyser will be dominated by the noise at the front end due to the various gain stages. Therefore the noise passing through the system will see the same responsivity changes that the RF level would see (except for the broadband noise smoothing of 2 dB as mentioned in section 3.4.6). Hence, in order to obtain the true sensitivity of the system the sensitivity of the system must be compensated by the measured responsivity. The true noise figure of the spectrum analyser is therefore given by the red dashed response shown in Figure 4-4.

By definition the sensitivity of a spectrum analyser is defined as the level of a sinusoidal signal which equals the noise level of the system and at this point the noise floor would rise by 3 dB. Hence, by applying an external RF signal to the spectrum analyser it may be possible to be able to assess the sensitivity of the system by introducing a modulation level which raises the noise floor by 3 dB. Then the noise figure of the system can be calculated from:

$$NF_{SA} = SG_{level} - 10\log(RB) + 174 \quad dB \tag{4-2}$$

where SG_{level} is the RF level (as measured on the signal generator) which on passing through the spectrum analyser represents a level which is 3 dB above the noise floor. This technique was used to assess the noise figure of the spectrum analyser as a function of frequency, shown in Figure 4-5, and shown along side the average displayed noise floor compensated by the measured responsivity (red dashed response).

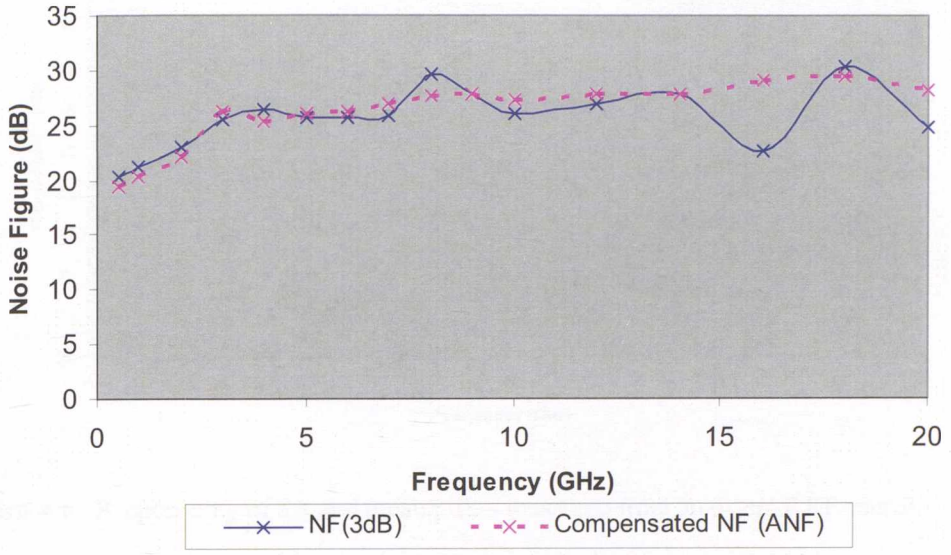

Figure 4-5: Comparison of noise figure techniques for the SA.

In summary, the SA measurements exhibit a noise figure nominally around 25dB which is somewhat higher than expected. There is a small difference in calculated noise figure between the 3dB noise floor rise and the average noise level approaches. This difference may be partially explained by the error in the signal generator and possible impedance mismatch between the two devices.

4.1.3 Specification of Preamplifier and Spectrum Analyser Combination

Following from the individual assessments of the preamplifier and SA, the responsivity of the preamplifier and SA combination was measured, Figure 4-6. This was achieved by applying a fixed input RF level from a signal generator (SMP22) and observing the RF level measured on the spectrum analyser. This includes the gain of the system (normalised 45.73dB @ 0.5|GHz).

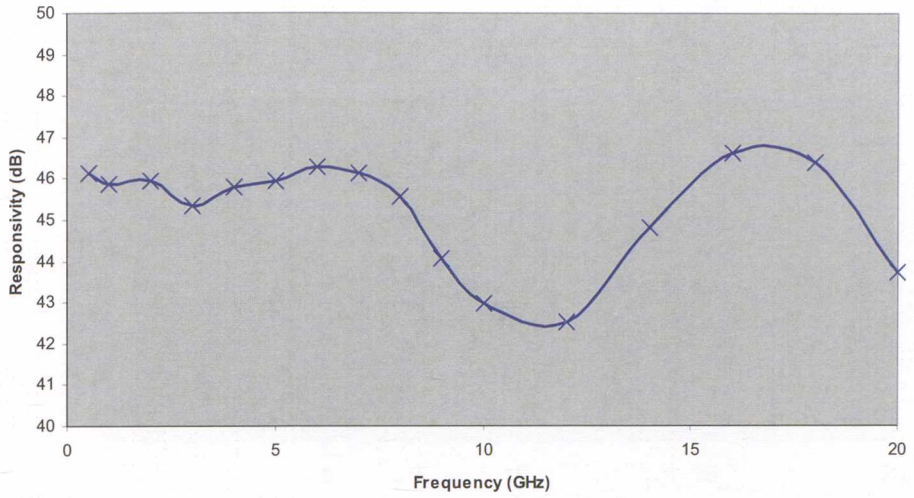

Figure 4-6: Responsivity of SA and preamplifier measured from an external RF source.

Pre amplifier gain variations do not significantly couple into the variation of the noise floor as discussed in an earlier section 3.4.7. A small offset of around 0.02 dB is estimated which, essentially can be ignore. The noise figure of the combination has been assessed using the average displayed noise floor and the 3 dB noise floor rise technique, Figure 4-7 and Figure 4-8 respectively. The dashed responses represent the noise figure calculated from the average displayed noise floor compensated by the measured responsivity of the system.

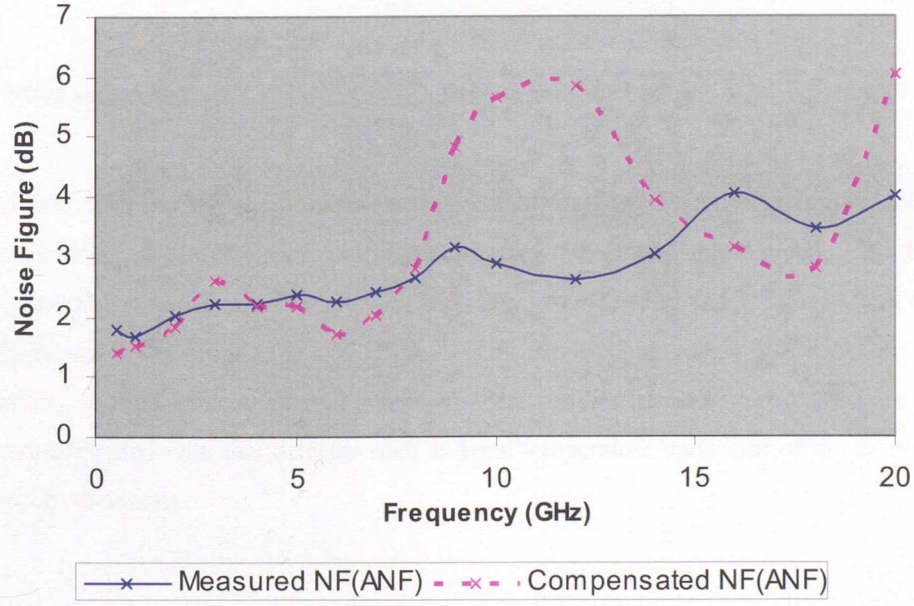

Figure 4-7: Noise figure of the SA and preamplifier measured from the average noise floor.

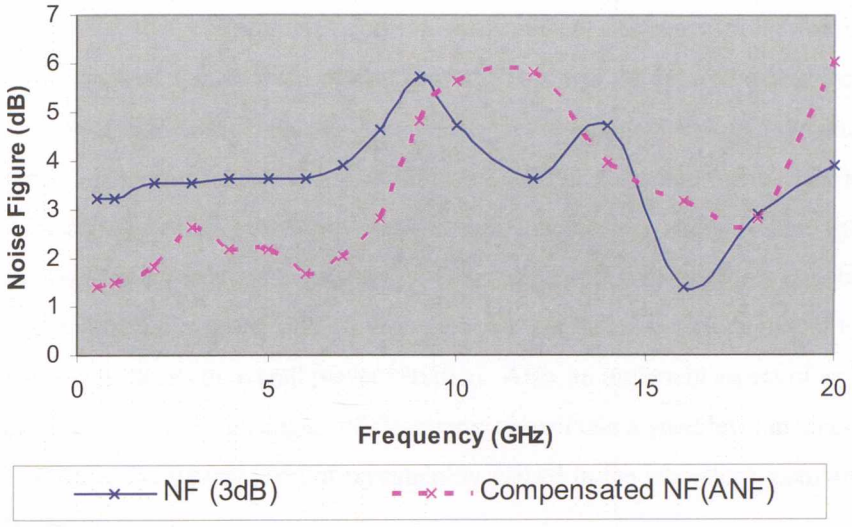

Figure 4-8: Measured noise figure of SA and preamp. (3dB noise floor rise technique).

Again there does appear to be a discrepancy between the techniques but clearly from the results the noise figure of the combination is typically less than 3.5 dB implying overall sensitivities of -170.5 dBm/Hz. This is likely to be marginally improved by a few tenths of dB's when the expected pre-selected spectrum analyser out of a batch of 50 is made available from Rohde and Schwarz.

4.2 Photodetector

This section describes the performance assessment of the New Focus 1414 high speed photo detector, looking at the dc and rf performance verses the optical input signal. The InGaAs detector covers the two main telecommunication windows (ie 1300 and 1550 nm), and offers a typical responsivity of around 0.6A/W. Assessments detailed here investigate optical connector repeatability, thermal effects, internal generated noise and linearity. Also discussed are several problems associated with this detector such as local temperature variations of the detector and responsivity variations.

4.2.1 Reproducibility and stability of power measurement

The optical input to this detector will form a measurement reference point for the RIN measurement in terms of the received optical power. This will be used to determine system responsivity and coupling loss. Thus, the input connectors ruggedness and reproducibility is of high importance. The connection is via an industry FC/PC connector which has a higher specification for durability than other fibre communication connectors, and is commonly used in test & measurement equipment and laboratories. Orientation of this connector is maintained by a mechanical slot or key down one side. It was observed that there is some degree of tolerance in this slot which contributes to overall power variation. Also, an important aspect of any optical connector is in maintaining a high degree of cleanliness to maintain a good level in repeatability. Figure 4-9 highlights the typical level of repeatability gained in the laboratory, combined with the effect of rotation.

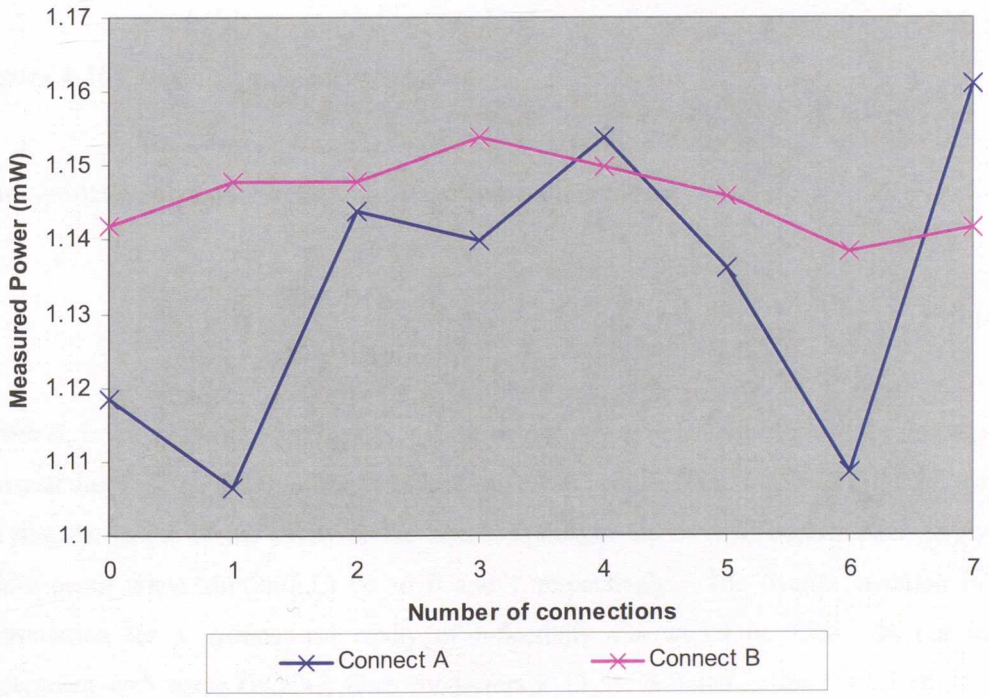

Figure 4-9: Optical power measurement reproducibility of the detector.

Here a 2mW optical power is repeat ably reapplied to the detector via a FC/PC uniter and the resultant dc photocurrent recorded. Optical power traceability is provided via an ILX lightwave power meter (Model No OMH-6725B InGaAs power/wavehead) before each reconnection. The power head consists of an integrating sphere which naturally provides high level repeatability as there is no optical contact interface. Results are given for connect A – connection uncleaned and unbiased in rotation, and B – connection cleaned before each measurement point and rotation

biased to one side. A variation of 4.7% was achieved for connect A and 1.3% for connect B. Due to the difficulty in cleaning the photo-detectors FC/PC connector a plane FC/APC connectorised fibre will be used which will also reduce wear on the photo-detectors input. A tighter tolerance uniter has also been fabricated to restrict the rotational variation and thus provide performance similar to connect B.

In performing each of the measurements in Figure 4-9 a significant level of instability was observed necessitating the use of averaging. This is associated with etalon\cavity effects mentioned briefly in section 3.4.1 and further described below.

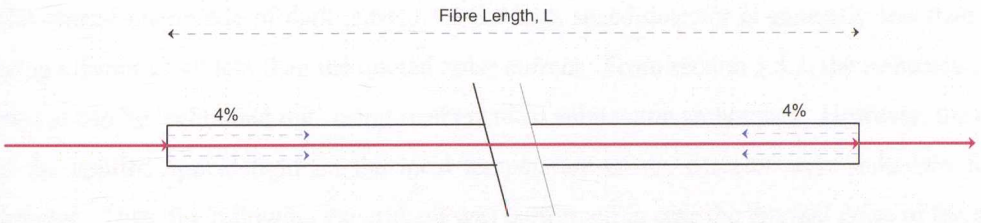

Figure 4-10: Etaloning problem exemplified

The transmitted irradiance of the Fabry Perot system is given by:

$$H_t = H_o \frac{(1-r)^2}{(1-r)^2 + 4r\sin^2 \frac{2\pi}{\lambda} L} \quad Watts/m^2 \tag{4-3}$$

where H_o is the incident power density, r is the optical power reflectivity, $2\pi/\lambda$ is the propagation constant and L is the length of the resonator cavity. It is clear from the above equation that by varying the length of the cavity or the laser wavelength the level of transmission may vary. These occur when $\sin^2(2\pi/\lambda.L)$ go to 0 and 1 respectively. The overall variation in the transmission for a symmetrical cavity of reflectivity 4% would be 15%. In our initial experiment with plane (FC/PC) fibre connectors a 12 % variation in the optical power was observed. Thus, it is possible that instability of the fibre optical length (due to temperature and strain effects) can explain the 12% fluctuation in the optical power when using plane FC/PC connectors. By using angled connectors (FC/APC) the effective finesse of the fibre cavity is degraded substantially and the above intensity variations can be minimised. In practice the use of angled fibre connectors reduces the optical power variations to less 1%.

The New Focus detector has an integral fibre lead to the active area of the detector and this does use plane fibre ends. However, the length of the fibre ~ 4 cm and the fact that it is enclosed

means that the intensity fluctuations may be reduced to < 5%. Angled connectors are used throughout and thus any intensity instability will be dictated by the FC/PC uniter at the photodetector. Thus, by ensuring a good contact at the photodetector connector it is possible to minimise this variation. In practice the stability in the optical power has been found to be < 1% when applying the reference laser described in section 3.5.2, over long periods of time (> 8 hours). If stability needs to be further improved then index matching gel can be used at the detector FC/PC surfaces.

4.2.2 Temperature Dependent Effects in the Photodetector

The quoted magnitude of dark current for the high speed detector is generally less than 1 μA, being a factor of 40 less than the quoted noise current. From section 3.5.2, the influence of dark current can be 'calibrated out' using mathematical subtraction techniques. However, the effects of the applied optical light on the local temperature of the detector were unknown for this detector. Thus, the following experiment was performed in case the thermal noise of the system was affected.

It is well understood that the dark current depends on the temperature of the detector which for silicon doubles every 11°C rise[51]. With this information, it may be possible to estimate the local temperature of the detector at a particular optical power level by blocking the light and instantaneously reading the dark current.

The New Focus detector is fibre pigtailed to the active area of the photodetector. The epoxy used for this may not survive temperatures in excess of 40°C. In order for measurements to be made at temperatures in excess of this value, a preassembled unit was acquired from New Focus without the fibre pigtail. Also, the mount holding the photodetector was rearranged so that the Peltier control of the temperature could be achieved efficiently. The dark current was measured via the detectors DC port connection.

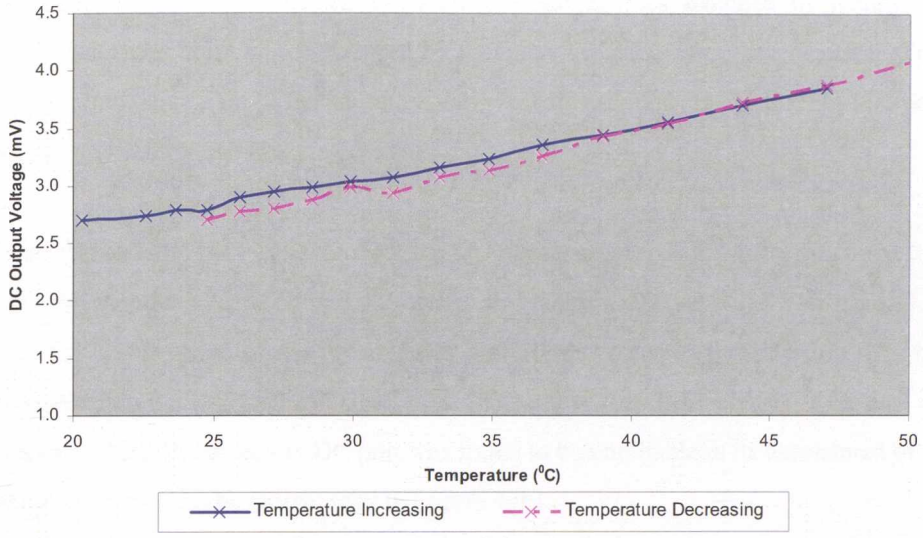

Figure 4-11: Photodetector dark current as a function of temperature.

The results show some variation from a linear graph but the exponential behaviour could not be seen. When light is now incident on the detector, if there are any variations in the local temperature, these can be monitored via the dark current when the light is blocked (provided that the bandwidth of the measuring equipment is sufficient). With this measurement it was found that the rise in the dark current was marginal when an optical power of between 1- 2 mW was used. This suggests that there are minimal changes in the local temperature of the detector and the effects of this error are insignificant.

4.2.3 Noise and Linearity of Detector

Another point of interest was the excess noise of the photodetector. The photodetector DC port measurement was out coupled via the standard internal transimpedance amplifier, and depending on the feedback resistance excess noise could be introduced into the system. From the manufacturers, the photodetector was quoted has being thermally noise limited by the 50 Ohm impedance. The Johnson current noise will be given by

$$\Delta i^2 = \frac{4kT}{R} \quad Amps \tag{4-4}$$

and for an impedance of 50 Ω the effective Noise Equivalent Power (NEP) of the detector was calculated to be 33 pW/√Hz. Hence on connecting a 50 Ohm termination to the preamplifier, the same noise levels should be registered on the spectrum analyser as the detector. However, there was an excess noise from the detector of ~ 2 dB. On disconnecting the transimpedance

amplifier circuitry, the noise levels between the two devices matched to within 0.2 dB. Therefore the excess noise was introduced by the internal electronics of the detector. Thus, the detector transimpedance amplifier circuitry was permanently disconnected from this point on, leaving just a 9V battery to bias the detector.

Since the standard DC port was removed, the DC photocurrent needed to be measured from the RF port. As mentioned in section 3.4.2 earlier and measured in section 4.3.1, the DC current degrades the performance of the preamplifier and this necessitates the insertion of a bias tee which outcouples the DC signal. This DC voltage signal can then be used to assess the DC photocurrent. Also, the detectors DC port was found to be unreliable in its assessment of the DC optical light and this can be clearly seen in Figure 4-12.

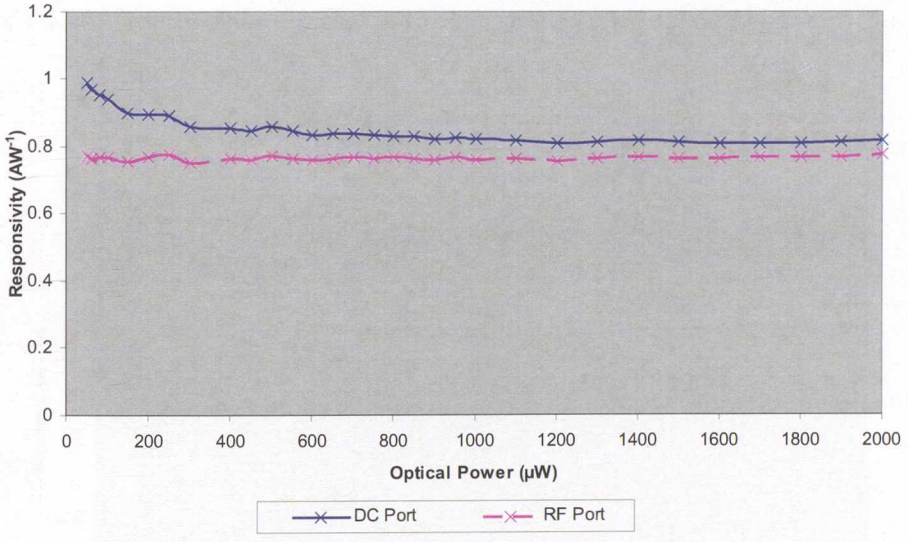

Figure 4-12: Responsivity of photodetector for various optical powers.

It can be seen, from Figure 4-12 that the DC port calibration tends to 1 for extremely low powers, < 100 μW. Whereas the DC measurement from the RF port provides a consistent value of responsivity, as a function of optical power.

The linearity of the photodetector was assessed at various laser wavelengths. The following results discussed are with reference to 1319 and 1533nm using the ILX power meter.

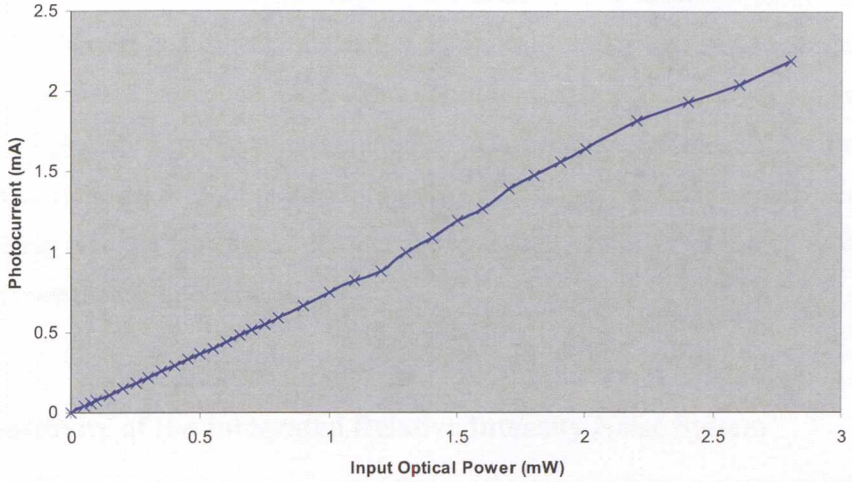

Figure 4-13: Linearity of the detector, at 1319nm, as a function of optical power.

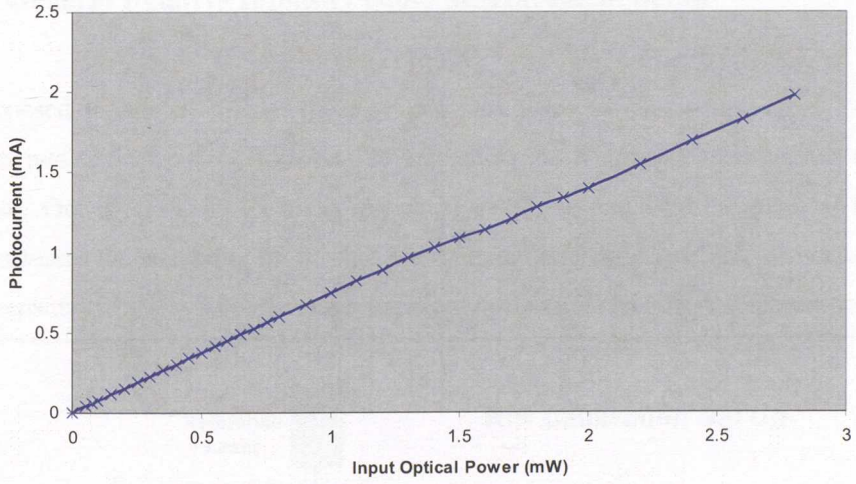

Figure 4-14: Linearity of the detector, at 1533nm, as a function of optical power.

Figure 4-13 and Figure 4-14 demonstrate the linearity of the detector at two wavelengths. These results become critical when the final RIN measurements are calculated since errors here will couple directly into the uncertainty budget. This error can be greatly reduced if the actual responsivity at a particular power be known. The maximum variation in the responsivity at one particular wavelength was measured to be 5%. All these results are traceable through the ILX lightwave power meter.

Due to the uncertainty of using the high speed detector as a calibrated power meter with respect to its ageing quality etc., the use of an optical transfer standard has been selected, previously discussed in section 3.4.2. This consists of a temperature stabilised germanium detector coupled to a photocurrent amplifier. Calibration performance for this unit is discussed in section 4.5. By first measuring the optical signal with the transfer detector and then applying it to the high speed detector the generated photocurrent can be calibrated for each RIN measurement performed.

4.3 Sensitivity of the Integrated Relative Intensity Noise System

In the preceding work the detector, preamplifier and SA have each been examined individually. This section now integrates these components and assesses in detail the overall noise level system performance.

4.3.1 General Relative Intensity Noise Measurement Setup

The proposed integrated measurement system was setup as shown in Figure 4-15. This identifies two optical paths which can be applied to the high speed detector via the optical attenuator. One is for the device under test signal and the second is for the reference laser. This section assesses the suitability of the shot noise limited reference laser and also determines the system sensitivity by way of the average displayed noise floor and 3dB rise approaches.

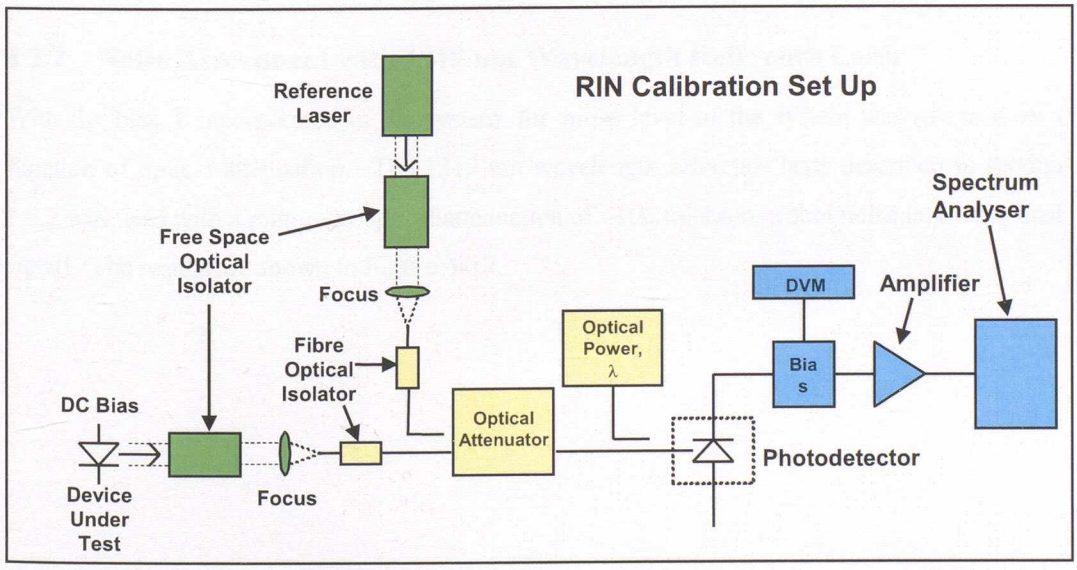

Figure 4-15: Integrated RIN measurement system.

As previously described in section 3.4.3, the bias T was necessary since the high speed photodetector with its DC photocurrent capability tended to saturate the preamplifier. The bias T forms a DC block allowing the DC photocurrent to be out coupled from the rf path. The saturation of the system with increasing optical power can be seen in Figure 4-16. The insertion of the bias T into the system introduces an additional loss in the RF signal path which will have an effect of increasing the overall noise figure of the system by the same amount. The Picosecond Pulse Labs bias T, 5541A selected has a frequency bandwidth of 80kHz to 26GHz with an insertion loss typically 0.4dB rising to 1.5dB at the higher frequency end.

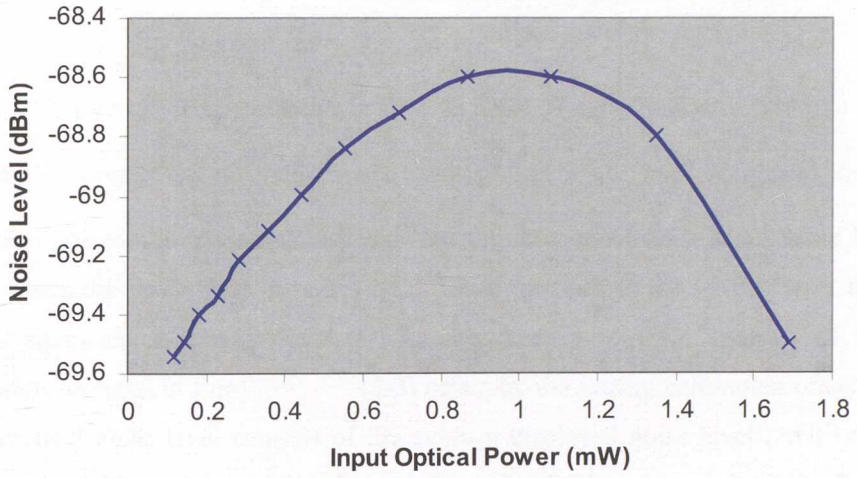

SA set to 12 GHz and resolution bandwidth 1MHz

Figure 4-16: SA noise level saturation as detected optical light incident increased.

4.3.2 Noise Assessment with 1319 nm Wavelength Reference Laser

With the bias T incorporated in the system, the noise level of the system was assessed as a function of optical attenuation. The 1319 nm wavelength reference laser described in section 3.5.2 was used with a minimum optical attenuation of ~100 to ensure a shot noise limited optical signal. The results are shown in Figure 4-17.

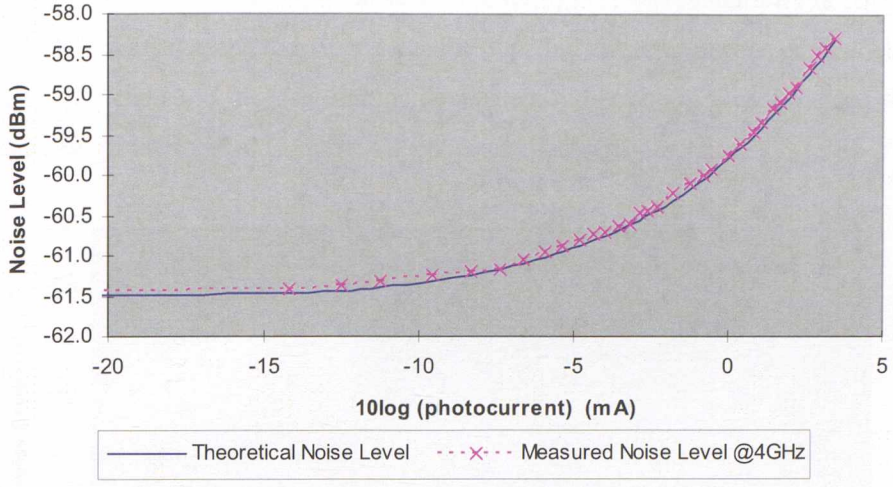

SA set to 4GHz, resolution bandwidth 3MHz, Correction factor 1.33dB

Figure 4-17: Measured & theoretical noise level as a function of incident optical power.

Figure 4-17 shows the measured response and the theoretical noise level, solid line. The point at which the noise floor increases by 3 dB corresponds to the sensitivity of the system which is examined in section 4.3.5. The measured noise level consists of the noise contributions defined in Eqn (3-3) offset by the system calibration offset (Syscal). The theoretical noise level consists of the average displayed noise level (ANF) measured, superimposed with the shot noise derived from the DC current at the bias T which is adjusted by the Syscal. Syscal essentially consists of the gain introduced by the amplifier and the resolution bandwidth of the SA.

Both the Shot and thermal noise power contributions will see the divider effect and broadband smoothing discussed in sections 3.1.1.1 and 3.4.6 respectively. After accounting for these contributions (6dB and 2dB respectively) it was observed that the responses did not match. By decreasing the theoretical level of Shot noise by 1.33dB (correction factor) a close match was obtained. The origins of the correction factor are most probably linked to the error associated with the 'nominal' 2dB broadband smoothing combined with effective impedance matching of the detector, amplifier and spectrum analyser.

Summary:

- Measured Noise = (Thermal Noise + Shot Noise + Spontaneous Noise) Syscal
- Theoretical Noise = ANF + (Derived Shot Noise) Syscal
- Syscal = RB of SA + Gain – 6dB – 2dB – Correction Factor

In Figure 4-18 the average displayed noise level of the system was subtracted from the previous result and the resultant graph then represents the Shot and any spontaneous noise contributions of the laser. Of course, if the laser light is dominated by Shot noise then the graph should be linear and any curvature would indicate a spontaneous contribution.

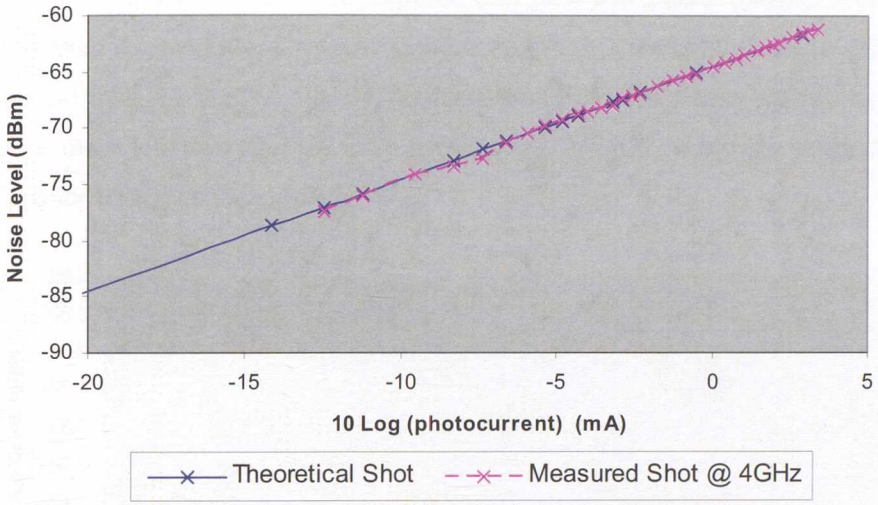

SA set to 4GHz, resolution bandwidth of 3MHz, Correction factor 1.33dB

Figure 4-18: Measured & theoretical Shot noise (average noise of system subtracted).

From Figure 4-18, the response is clearly linear having a least squares gradient of 1.02 and a standard uncertainty, u(x) of 0.033dB derived from the standard deviation (σ) of the errors divided by the square root of the number of samples.

$$u(x) = \frac{\sigma}{\sqrt{n}} \tag{4-5}$$

Typically the spectrum analyser used in this technique will contribute significant errors in terms of reproducibility (with no averaging this was observed as ~0.3dB (7%)), linearity and log scale fidelity. These are further discussed later in the uncertainty budget calculations, 4.5. The theoretical gradient for the Shot noise variation with optical attenuation should be 1 and this fits in well with the findings. The gradient for spontaneous noise as function of optical attenuation would be 2. If the spontaneous noise is a factor of 20 dB down on the Shot noise we would expect a change in the gradient of 2×1/100 (since 2 would be the gradient of any spontaneous noise). This is an error of 2 % which is well within the quoted error for this technique. However, the actual value of the least squares gradient is 2% out from the correct gradient of Shot noise. Thus, the results are consistent with the reference laser being 'shot noise limited'.

4.3.3 Noise Assessment with 1533 nm Wavelength Reference Laser

The previous test method was repeated with another available low noise laser of wavelength 1533 nm. This provides an opportunity to confirm that the Shot noise correction factor was similar at different wavelengths. The reference laser used was a diode pumped Erbium doped glass laser from Amoco Laser Company (Model: ALC 1535- 50EHS OPT f3.160) and has an output optical power of 35 mW. Clearly, the attenuation factor required to obtain optical powers of 1 mW is much less than the 1319 nm reference laser. Even so, due to the cavity design this laser is predicted to be extremely *clean.*

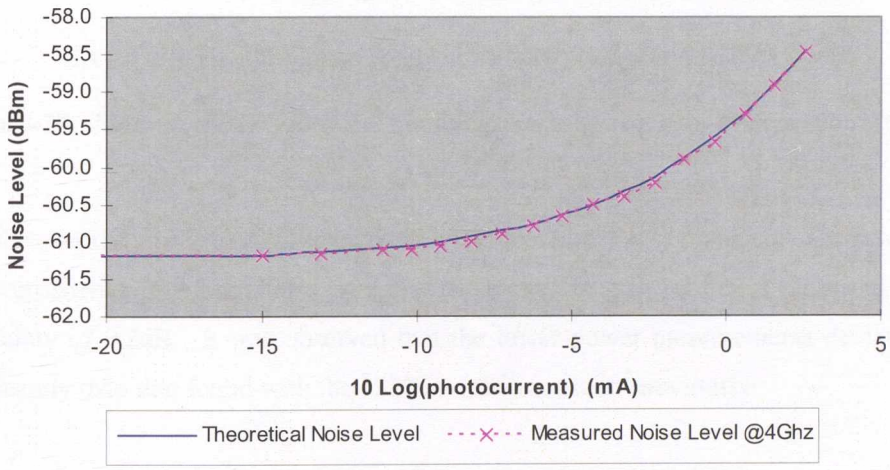

SA set to 4GHz, resolution bandwidth 3MHz, Correction factor 1.4dB.

Figure 4-19: Measured & theoretical noise level as a function of incident optical power.

The measured noise level varies as a function of the DC photocurrent and the result was fitted in the same way as the previous case for the 1319nm reference laser. The correction factor in this case was found to be 1.27 dB which is close to the previous value of 1.33dB. It does appear that the correction factor will be dependent on the laser wavelength.

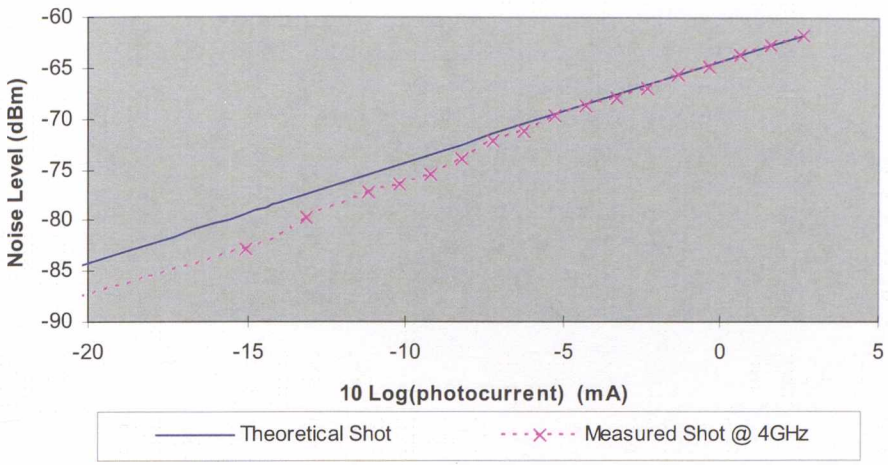

SA set to 4GHz, resolution bandwidth 3MHz, Correction factor 1.27dB.

Figure 4-20: Measured and theoretical Shot noise (average noise of system subtracted)

With the average noise floor subtracted the linear plot above was obtained. The results were again consistent with a Shot noise limited laser source, the gradient being 1.026 and standard uncertainty of 0.2dB. It was observed that the lower power measurements deviated more significantly than that found with the 1319nm reference laser previously.

Next the frequency dependency of the correction factor was investigated using the same set up and the 1533nm reference source. Further measurements using the 1319nm reference laser have also been performed over frequency and are reviewed in 4.5.10.3. The following plots show shot noise limited performance at 10GHz.

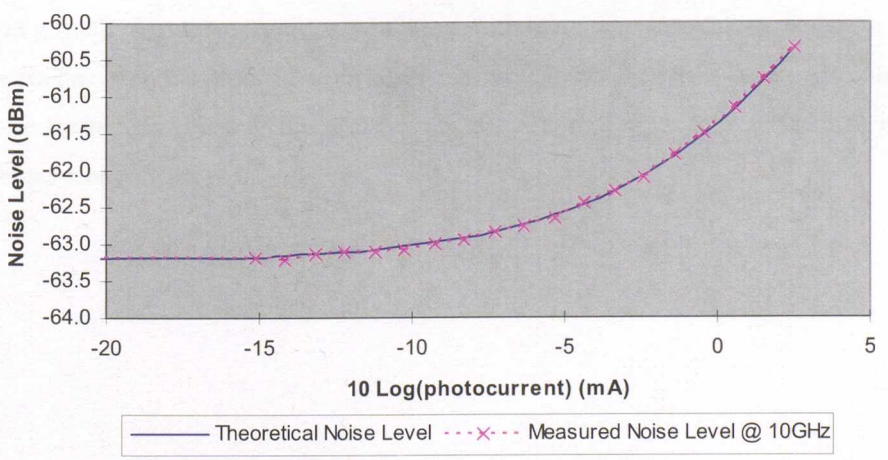

SA set to 10GHz, resolution bandwidth of 3MHz, Correction factor 0.95dB.

Figure 4-21: The measured & theoretical noise level (function of incident optical power).

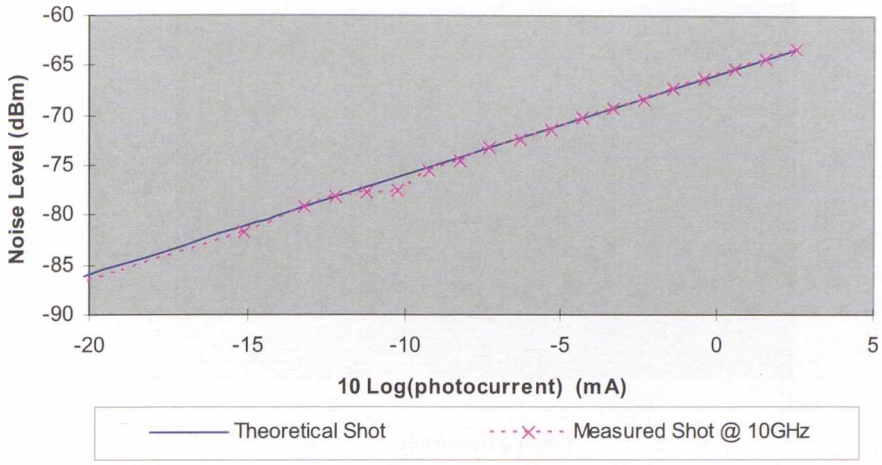

SA set to 10GHz, resolution bandwidth 3MHz, Correction factor 0.95dB.

Figure 4-22: The measured & theoretical Shot noise (avg. noise of system subtracted).

The fitted data suggests a correction factor in the shot noise at 10 GHz of 0.95dB, thus the correction factor is frequency dependent. Completing the least squares linear fit to the shot noise response, Figure 4-22, we obtain a gradient of 1.031 with a standard uncertainty of 0.24dB. Again, this is consistent with a shot noise limited source. One data point shows a large deviation against the full data set which is thought to be a measurement glitch due to the automated scanning routine. No variations of this magnitude have been found to be repeatable. Thus, by excluding this data point the fitted gradient becomes 1.0127 with a standard uncertainty of 0.08dB.

4.3.4 Correction Factor Measured as a Function of Frequency

Continuing with the theoretical noise fitting technique, the correction factor at various frequencies has been assessed using the 1319 nm wavelength reference laser. Also, the laser's shot noise limited performance has also been assessed at each frequency and similar results to the previous section were obtained.

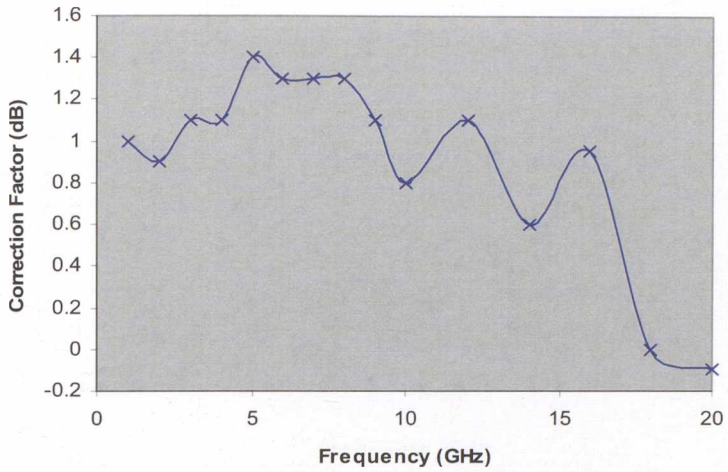

Figure 4-23: Correction factor as a function of frequency (1319nm reference laser).

The overall correction factor has been found to vary over the frequency range by 1.5dB. These results have been repeated several times and the reproducibility in the correction factor appears to be less than < 0.2 dB.

4.3.5 Sensitivity of System using the 1319 nm Wavelength Reference Laser

Following on from the correction factor assessment, the same reference laser v frequency data can be used to extract the sensitivity of the system. This is achieved by determining the point at which a 3dB rise is observed in the spectrum anaylsers average displayed noise floor as incident optical power is increased. The DC photocurrent at this point then represents the level of noise (shot) introduced and hence the sensitivity of the system. By accounting for the divider effect (6dB) and subtracting from the noise floor, -174dBm (referenced at the I/P of the rf amplifier) we obtain the following responses referred to as the systems 'noise figure'.

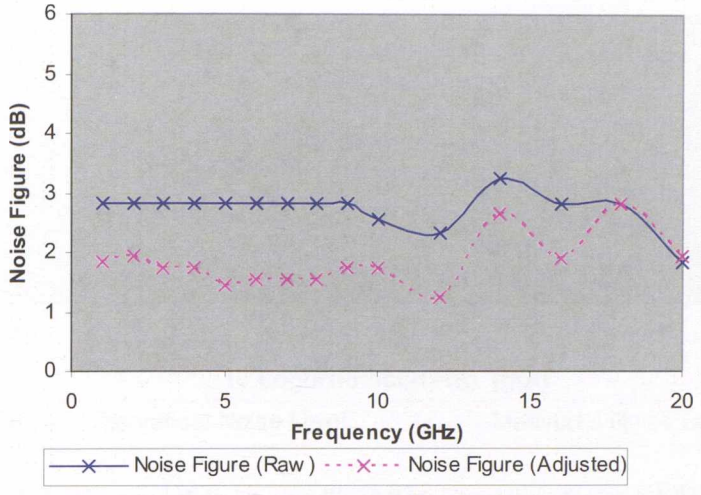

Figure 4-24: System noise figure as a function of frequency. 1319nm reference laser.

The 'Raw' noise figure shows a typical noise figure of <3dB (i.e. sensitivity of <-171dBmHz^{-1}) using the 3dB technique. However, system sensitivity refers to the ability to measure RF signals which do not see the Correction factor. Hence, in order to obtain the actual sensitivity of the system the Correction factor must be accounted for and this is shown by the 'adjusted' noise figure. Typically, this results in a noise figure of <2dB (i.e. sensitivity of <-172dBmHz^{-1}), and peaks at 2.83dB at 18GHz. This is similar to previously gathered data for the bias T, rf amplifier, spectrum analyser and detector combination, after considering variation in impedance matching and the frequency responsivity of the detector.

4.3.6 Noise Assessment with Noisy Laser Source

The lasers reported so far are *high power low noise* lasers which, with attenuation achieve even better laser performance with diminished spontaneous noise contributions. The theoretical noise fitting measurement technique has been repeated with a practical telecomm's laser such as the Fabry Perot laser from Hitachi (HLP 5400) for comparison.

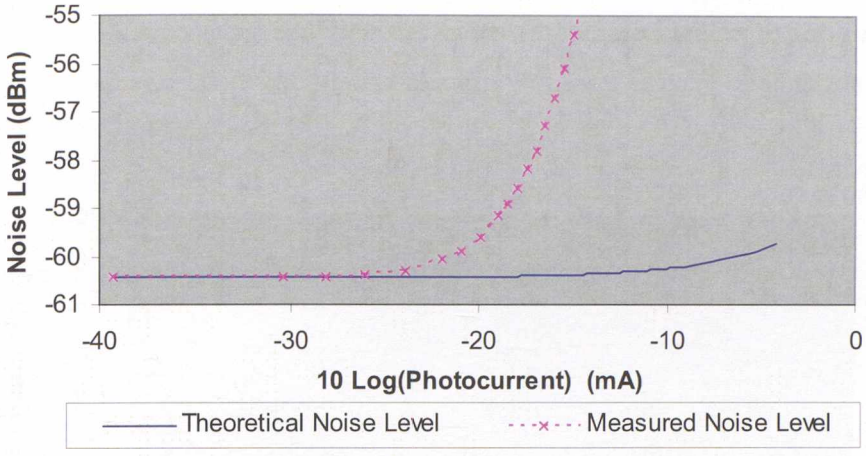

SA 4GHz, resolution bandwidth 3MHz, Correction factor 1.4dB

Figure 4-25: Measured & theoretical noise level as a function incident optical power.

It is clear from the above response that the laser under test has enormous amounts of spontaneous noise shown by the departure from the theoretical noise level which assumes no spontaneous noise contribution. Figure 4-26 shows the spontaneous contribution fitted to the thermal and shot noise.

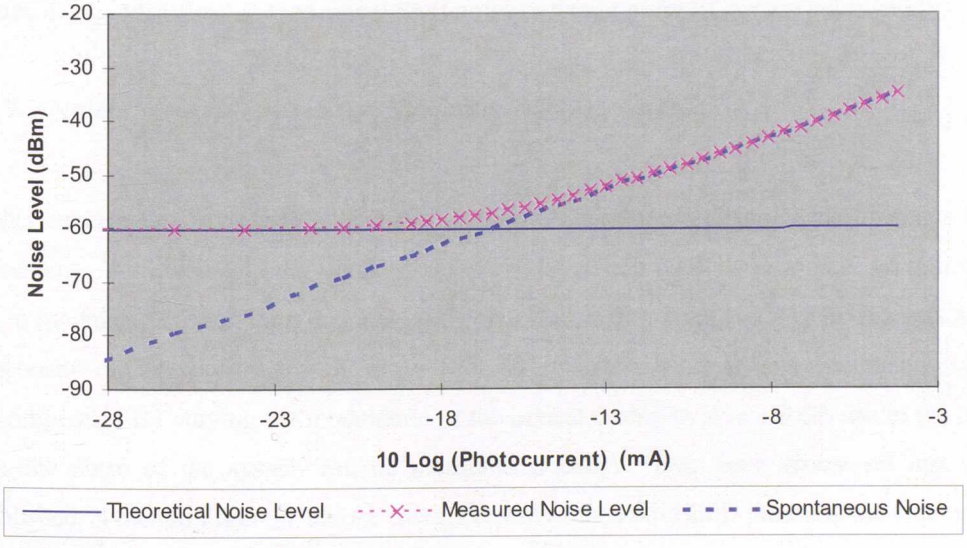

SA 4GHz, resolution bandwidth 3MHz, Correction factor 1.4dB

Figure 4-26: Spontaneous noise contribution shown as a function of optical power.

With the average noise floor subtracted the linear plot in Figure 4-27 was obtained. This time we see the measured response has a gradient of 2.03 due to the dominance of the lasers spontaneous noise contribution. Standard uncertainty was 0.04dB. Also shown is the theoretical response which only consists of the shot noise contribution, clearly different from that measured. An important point observed through the experiments in this section is the

spontaneous noise of the laser will see the same offsets as the shot noise, i.e. voltage divider effect and the SA smoothing and thus this needs to be accounted for when quoting the spontaneous noise of a laser. As far as I'm aware this level of compensation has not been recognised in any previous work.

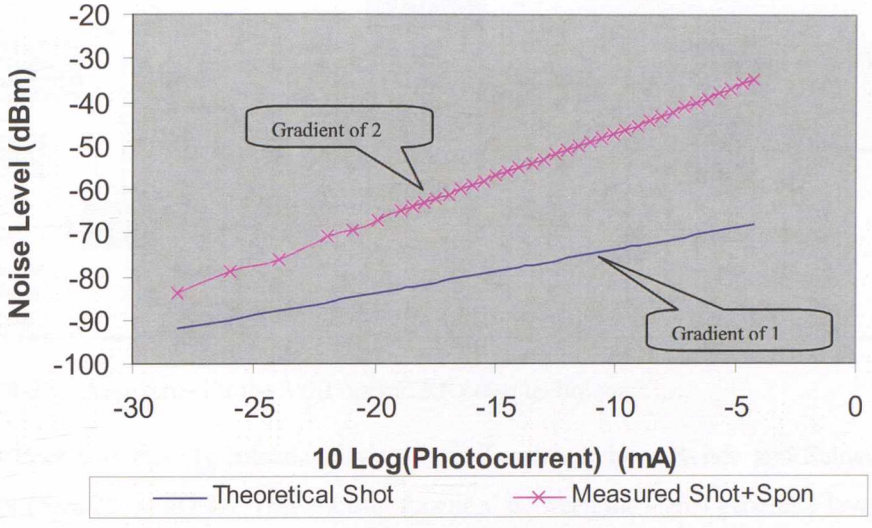

SA 4GHz, resolution bandwidth 3MHz, Correction factor 1.4dB

Figure 4-27: Measured & theoretical Shot noise (average noise of system subtracted).

4.3.7 Noise Assessment via the Modulated Light Carrier

Further experiments have been undertaken to cross-examine the findings of the reference laser assessment. A variation to the previous sensitivity approach (wideband signal), section 4.3.5 was to modulate the laser light incident on the detector (narrowband signal). In this way a DC component of the light as well as a relatively narrow band optical modulation were superimposed. By varying the modulation of the optical carrier to give a 3 dB rise in the noise floor the noise of the system can be measured directly. Two laser source set ups were established, shown in Figure 4-28 one using a directly modulated DFB laser and the other using the 1533nm reference laser combined with an external optical modulator.

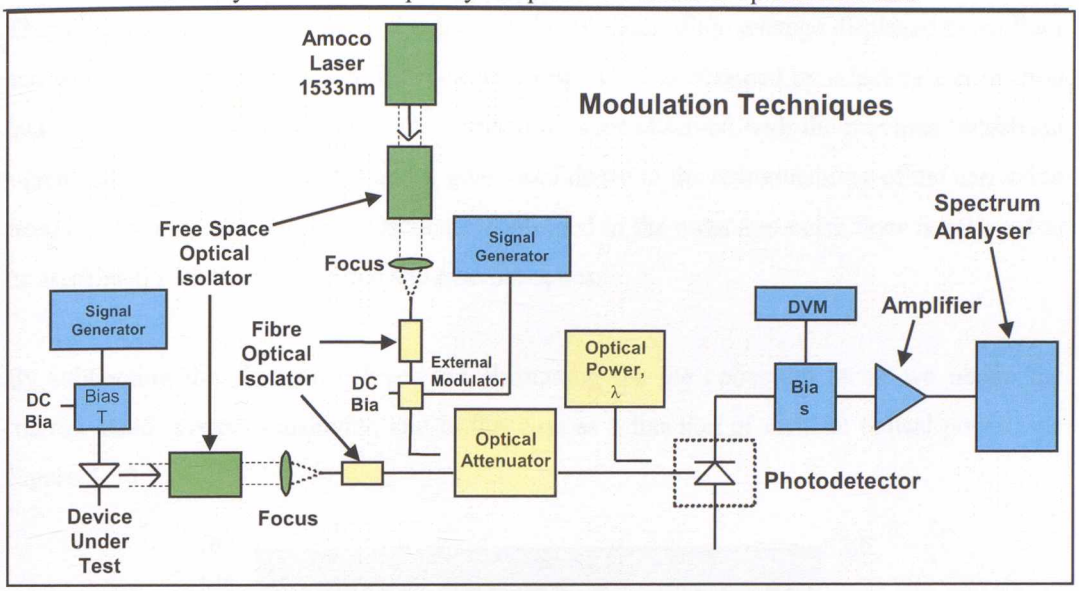

Figure 4-28: Apparatus for the 3 dB optical RF noise technique.

A DFB laser was directly modulated via a bias T network by a Rohde and Schwarz signal generator (SMP22) at 4GHz. The 'transfer function' between the signal generator level and that displayed on the spectrum analyser was first determined at RF levels above the 3 dB rise in the noise floor. Following this the 3dB sensitivity level was determined at various incident optical powers. The laser rf input level was increased via the signal generator until a 3dB rise was observed in the average displayed noise floor. At this point the input level was noted and adjusted by the 'transfer function' and the amplifier gain and SA resolution bandwidth to determine the equivalent signal level at the input of the amplifier, see Figure 4-29. Note: the signal level increases with incident power due to the shot noise component.

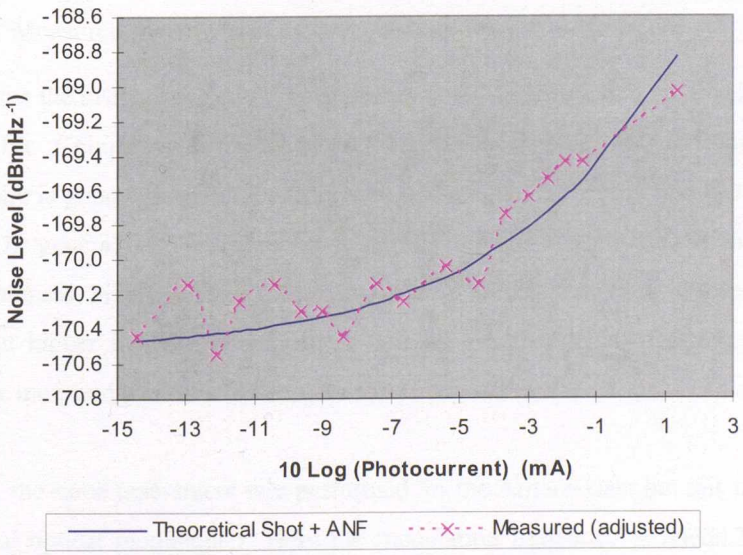

SG 1GHz, resolution bandwidth 3MHz, Correction factor of 1.4dB

Figure 4-29: Measured & theoretical level for 3dB increase (function of incident power).

The solid line shows the theoretical signal level consisting of the average displayed noise floor and shot noise. A good fit with the measured response was obtained by selecting a correction factor of 1.4dB. This is similar to the correction factor observed with the previous 'wideband signal' reference laser technique and it gives confidence in the reproducibility of the correction from one technique to another. Oscillation observed in the measured noise floor is believed to be associated with the laser source and external optics.

By subtracting the shot noise level and accounting for the correction factor we obtain the 'narrow band' system sensitivity, and in this case as a function of incident optical power, see Figure 4-30

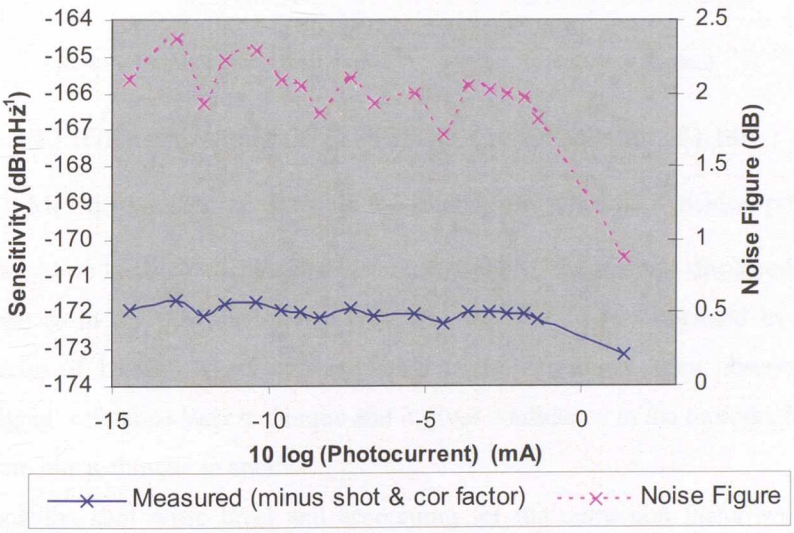

SG 1GHz, resolution bandwidth 3MHz, Correction factor of 1.4dB

Figure 4-30: Measured 'narrowband' system sensitivity and noise figure.

Here we can see the average sensitivity is approximately -172dBmHz^{-1}, i.e. system noise figure of 2dB @ 1GHz. Comparing to the 'wideband' sensitivity approach (NF = 1.83dB, CF = 1dB) we can see there is good agreement regarding the noise figure and correction factor between the techniques. The general decrease *observed* is significantly governed by the initial measurement stability randomness, highlighted by the deviation from the fitted theoretical response in Figure 4-29. Also at higher incident powers there will be a higher level of error associated with subtracting the increasingly dominant shot noise term.

Following on, the same assessment was performed for the Amoco laser but this time modulated via an external optical modulator. Here the modulation frequency provided by the SMP22 signal generator was set to 1GHz and connected to a GEC Marconi Ltd amplitude modulator (8GHz, 1.5 μm, Y-35-8931-02). Optical attenuation was used to control the incident power at

the photo detector. Figure 4-31 shows the measured response together with the fitted theoretical noise.

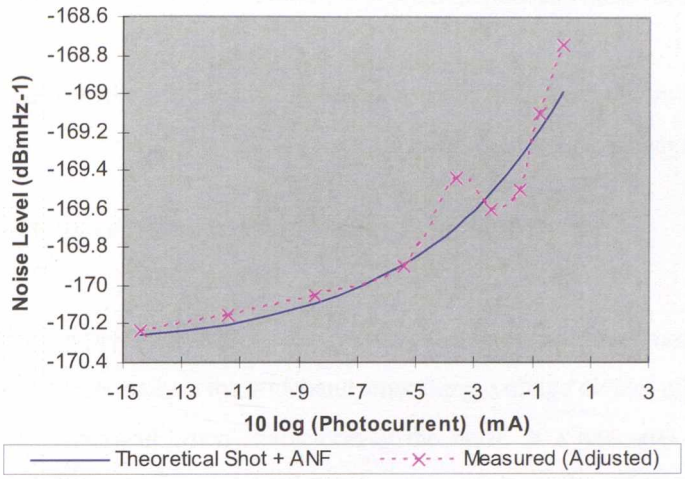

SG 1GHz, resolution bandwidth 3MHz, Correction factor of 1.1dB

Figure 4-31: Measured & theoretical level for 3dB increase (function of incident power).

The solid line shows the theoretical signal level consisting of the average displayed noise floor and shot noise as in the previous case. This time the best fit was obtained by selecting a correction factor of 1.1dB. Again, this is similar to the correction factor observed with the 'wideband signal' reference laser technique and it gives confidence in the reproducibility of the correction from one technique to another.

On subtracting the shot noise level and accounting for the correction factor we obtain the 'narrow band' system sensitivity as a function of incident optical power shown in Figure 4-32.

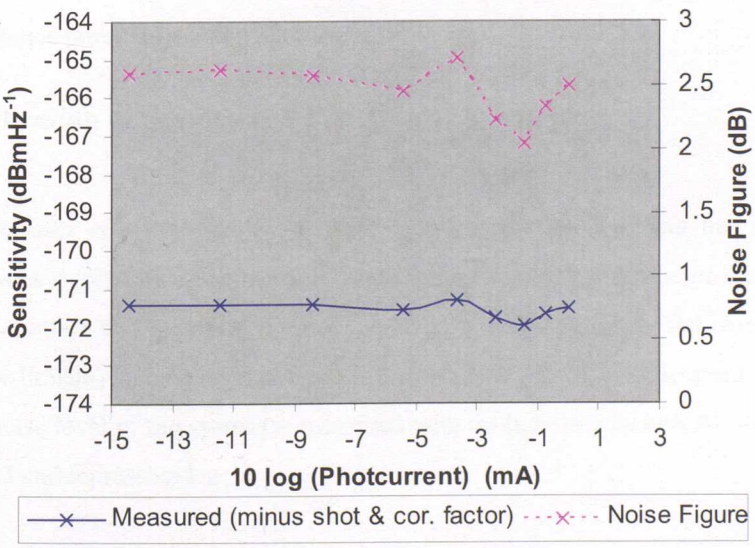

SG 1GHz, resolution bandwidth 3MHz, Correction factor of 1.1dB

Figure 4-32: Measured 'narrowband' system sensitivity and noise figure.

Here we can see the average sensitivity is approximately -171.6 $dBmHz^{-1}$, i.e. system noise figure of 2.4dB @ 1GHz. Again, comparing to the 'wideband' sensitivity approach (NF = 1.83dB, CF = 1dB) we can see there is reasonable agreement between these techniques.

All the wideband and narrow band techniques demonstrated here have shown a good degree of consistency and therefore provide confidence in the noise measurement system approach.

4.4 Relative Intensity Noise Measurement Procedure

As can be seen from the previous sections determining accurate noise level measurements is not without its pitfalls. Factors such as the wideband smoothing, voltage divider effect, rf mismatch etc. require careful assessment when characterising the noise of a telecoms laser. All these factors also have knock-on affects on the measurement sensitivity and confidence level which, in this application needs to be of the up-most precision representing a national standard. The procedure outlined below assumes nothing about the various mechanisms in the system and makes the resultant traceable via the DC photocurrent, and optical power measured. This significantly relies on a simple referencing technique, the first application of using a low noise reference laser as a variable cold noise source. A more detailed operational procedure is detailed in Appendix D.

Measurements of:

- Dark or thermal noise
- Device under test, at specific optical power, and photocurrent
- Reference laser, at matched photocurrent

4.4.1 Calibration of System as a Function of Frequency

The reference laser is a key element in this measurement standard and has shown, in the previous sections significant advantages in determining frequency response of the system. This follows from the fact that the noise floor of the laser light is completely flat over the spectrum (i.e. shot noise limited) and the level of noise is traceable via the DC photocurrent. In this system the average noise level of the system is measured with no light incident on the detector, shown in Figure 4-33 and represented as;

$$(N_{drk}) = \text{Syscal}(N_{th}) \quad \textit{Watts} \tag{4-6}$$

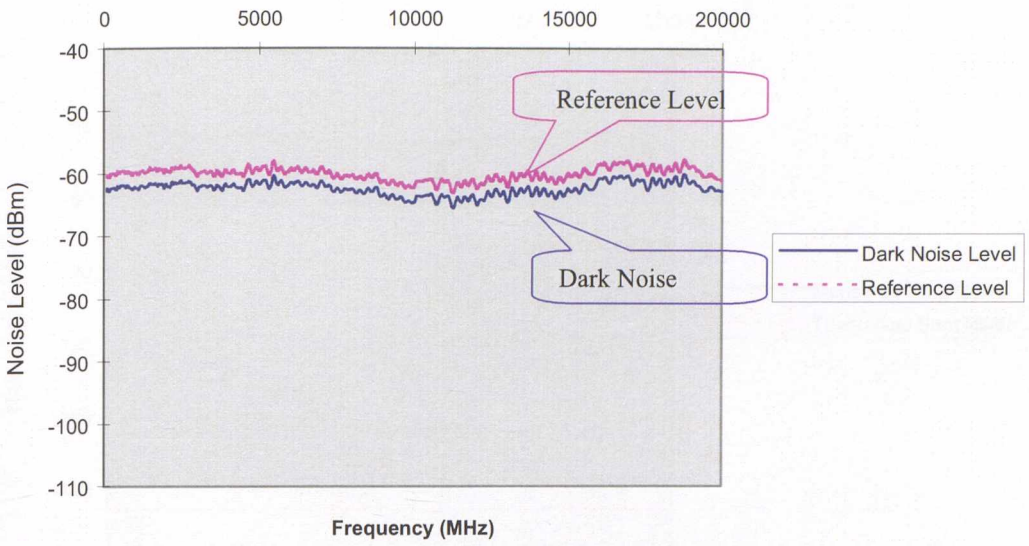

Figure 4-33: Incident detector noise level with and without reference laser.

Now the light from the reference laser is increased to the level of light that will be expected from the DUT and the noise spectrum is re-measured (i.e. matched photocurrent)

$$(N_{ref}) = \text{Syscal}(N_{th}) + \text{Syscal}(N_q) \quad \textit{Watts} \tag{4-7}$$

As can be seen from the upper response (red) the noise level has just shifted up by a very small amount which is equivalent to the shot noise introduced. By subtracting the (N_{drk}) response from the (N_{ref}) response the system calibration factor (Syscal) and the shot noise terms will remain.

$$(N_{ref}) - (N_{drk}) = \text{Syscal}(N_{th}) + \text{Syscal}(N_q) - \text{Syscal}(N_{th}) = \text{Syscal}(N_q) \quad \textit{Watts} \tag{4-8}$$

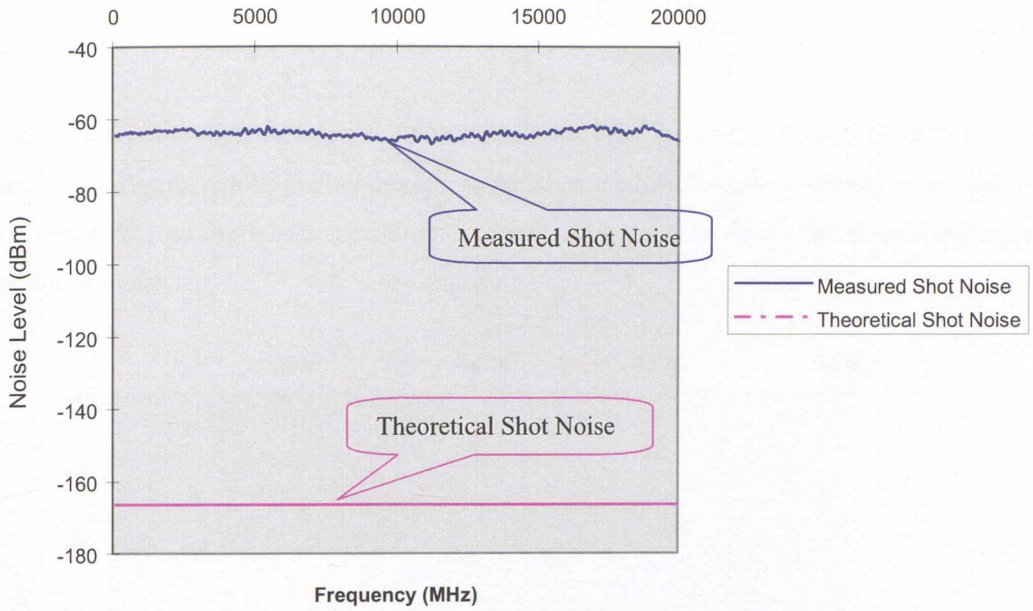

Figure 4-34: Measured Shot noise level response (dark noise subtracted).

As the reference laser operates at a fixed wavelength and the dut could operate anywhere in the telecommunications windows an adjustment factor needs to be incorporated to take into account detector responsivity differences. This will enable the system calibration factor to be corrected for the wavelength of the DUT.

$$\text{Responsivity Factor} = \frac{\beta_{dut}^2}{\beta_{ref}^2} \tag{4-9}$$

The responsivity (β) of the detector at the wavelengths of interest can be derived from the measured optical power (P_{opt}) at the input of the ultrafast detector and the recorded photocurrent i_{dc} as follows:

$$\beta = \frac{i_{dc}}{P_{opt}} \quad A/W \tag{4-10}$$

Using this photocurrent the equivalent shot noise power (N_q) can be calculated to derive the system calibration factor for the wavelength of the laser under test.

$$\text{Syscal} = \frac{\beta_{dut}^2}{\beta_{ref}^2} \frac{(N_{ref}) - (N_{drk})}{2qi_{dc}R} \tag{4-11}$$

The system calibration factor will automatically account for system frequency responsivity, gain, noise figure, resolution bandwidth, impedance mismatch, voltage divider effect etc., of the system across the whole measurement range. Figure 4-35 shows the system calibration for this example.

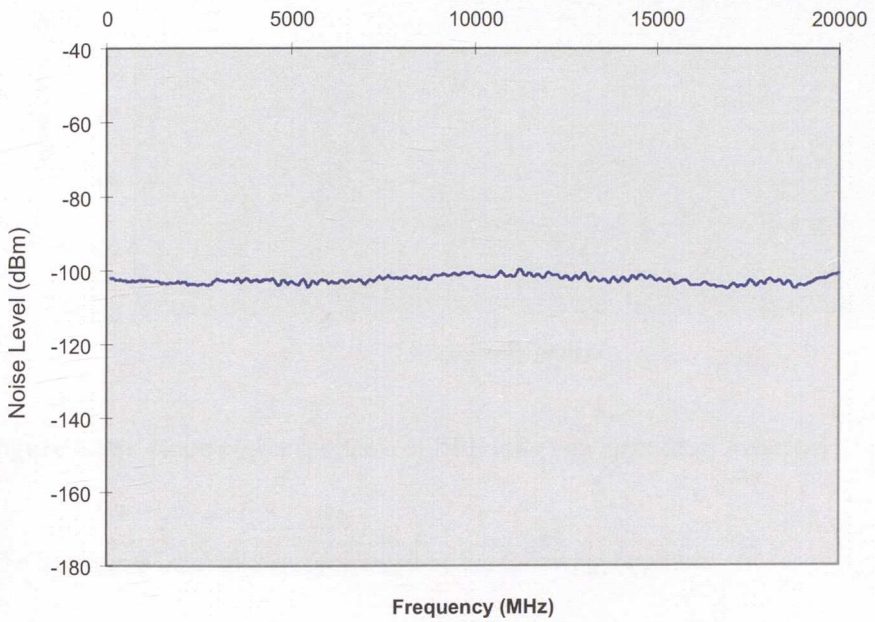

Figure 4-35: Calibration factor as a function frequency.

Its worth noting that the calibration factor calculated here is appropriate for wideband noise. If the signal to be measured was narrowband an adjustment in the above calibration factor of 2 dB would be necessary, as discussed in section 3.4.6. However, for the type of measurements undertaken in this report the spontaneous noise contributions are generally broadband and the calibration factor demonstrated will be appropriate.

4.4.2 Measurement of Relative Intensity Noise of the Device Under Test

For demonstration purposes the 'device under test' measurements have been carried out on a DFB laser manufactured by GEC Marconi. The laser was driven from a low noise (IEEE controlled) power supply and from rechargeable batteries. The laser was optically isolated in free space and a further fibre isolator incorporated in the optical fibre path. Martock mounts

were used throughout to aid stability and alignment of the singlemode optical fibres. The noise spectrum of the DUT was measured as a function of frequency at the same photo current as the reference laser. This can be seen in the graph below.

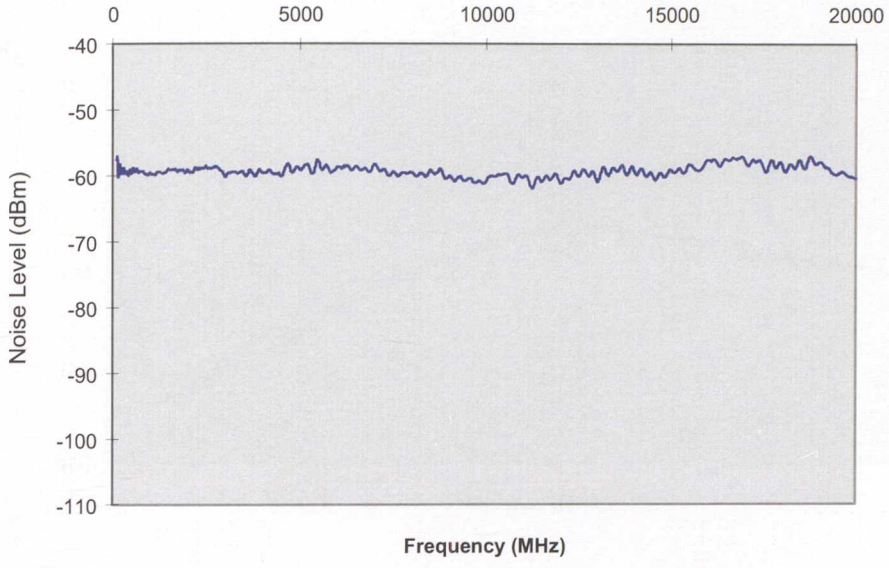

Figure 4-36: Noise power spectrum of DFB laser as a function of frequency.

The laser noise measured is represented by the following equation:

$$(N_{dut}) = Syscal(N_{th}) + Syscal(N_q) + Syscal(N_L) \quad Watts \tag{4-12}$$

Having previously determined the Syscal factor and measured the thermal and shot noise terms the laser spontaneous noise (N_L) can be simply deduced by the following steps:

The reference laser (N_{ref}) response is subtracted from the device under test (N_{dut}) response. As the photocurrents for both measurements have been matched the resultant shot noise can be cancelled along with the thermal noise component hence leaving the spontaneous noise power of the dut and the system calibration factor, see Figure 4-37.

$$(N_{dut})-(N_{ref}) = Syscal(N_{th}) + Syscal(N_q) + Syscal(N_L) - Syscal(N_{th}) + Syscal(N_q) = Syscal(N_L) \quad Watts \tag{4-13}$$

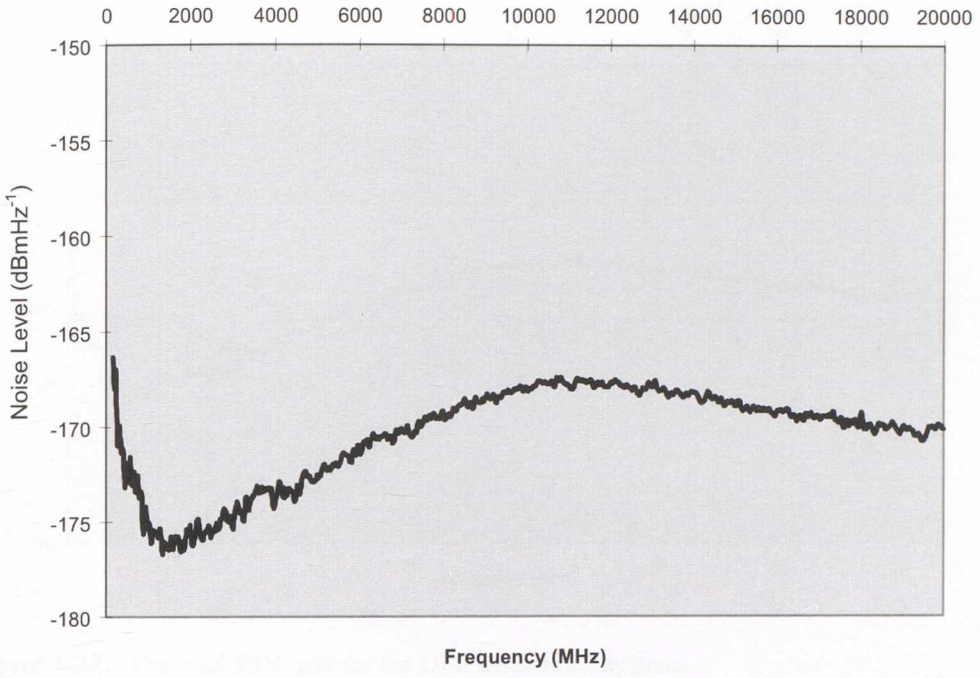

Figure 4-37: Spontaneous noise of the laser under test as a function of frequency.

As we have already derived the system calibration factor (Syscal) for the wavelength of interest the laser spontaneous noise (N_L) can be determined.

$$N_L = \frac{(N_{dut}) - (N_{ref})}{\text{Syscal}} \quad Watts \tag{4-14}$$

The remaining noise power (N_L) is divided by the average electrical power to obtain the spontaneous RIN level of the DUT at each frequency point.

$$RIN_{Laser} = 10\,Log_{10}\frac{N_L}{i_{dc}^2 R}\,dBHz^{-1} \tag{4-15}$$

This measurement procedure is repeated five times and the mean value quoted as the Laser spontaneous noise present at the input of the photo-detector.

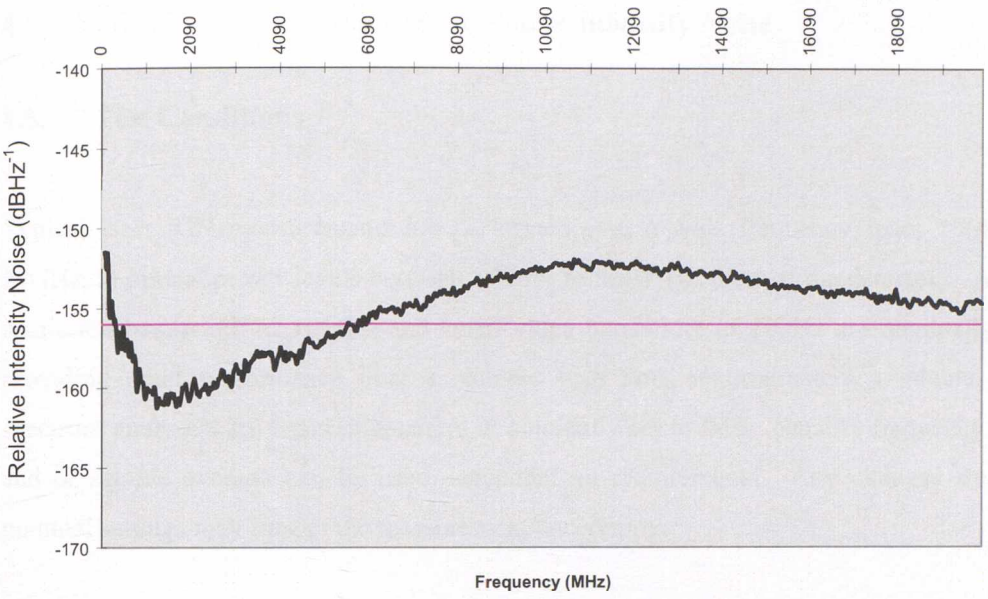

Figure 4-38: The final RIN data for the DFB laser diode system.

Figure 4-38 shows the spontaneous noise spectrum in the classical units of RIN ($dBHz^{-1}$) after compensating for system frequency response. Also plotted is the shot noise of the system at the tested optical power (red solid line). It can be seen that the spontaneous noise of the laser under test is greater than the shot noise except for the frequency band from 200MHz to 5.5GHz. This is the main modulation bandwidth window for sub 2.5Gb/s systems which this laser is intended.

4.5 Definition of Uncertainties – Relative Intensity Noise

4.5.1 Test Conditions

Typical laser RIN measurements are performed over a wide frequency span, 10MHz to 20GHz, at optical power levels between 100uW to 5mW (incident at the detector). A large resolution bandwidth of 10MHz and small video bandwidth of 100Hz are nominally used providing good performance over a realistic scan time, approximately a minute. The spectrum analysers RF input attenuation is nominally set to 0dB. Smaller frequency spans and or sample average can be used dependant on requirements. Any changes from the nominal settings may impact the measurement uncertainty.

It is imperative that high levels of optical isolation (60dB minimum) and counter angled fibre connectors are used within the system to minimise the effects of reflections. Laser RIN will vary as a function of diode temperature and drive current, therefore it is important that these parameters are specified by the customer as well as the optical power. RIN levels can also be affected by the laser power supply used, i.e. contributing noise itself. For these reasons customers are encouraged to provide necessary laser diode power supplies and coolers, as would be used in an end application so as to provide meaningful RIN measurements that can be applied to optical communication systems.

The reference plane for the laser RIN measurement is the light incident on the ultra fast photo detector. Laser RIN values are quoted at the optical power incident on the detector together with frequency tested following the test procedure described in Appendix D. The high system sensitivity allows laser RIN measurements down to the shot RIN level and even below to be achieved, although at a higher uncertainty level.

4.5.2 Equipment

Table 4-1: Equipment used in the Relative Intensity Noise system

Description	Model No.	Manufacturer	Serial Number	Cal Interval	Cal by
DUT PSU	LDC404B	Profile	02210	1 yr	SESC
Optical Attenuator	8156A	HP	3328G01374	1 yr	HP
Fibre Isolator 1300nm 1550nm	M-PI-2-13-S-B-B-A-1 M-PI-2-15-S-B-B-A-1	FOCI FOCI	011414 011409	------- -------	
Reference Laser	125-1319-100	Lightwave	139	1 yr	In-house
Detector System 1 Ge photodiode Thermoelectric cooler Amplifier	J16TE2 TEC2-030 SP043	EG&G Alpha Omega Vinculum	802043 2-9911 C125/1	6 months 6 months 1 yr	NPL as Pair SESC
Ultra Fast Detector	1414	NewFocus	0761	1 yr	In-house
Electrical DMM	2000	Keithley	0636295	1 yr	SESC
Bias Tee	5541A	Picosecond Pulse Labs	415 10/96	1 yr	SESC as system
RF Amplifier	JS42-00102000-25-8P-42	Miteq	394841	1 yr	SESC as system
Spectrum Analyser	FSEM30	Rohde & Schwarz	1079850030	1 yr	SESC as system
Optical DMM & Head	OMM6810B OMH6725B	ILX ILX	68102033 67252016	1 yr 1 yr	OTC OTC

4.5.3 Measurement Uncertainties

The overall expression to obtain Laser RIN from the measurements obtained is as follows:

$$RIN = 10Log\frac{P_{optdut}^2.i_{ref}^3.2.q\Delta f\left(N_{dut}-N_{ref}\right)}{P_{optref}^2.i_{dut}^4\left(N_{ref}-N_{Drk}\right)}\ dB/Hz \qquad (4\text{-}16)$$

From this expression it can be seen that there are eight separate systematic measurement quantities which will have their own measurement uncertainty consisting of systematic and random elements. Uncertainty budgets for each measurement have been established and can be seen in the following sections.

A complete combined uncertainty budget consists of these systematic uncertainties and also any random components associated with the RIN measurement. Due to the complexity of the RIN expression and that some of the input quantities are correlated, for instance the RF noise level measurements, the functional relationship of each input quantity has been derived. This was achieved using partial differentiation and enables the calculation of change in RIN for any change in input quantity. This also enables uncertainties to be derived specifically for each RIN measurement performed.

These functional relationships are used to obtain the systematic uncertainties of each input quantity in the combined uncertainty budget. Often functional relationships have the effect of reducing the overall uncertainty but the uncertainties calculated in this report do not account for this. Also the highest levels of individually calculated systematic uncertainties have been used regardless of test conditions, e.g. frequency point, wavelength, optical power.

Hence these two points indicate that the combined systematic uncertainty represents an extreme **worst case** uncertainty.

The Uncertainty Budget outlined here represents a base line from which many improvements can be made in reducing the uncertainty level by:

- compiling measurement parameter specific uncertainty budgets
- performing further repeat measurements, building history
- minimising calibration uncertainties of components
- reducing measurement span, focusing on one frequency point, increasing accuracy
- perform measurements at different optical powers to enable linear fitting procedure.

4.5.4 Combined Uncertainty Budget

Formulation of the RIN uncertainty budget follows the guidelines laid down by the UKAS, formally NAMAS, NIS3003 Edition 8 and the Qinetiq Quality System.

Table 4-2: Combined uncertainty budget – Relative Intensity Noise

Symbol	Source of uncertainty	Value (± %)	Probability Distribution	Divisor	Ci	Ui(RIN) (± %)	Vi or Veff
δPoptref	Optical Power - Ref	1.463	normal	1.000	2.000	2.927	∞
δPoptdut	Optical Power - DUT	1.537	normal	1.000	2.000	3.074	∞
δIref	Photocurrent - Ref	0.586	normal	1.000	3.000	1.758	∞
δIdut	Photocurrent - DUT	0.586	normal	1.000	4.000	2.344	∞
δNdrk	Dark noise level	1.145	normal	1.000	0.804	0.921	∞
δNref	Ref noise level	5.023	normal	1.000	-3.831	-19.245	∞
δNdut	DUT noise level	4.477	normal	1.000	0.804	3.600	∞
δf	Bandwidth Error	5.000	normal	1.000	1.000	5.000	∞
δT	Temperature Stability (19-23)	5.158	rectangular	1.732	1.000	2.978	∞
	Repeatability	10.875	normal	1.000	1.000	10.875	4
Example: High optical power, Laser RIN = Shot RIN							
				Nref	-59.23	Ndrk	-62.737
				Ndut	-57.49	RIN(dB/Hz)	-158.18
Uc(RIN)	Combined uncertainty (%)		normal			23.726	>100
U	Expanded uncertainty (%)		normal(k=2)			47.452	>100
Uc(RIN)	Combined uncertainty (dB)		normal			1.176	>100
U	Expanded uncertainty (dB)		normal(k=2)			2.352	>100

Notes:

1. RIN measurement is based on an average of five repeats
2. RIN measurement consists of a complete scan from 10MHz to 20GHz
3. Resolution bandwidth 10MHz, video bandwidth 100Hz, RF attenuation 0dB
4. dut laser RIN equal to shot RIN, i.e. **worst case spec**

It can be seen that the combined uncertainty for this worst case laser (i.e. down to RIN shot level) is <±1.18dB, giving an expanded uncertainty of ±2.35dB at 95% confidence level.

The dominant uncertainties for the measurement of RIN are in determining the dut noise level, reference laser confidence, and RIN measurement repeatability. The dut uncertainty consists primarily of spectrum analyser log scale fidelity, system linearity and wavelength dependant frequency response. Initial assessments have been performed on these uncertainties forming a pessimistic view which, and after further assessment are predicted to fall.

Confidence in the reference laser spontaneous noise content is within ±4%. In the measurement example above, i.e. worst case, we are subtracting very small values which increase the measurement uncertainty. If higher values of laser RIN are measured this uncertainty will reduce significantly. For example, a laser RIN 8dB above the shot RIN decreases the RIN systematic δN_{ref} to 11.68% with a combined uncertainty of 0.877dB worst case.

The random uncertainty, RIN repeatability has been based on previous repeat measurements on individual devices, and also by assessing the system calibration factor repeatability. This represents a conservative uncertainty which when assessing a well isolated, FC/APC coupled dut will be less. Effects of laboratory temperature variation have been assessed concerning RIN over a 5°C range. This forms an extreme case as laboratory temperature is controlled to within 21°C ±2 and rapid excessive changes, from previous monitoring are not experienced. A maximum variation of 0.23dB was observed. It will be possible, in time to minimise this uncertainty further.

The following sections identify the uncertainty budgets for each of the combined uncertainty terms.

4.5.5 Optical Power Measurement Uncertainty Budget

Two optical power measurements are performed for the derivation of laser RIN, one being that incident on the photodetector by the DUT and the other being the reference laser, P_{optdut} and P_{optref} respectively. Due to poor stability over long periods of time the New Focus Detector is not operated as a calibrated power meter. Instead it is effectively calibrated during each laser RIN measurement using a established transfer detector, calibrated by NPL, and an allowance has been made for connectivity errors. Optical power measurement provides the traceable link to National Standards for the RIN measurement system.

Table 4-3: DUT optical power budget

Symbol	Source of uncertainty	Value (± %)	Probability Distribution	Divisor	Ci	Ui(Poptdut) (± %)	Vi or Veff
	Standard Detector Uncert (NPL)	1.000	normal	2.000	1.000	0.500	∞
	Detector Linearity Error (NPL)	1.500	normal	2.000	1.000	0.750	∞
	Detector Amp Resolution Error	0.200	rectangular	1.732	1.000	0.115	∞
	Detector Amp Uncert (SESC)	0.050	normal	2.000	1.000	0.025	∞
	Detector Amp Linearity Error	0.026	rectangular	1.732	1.000	0.015	∞
	Detector Amp Drift over 6 mths	0.100	rectangular	1.732	1.000	0.058	∞
	Wavelength Error	0.553	rectangular	1.732	1.000	0.319	∞
	Responsivity Interpolation Err	0.600	rectangular	1.732	1.000	0.346	∞
	Repeatability	1.145	normal	1.000	1.000	1.145	49
Uc(Poptdut)	Combined uncertainty		normal			1.537	>100
U	Expanded uncertainty		normal (k=2)			3.074	>100

Table 4-4: Reference optical power budget

Symbol	Source of uncertainty	Value (± %)	Probability Distribution	Divisor	Ci	Ui(Poptref) (± %)	Vi or Veff
	Standard Detector Uncert (NPL)	1.000	normal	2.000	1.000	0.500	∞
	Detector Linearity Error (NPL)	1.500	normal	2.000	1.000	0.750	∞
	Detector Amp Resolution Error	0.127	rectangular	1.732	1.000	0.073	∞
	Detector Amp Uncert (SESC)	0.050	normal	2.000	1.000	0.025	∞
	Detector Amp Linearity Error	0.026	rectangular	1.732	1.000	0.015	∞
	Detector Amp Drift over 6 mths	0.100	rectangular	1.732	1.000	0.058	∞
	Wavelength Error	0.127	rectangular	1.732	1.000	0.074	∞
	Responsivity Interpolation Err	0.100	rectangular	1.732	1.000	0.058	∞
	Repeatability	1.145	normal	1.000	1.000	1.145	49
Uc(Poptref)	Combined uncertainty		normal			1.463	>100
U	Expanded uncertainty		normal (k=2)			2.927	>100

The transfer detector used is a EG&G germanium photodiode combined with a thermoelectric cooler and amplifier unit. Traceability is obtained via NPL and SESC, summary of results shown in Appendix B and following sections.

4.5.5.1 Calibration of the SP043 amplifier

The following uncertainties are included in the optical power measurement uncertainty budget. Some uncertainties, such as amplifier offset are compensated for before measurements are performed.

4.5.5.1.1 Linearity of amplifier :

From the calibration certificate the worst case deviation from the applied value is 0.026% (0.001dB)

4.5.5.1.2 SESC uncertainty of measurement

The worst case value is ±0.05%. (0.002dB)

4.5.5.1.3 Drift in amplifier calibration during one year calibration period

The worst case value is ±0.1% (0.004dB), derived from previous history of similar amplifiers.

4.5.5.1.4 Amplifier resolution error

Scale range used is the preamp (1mA), providing 0.0000 scale. The worst case resolution uncertainty for the P_{optref} and P_{optdut} is as follows:

P_{optref}, 1319nm Responsivity = 0.786A/W

Worst case optical power 100uW, hence 78.6μA

Error = 0.0001/0.0786 = **0.127%**

P_{optdut}, 1600nm Responsivity = 0.501A/W

(worst case) Worst case optical power 100uW, hence 50.1μA

Error = 0.0001/0.0501 = **0.2%**

4.5.5.2 Additional optical power measurement uncertainties

The following uncertainties are included in the optical power measurement uncertainty budget. Some uncertainties, e.g. ref & dut wavelength stability (0.0003 & 0.1nm respectively) has been established as having minimal affect on responsivity uncertainties. This is also the case for Polarisation Dependant Loss (PDL) of both the transfer detector and

ultrafast detector, when overall uncertainties are > 1%. Both types of detector are historically known to be very uniform devices and due to the incident optical light being significantly small (i.e. single mode fibre) this reduces uncertainties regarding PDL.

4.5.5.2.1 Wavelength accuracy uncertainty on responsivity.

The ILX optical DMM has a wavelength uncertainty of ±1nm

P_{optref}, 1319nm ±1	Responsivity	@ 1318nm 0.785A/W
		@ 1319nm 0.786A/W
	Corresponding Error = 0.001/0.786 = **0.127%**	
P_{optdut}, 1600nm ±1	Responsivity	@ 1599nm 0.5038A/W
(worst case)		@ 1600nm 0.501A/W
	Corresponding Error = 0.0028/0.501 = **0.553%**	

4.5.5.2.2 Drift in transfer detector calibration during 6 month calibration period

Only one calibration has been carried out by NPL at present, hence an uncertainty estimate for drift will be assessed after the next 6 month calibration.

4.5.5.2.3 Optical power repeatability (random).

Repeatability of absolute power measurements has been found to be no worse than 0.1dB, 1.145%. This includes stability uncertainties of the ref laser and typical dut lasers expected and connectivity uncertainties.

4.5.6 Photocurrent measurement uncertainty budget

Two measurements of dc photocurrent are performed, for the reference and dut signals, to establish the shot noise level enabling matching and calculation of system calibration.

The dc photocurrent is derived by measuring the dc voltage across the nominal 50Ω ultra fast photodetector termination, ie I = V/R, using the Keithley 2000 DMM. Assessments of dark current offset, resistance stability & bias current stability have negligible influence. Due to the transfer detector and reference laser technique the linearity of the ultrafast detector does not need to be known, it is naturally compensated for during each RIN measurement.

Table 4-5: DUT photocurrent uncertainty budget

Uncertainty Budget for measurements of DUT photocurrent (Idut) using Keithley 2000 DMM							
Symbol	**Source of uncertainty**	**Value (± %)**	**Probability Distribution**	**Divisor**	**Ci**	**Ui(Idut) (± %)**	**Vi or Veff**
dV	Uncertainty of voltage	0.149	rectangular	1.732	1.000	0.086	∞
dR	Uncertainty of resistance	0.013	rectangular	1.732	1.000	0.008	∞
	Photocurrent Match (max)	0.500	normal	1.000	1.000	0.500	∞
	Photocurrent Drift	0.500	rectangular	1.732	1.000	0.289	∞
	Repeatability	0.051	normal	1.000	1.000	0.051	99
Uc(Idut)	Combined uncertainty		normal			0.586	∞
U	Expanded uncertainty		normal (k=2)			1.172	∞

Table 4-6: Reference photocurrent uncertainty budget

Uncertainty Budget for measurements of Reference photocurrent (Iref) using Keithley 2000 DMM							
Symbol	**Source of uncertainty**	**Value (± %)**	**Probability Distribution**	**Divisor**	**Ci**	**Ui(Iref) (± %)**	**Vi or Veff**
dV	Uncert of voltage	0.149	rectangular	1.732	1.000	0.086	∞
dR	Uncert of resistance	0.013	rectangular	1.732	1.000	0.008	∞
	Photocurrent Match (max)	0.500	normal	1.000	1.000	0.500	∞
	Photocurrent Drift	0.500	rectangular	1.732	1.000	0.289	∞
	Repeatability	0.051	normal	1.000	1.000	0.051	99
Uc(Iref)	Combined uncertainty		normal			0.586	∞
U	Expanded uncertainty		normal (k=2)			1.172	∞

4.5.6.1 Voltage Measurement Uncertainty

The input impedance of the DMM itself is large enough (>10GΩ) to have negligible uncertainty contribution. Also noise immunity has been addressed by using minimum length screened lead. The nominal value of the resistor is 50Ω, this value being used for the purpose of the following voltage uncertainty calculations.

The following DMM ranges (DC voltage) are used to measure the voltage across the resistor for typical photocurrent range of 50uA to 4mA:

100mV: Photocurrent 50uA to 2mA

1V: Photocurrent >2mA

The % uncertainty of the measurement will decrease as the voltage measured increases, therefore only the minimum values of voltage for each range are used to calculate the uncertainty.

100mV Range: Photocurrent 50uA to 2mA

Slow rate response selected

Instrument Accuracy (1 Year, 23°C ±5°) = ±50ppm of reading + 35ppm of range

Number of digits displayed = 000.0000

Resolution = 0.1uV

Uncertainty at 50uA

Voltage measured 50uA x 50Ω = 2.5mV

Accuracy @ 2.5mV = (2.5mV x 50ppm/2.5mV) x 100 = ±0.005%

Uncertainty due to range = (0.0035mV/2.5mV)x100 = 0.14%

Uncertainty due to resolution = (0.0001mV/2.5mV)x100 = 0.004%

Total Uncertainty 0.005 + 0.14 + 0.004 = **±0.149%** (Worst case)

1V Range: Photocurrent > 2mA

Slow rate response selected

Instrument Accuracy (1 Year, 23°C ±5°) = ±30ppm of reading + 7ppm of range

Number of digits displayed = 0.000000

Resolution = 1.0uV

Uncertainty at 2mA

Voltage measured 2mA x 50Ω = 100mV

Accuracy @ 100mV = (100mV x 30ppm/100mV) x 100 = ±0.003%

Uncertainty due to range = (7.0uV/100mV)x100 = 0.007%

Uncertainty due to resolution = (1.0uV/100mV)x100 = 0.001%

Total Uncertainty 0.003 + 0.007 + 0.001 = **±0.011%** (Worst case)

The temperature coefficient of the DMM for conditions between 23°C±5°C, has already been compensated for in the above uncertainties and as the laboratory temperature is controlled to 21°C±2°C temperature variations can be considered negligible.

The Maximum Uncertainty due to the DMM voltage measurements is **±0.149%** over the range of interest.

4.5.6.2 Resistance Measurement Uncertainty

The photo detectors output resistance nominally 50Ω, is measured by the Keithley 2000 DMM in two terminal mode with the photo detector unbiased. Range used: 100Ω

100Ω Range: Nominal 50Ω

Slow rate response, two termination selected

Instrument Accuracy (1 Year, 23°C ±5°) = 100ppm of reading + 40ppm of range

Number of digits displayed = 000.0000

Resolution = 0.1mΩ

Uncertainty at 50Ω

Accuracy @ 50Ω = (50 x 100ppm/50) x 100 = ±0.005%

Uncertainty due to range = (0.004/50)x100 = 0.008%

Uncertainty due to resolution = (0.0001/50)x100 = 0.0002%

Total uncertainty 0.005 + 0.008 + 0.0002 = **±0.0132%** (Worst case)

The temperature coefficient of the DMM for conditions between 23°C±5°C, has already been compensated for in the above uncertainties and as the laboratory temperature is controlled to 21°C±2°C temperature variations can be considered negligible.

The maximum uncertainty due to the DMM resistance measurements is **±0.0132%** over the range of interest.

4.5.6.3 Photocurrent matching and drift uncertainty

An important area of the laser RIN measurement is the matching of the reference shot noise to the dut. *Trade-off's* occur between improving the match, hence reducing uncertainties

and in operating a practical facility. Experience has shown that reliable measurements are obtained when matching of <1% is achieved. Both matching and drift uncertainties are largely dependant on the dut and fibre coupling used. Improvements can be made by tracking the photocurrent during RF sampling which allows matching & drift to be calculated for each measurement and included in the uncertainty budget and or by reducing the measurement scan time.

The affect of different matching and drift uncertainties on the combined RIN uncertainty level is shown in Figure 4-39.

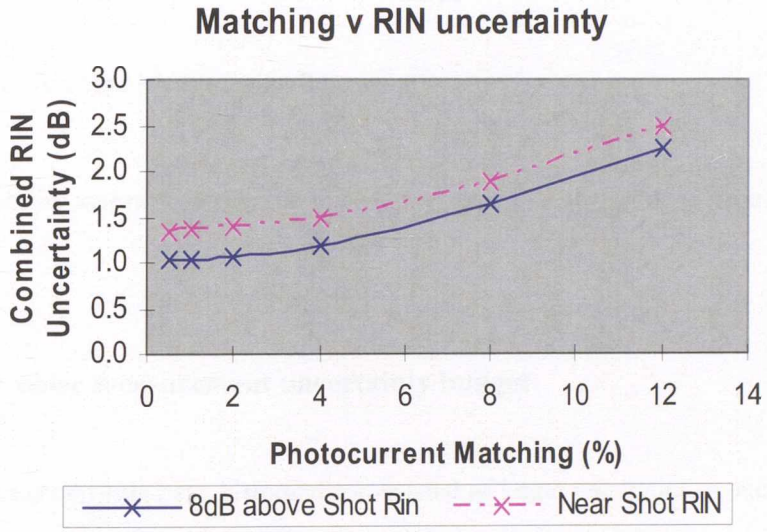

Figure 4-39: Impact of photo current matching on overall uncertainty.

4.5.6.4 Random Uncertainties

The repeatability of measurement is largely dominated by the source laser power stability, as there are no disconnection/reconnection uncertainties involved. Hence a generous uncertainty as been established for the voltage repeatability using the reference laser as a source. One hundred samples were taken resulting in an uncertainty of 0.0507% for 50μW optical input and reduced uncertainties at higher powers.

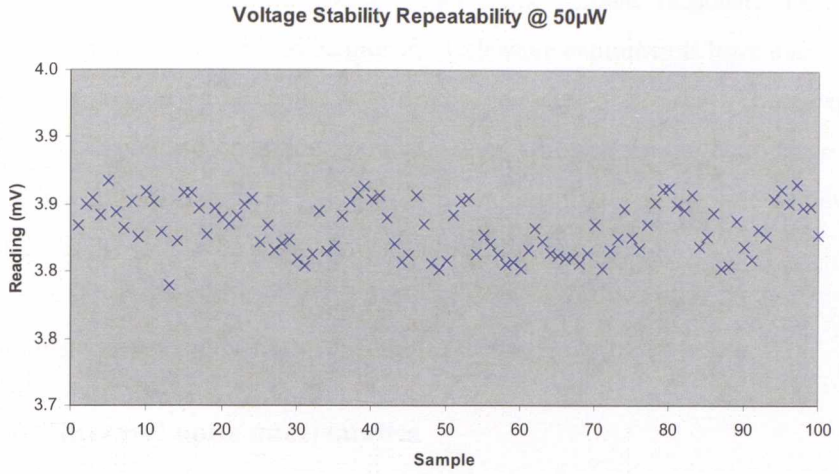

Figure 4-40: Voltage Measurement Repeatability.

Resistor stability assessments, similar to above resulted in a negligible uncertainty being observed.

4.5.7 RF noise measurement uncertainty budget

RF noise measurements have historically consisted of larger uncertainties due, in part to the randomness nature of noise. Many uncertainties have to be addressed for absolute measurements, for example mismatch losses, noise figure, connector losses, wideband smoothing effects, etc. The referencing measurement technique discussed in section 3.4 was developed to reduce the level of noise measurement uncertainty.

The key feature of the RIN measurement technique is in the use of a reference laser, providing a source to enable ratio metric techniques to be performed. Ratio methods naturally compensate for a number of systematic uncertainties which in regard to RF measurements can be significantly high. Examples of these compensated uncertainties are system gain, noise figure, mismatch losses, spectrum analyser filters, offsets, etc.

Another significant advantage of the reference source is in the fact that the device under test (dut) noise is compared on a *like for like* basis, i.e. the reference laser acts as a wideband noise source like the dut. From the previous section 3.4.6, regarding measurement of wide band and narrow band signals using a spectrum analyser, disparity was shown to exist, hence errors may result regarding existing RIN measurement techniques. For this technique to be

valid confidence in the reference laser's shot noise limited response (i.e. negligible spontaneous noise content) needs to be gained. Extensive experiments have been performed to test the confidence of the reference laser source, see section 4.5.10.3. These experiments have increased our confidence and are now at a level whereby further confidence will only be gained when improvements in associated measurement technology are achieved. The reference laser is proving to be a very powerful measurement tool.

The measurement uncertainties of the three noise scans are discussed below.

4.5.8 Dark/thermal noise uncertainties

The uncertainty components of N_{drk} are shown in Table 4-7. Due to the referencing measurement technique only two uncertainties have any significant affect.

Table 4-7: Dark/thermal noise uncertainty budget

Symbol	Source of uncertainty	Value (±dB)	Probability Distribution	Divisor	Ci	Ui(Ndrk) (±dB)	Vi or Veff
	SA Resolution Error	0.0001	rectangular	1.7321	1.0000	0.0001	∞
	Repeatability	0.0500	normal	1.0000	1.0000	0.0500	>1000
Uc(Ndrk)	Combined uncertainty		normal			0.0500	>100
U	Expanded uncertainty		normal (k=2)			0.1000	>100

4.5.8.1 Spectrum analyser resolution error

The absolute noise power reading on the spectrum analyser provides four decimal places, i.e. 0.0001dB's. This represents the resolution uncertainty for the spectrum analyser.

4.5.8.2 Random uncertainties

RF Random uncertainties are significantly dependant on the spectrum analyser bandwidths and sampling time. Hence repeatability has been assessed under the same conditions that the system will be nominally used, ie resolution and video bandwidth of 10MHz and 100Hz. Results from over 1000 samples, provides a maximum uncertainty of 0.05dB. Repeat measurements have been performed at other spectrum analyser conditions.

4.5.9 DUT noise uncertainties

The power behind this measurement technique in reducing uncertainties is in the use of a reference source. For this reason it is important to identify possible causes of error between the reference and dut as these will be dominant. The N_{drk} term is common to both N_{ref} and N_{dut} terms hence measurement uncertainties will only be applicable over the range difference between N_{ref} and N_{dut}.

The worst case measurement scenario is when measuring a low noise laser, i.e. subtracting a small number away from another small value. Uncertainties in this measurement will significantly affect the end result, giving a higher combined uncertainty. With this in mind, the test procedure has been developed to minimise uncertainties at lower RIN levels.

Table 4-8: Device Under Test (DUT) noise measurement uncertainty

Uncertainty Budget for measurements of Dut noise (Ndut)							
Symbol	**Source of uncertainty**	**Value (±dB)**	**Probability Distribution**	**Divisor**	**Ci**	**Ui(Ndut) (± dB)**	**Vi or Veff**
	SA Log Fidelity Error	0.0100	normal	1.0000	1.0000	0.0100	∞
	System Linearity (20dB)	0.2500	rectangular	1.7321	1.0000	0.1443	∞
	SA Resolution Error	0.0001	rectangular	1.7321	1.0000	0.0001	∞
	Wavelength Dependant Freq Error	0.2200	rectangular	1.7321	1.0000	0.1270	∞
	Repeatability	0.0500	normal	1.0000	1.0000	0.0500	>1000
Uc(Ndut)	Combined uncertainty		normal			0.1989	>100
U	Expanded uncertainty		normal (k=2)			0.3978	>100

4.5.9.1 Spectrum Analyser Log Scale Fidelity Error

The log scale fidelity error is often quoted as a linear/log error per division, up to a maximum value[52]. The nature of the RIN measurement, i.e. the N_{ref} and N_{dut} scans may be at different locations on the spectrum analyser screen, requires this error to be included as a systematic. Assessment of the spectrum analyser Log scale fidelity error has established an error of 0.1dB/10dB.

To minimise Log scale fidelity errors for RIN measurement the spectrum analyser reference level is adjusted to obtain signal traces on the same area of the screen for the lowest noise levels (i.e. worst case). By achieving a match of < 1dB on the screen for the lowest noise level, the maximum error will be 0.01dB. As laser RIN peaks at the resonant frequency the highest noise level may be say 20dB or more higher than the reference trace which will result in a corresponding log scale fidelity error of 0.2dB. However, the actual reference

noise signal in this case is 20dB less than the dut, equivalent to 1% (i.e. has negligible affect when subtracted) which has the effect of reducing the error to less than 0.01dB. Hence the worst case Log scale fidelity error is 0.01dB.

For duts that are significantly noisy over the whole scanning range, the log scale fidelity error will effectively be reduced as the reference signal will have negligible influence after subtraction.

4.5.9.2 System Linearity Uncertainty

Linearity of the system, i.e. bias Tee, Amplifier and Spectrum Analyser have been assessed together using a number of techniques by SESC. Linearity of the system is predominantly limited by the saturation point of the amplifier. The saturation input level is typically -10dBm which over a 20GHz bandwidth corresponds to an input noise level of -113dBm/Hz. N_{dut} noise levels expected will be typically up to 20dB above the thermal noise floor (-154dBm/Hz), hence well within the linear range of the amplifier.

Assessments carried out to establish the small linearity error over this low signal range indicates a maximum error of <0.25dB over a 50dB range. This is a pessimistic uncertainty, but further confidence needs to be gained before this uncertainty can be reduced. Assessments performed on the spontaneous noise content of the reference laser, 4.5.10.3 provides evidence that system linearity error is less than 0.25dB. In the future the reference laser may enable assessment of system linearity errors to better accuracies than traditional methods.

As we are performing a ratio metric measurement the linearity uncertainty of interest will be over the range between the two noise levels, N_{ref} and N_{dut} which will typically be <20dB. Noise levels over a wider range than this will have the effect mentioned in section 4.5.10.1, whereby N_{ref} becomes negligible compared to N_{dut} . Hence an uncertainty of 0.25dB over 50dB represents a pessimistic level which is expected to reduce in due course.

4.5.9.3 Wavelength Dependant Frequency Response Uncertainty

In most cases when performing measurements the DUT wavelength will not be the same as the reference source. For this reason the wavelength dependence of the ultrafast detector has been assessed. Detector responsivity is derived by the dc photocurrent and optical power, which is compensated for by the system calibration factor. But slight variations in the

frequency response characteristic from wavelength to wavelength will give rise to an error. For this reason a diode pumped Erbium doped glass laser from Amoco Laser Company was borrowed to be able to assess frequency response variation from 1533nm to 1319nm (i.e. the reference laser). The Amoco laser provides a shot noise limited response, similar to the reference laser. This has been assessed in the same manner as the reference laser, 4.5.10.3. Frequency response measurements at each wavelength indicate a maximum variation of < 0.22dB being observed. This ties in well with published work in this area of <0.2dB[53]. Other measurement methods are being considered, i.e. Hetrodyne, but the broadband method has the advantage of providing an approach of a similar nature to the RIN measurement system i.e. noise derived. From previous research narrowband and broadband signals couple through measurement systems in different ways due to Rayleigh distribution effects, etc.

Further experiments are planned to examine the exact origin of detectors frequency response characteristic which, due to this broadband approach may become more evident, increasing system understanding and confidence.

4.5.9.4 Random Uncertainty

The repeatability of N_{dut} has been assessed in a similar manner to the dark noise term, with the inclusion of a laser source. Standard uncertainties of far less than 0.05dB were obtained, but due to the dut dependence a pessimistic repeatability of 0.05dB is quoted.

4.5.10 Reference Laser Noise Uncertainties

The RIN measurement technique described in this report relies significantly on the low noise reference source. This reference source N_{ref} enables subtraction of the thermal and shot noise contributions from N_{dut} and also provides a means to calculate the responsivity of the system (Syscal). This is derived by subtracting the thermal noise level, N_{drk} and by substituting the measured shot noise. Similar to the N_{ref} and N_{dut} subtraction, we are only concerned with uncertainties over the range difference between N_{drk} and N_{ref}.

The uncertainty associated with the reference noise measurement consists mainly of the system linearity and assessing the spontaneous noise content of the laser, see Table 4-9.

Table 4-9: Reference noise measurement uncertainty

Uncertainty Budget for measurements of reference noise (Nref)							
Symbol	**Source of uncertainty**	**Value (±dB)**	**Probability Distribution**	**Divisor**	**Ci**	**Ui(Nref) (±dB)**	**Vi or Veff**
	SA Log Fidelity Error (Matched)	0.0100	normal	1.0000	1.0000	0.0100	∞
	System Linearity (12dB range)	0.1500	rectangular	1.7321	1.0000	0.0866	∞
	Spontanteous Noise content	0.2000	normal	1.0000	1.0000	0.2000	∞
	SA Resolution Error	0.0001	rectangular	1.7321	1.0000	0.0001	∞
	Repeatability	0.0500	normal	1.0000	1.0000	0.0500	>1000
Uc(Nref)	Combined uncertainty		normal			0.2238	>100
U	Expanded uncertainty		normal (k=2)			0.4477	>100

4.5.10.1 Spectrum Analyser Log Scale Fidelity Error

The Log scale fidelity error between the reference and dark noise levels is minimised by adjusting the spectrum analyser reference level to obtain N_{ref} at the same screen position as the N_{drk} trace (see test procedure, 7 Appendix A. Due to the flat frequency response of the reference laser, matching of < 1dB is easily achieved which corresponds to a pessimistic worst case log scale fidelity error of 0.01dB.

4.5.10.2 System Linearity Uncertainty

As described previously, 4.5.9.2, system linearity has been assessed over a 50dB range. The range of interest will be between the N_{drk} and N_{ref} levels, which will be a maximum of 12dB (Popt of 5mW).

Over this range the linearity uncertainty will be typically less than 0.25dB, and further assessments suggest the error to be <0.15dB, representing a pessimistic level. This is expected to be reduced in the future when further confidence is gained relating to the reference laser spontaneous noise content.

4.5.10.3 Reference Laser Spontaneous Content Uncertainty

The prime uncertainty which determines the effectiveness of this reference source lies in assessing its spontaneous noise content, to establish a confidence level. A technique has been developed to assess the reference source using least squares fitting routines against known mathematical noise behaviour 3.5.1.

By attenuating the reference laser optical power incident on the ultra fast detector and recording and plotting (in log terms) the dc and rf levels, a linear response (slope = 1) will be observed if the source is shot noise limited. Any spontaneous content will increase the slope factor, hence providing a measure of the reference source performance.

Below demonstrates a typical response gained at 20MHz.

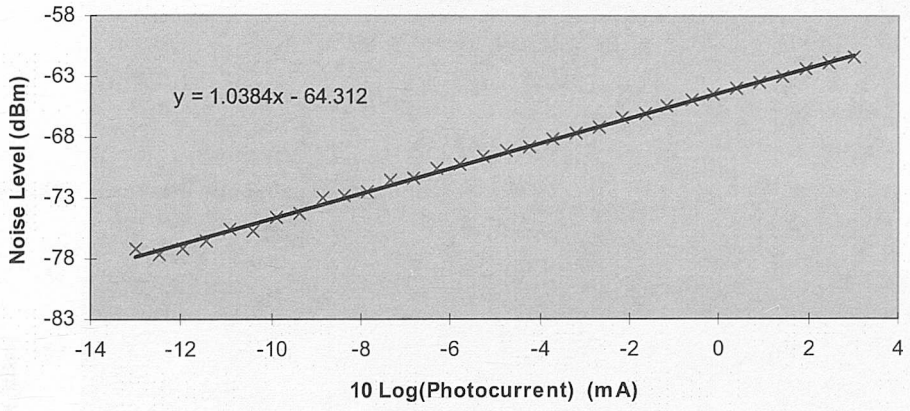

Figure 4-41: Spontaneous noise content at 20MHz.

The gradient of the 20MHz response suggests a spontaneous uncertainty of better than 4%, ie 0.17dB and a standard measurement uncertainty of 0.046dB. From Figure 4-41 it can be seen that the uncertainty level may be improved if the lower signal level stability is improved. Assessing the spontaneous content using the higher level signals only, provides an uncertainty well below 4%. Measurement uncertainties associated which this technique ie system linearity, log scale fidelity, are also contained within this assessment. Hence the spontaneous content will actually be less and the high spontaneous uncertainty in the reference laser budget (N_{ref}) is significantly due to the ability to measure the source rather than the noise of the source itself. Until measurement improvements are made a pessimistic uncertainty of 0.2dB will be used.

The following three responses represent typical responses gained across the frequency range of interest, all being within 4% uncertainty.

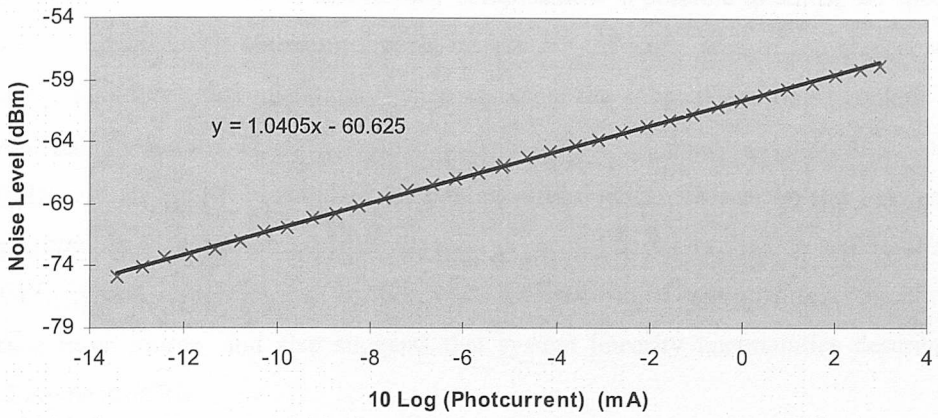

Figure 4-42: Spontaneous noise content at 1GHz.

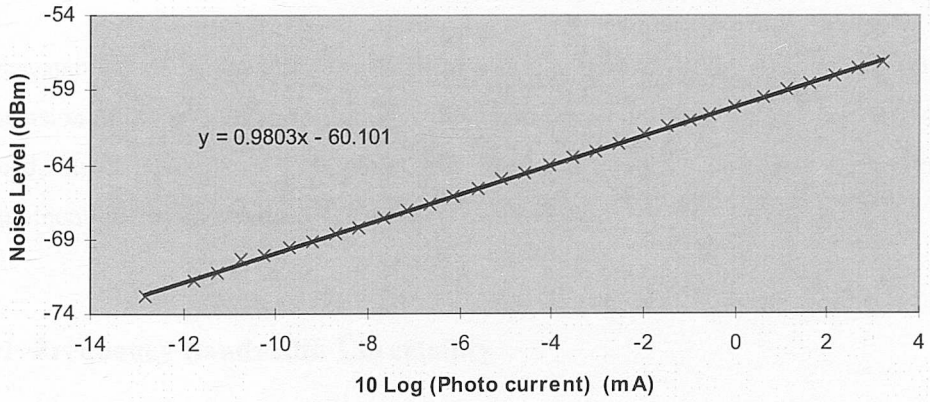

Figure 4-43: Spontaneous noise content at 15GHz.

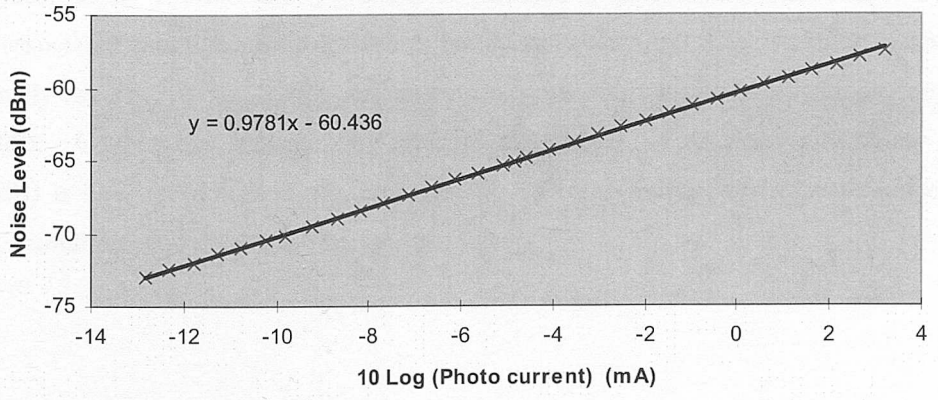

Figure 4-44: Spontaneous noise content at 20GHz.

As mentioned previously, the measurement uncertainties associated which this technique i.e. system linearity, log scale fidelity, are also contained within this assessment. To assess the

impact of the Log scale fidelity uncertainty component it is possible to adjust the spectrum analyser reference level, obtaining signals on exactly the same area of the screen, which effectively eliminates this uncertainty when assessing the spontaneous noise content. The response gained for the 1GHz assessment resulted in a spontaneous contribution of 1% (0.043dB) and an improved standard uncertainty of 0.008dB. This technique has reduced the measured spontaneous by >0.1dB, which is as predicted, due to the Log scale fidelity of 0.1/10dB. Hence, a high level of confidence has resulted from continued assessment of the reference laser source, and also suggests that system linearity uncertainties described in 4.5.9.2 are pessimistic.

4.5.10.4 Random Uncertainty

The repeatability of N_{ref} has been assessed in a similar manner to the dark noise term, with the inclusion of the reference laser source. Standard uncertainties of far less than 0.05dB are obtained, but a pessimistic view of 0.05dB has been quoted. This may be reduced as measurement history increases.

4.5.11 Frequency Bandwidth Uncertainty

To be able to convert the spectrum analyser measurements back to dB/Hz (1Hz bandwidth) we need compensate for the resolution bandwidth used. This is naturally accounted for by the Syscal factor. An uncertainty needs to be included in the combined RIN budget, i.e. the error associated with the spectrum analyser bandwidth switching. The resolution bandwidth nominally used is 10MHz, which corresponds to a maximum bandwidth switching error of <0.22dB. Calibrations indicate this error to be <0.1dB. Hence the uncertainty used (0.22dB) is likely to reduce in the near future. This uncertainty level may be reduced if lower resolution bandwidths (<10MHz) are used.

4.5.12 Associated RIN Measurement Parameters

4.5.12.1 Wavelength Measurement Uncertainty

Wavelength of the dut lasers is measured using the ILX optical multi meter and head, calibrated by OTC. An uncertainty budget has been formed which combines to an uncertainty level of ±1.01nm, or @ 95% confidence ±2.02nm.

4.5.12.2 Frequency Measurement Uncertainty

The frequency measurement is provided by the spectrum analyser having a worst case uncertainty <0.5% @ 95% confidence level.

4.6 Chirp System Assessment

Following the theoretical discussions on the performance of self homodyning interferometers this section sets out to confirm the predicted performances through laboratory controlled testing. This includes assessments of linewidth and chirp under various modulation frequency and amplitude levels. Comparisons are also made between techniques / set ups.

4.6.1 General Chirp Set Up

As previously defined in section 3.6.2, the set up shown in Figure 4-45 is essentially based on the photo detector, amplifier and spectrum analyser used for RIN measurements. Inserted within the optical fibre path is the 'birefringence insensitive' interferometer (BII), utilising Faraday rotating mirrors. Additionally a second interferometer was assembled consisting of two couplers and 2 optical paths (long and short) and a polarisation adjuster. This represents the traditional or standard self homodyning approach and allowed comparisons to be investigated.

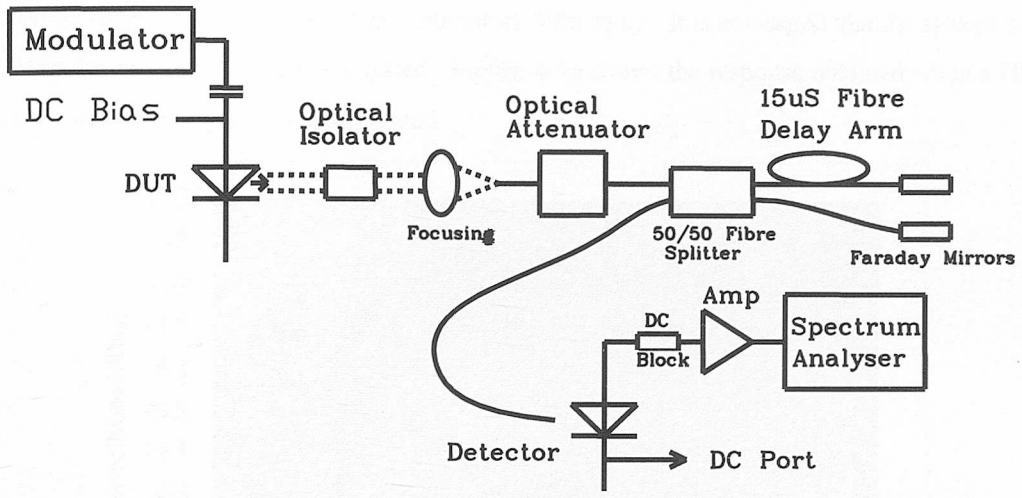

Figure 4-45: General chirp / linewidth measurement set up.

A fibre path length 1.5km of standard single mode fibre was selected for the BII, providing a round trip delay of nominally 15uS resulting in a resolution < 70kHz. This was replicated for the standard interferometer. Optical insertion loss through the birefringence insensitive interferometer was measured as approximately 10dB, similar to the standard interferometer.

Most of the assessment has been under taken with a DFB laser manufactured by GEC Marconi. Initially, this section looks at the un-modulated laser spectrum in assessing the lasers linewidth. Following this we look at chirp measurement capabilities using the BII and standard interferometer, gated and non-gated self homodyne.

4.6.2 Linewidth

A DFB laser was set up and operated at 140mA, being well above threshold and the optical power coupled to the photo detector via the isolators and interferometer. Initially, the responses gained showed periodic cycling on the linewidth response. This was pin pointed to a reflection from the coupling optics back into the laser. By angling the DFB laser and incorporating in-fibre-isolators this cycling was minimised. Also, the low frequency response, <10MHz was found to be dominated by the 1/f noise discussed earlier and suffered from a drop off in system sensitivity due to the rf amplifier and bias T used. Another bias T device manufactured by Pico second pulse labs, with a lower quoted frequency range was compared and found to improve the low frequency sensitivity, but only if the amplifier is taken out. One side affect of the Pico Bias

T was its poor noise immunity which left various signal peaks on the linewidth response such as a 10MHz frequency standard sited in a laboratory 50m away. It is envisaged that the system set up will vary to suit the laser being tested. Figure 4-46 shows the response obtained when a HP Bias T and Miteq amplifer is incorporated.

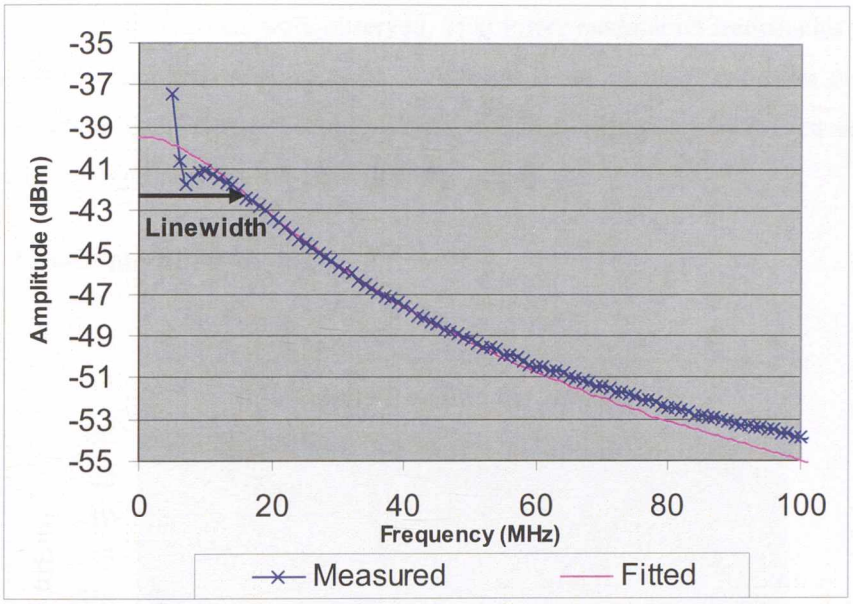

Figure 4-46: Linewidth measurement of DFB Laser – un-modulated.

Since the displayed spectrum is the autocorrelation function of the laser's line shape, its spectral width is twice that of the laser linewidth. For the special case of Lorentzian lineshapes, the autocorrelation function is also Lorentzian and has a linewidth exactly twice that of the original line shape as previously discussed. For Gaussian lineshapes, the autocorrelation function is also Gaussian but has a linewidth equal to $\sqrt{2}$ times that of the original lineshape. Currently, most single frequency semiconductor lasers are accurately described by Lorentzian lineshapes. From the above result the linewidth of the laser was manually recorded as approximately 15MHz, i.e. 3dB drop from an approximation of the laser signal peak at very low frequency. The second response is based on the standard lorentzian function which is fitted to the linewidth response measured. The linewidth and amplitude offset were adjusted to obtain the optimum fit, resulting in a linewidth of 17MHz, average frequency delta of 0.16MHz, and standard uncertainty U(x) of 0.12MHz based on range 10MHz to 60MHz.

A cross correlation for linewidth is provided in the next section utilising the modulated Bessel functions. Unfortunately due to limitation of available lasers the system capabilities at lower linewidths approaching the resolution limit (<100kHz) could not be obtained.

4.6.3 Gated Delayed Self-homodyne Technique

The DFB laser characterised for linewidth was then amplitude modulated using the signal generator and resulting response observed on the spectrum anaylser via each of the two interferometers. Two regimes were observed, 1) at lower modulation frequencies (<2xLW) where the chirp characteristic consists of convoluted Bessels and 2) at greater modulation frequencies where each Bessel becomes distinguishable. Modulation frequencies greater than 10MHz are dominated by the carrier density effect.

4.6.3.1 Lower modulation

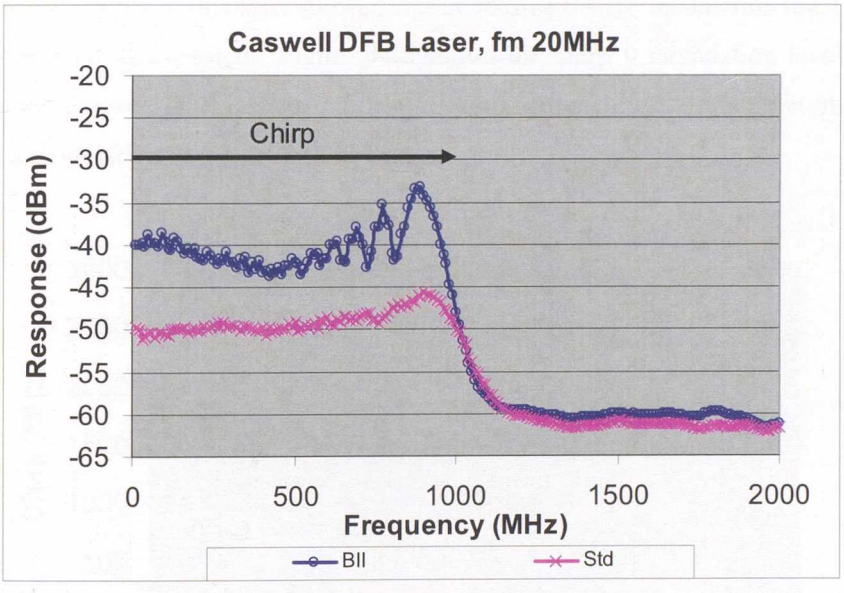

Figure 4-47: Chirp response obtained from a DFB laser modulated at 20MHz.

Figure 2-3 shows the chirp encountered under a modulation of 20MHz, 4dBm applied modulation, for both the BII and standard interferometer. Resolution bandwidth 3MHz, video bandwidth 300Hz, x10 averaging, 10MHz steps. At this low modulation frequency the Bessel functions are not resolvable and thus the spectrum takes on the shape of the probability density function for wideband sinusoidal FM modulation. By establishing the frequency for a 3dB drop from the averaged low frequency points, large frequency chirp excursions were observed. The BII gave a frequency chirp of 970MHz, and the standard 1040MHz. These initial measurements suggest a 7% difference between the interferometers which is consistent with the expected birefringence effects under lower chirp excursions. Also noted was the observed -10dB shift in the overall signal spectrum for the standard

interferometer, suggesting a lower amplitude sensitivity. Large chirp at low modulation frequencies yields a high FM index (M) as discussed in 3.1.2, for this case being (M) = 24.

The level of amplitude modulation index can be obtained via measurement of the received power at the photo-detector (Pc) and the relative sideband level (Ps). The former can be obtained simply from the voltage measured at the bias T dc port. The latter is found from the spectrum analyser with the interferometer taken out of the system, adjusted to provide the side band level at the same reference plane as the carrier power. This adjustment can be derived by use of the calculable reference laser source, in a similar manor to the RIN measurement. Knowing both the AM and FM indexes the alpha coefficient can be derived.

Further measurements of this laser showed that increasing the RF modulation level increased in chirp observed as expected. Figure 4-48 shows the chirp v modulation level response gained for the Caswell DFB laser using the 3dB drop approach for both interferometers, this time with a modulation frequency of 30MHz.

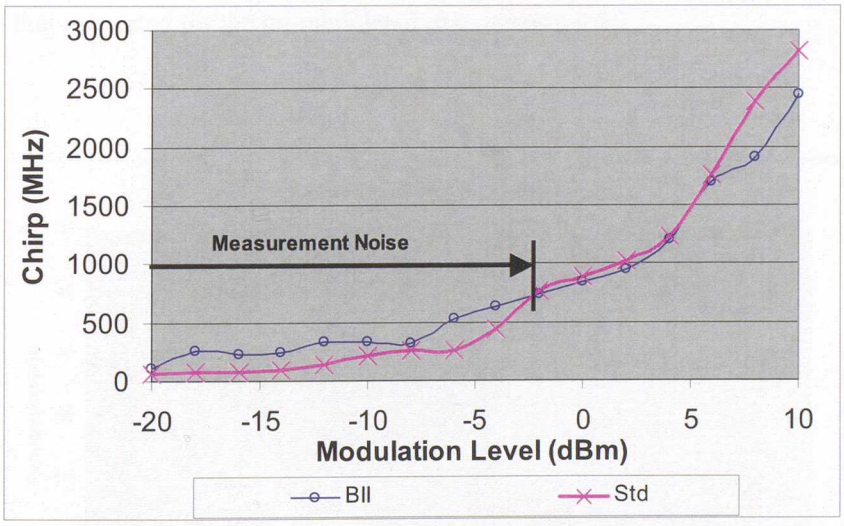

Figure 4-48: Increase in chirp with increased modulation level for 30MHz frequency.

Some difficulty was observed when measuring chirp at very low modulation levels (sub -4dBm) as noted on the response. This was significantly due to the 1/f noise contribution being more significant for lower chirp responses. This aside, there does appear to be a generally higher chirp value derived from the standard interferometer. Further improvements to the measurement technique should provide further confidence.

Converting modulation level to injected current and performing a linear fit with chirp we obtain a response of 0.175GHz/mA with a 4% standard uncertainty, typical for a DFB laser.

4.6.3.2 Higher Modulation

At modulation frequencies greater than 2x linewidth the laser is more dominated by the carrier density effect. In this case the Bessel functions are un-convoluted and thus it is possible to obtain the frequency modulation index (M) by effectively 'nulling' a specific Bessel sideband. This is achieved by adjusting the RF input modulation level. Shown previously, knowing M and the modulation frequency, f_m the effective frequency chirp can be derived by:

$$\Delta v_o = 2(M+1)f_m \quad Hz \tag{4-17}$$

Figure 4-49 shows the Bessel function response gained for a DFB laser modulated at 150MHz, modulation level of +5.2dBm. Each Bessel function is clearly separated by the frequency of modulation as demonstrated previously using classic FM theory. Also, the 3dB width of these Bessels directly relates to the lasers un-modulated linewidth. By centring and focusing the spectrum analyser to one of these peaks we obtained a linewidth of 15MHz, similar to that measured for the un-modulated case, section 4.6.2.

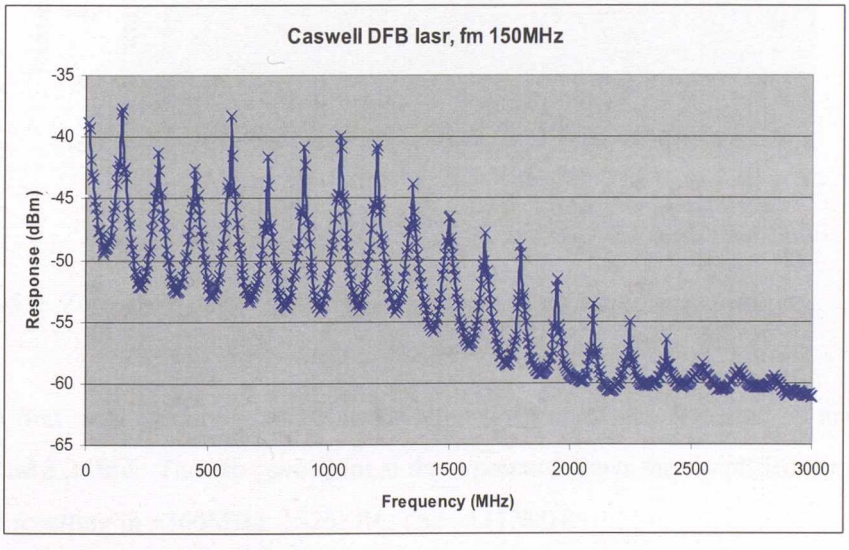

Figure 4-49: Chirp response obtained from a DFB laser modulated at 150MHz.

By tracking the zero order Bessel peak whilst adjusting the frequency modulation level it is possible to determine known M values when nulled and thus calculate the effective chirp. Figure 4-50 shows the nulled Bessel function response and Figure 4-51 the amplitude variation of the zero order Bessel as a function of modulation level.

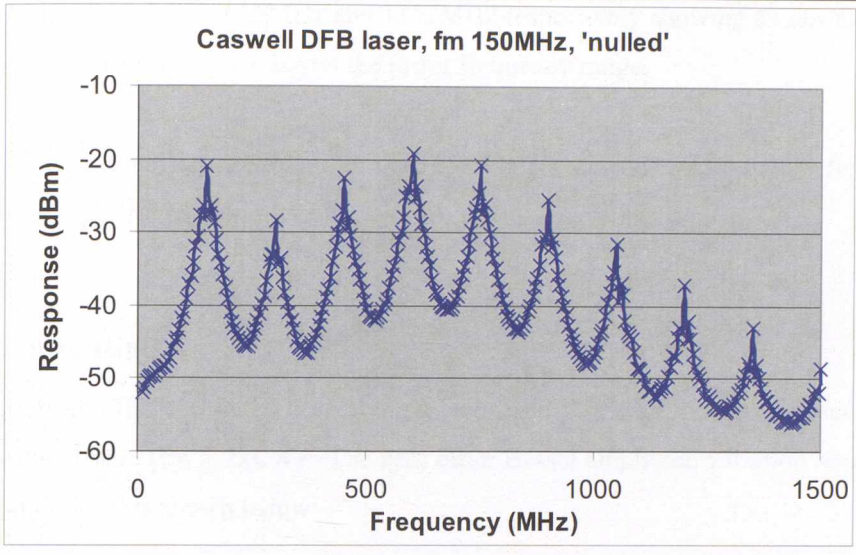

Figure 4-50: RF modulation adjusted to null zero order Bessel.

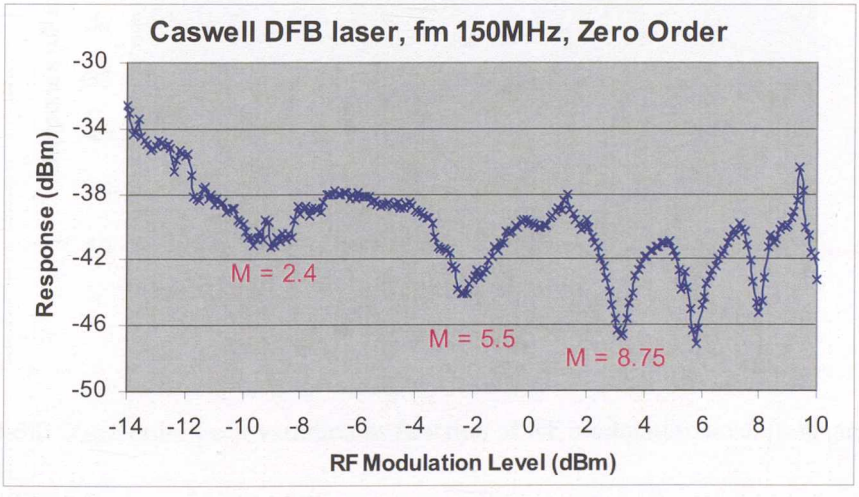

Figure 4-51: Zero order peak variation as a function of RF modulation level.

Here, the first 'null' occurs at an RF modulation level of -9dBm followed by another at -2.3dBm and 3.2dBm. The effective chirp at these points follows the simplified form, ±Chirp = M x fm resulting in ±360MHz, ±825MHz and ±1312MHz.

From Figure 3-2, typically the chirp response is relatively flat over from 10MHz to 500MHz Thus an approximate comparison can be drawn between the convoluted and unconvoluted techniques based on the measurements at 20MHz and 150MHz respectively. Using the derived 0.175GHz/mA from Figure 4-48 and the injected current at each Bessel null one

obtains chirps of 296MHz, 619MHz and 1152MHz respectively showing a reasonably good agreement between approaches across the lower frequency range.

This single Bessel nulling technique is thus capable for extended modulation frequencies, limited by the spectral bandwidth of the system, in this case being 20GHz.

4.6.4 Self Beating

For completeness the non gated homodyning technique was additionally assessed over the non convoluted state (fm > 2xLW). The zero order Bessel amplitude variation as a function of modulation level is shown below:

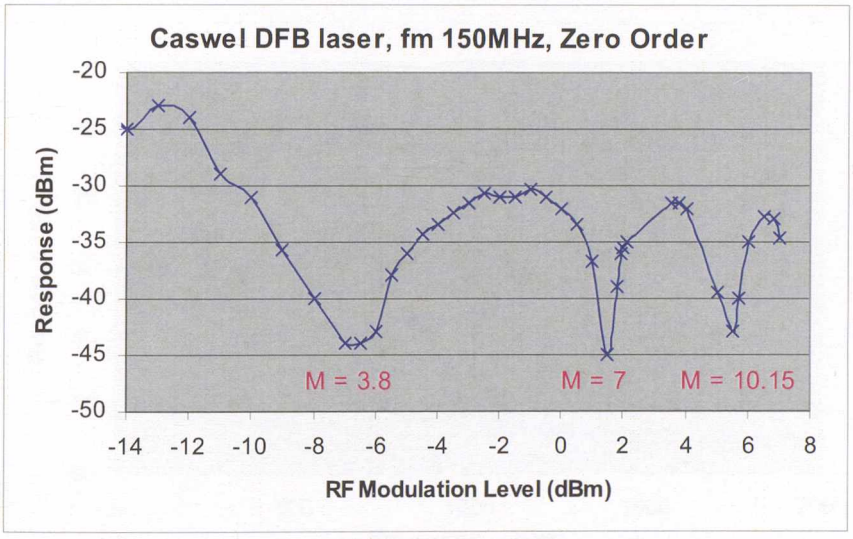

Figure 4-52: Zero order peak variation as function of RF modulation level (non gated).

As discussed in 7.1.3, the M corresponding to each null point will be different from the gated technique. The first 'null' occurs at an RF modulation level of -6.75dBm followed by another at 1.5dBm and 5.5dBm. The effective chirp is thus; ±570MHz, ±1050MHz and ±1522MHz respectively.

Cross correlating to the previously defined 0.175GHz/mA from the gated technique (low modulation frequency) we obtain chirps of 378MHz, 950MHz and 1497MHz for the injected current at each null point. Again we see reasonably good agreement between approaches particularly at higher injection currents, thus providing confidence in the approaches.

4.6.5 Nulling Ratio Technique

One disadvantage of the null point technique is the potentially limited modulation level applied which will in turn limit the Bessel amplitude range, i.e. may not reach a null. A possible solution to this is to look at the relative ratios of the neighbouring Bessel orders and compare to modelled classic FM theory. This would limit the modulation frequency range to less than half the system frequency range and also care should be exercised regarding relative responsivity changes between the Bessel frequency points. Knowing the linewidth and modulation level index it is possible to fit classic FM theory to the measured response. This allows the frequency modulation index to be gained at transitional points between nulls and thus derive the effective chirp. The following example looks at tracking just the zero order Bessel at a modulation frequency of 500MHz.

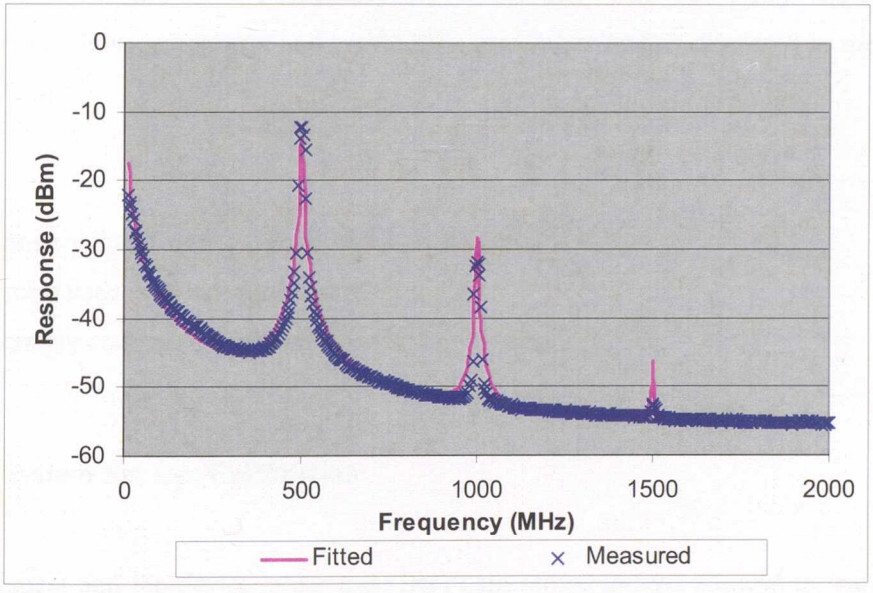

Figure 4-53: Response fitting using classic FM theory, DFB laser at fm 500MHz.

Here the linewidth, AM and FM index are adjusted to obtain a good match to the measured response. In this case a frequency modulation of 0.66 and linewidth of 1.3MHz achieved the best match. This results in an estimated chirp of 333MHz which is typically when, in the flat area of the modulation frequency v chirp range. Incorporating modelling theory in this way should also improve measurement uncertainty.

The linewidth parameter can be gained directly by measuring the Bessel response width at half height, for low modulation levels). Good agreement for the Caswell DFB was found when compared to the 'un-modulated' linewidths measured in 4.6.2, previously. An

advantage with this LW technique is analysis can be performed away from the system 1/f noise (<10MHz).

4.7 Chirp Measurement Procedure

Early chirp measurements centred on the low modulation frequency (convoluted) state where the 3dB power drop derives the frequency excursion. This section focuses on this approach. More analysis is required for the higher modulation frequency (un-convoluted) state to be able to lock a measurement procedure and uncertainty level.

The overall procedure for low frequency modulation chirp measurements is shown below with test conditions, equipment and preliminary uncertainty budget discussed in subsequent sections

Note:

1. All terms are linear values unless otherwise stated
2. Equipment used is as listed in section 4.8.2
3. Temperature controlled laboratory is used for all tests, 21±2°

4.7.1 System Set Up, Calibration

- Equipment and the device under test (DUT) are turned on and allowed to warm up, 2 hours minimum.
- Initial equipment calibration is performed, i.e. zeroing etc.

4.7.2 Setting Amplitude Modulation Index

The approach taken avoids calibration back to the injected signal from the RF signal generator. Instead, the spectrum analyser is used to measure the amplitude of the received sideband with the interferometer disconnected. Calibration of the spectrum analyser / amplifier is provided via the reference laser, similarly to the RIN measurement. The ratio of the received signal power and carrier power then derives the amplitude modulation index as below. Essentially this removes additional uncertainties associated with the applied signal

advantage with this LW technique is analysis can be performed away from the system 1/f noise (<10MHz).

4.7 Chirp Measurement Procedure

Early chirp measurements centred on the low modulation frequency (convoluted) state where the 3dB power drop derives the frequency excursion. This section focuses on this approach. More analysis is required for the higher modulation frequency (un-convoluted) state to be able to lock a measurement procedure and uncertainty level.

The overall procedure for low frequency modulation chirp measurements is shown below with test conditions, equipment and preliminary uncertainty budget discussed in subsequent sections

Note:

1. All terms are linear values unless otherwise stated
2. Equipment used is as listed in section 4.8.2
3. Temperature controlled laboratory is used for all tests, 21±2°

4.7.1 System Set Up, Calibration

- Equipment and the device under test (DUT) are turned on and allowed to warm up, 2 hours minimum.
- Initial equipment calibration is performed, i.e. zeroing etc.

4.7.2 Setting Amplitude Modulation Index

The approach taken avoids calibration back to the injected signal from the RF signal generator. Instead, the spectrum analyser is used to measure the amplitude of the received sideband with the interferometer disconnected. Calibration of the spectrum analyser / amplifier is provided via the reference laser, similarly to the RIN measurement. The ratio of the received signal power and carrier power then derives the amplitude modulation index as below. Essentially this removes additional uncertainties associated with the applied signal

generator level, connection, Voltage Standing Wave Ratio (VSWR) loss etc. providing a measurement reference plane at the photo-detector.

$$m = 2\sqrt{\frac{P_s}{P_c}} \tag{4-18}$$

where m is the AM index

P_s is the modulation power, obtained via the spectrum analyser

P_c is the carrier power, obtained via the detector current (V^2/R)

- With the interferometer disconnected, the reference laser is applied to the detector to provide calibration of the system, set up for narrowband signals at the test modulation frequency (similar manor to RIN calibration described previously.
- The DUT is then applied to the detector and modulation level adjusted to obtain required AM index, via measurements of carrier and sideband power.

4.7.3 Deriving Chirp

Essentially, derivation of the frequency chirp is obtained from measuring the frequency that which the signal amplitude drops by 3dB. From this the frequency modulation index can be derived using the following relationship.

$$\Delta v = M.f_m \quad Hz \tag{4-19}$$

where $\Delta\upsilon$ is the chirp excursion, M is the frequency modulation index and f_m is the modulation frequency, for low modulation levels

- Connecting the interferometer into the system the spectrum analyser is then adjusted to obtain the optimum span etc to assess the 3dB drop.
- The frequency excursion from the laser centre frequency to the lower 3dB marker is then measured
- The reference laser is then used to calibrate system gain over this region, compensating for gain variations.
- Chirp is then quoted in electrical terms ± from the laser frequency at the modulation frequency and level.

Repeat measurements are normally performed to reduce repeatability uncertainties.

4.8 Definition of Uncertainties - Chirp

4.8.1 Test Conditions

Typical laser chirp measurements are performed over a wide modulation frequency range from 10MHz. Spectrum analyser bandwidths are adjusted to obtain the optimum signal level, being wideband (chirp) or narrowband (modulation level). RF input attenuation is nominally set to 0dB. Smaller frequency spans and or sample average can be used dependant on requirements.

It is imperative that high levels of optical isolation (60dB minimum) and counter angled fibre connectors are used within the system to minimise the affects of reflections. Laser chirp will vary as a function of diode temperature and drive current, therefore it is important that these parameters reflect the conditions required for the end application as well as the modulation level required. Chirp levels may also be effected by the power supply and signal source used, **i.e. introducing noise themselves**. For these reasons it is important to provide necessary laser diode power supplies and coolers, as would be used in an end application so as to provide meaningful chirp measurements that can be applied to optical communication systems.

The reference plane for the laser chirp measurement is the light incident into the interferometer system. Laser chirp values will be quoted at the modulation level incident to the interferometer, in electrical domain at the specified modulation frequency. The high sensitivity of the birefringence insensitive interferometer allows laser chirp measurements to be assessed at low modulation levels.

4.8.2 Equipment

Table 4-10: Equipment list for the chirp facility

Description	Model No.	Manufacturer	Serial Number	Cal Interval	Cal by
DUT PSU	LDC404B	Profile	02210	1 yr	SESC
Signal Generator	SMP22	Rohde& Schwarz	835695/010	1 yr	SESC
Optical Attenuator	8156A	HP	3328G01374	1 yr	HP
Fibre Isolator 1300nm 1550nm	 M-PI-2-13-S-B-B-A-1 M-PI-2-15-S-B-B-A-1	 FOCI FOCI	 011414 011409	 ------- -------	
Reference Laser	125-1319-100	Lightwave	139	1 yr	In-house
Detector System 1 Ge photodiode Thermoelectric cooler Amplifier	 J16TE2 TEC2-030 SP043	 EG&G Alpha Omega Vinculum	 802043 2-9911 C125/1	 6 months 6 months 1 yr	 NPL as Pair SESC
Ultra Fast Detector	1414	NewFocus	0761	1 yr	In-house
Electrical DMM	2000	Keithley	0636295	1 yr	SESC
Bias Tee	5541A	Picosecond Pulse Labs	415 10/96	1 yr	SESC as system
RF Amplifier	JS42-00102000-25-8P-42	Miteq	394841	1 yr	SESC as system
Spectrum Analyser	FSEM30	Rohde & Schwarz	1079850030	1 yr	SESC as system
Interferometer	BII	DERA	BII01	-------	
Optical DMM & Head	OMM6810B OMH6725B	ILX ILX	68102033 67252016	1 yr 1 yr	OTC OTC

4.8.3 Measurement Uncertainties

The following combined uncertainty budget shown consists of systematic uncertainties and also any random components associated with the chirp measurement. Due to the complexity of the chirp measurement and that some of the input quantities are correlated, effectively the

combined uncertainty will be over estimated. In time the budget can be tailored more closely to the errors which couple through by deriving the functional relationship of each input quantity using partial differentiation.

Worst case systematic uncertainties have been used regardless of test conditions, e.g. modulation level, chirp level etc. Therefore the combined systematic uncertainties represent the **worst case** chirp uncertainty. This represents a base line from which many improvements can be made in reducing the uncertainty level further by:

- compiling measurement parameter specific uncertainty budgets
- performing further repeat measurements, building history
- minimising calibration uncertainties of components
- reducing measurement span, focusing on one frequency point, increasing accuracy
- perform measurements at different modulation frequencies and levels to enable line fitting procedure.

4.8.4 Combined Uncertainty Budget

Formulation of the Chirp uncertainty budget follows the guidelines laid down by UKAS, formally NAMAS, NIS3003 Edition 8 and the DERA Quality System.

Table 4-11: Combined uncertainty budget for low frequency modulation

Uncertainty Budget for measurements of Chirp (fm 10MHz to 2*LW)							
Symbol	Source of uncertainty	Value (± %)	Probability Distribution	Divisor	Ci	Ui(chirp) (± %)	Vi or Veff
	Modulation Index Error	6.0	normal	1.0	0.7	4.2	∞
	3dB Measurement Error	1.0	normal	1.0	1.0	1.0	∞
	Frequency Accuracy	1.0	normal	1.0	1.0	1.0	∞
	Linewidth Error	0.1	normal	1.0	1.0	0.1	∞
	Pulse Alignment Error	1.5	normal	1.0	1.0	1.5	∞
	Repeatability	3.0	normal	1.0	1.0	3.0	5
Uc(Chirp)	Combined uncertainty		normal			5.6	>100
U	Expanded uncertainty		normal (k=2)			11.1	>100

Notes:

1. Uncertainty based on an average of five repeats
2. The DUT has a lorentzian linewidth profile
3. DUT is characterised with its own signal source and PSU.

It can be seen that the combined uncertainty for this worst case chirp is ±5.6%, giving an expanded uncertainty of ±11.1% at 95% confidence level.

The dominant uncertainties for the measurement of chirp are in determining the calibration of the system and in measuring the modulation index. Future improvements in this area have the prospect of reducing these error terms. This could be in the form of line fitting from Bessel function modelling knowing LW, m and M. In this way chirp can easily be derived for other modulation frequencies.

The systematic error terms listed in the combined budget are derived from further sub budgets consisting of further measurement uncertainties which are summarised below.

4.8.5 Modulation Index Error

Determining the modulation index of the optical signal consists of measurements of detector current and resistance, modulation level and system calibration using the reference laser. A typical relationship between modulation level/index and chirp can be used to estimate the resulting maximum uncertainty that can be expected in chirp measurement resulting from an error in setting the modulation index. A modulation index uncertainty of 6% has been estimated to influence the chirp level be <4%.

4.8.6 3dB Measurement Error

The ability to measure the 3dB amplitude drop on the wideband signal trace is largely dominated by the spectrum analyser settings. Minimising the uncertainty can easily be achieved by focusing in on the area of interest to improve the resolution in the amplitude and frequency scales. System gain variations can be compensated for and hence measurement uncertainties within 1% are achievable.

4.8.7 Frequency Accuracy

The spectrum analyser frequency accuracy is governed primarily by the span and resolution bandwidth selected. As mentioned above, by focusing on the area of interest the frequency uncertainty will be less than 1%.

4.8.8 Linewidth Error

The interferometer relies upon a long time delay to provide incoherence. The affect of decreasing linewidth has the effect of increasing the coherence of the laser which will in turn result in a small error from the interferometer action. Typically DFB lasers will have linewidths of >1MHz and if we take this as a worst case the resultant influence in terms of chirp will be no more than 0.1%.

4.8.9 Pulse Alignment Error

Setting the gating source to the time delay of the interferometer can be reliably achieved by fine adjustment to obtain the maximum chirp signal level on the spectrum analyser. Other gating errors, for instance rise/fall time errors are dependant on customer systems but will typically not exceed an overall uncertainty of 1.5%.

5 Intercomparisons

During this project good contacts were established with Hewlett Packard (HP), Santa Rosa, whom has significantly lead laser noise metrology in earlier years. This lead to the opportunity of a loan HP70810A Lightwave receiver and HP11980A (Pilot) Interferometer allowing a level of inter comparison to be performed of which, results would be shared with HP in return. The USA's National Institute of Standards & Technology (NIST) in Colorado also have been involved with discussions to perform further intercomparisons. Unfortunately, other NIST project commitments have prevented us completing an these measurements, although resulting discussions have proved useful in gaining support for the projects findings.

This chapter discusses the HP Lightwave comparisons undertaken, interrogating the commercial measurement system and draws conclusion on the capability level of the RIN/Chirp systems. The aim here is to provide increased confidence in the established National Standard facility.

5.1 Equipment

The following equipment was loaned by Hewlett Packard (HP) to enable comparison measurements for RIN and chirp to be performed.

1. 70810B (2883A00055) LW Section
2. 70908A (2713A00147) RF Section
3. 70810-10002 (NSN) RIN DLP
4. 11980A (Pilot) Interferometer
5. 70880A (NSN) Linewidth DLP

These *plug in modules* were combined with an available HP70000 series mainframe and set-up along side the DERA noise standard under controlled laboratory conditions. A temperature controlled GEC DFB laser diode was set-up along with an OTC DFB bench type laser to provide suitable noise sources to measure.

5.2 Relative Intensity Noise System

A significant proportion of the loan unit available time has been spent assessing the RIN parameter, due to the more advanced measurement capability. Focus has been on determining any measurement differences, methodically understanding HP's software/firmware and also to evaluate an effective way to calibrate these units in the future. Comparison laser sources used cover a dynamic range of >30dB and provide low RIN's below the shot noise level to assess system sensitivities. Results gained suggest that measurement discrepancies between the two systems increase proportionally with reducing RIN, clearly indicating sensitivity limitations of the HP system.

5.2.1 Hewlett Packard System

The HP system calculates RIN from measurement of the dc optical power and two RF scans - Dark and Signal. The laser RIN is calculated at the end of the second scan along with other RIN levels as below. Both scans are automatically controlled on activation of the single or continue mode buttons with a delay between scans of approx. 2 seconds allowing for stabilisation.

- RIN laser
- RIN system
- RIN thermal
- RIN shot

The relationship between these terms and the measured units is:

$$RIN_{laser} = RIN_{system} - RIN_{therm} - RIN_{shot} \quad Hz^{-1} \tag{5-1}$$

$$RIN_{system} = \frac{N_T}{P} \quad Hz^{-1}$$

$$RIN_{therm} = \frac{N_{th}}{P} \quad Hz^{-1} \tag{5-2}$$

$$RIN_{shot} = \frac{2q}{I_{dc}} \quad Hz^{-1}$$

5.2.2 Comparison Measurements

5.2.2.1 Set-up

In order to gather comparison information efficiently, the GPIB interface provided on the HP system was configured to operate from the DERA system controller. The HP system RIN derivation can only be performed at one spot frequency per scan sequence. Hence to enable a full frequency span of RIN measurements to be obtained the level marker was scanned over the thermal and laser frequency traces similar to the DERA system, and then the data transferred to a spreadsheet to determine laser RIN using (5-1) and Eqn.(5-2) as the HP software performs.

HP parameters were set as follows, which are considered to be the ideal measurement conditions, gained from HP application notes.

Resolution Bandwidth	3MHz
Video Bandwidth	300Hz
Frequency Span	500MHz - 20GHz
Internal Optical Attenuation	0dB
Lambda	1550nm
Trace	Top 1/3 of screen
Range	1dB/div
SA Ref. Level	-36dBm
LW mode	Elect
SYSCOR	Auto

The DERA system was set-up to suit the above setting, providing a close comparison.

The GEC laser source was operated at 100mA, 1mW and temperature controlled. An ETEK isolator coupler device was used to gather the free-field light through a FOCI in-fibre isolator which combined provided approximately 120dB optical isolation, hence minimising back reflections. Basic optical and RF accuracy assessments are summarised in Appendix C.

5.2.2.2 System Responses

The RIN response shown in Figure 5-1 consists of two RIN measurements performed by the HP system and the corresponding DERA RIN level measured using the GEC laser source.

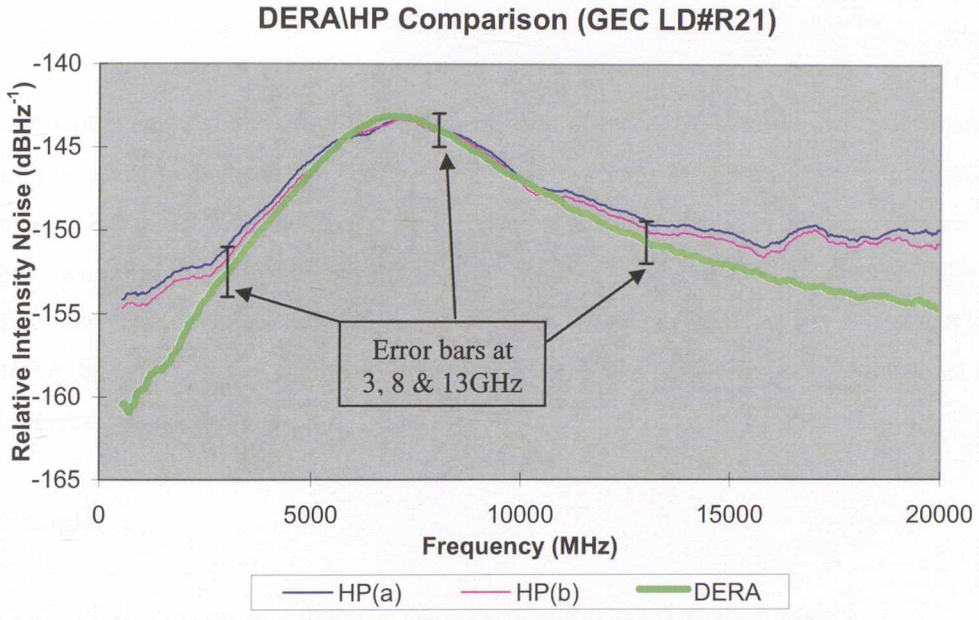

Figure 5-1: RIN Comparison.

Optical power stability between the HP scans was 0.1dBm. All RIN responses shown are referenced to the input of the detector. Three error bars have been inserted representing DERA system measurement uncertainty (@95% confidence level) under these conditions, i.e. 3GHz @ ±1.5dB, 8GHz @ ±1dB, 13GHz @ ±1.27dB.

Although the noise levels agree well between 3 to 13GHz, we can see a progressive shift apart as the laser noise decreases below the shot noise level. Assessing the trend of the responses suggests that the sensitivity of the HP system is limiting its ability to measure low noise levels.

5.2.2.3 Optical Attenuation Affects

The HP system follows similar methodology as the DERA system in that dc and rf levels are measured at the output of the detector and the RIN calculated and referenced to the optical

input, compensating for any offsets. An important consideration which came to light during the early stages of this project was the affect of optical attenuation on shot & spontaneous noise, mentioned in 3.5.1 particularly concerning the reference laser. Attenuating by a factor of 2 will reduce the optical power and the shot noise present by 2 but the spontaneous noise will reduce by a factor of 2^2. Hence the shot-spontaneous ratio each side of the attenuation will be different and this needs to be remembered when measuring laser RIN, to avoid effectively a systematic error.

Any optical attenuation before the reference point of these two systems does not require any compensation to be made to the measured RIN as long as the incident optical power is stated. From the reference point onwards compensation needs to be incorporated. The reference point of the DERA system is at the input of the detector. This detector, like most, effectively causes some attenuation related to its responsivity (typically 0.6 to 0.8). The DERA system therefore includes spontaneous noise loss compensation, proportional to the detector responsivity measured.

Example:

Responsivity @ 1550nm = 0.717 $\therefore$ attenuation factor of 1/0.717 = 1.395

Shot Noise attenuation factor = 1.395

$\therefore$ decrease in noise = 10 Log 1.395 = 1.445dB

Spontaneous Noise attenuation factor = $(1.395)^2$

$\therefore$ decrease in noise = 10 Log $(1.395)^2$ = 2.89dB

As we are referencing in terms of relative noise levels only the difference between the shot & spontaneous attenuation affect needs to be incorporated as an offset correction. In the example previous this would require 1.445dB be added to the laser RIN measured.

The HP system, which has a detector similar to the DERA system, also has an internal optical attenuator which if set to other than 0dB will increase the relative offset required to correct this systematic affect. Unfortunately there seems to be no means of accounting for this affect by software control or calibration. To my knowledge this attenuation affect has not been discovered before and as the HP system was designed some greater than ten years ago this would explain the lack of compensation.

Communications with HP has established that this systematic offset has not been considered before. Discussions with NIST (Colorado) provided further support for this effect which they will be looking into.

To enable comparison of the HP RIN responses with the DERA response, this systematic error needs to be compensated for by establishing the detector responsivity. Using Eq. (9-1) and knowing the recorded average power detected and the incident optical power the responsivity was found to be 0.669. The compensation required therefore is 1.746dB (10Log 1/0.669). With the internal optical attenuator set to 0dB no further compensation was required. Figure 5-2 now shows the compensated responses.

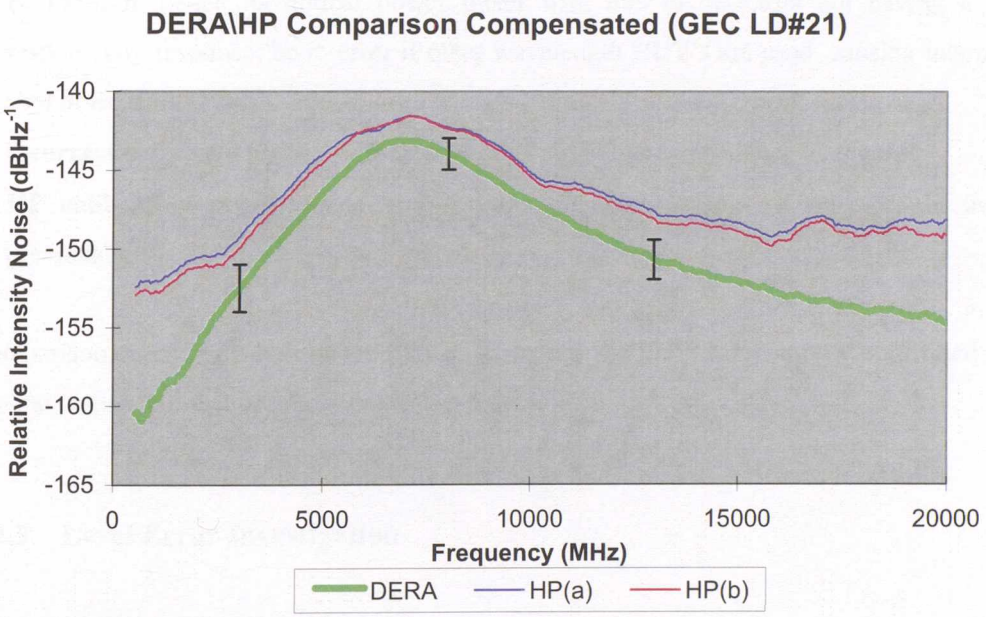

Figure 5-2: RIN Comparison, compensated for responsivity attenuation.

This has increased the offset between the two systems, now compared on equal terms. Errors which may be combining to cause this offset are investigated in the following sections and summarised below.

- **rf amplitude calibration error:** the impact on laser RIN caused by a level error will be proportional to the difference level between the thermal and system noise and the shot noise present.

- **smoothing error:** HP system calibration using narrow band techniques will not provide absolute rf level accuracy for noise signals under test. Instead will be approximately 2dB higher.
- **thermal level error:** due to the thermal noise being independent of the detector frequency responsivity a different calibration offset is required compared to the system noise level (ideally).
- **frequency response errors:** HP's detector and amplifier responsivity is only calibrated at 300MHz using a narrowband source. The whole frequency range is quoted as a flatness uncertainty instead, unlike the DERA system which naturally compensates for variations using the reference source.
- **wavelength error:** The HP system only provides two DUT wavelength selections 1300 & 1550nm, hence its optical power meter will, due to detectors not having a flat responsivity response, be in error if other wavelength DUT's are used, causing incorrect shot noise subtraction.
- **incorrect reference plane:** 6dB elect error - caused by rf impedance matching
- **HP calibration process:** does not consider spontaneous loss of detector, discussed previously.

Comparison measurements obtained when assessing the OTC laser source confirmed the general response offset between the two systems.

5.2.3 Level Error Investigation

5.2.3.1 Reference Laser Method

The 1319nm reference laser provides a substantially shot noise limited response above 10MHz with the inclusion of the optical attenuation technique as demonstrated in 4.5.10.3. This reference signal essentially consists of shot noise which can be varied by adjusting the optical power, providing a variable flat noise signal. Applying this signal to a RIN system will introduce thermal noise and system responsivity terms along with any system calibration errors (calerror) as

$$N_T = N_q(calerror) + N_{th}(calerror) \quad Watts \tag{5-3}$$

The reference laser was applied to the HP system to investigate the rf level calibration. Figure 5-3 shows four reference level responses at different optical powers along with a thermal response (dark) when no signal was applied.

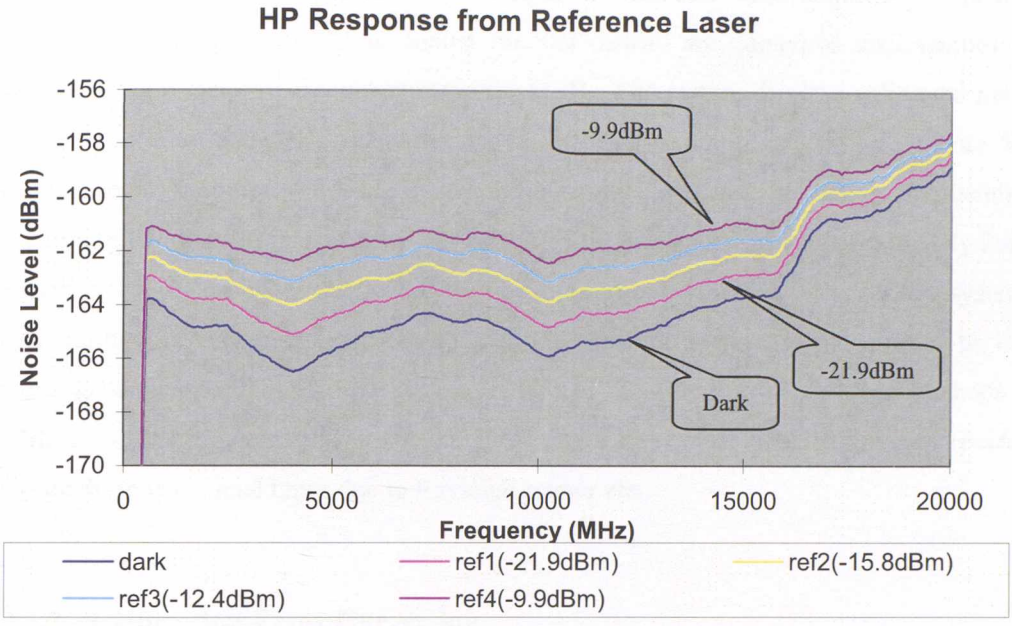

Figure 5-3: HP Response gained on application of the Reference Laser.

The calerror term of the HP system shown in Figure 5-4 is found by subtracting the dark response and the shot noise (N_q) derived by the photocurrent from the total noise (N_T).

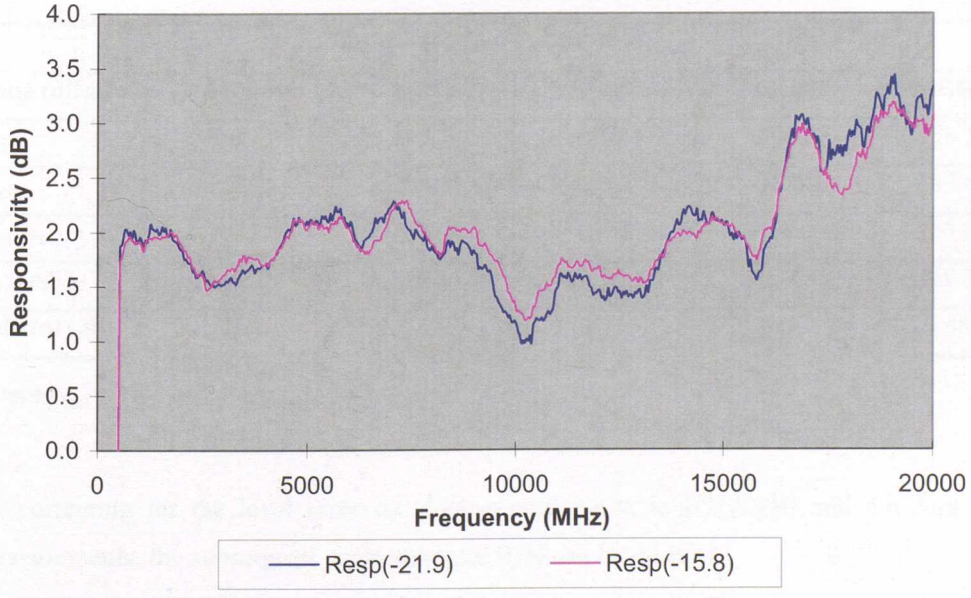

Figure 5-4: Calculated Responsivity of the HP system.

Some error is expected with the HP system as detector and amplifier frequency responsivities are not normally accounted for, but instead are quoted as uncertainties of measurement e.g. detector frequency response ±1dB. The system displays calibrated noise levels referenced at 300MHz, accounting for mismatch loss, amplifier gain etc. Figure 5-4 indicates level variation of >±1dB which generally increases at higher frequencies representing the detector responsivity roll-off. Also there is an offset of approximately 2dB. This error is most probably due to the way calibration is performed. The DERA system, incorporating the reference laser provides a wideband calibration signal similar to test devices to be measured, but the HP system, as far as I'm aware uses narrowband methods at 300MHz. It has previously been shown, 3.4.6 that a level error of 2dB will be expected between these two signal types due to Rayleigh scatter etc.

5.2.3.2 Calibration Error Correction

Using the reference laser calibration process just described enables any rf level error to be established across the whole frequency range. The following table shows a spread of calibration errors found across the frequency range.

Table 5-1: Calibration Error Correction

RF Level Error Calibration					
Noise (dBm)	**1GHz**	**3GHz**	**8GHz**	**13GHz**	**20GHz**
N_{th}	-163.92	-165.71	-163.86	-164.83	-158.16
N_{ref}	-162.23	-163.69	-162.21	-163.10	-157.48
N_{ref}-N_{th}	-167.15	-167.99	-167.21	-167.93	-165.87
N_q (2eiR)	-169.35	-169.35	-169.35	-169.35	-169.35
Calerror (dB)	2.2	1.36	2.14	1.42	3.48

where $N_{ref} = N_T$, and $Popt_{elect} = -15.8dBm$

By correcting for the level error for devices under test, ie HP(A&B) and the dark level measurements, the subsequent corrected laser RIN can be derived.

Table 5-2: HP RIN corrected for Calibration Error

RIN, Correcting for RF Level Error					
Noise (dBm)	**1GHz**	**3GHz**	**8GHz**	**13GHz**	**20GHz**
N_{th}	-166.32	-166.84	-166.70	-166.11	-162.19
N_{dut}	-164.60	-164.02	-160.94	-163.16	-161.34
$RIN_{laser}(dBHz^{-1})$ Corrected	-163.66	-152.60	-144.90	-150.58	-158.01
$RIN_{laser}(dBHz^{-1})$ Uncorrected	-152.66	-149.94	-142.40	-148.27	-149.10
RIN_{laser}(DERA)	-159.55	-152.06	-144.06	-151.06	-154.56
HP-DERA Error Uncorrected	6.90	2.12	1.66	2.79	5.46
HP-DERA Error Corrected	**-4.10**	**-0.54**	**-0.84**	**0.48**	**-3.45**
DERA Uncert 2σ		±1.50	±1.00	±1.27	

This has now pulled the HP RIN response closer to the DERA standard. The remaining relatively small errors at 3, 8 & 13GHz are caused by a combination of errors such as; wavelength dependence of the detector frequency response between the reference and dut lasers, calibration error for the dark noise level will be different to the DUT scan (i.e. detector frequency responsivity not influent on dark noise) etc. At 1 and 20GHz the offset error is still large. If we consider the sensitivity of the system, it becomes clear that at these frequencies RIN levels are below the system sensitivity and therefore the signal level error will increase proportionally.

5.2.3.3 Hewlett Packard Amplifier/Analyzer Sensitivity

An indication of the HP amplifier/analyser combination sensitivity can be found by subtracting the thermal noise (4KTB) from the dark level measurements, Figure 5-5. Compensation for the 2dB wideband smoothing also needs to be considered.

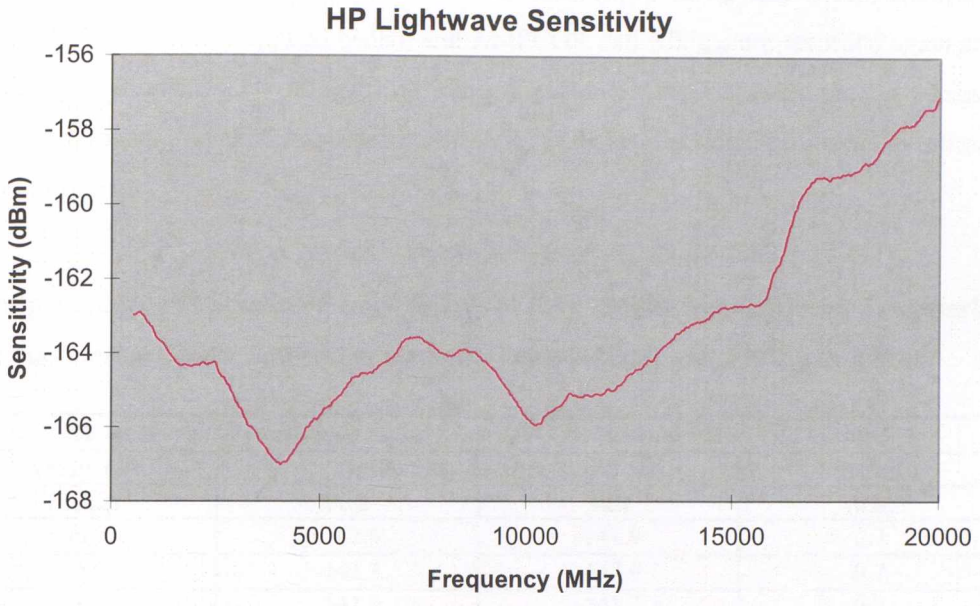

Figure 5-5: Sensitivity Level of the HP Lightwave system.

Product literature suggests that the HP lightwave analyser has a sensitivity of -166dBm[54]

The relatively small RIN offset errors between the two systems implies that the 6dB(elect) loss caused by impedance matching has been considered in HP's calibration process. This issue was raised early on in the development of the RIN standard after observing some HP application notes[54]. It should be emphasised that these notes plus a HP publication[55] are inconsistent in defining impedance matching of the noise terms.

5.2.3.4 Attenuation \ AMPCOR Method

Discussions with HP, Santa Rosa lead further into their measurement assessments. This included uncertainty estimates and additional internal papers one of which described a method of determining if the lightwave analyser has any rf level error.

The method forms a self assessment incorporating optical attenuation and rf amplitude correction (AMPCOR) sequences. The principle is that the RIN_{laser} level will not vary under different internal optical attenuation levels due to the way the HP system is calibrated. An inconsistent RIN_{laser} measured at different attenuation's will be found if the trace calibration is wrong.

RIN_{laser} measurements are recorded at several attenuation levels and if inconsistent, the amplitude correction is applied (±dB), and AMPCOR and RIN_{laser} are recorded again at the same attenuation's. This is again repeated at other AMPCOR levels until a consistent RIN_{laser} is found. When this is obtained the AMPCOR level selected provides the estimated level of rf error.

This procedure has been performed at 1, 3, 8, 13 & 20GHz frequencies as a comparison for the reference laser calibration method. Table 5-3: HP system RF Level Error

RF level error detection @ 8GHz using HP Attenuation\AMPCOR Method			
AMPCOR	**Optical Attenuation Level**		**Variation**
(dB_{opt})	**0dB**	**3dB**	**(dB)**
off	-142.6	-141.9	0.7
-0.5	-143.3	-142.6	0.7
-1.0	-143.9	-143.2	0.7
-1.5	-144.5	-143.9	0.6
-2.0	-145.0	-144.5	0.5
-2.5	-145.6	-145.2	0.4
-3.5	***-147.2***	***-147.1***	***0.1***
-4.5	-148.3	-148.5	-0.2
-5.5	-149.8	-150.5	-0.7

shows measurements obtained at 8GHz, resulting in an almost consistent RIN_{laser} when -3.5dB amplitude correction is applied. Since AMPCOR is in optical terms the electrical equivalent will be -1.75dB.

Table 5-3: HP system RF Level Error

RF level error detection @ 8GHz using HP Attenuation\AMPCOR Method			
AMPCOR	**Optical Attenuation Level**		**Variation**
(dB_{opt})	**0dB**	**3dB**	**(dB)**
off	-142.6	-141.9	0.7
-0.5	-143.3	-142.6	0.7
-1.0	-143.9	-143.2	0.7
-1.5	-144.5	-143.9	0.6
-2.0	-145.0	-144.5	0.5
-2.5	-145.6	-145.2	0.4
-3.5	***-147.2***	***-147.1***	***0.1***
-4.5	-148.3	-148.5	-0.2
-5.5	-149.8	-150.5	-0.7

Comparing this level error, **1.75dB** with that found by the reference laser of **2.14dB**, we have established a quite close agreement. This has also been found at 3 & 13GHz but the method was not able to establish a level error for 1 & 20GHz due to the HP system having difficulties measuring the low noise signal applied.

Although this comparison provides further confidence in the reference laser calibration concept, the HP method described here does not account for the attenuation affect on spontaneous noise described in 5.2.2.3. Hence the AMPCOR obtained will in fact be in error by an amount dependant on the laser noise level applied and the detector responsivity.

5.3 Chirp System

5.3.1 Interferometer Systems

Laser diode modulation responses can be characterised by the HP Lightwave Analyser when the HP 11980A interferometer is incorporated before the detector. This interferometer consists of two optical fibre paths, long and short in parallel, coupled each end by fibre splitters. The resulting interference converts phase information into amplitude information. Since the optical fibre does not preserve the polarisation state, a polarisation state controller is included in one path allowing adjustment to provide the maximum interference signal. The differential delay between both paths is 3.5μS which corresponds to a resolution of approximately 280kHz

The Birefringence Insensitive Interferomter (BII) is based on the same concept, but incorporates faraday fibre rotating mirrors at the end of each path, requiring only one fibre coupler. This system naturally compensates for any fibre birefringence and eliminates the need for a polarisation state controller. A differential delay of 14.6μS was selected to provide an increased resolution capability of <100kHz. This interferometer was then coupled to the DERA RIN system to assess the response.

5.3.2 Set-up

The interferometer systems described here provide the means to obtain the frequency chirp response. From this, techniques are used to determine a level measure of chirp, in this case being the commonly used 3dB drop method (low modulation frequency). Comparison measurements performed here essentially assess the performance difference between:

- Interferometers
- Optical power efficiencies
- Frequency accuracy's

The GEC Laser diode sources used previously in the RIN comparisons were modulated by an external Rohde & Schwarz signal generator. The modulation signal was gated on/off, with the time delay set to the delay path of the interferometer used. The input signal modulation index was not set the same for all modulation frequencies assessed but instead only maintained for each comparison.

Due to the small linewidth of the laser, low modulation frequencies, upto 200MHz were assessed. Measurements were taken one after the other in quick succession to minimise any laser diode variation. The BII system repeatability day to day was <1.5% and <1% measurement to measurement. The HP system repeatability was typically >5% measurement to measurement but by averaging this is reduced <2%.

5.3.3 Comparison Measurements

The summary table below shows close agreement of the HP and BII systems for these low modulation frequencies, well within uncertainty of measurement (±11%@2σ). The electrical modulation input to the laser diode was set to -10dBm

Table 5-4: Comparison of Chirp between BII and HP Interferometers

BII / HP Chirp Comparison										
Mod. Freq (MHz)	**5**	**11**	**15**	**20**	**25**	**35**	**50**	**70**	**100**	**200**
HP (MHz)	302.5	459.0	419.9	455.0	429.3	454.5	425.0	400.0	375.0	335.0
BII (MHz)	302.6	454.8	422.7	454.4	428.3	440.5	420.0	393.4	375.0	324.0
Error (%)	**0.0**	**0.9**	**-0.7**	**0.1**	**0.2**	**3.2**	**1.2**	**1.7**	**0.0**	**3.4**

There is some evidence that the error generally tends to increase proportionally with modulation frequency. This, in part is due to the difficulty in assessing frequency chirps at higher modulation frequencies due to the Bessel functions becoming non convoluted. It may also be due to our understanding of fibre birefringence which may form a systematic error in the HP interferometer. This will only become evident at higher modulation levels. Unfortunately due to time constraints and the immaturity of the chirp capability these measurements could not be obtain.

Further development of high modulation level and frequency technique needs to be made before further comparisons can confirm this. It is hoped that the loan interferometer module HP11980A will be available for further comparisons when appropriate.

The average optical power efficiency of both systems is similar, <10dB, implying the increased loss of the rotating mirrors is offset by the reduction in fibre couplings. But the frequency signal efficiency is improved with the DERA system, providing better sensitivity as found previously when compared with the mimic HP interferometer.

6 Conclusions

This chapter summarises on the development and investigation discussed in this research project. It draws on data collected observations made and defines key advantages of the novel techniques selected along with their limitations. Following this, suggestions of future developments are outlined for the capability and also to the wider metrology field.

6.1 RIN Measurement

Initial measurements during the construction of the detector/amplifier/spectrum analyser system confirmed the expected performance of each of the components and the suitability to the overall system. In determining the sensitivity / noise figure two approaches were compared, based on average displayed noise floor subtraction and the 3dB rise technique. Good agreement was found for the spectrum analyser after consideration for responsivity and the industry accepted nominal 2dB broadband noise smoothing. Further agreement was found with the combined spectrum analyser and amplifier configuration. Noise figure for the combined spectrum analyser and rf amplifier was, as predicted, dominated by the amplifier noise, established as typically better than 3.5dB thus providing sensitivity to -170.5dBm. This is some 4-5dB better than any previously published work for amplifier / spectrum analyser configuration and at some frequencies sensitivities, better than -172dBm.

Experimental measurements of the photo detector established the optical connector repeatability to be sufficient, <1% and local temperature dependence as being insignificant in a temperature controlled laboratory. It was identified that the detectors DC port trans-impedance amplifier, introduced 2dB of noise and had a poor linear response at power levels below 0.5mW. By isolating the DC port circuitry and inserting an external bias-T device to the rf port we effectively provided an alternative DC port to measure the photocurrent without any significant noise being introduced and minimal rf signal loss (0.6dB).

Integrating the photo detector to the rf amplifier / spectrum analysers combination gave, for the first time the ability to assess the system sensitivity optically. Here, the shot noise limited reference laser was used as a source, whose power level was controlled by an optical attenuator and monitored by way of an external optical power meter, traceable to national standards. Extensive data over the wide frequency range 10MHz to 20GHz was gathered plotting rf noise level as a function of applied optical power. Overall system sensitivity was

initially assessed using the 3dB rise principle at each frequency. Results gained showed noise figure's typically sub 3dB for most of the frequency range peaking at 14GHz, 3.25dB. By linear fitting the theoretical noise level to the measured response the effective system calibration factor (Syscal) was extracted. This was achieved by subtracting the effect of resolution bandwidth setting, thermal noise, 6dB divider effect and broadband smoothing leaving a small level of up to 1.4dB remaining. This system correction factor consists of impedance matching errors, 'nominal' broadband smoothing errors and the effect of system responsivity. Establishing this system correction factor is a key feature of the broad band reference laser noise source employed. Using traditional test methods this would be very tedious to determine and quite likely that the uncertainties associated with the measurements would be greater than the correction factor itself!

The previously derived 3dB rise noise figure was then adjusted by this derived system correction factor over frequency resulting in the true system noise figure and thus system sensitivity. Results show approximately 2dB noise figure for frequencies to 12GHz rising to a peak at 18GHz of <3dB, thus providing sensitivity levels of -172dBm and <-171dBm respectively. A peak is evident at 14GHz similarly found with the rf amplifier / spectrum analyser combination but with an improvement in noise figure at 20GHz thought to be attributed to the known photo detector responsivity variations at these higher frequencies.

The theoretical line fitting not only provided system correction factors but additionally provided a means to assess the broad band nature of the reference laser source, governed by the gradient. Measured noise gradients indicate spontaneous noise content to be <2% as predicted due to the inherent design of the reference laser source and the effect of optical attenuation. Essentially this provides a known broadband reference source with a 'flat' frequency profile, a significant feature of this system approach.

Further measurements using a second 'reference' laser of a longer wavelength (1533nm) provided similar sensitivity and correction factors, providing confidence in the systems ability to cater for telecommunication lasers in both the commonly used wavelength windows. A 'shot noise limited' response was also found for this laser source.

Noise measurement observations using a Fabry Perot constructed telecommunication laser provided confirmation of response behaviour in the presence of spontaneous noise. Here a linear response gradient of approximately 2 was derived as predicted by theory.

A second alternative system sensitivity measurement approach was investigated by way of modulating the light carrier to allow cross examination of reference laser findings. This is effectively a 'narrowband' optical signal rather than the previous 'broadband' with sensitivity determined by the 3dB rise in the noise floor. Results from directly modulating a DFB laser and also externally modulating a light carrier provided *worst case* correction factor and noise figure delta's of less than 0.4dB and 0.6dB respectively compared to the 'wideband' technique. This small difference between broad / narrowband approaches confirms the nominal 2dB offset previously reported (broad band level already compensated). Indeed, some of the remaining offset may be attributed to the nominal nature of this 2dB. Thus, good agreement has been obtained between narrow and broad band techniques technique's, considering the difficulty of measuring these small values.

The measurement of RIN itself is discussed in section 4.4. Here, the true benefit of the reference laser can be seen. Not only does it allow system correction factor adjustment but also provides a known 'wideband' reference source which can be used to simply subtract unwanted noise terms from the device under test. This consists of three measurement stages, obtaining the dark level, DUT level and the 'matched' reference level. From this a simple formula linked to a spread sheet can be used to determine the calibrated RIN. DUT RIN levels of below -170dBHz^{-1} have routinely been achieved on a number of different lasers. The improved system sensitivity level provides the ability to accurately measure RIN levels below the shot level, providing further test capability in the development of 'cleaner' lasers for tomorrow's optical networks.

Measurement uncertainty has been extensively defined with dominant terms being the reference noise level, DUT noise level and detector responsivity. The budget is based on a pessimistic view which in time is expected to reduce further on acquisition of more data history and further improvements. The level of RIN measured plays an important role in the resulting overall uncertainty level. For this reason the uncertainties defined are dynamically linked to the actual levels measured through partial differentiation. RIN levels below Shot noise are dominated by the DUT and reference contribution terms. At higher RIN levels the detector responsivity becomes more dominate. Based on five repeat measurements it has been shown that uncertainty levels of ±1dB are achievable for RIN levels approaching the shot noise level. Depending on the incident optical power this level of uncertainty has been achieved for RIN levels 10dB below shot noise. Analysis of the reference / DUT photo-current matching shows that improving the match <1% provides a diminishing improvement in the overall uncertainty. This may change if and when other dominant terms reduce in the future.

RIN traceability is essentially gained through the measured dc photo current, optical power and rf frequency. Compared to existing techniques, where the spectrum analyser provides traceability via the calibrated rf level and frequency, this referencing technique offers a more direct alternative traceable path to SI units.

The improved accuracy of the referencing technique eliminates the need to perform time consuming linear fitting at numerous optical power levels as reviewed in previous papers and NIST. This may open up an opportunity to reduce the dynamic range spec of the spectrum analyser / amplifier which may allow selection of a lower noise figure amplifier.

Direct comparisons have been performed on a loan HP Lightwave Analyser detailed section 5. Experiments and communications with HP have allowed a better understanding of the equipments capabilities and limitations. For instance, there is no accounting for the spontaneous noise loss over attenuation, either for the internal attenuator or the responsivity loss of the photo detector, 5.2.2.3. This effect was highlighted in section 3.5.1. Laser RIN comparison measurements have been performed between the two systems. After accounting for the attenuation affect an offset of approximately +1.75dB was found for 3 to 16GHz. Either side of this window the RIN response was limited by the HP's system sensitivity, whereas the referencing technique shows a trace which is much more inline with that expected for RIN.

More detailed experiments looked into the HP's calibration accuracy. The system is calibrated via a 300MHz narrow band signal and then a wide flatness tolerance of ±2dB stated for all other frequency points. Applying the reference laser we have established the actual response flatness to be approximately ±1dB. Correcting for this pulls in the comparison offset to <1dB for RIN's between 3 to 16GHz. The HP Lightwave Analyser provided a further software feature to correct for amplitude errors, referred to as 'AMPCOR'. Basically, this relied on performing multiple measurements at 0 & 3dB attenuation settings, described in section 5.2.3.4. Testing performed agreed well with the reference laser technique at 3, 8 & 13GHz tested, indicating that this feature does reduce error terms such as frequency dependence, broadband noise smoothing etc. Indeed, the electrical equivalent of the AMPCOR factor, 1.75dB (8GHz) shows some comparison with the calibration error term, 2.1dB derived by applying the reference laser, 5.2.3.2. But, it remains to be seen if this approach can account for the spontaneous noise attenuation affect. The remaining AMPCOR measurements either side of this range at 1 & 20GHz proved unsuccessful due to sensitivity limitations of the HP Lightwave Analyser.

Sensitivity of the HP Lightwave Analyser was found to range from -157dBm to -167dBm over the full frequency range based on subtracting thermal noise from the dark level response. This suggests the RIN referencing technique outlined in this report provides between 4dB to 14dB better sensitivity over the frequency range, which is a significant step forward. Loan time restrictions prevented the inclusion of further sensitivity tests based on the 3dB rise technique.

6.2 Chirp Measurement

Development of the fibre interferometer for the chirp measurement capability inherently offers high resolution (<100KHz) due to the fibre delay selected, wide dynamic range as well as flexibility in terms of the overall RIN/Chirp utilisation. Inclusion of the faraday rotating mirrors has not impacted overall optical insertion loss compared to the standard and HP interferometers. This is partly due to the reduced connector count and removed need for a polarisation state controller. Simple polarisation testing of the Birefringent Insensitive Interferometer (BII) confirmed its insensitive nature early on which has a secondary effect of improving stability over temperature and to physical movement during measurement.

Performance investigations have been somewhat hampered by equipment delivery and thus experiments have been largely limited to the lower modulation frequencies for gated signals. This has prevented drawing conclusion on the full benefits of the approach taken at this time. Even so, significant testing has been performed covering modulation frequencies from MHz to GHz, resulting in frequency chirps of MHz to GHz. Both convoluted and un-convoluted Bessel states have been observed, details of which are discussed below.

Initial linewidth response observations showed the importance of optical isolation between the laser and interferometer. With no isolation a recurring 33MHz ripple was super imposed on the response which equates to a fibre path length of 3.3m. This happened to be the length of fibre between the collimating lens and the FC/PC connector at the interferometer input, subsequently eliminated by inclusion of a 60dB 'in-fibre' isolator. Linewidth measurements have shown good agreement from the simple 3dB drop approach to lorenztian line fitting and later from the width of a resolvable Bessel function when modulated. Benefit was seen in performing linewidth assessment with the rf amplifier removed due to the amplifier gain drop off at <10MHz. Laser sources available consisted of DFB's providing linewidths from 2MHz to 20MHz.

Under low modulation frequencies (<2xLW) the convoluted response provides a clear image of frequency chirp. Comparisons have been carried out to the standard interferometer which indicates the BII to have approximately 7 to 10dB improved amplitude sensitivity. This will benefit the measurement resolution for determining the response 3dB drop point. The amplitude reference point, from which to determine the 3dB drop frequency has not been defined clearly in previously literature. The reference point assumed in this report is based on the average level obtained from MHz to the highest amplitude level before the response rolls off. Graphically, this best describes the chirp effect on linewidth when modulated and has been used for all correlations.

Benefits of the gated delayed self homodyne approach have been observed, which prevents the cyclic nature of resultant chirp as the modulation frequency is increased. A linear relationship has been reported between injected current and chirp ($GHzmA^{-1}$) for DFB lasers inline with previous published papers. Additionally, initial chirp measurements show an approximate -7% difference for the BII compared to the standard interferometer which is believed to be as a result of birefringence removal. More data measurements are needed at higher chirp frequencies to confirm this effect is proportional to the resultant chirp.

To aid the calibration and traceability of the DUT set up conditions, a routine to determine the amplitude modulation index at the interferometer input has been defined and performed. This takes advantage of the calculable reference laser to calculate the systems amplitude offset and thus provide a modulated power level. The approach avoids the requirement to calibrate the applied rf input signal level for every DUT setup, which would otherwise need to have consider VSWR matching dependence.

For higher modulation frequencies the resultant un-convoluted lower order Bessels have been analysed and compared to the classic FM theory expected. The carrier signal width, evident on top of each Bessel, is dependent on the spectrum analyser resolution bandwidth selected, thus better Bessel amplitude tracking is obtained when the resolution bandwidth is set lower. This tracking has provided the re-occurring null point response as predicted in 7.1.3 for both gated and non gated techniques. The FM index at these points together with the modulation frequency applied has provided the effective chirp excursion, which has shown good cross correlation to the 3dB drop technique (convoluted response). Due to the lower FM index for the first null point the gated technique offers a slight improvement in terms of chirp measurement points across applied modulation level.

Further, a nulling ratio technique has been described and demonstrated, 4.6.5 which came improve the modulation level capability, thus providing a more versatile system.

6.3 Summary

This programme of work was initiated in response to the DTI National Measurement System Policy Unit's requirement to further advance the measurement and understanding of laser noise, typically for telecommunications. Project focus centred on two noise parameters, RIN and Chirp, initially reviewing measurement theory and appraising existing techniques forming the following observations;

RIN

- Shortfall in sensitivity for today's DFB laser diodes
- Large number of tedious measurements required to obtain confidence
- Ambiguity in accounting for sources of noise loss
- No in-depth consideration of measurement uncertainty

Chirp

- Resolution capability
- Potential systematic offset caused by birefringence
- No in-depth consideration of measurement uncertainty
- No technical pull observed for temporal chirp

Project objectives were then outlined:

The calibration standard must be able to measure laser noise down to the shot noise level for optical power levels which range between 100 μW to 5 mW. Laser RIN measurement sensitivities should be capable of measuring levels as low as -170 dBHz^{-1} @1mW over a frequency range of 10MHz to 20 GHz to better than ±1dB uncertainty. The dynamic range of the RIN measurement should be at least 70 dB so that the versatility in the measurement can be achieved. The system must be able to measure frequency chirps as large as 50 GHz and as low as 100 KHz, over as wider modulation frequency range as possible to better than ±10%. Both parameters should focus on the two telecommunications windows at wavelengths of 1300nm and 1550nm (±50nm).

Additional capabilities within the system developed should consider;

- back-scatter degradation
- linewidth of laser sources
- frequency response of detection systems
- noise figure of optical amplifiers
- gain of optical amplifiers

The novel RIN measurement developed, utilising a reference laser has significantly advanced the understanding of the observations mentioned previous. Sensitivity has improved by some 4 to 14dB to that available commercially and in national laboratories, significantly through component selection and the referencing calibrations implemented. The overall impact of incorporating the referencing measurement has actually simplified the measurement process, essentially by providing a far more accurate result based on fewer samples. Its inclusion effectively provides specific system calibration for each and every measurement undertaken, whether the signal is high or low level thus minimising measurement uncertainties such as linearity over range etc. It provides a like-for-like simplistic subtraction for unwanted noise terms such as Shot and thermal noise, naturally compensating for losses and additionally provides traceability. A thorough break down of the measurement uncertainty contributions has been created, analysed, tabulated and dynamically linked incorporating random and systematic uncertainties. Example measurements have shown capability close to the ±1dB target when laser noise is equal to the shot noise level and considerably more favourable as the laser noise increases.

This development is believed to have the greatest sensitivity and most accurate RIN capability achieved to date, demonstrating enhanced performance over the HP Lightwave Anaylser. The research has improved understanding of systematic noise contributions such as broadband smoothing, impedance match loss and importantly the observation of spontaneous noise loss under attenuation compared to shot noise. These findings have been reviewed with NIST and HP both of which had not considered the spontaneous loss over attenuation. Papers outlining these findings have been presented at the Optical Fibre Measurement Conference, British Electro-Magnetic Conference, London Metropolitan University, International Symposium on Telecommunication and subsequent publication in IEE Proceedings, see 'Published Papers' section. Detailed reports have been submitted to the DTI's NMSPU and the reference laser concept has been patented. A number of laser diode

companies have now used the facility, specifically looking at better defining their products noise contribution.

For the measurement of Chirp the assembled homodyning system provides a resolution capability of 100kHz which has proved appropriate and also suitable for the majority of DFB lasers when measuring line width. Findings are generally in line with previously reviewed papers with the addition of improved amplitude sensitivity, 7 – 10dB and increased measurement stability due to the use of faraday rotating mirrors. These improvements aid the ability to analyse line width and Bessel responses for chirp. A maximum chirp of 25GHz can be assessed, representing FWHM(optical) which is considered adequate for most telecom lasers. Larger chirps could be measured by selecting wider bandwidth system components but this would be at the expense of sensitivity. Optical isolators have been seen as crucial to prevent reflection ripples within the line width / chirp responses, typically >60dB required. The original intention of the faraday rotating mirrors was to naturally cancel out the predicted theoretical systematic error caused by fibre birefringence in the delay arm. Some constraints have prevented drawing conclusions on this, however, some lower frequency analysis has demonstrated a small systematic offset between the BII system and the standard interferometer method. The reference laser has once again proved useful, this time to determine the applied amplitude modulation index for a given chirp thus avoiding more complex calibration. The effective chirp under low modulation frequencies has been observed and calculated using the 3dB drop technique, similarly to line width. Initial uncertainty budget shows that a 10% uncertainty level is reasonable for chirp. At higher modulation frequencies chirp has been demonstrated and assessed using a Bessel nulling technique as well as a Bessel ratio technique coupled to modelled classic FM theory. This latter technique provides a more flexible capability to suit amplitude modulation levels which may not coincide with a 'null' condition.

6.4 Way Forward

Following the initial assembly of the uncertainty budget a number of incremental developments should be pursued to improve measurement uncertainty and capability. Examples include;

6.4.1 Relative Intensity Noise

- operating noise traces as close as possible to the top of the spectrum analyser screen to reduce log scale fidelity errors
- increasing linearity data for the reference source to thus reduce its systematic contribution
- incorporating optical switching of ref and DUT signals
- analysing best repeatability procedure
- incorporation of slightly improved noise figure spectrum analyser
- incorporate controllable reflector to allow for RIN backscatter degradation assessment
- compare to NIST when system becomes available

Further uses of this combined facility have been identified during this research. The reference laser is effectively a shot noise limited calculable noise source. This essentially flat frequency signal can be used for the frequency response characterisation of optical detectors. Initial measurements performed have shown comparable responses to that gained using heterodyning technique. The reference source could additionally be used to determine noise figure / gain of optical amplifiers and also may provide an alternative microwave rf noise source standard. The main obstacle to over come for the latter example is the large difference in noise level between the laser, typically -160dBm compared to a useful mircowave rf standard of -10dBm for instance.

6.4.2 Chirp

- further develop classic FM modelling capability for high frequencies
- demonstrate fibre birefringence systematic effect at higher modulation frequenc
- develop a corresponding uncertainty budget for high modulation frequency
- assess the use of a fibre grating as a transfer standard
- potentially could adapt system to provide alpha co-efficient of lasers and external modulators

An application realised during development relates to an alternative approach to measure optical fibre length. This utilises the un-gated approach, where there is a phasing in and out of chirp as the modulation frequency is adjusted. National Standard techniques rely on pulse

timing methods, achieving accuracies approaching 2 parts in 10^4. A comparative test was performed using a 'golden' fibre loaned from NPL, Teddington with an uncertainty of ±0.8m. Here, an average offset of <-0.25m was achieved over a single mode fibre length of 4,459.6m. Further testing over a range of fibre reels from 30m to 10km concluded that fibre path length can be measured to a resolution of 10^5 for single mode fibre with standard deviation <0.002%. Measurement performed on a multimode fibre reel, 100m @ 1300nm also provided favourable results although due to the greater inter-modal dispersion, at a larger uncertainty level. A paper outlining the theory, results and benefits of this approach has been published at OFMC, see published papers section. This paper includes experimental results of a crude low-cost approach, utilising a photo-detector connected to an rms volt meter. Without filtering or amplification the oscillating E-field behaviour was clearly evident. Measurements gained enabled the period frequency to be determined, typically to within $5x10^4$. Refinements to this system could improve on this further.

7 Appendix A – Interferometer Theory

7.1.1 Laser Linewidth Theory

In this analysis the system below is considered:

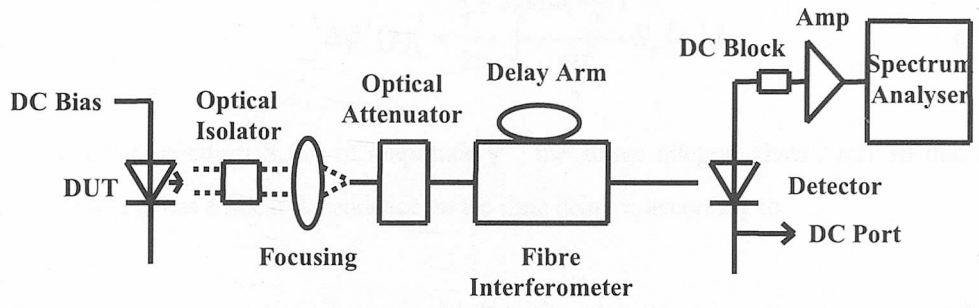

Figure 7-1: Apparatus for Linewidth Measurement Technique.

From Figure 7-1 it can be seen that no direct modulation of the laser takes place except for a frequency change in the one arm of the interferometer. This would normally be done using an acoustic optic modulator. Thus the total E field incident on the detector will be given by:

$$E_d(t) = E[e^{i((\omega+\omega_m)t+\phi(t))} + e^{i(\omega+\omega_m)(t+\tau_o)+\phi(t+\tau_o)}] \quad (7\text{-}1)$$

where, ω is the laser frequency, ω_m is the frequency change, τ_o is the optical delay difference in the interferometer and $\phi(t)$ is the associated phase. The current generated in the photodetector will be given by

$$\rangle E_d(t) * E_d^*(t) \langle \quad (7\text{-}2)$$

where brackets indicate the time average.

$$i_d(t) = E^2 * [2 + e^{-i(\omega_m\tau_o+\omega\tau_o+\phi(t+\tau_o)-\phi(t))} + e^{i(\omega_m\tau_o+\omega\tau_o+\phi(t+\tau_o)-\phi(t))}] \quad (7\text{-}3)$$

The responsivity of the detector has been assumed to be 1 throughout all the modelling. The spectrum analyser measures the fourier transform of the (photocurrent)^2 given above. First the photocurrent auto correlation will be derived,

$$R(\tau) = \left\langle i_d^*(t) * i_d(t+\tau) \right\rangle \tag{7-4}$$

where τ is different from the τ_o introduced by the interferometer. During the mathematical procedures an assessment of the phase jitter will be required [17]. Assuming the phase jitter to be a zero-mean random process having a Gaussian probability distribution, its variance σ^2 is related to the instantaneous frequency fluctuation spectrum $S_\varphi(\omega)$ by

$$\left\langle \Delta\phi^2(\tau) \right\rangle = \frac{\tau^2}{2\pi} \int_{-\infty}^{+\infty} \frac{\sin(\frac{\omega\tau}{2})}{\frac{\omega\tau}{2}} S_\varphi(\omega) d\omega \tag{7-5}$$

Assuming a flat spectrum $S_\varphi(\omega)$ of amplitude γ[57], the above integral gives $2\gamma\pi/\tau$ so that the variance $<\Delta\phi^2(\tau)>$ has a linear dependence on the time delay τ, according to

$$\left\langle \Delta\phi^2(\tau) \right\rangle = \gamma|\tau| \tag{7-6}$$

The other expression that has been used is

$$\left\langle e^{i\Delta\phi(t,\tau)} \right\rangle = \exp\left[\frac{-\left\langle \Delta\phi^2(\tau) \right\rangle}{2} \right] \tag{7-7}$$

which holds for random phase jitter[56,57]. The derivation is further simplified if one ignores some of the DC contributions (such as $\omega\tau_o$) and the use of the fact that in the final expression that $<e^{i\omega_m t}>$ tends to 1. This provides the following expression for the case when;

$\tau_o > \tau$

$$R(\tau) = E^4 \left[4(1 + e^{-\frac{\gamma\tau_o}{2}}) + (4e^{-\frac{\gamma\tau_o}{2}} + 2e^{-\gamma\tau_o}) \cos\omega_m\tau + 2e^{-\frac{\gamma\tau}{2}} \cos\omega_m\tau \right] \tag{7-8}$$

Similarly for the case when;

$\tau > \tau_o$

$$R(\tau) = 4E^4 \left[(1 + e^{-\frac{\gamma\tau_o}{2}}) + (1 + e^{-\frac{\gamma\tau_o}{2}}) \cos\omega_m\tau \right] \tag{7-9}$$

The spectrum analyser will display the fourier transform of the above expressions. For $\tau_o > \tau$ the last term contains the important information and its fourier transform is given below.

$$\int_0^{\tau_o} \exp(-\gamma\tau + i\omega_m\tau)\exp(-i\omega\tau)d\tau \qquad (7\text{-}10)$$

However, after some derivation of the above the following expression is obtained.

$$S(\omega) = \frac{E^4}{\pi}\frac{\gamma}{\left[\gamma + (\omega-\omega_m)^2\right]}\left[1 - e^{-\gamma\tau_o}\left[\cos(\omega-\omega_m)\tau_o + \frac{(\omega-\omega_m)}{\gamma}\sin(\omega-\omega_m)\tau_o\right]\right] + E^4\left|4\delta(\omega) + e^{-\gamma\tau_o}\delta(\omega-\omega_m\right| \qquad (7\text{-}11)$$

It can clearly been seen in the above spectrum that as the delay time τ_o is increased the spectrum will dominated by the Lorentzian linewidth profile centred at the modulation frequency. At short delays the expression above predicts a monochromatic term. This is demonstrated in the following modelled plots.

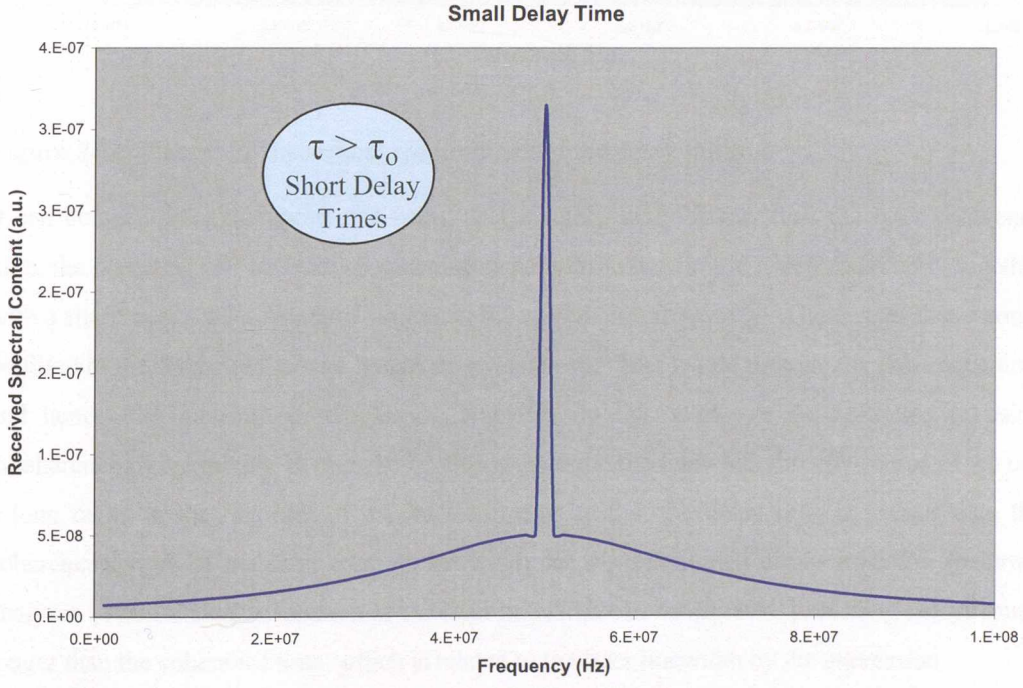

Figure 7-2: Plot of the theoretical spectrum with short delay times.

Both the plots Figure 7-2 & Figure 7-3 are modelled for a laser of linewidth 20 MHz and the modulating frequency of 50 MHz. Figure 7-2 represents an interferometer with an optical delay of 0.7 μs and Figure 7-3 has an optical delay of 30 μs.

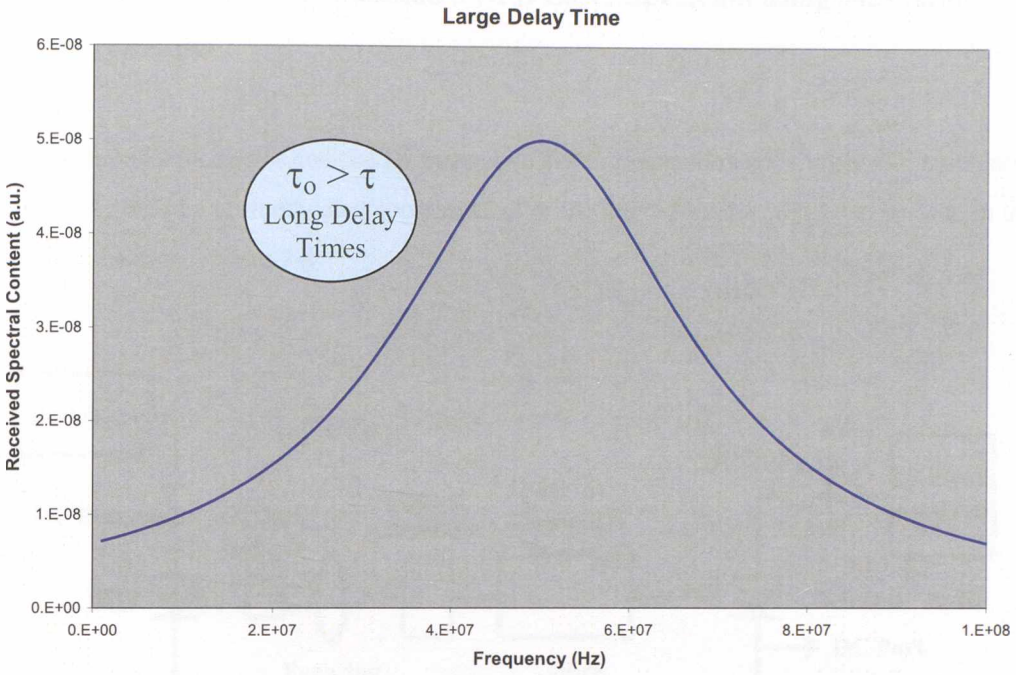

Figure 7-3: Plot of the theoretical spectrum with long delay times.

It can be seen from the above that using delays significantly shorter than the laser coherence time, the observed self-heterodyne spectrum departs from the simple Lorentzian curve, together with a sharp peak (delta function) centred at the modulation frequency. The results above could be fitted to the theoretical power spectrum given above. This would provide the coherence time and hence the linewidth of the laser. However, in this work we are restricted to using incoherence of the mixing in order to be able to measure the linewidth directly. Thus, if we use a long delay in the one arm of the interferometer so that the delay time is greater than the coherence length of the laser then its linewidth can be determined easily from the spectrum analyser. Thus, a clear evaluation of the laser linewidth can be achieved providing delays much longer than the coherence time, which is related to the laser linewidth by the expression

$$\tau_{co} \geq \frac{2}{\Delta\omega} \tag{7-12}$$

for a Lorentzian lineshape. For an optical delay of 30 μs the spectral resolution limit will be < 100 KHz. Also, for large laser linewidths, the acoustic optic modulator could be removed, and the Lorentzian profile above will be centred at DC. This is only appropriate if the contribution of the 1/f noise at DC is assessed to be a very small fraction of the measured linewidth.

7.1.2 Measurement of a Modulated DFB Laser Spectrum using the Gating Technique

In this technique the laser is switched between two states of operation allowing an RF modulated laser to mix with an un-modulated component after the interferometer. This can be seen in the following diagram, Figure 7-4.

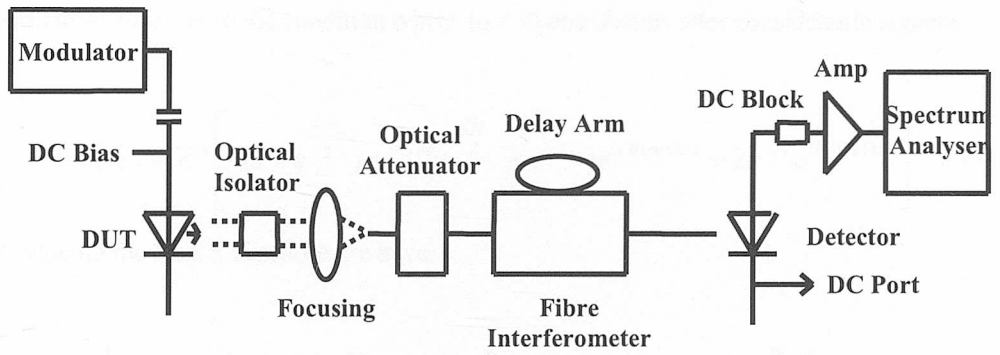

Figure 7-4: Gated Delayed Self-Homodyne Technique Set-up.

In this situation the period of the switching will be determined by the length of the optical delay introduced and in its simplest form will be twice the optical delay time. The complete equation for the modulation will be given by:

$$E(t) = E\sqrt{(1 + m\sin\Omega t)} \times e^{i(\omega t + \phi(t) + \beta\sin\Omega t)} \tag{7-13}$$

where M is the frequency modulation index, m is the amplitude modulation index and Ω is the RF modulation frequency. This expression simplifies for small modulation levels:

$$E(t) = E\left[1 + \frac{m}{2}\sin\Omega t\right] e^{i(\omega t + \phi(t) + \beta\sin\Omega t)} \tag{7-14}$$

Clearly, the intensity and frequency modulation index are inter-related via the well known α coefficient of the laser. This is essentially an indication of the coupling between the real and imaginary components of the refractive index. This means that changes in the carrier densities in the laser cavity will be followed by changes in the absorption/stimulation which will change the imaginary component. The effects of this on the real component of the refractive index will be dictated by the magnitude of the α coefficient. The change in the refractive index changes the optical cavity length and the lasing frequency and hence gives rise to a chirp.

In this gated delayed self-homodyne technique the total E-field incident on the detector will be:

$$E_d(t) = E\left[e^{i(\omega t+\phi(t)+\beta\sin\Omega t)} + e^{i(\omega(t+\tau_o)+\phi(t+\tau_o)}\right] \quad (7\text{-}15)$$

the amplitude modulation term being ignored at this stage. Thus, the photocurrent generated will be:

$$i_d(t) = \left\rangle E_d^*(t)E_d(t)\right\langle = E^2\left[2 + e^{i(\phi(t+\tau_o)-\phi(t)-\beta\sin\Omega t)} + e^{-i(\phi(t+\tau_o)-\phi(t)-\beta\sin\Omega t)}\right] \quad (7\text{-}16)$$

Now in a similar manner to section 7.1.1 the auto correlation function of the photocurrent (restricting ourselves to the condition where τo > τ) one obtains after considerable algebra:

$$R(\tau) = E^4\left[4(1+e^{\frac{-\gamma\tau_o}{2}}) + 2(2e^{-\frac{\gamma\tau_o}{2}} + e^{-\gamma\tau_o})e^{i(\beta\sin\Omega\tau)} + 2e^{-\gamma\tau}e^{i(\beta\sin\Omega\tau)}\right] \quad (7\text{-}17)$$

Introducing the Bessel functions we have:

$$R(\tau) = E^4\left[4(1+e^{\frac{-\gamma\tau_o}{2}}) + 2(2e^{-\frac{\gamma\tau_o}{2}} + e^{-\gamma\tau_o})\sum_{n=-\infty}^{\infty} J_n(\beta)\cos(n\Omega\tau) + 2e^{-\frac{\gamma\tau}{2}}\sum_{n=-\infty}^{\infty} J_n(\beta)\cos(n\Omega\tau)\right] \quad (7\text{-}18)$$

The inclusion of the Bessel functions introduces sidebands which will be separated by the modulation frequency. Thus, one can see that this is very similar to the expression derived in section 7.1.1 except that there are a large number of sidebands instead of one sideband created by the acoustic optic modulator. Again each sideband will be convolved with the Lorentzian lineshape of the laser.

The amplitude of each sideband should be determined by the appropriate Bessel coefficients, however, because of the intensity modulation term in the original equation the amplitudes of the sidebands will not be predicted directly from the Bessel coefficients of that order. The actual amplitudes of the sidebands can be predicted from the following expansion:

$$E(t) = [1+\frac{m}{2}\sin\omega t][J_o(\beta)\cos\omega_m t - J_1(\beta)[\cos(\omega_m+\omega)t - \cos(\omega_m-\omega)t] + J_2(\beta)[\cos(\omega_m+2\omega)t - \cos(\omega_m-2\omega)t] + \ldots\ldots \quad (7\text{-}19)$$

where $J_o(\beta)$ etc are the Bessel coefficients. Multiplying the terms out, a standard set of Bessels function are obtained as well as a set of expressions multiplied by $m/2\sin(\omega t)$. Considering each of these terms in order we obtain:

$$J_o(\beta)\frac{m}{2}\sin\omega t\cos\omega_m t = \frac{J_o(\beta)m}{4}[\sin(\omega_m+\omega)t-\sin(\omega_m-\omega)t] \quad (7\text{-}20)$$

From this expression it can be seen that a contribution is made to the first sideband from the zero order Bessel coefficient.

$$-J_1(\beta)\frac{m}{2}\sin\omega t[\cos(\omega_m+\omega)t-\cos(\omega_m-\omega)t] = -J_1(\beta)m\sin^2\omega t\sin\omega_m t$$
$$= -J_1(\beta)m\sin\omega_m t[1-\cos^2\omega t] \quad (7\text{-}21)$$

This demonstrates that there is a component of the first order Bessel coefficient at the carrier frequency. Also, it can be shown that the term involving the second order Bessel function will be given by:

$$J_2(\beta)\frac{m}{2}\sin\omega t[\cos(\omega_m+2\omega)t-\cos(\omega_m-2\omega)t]=\frac{-J_2(\beta)m}{4}[\sin(\omega_m+\omega)t+\sin(\omega_m-\omega)t]$$
$$+\frac{J_2(\beta)m}{2}\sin\omega_m t\cos^3\omega t \quad (7\text{-}22)$$

where there is clearly an influence of the second Bessel coefficient on the first sideband. The power at the carrier frequency (zero order Bessel) will be given by:

$$\text{Carrier frequency}\quad J_o^{\,2}(\beta)+J_1^{\,2}(\beta)m^2 \quad (7\text{-}23)$$

$$\text{First sideband}\quad J_1^{\,2}(\beta)+[\frac{J_o(\beta)m}{4}-\frac{J_2(\beta)m}{4}]^2 \quad (7\text{-}24)$$

The variation of the zero order and first order as a function of modulation level is shown in Figure 7-5.

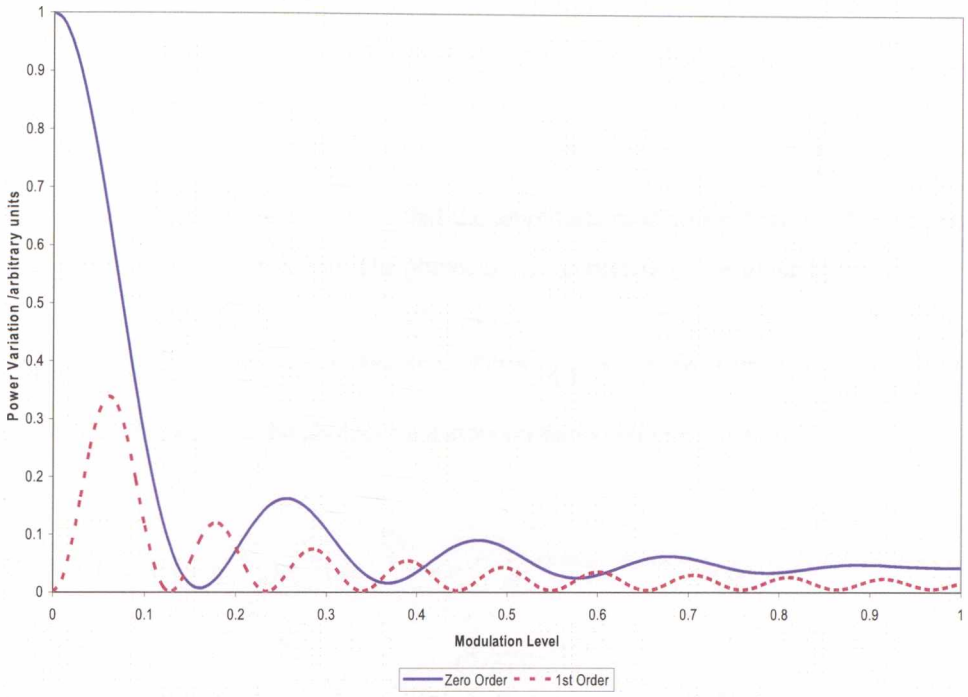

Figure 7-5: Zero and first order sidebands as a function of the RF modulation level.

The zero order goes through a zero (or a minimum) at M 2.4 which is inline with standard frequency modulation theory for a carrier signals amplitude. Thus, for low modulation levels the frequency modulation index could potentially be measured very efficiently. In contrast the first sideband goes through to a minimum at M 3.8. It can be seen that the sidebands go to a minimum at nearly the same point as the straight forward Bessel coefficients and hence this technique can be used efficiently to determine the chirp.

7.1.3 RF Modulation Self Beating Interferometer

In this system the same interferometer is used but there is no switching of the RF modulation i.e., the modulated laser beats with modulated laser light. In the previous example the laser frequency effectively beats only with each of the Bessel sidebands. However, in this system we have a case where each sideband beats with itself and each sideband in turn, so that there may be a number of cross multiplying terms. For example the first sideband obviously is a result of the beating of the first sideband with the laser frequency (as in section 7.1.1) but also there may be contributions from the beating of the second and first sideband, third and second sideband etc. Thus, the amplitudes of the sidebands are expected to be strongly dependent on the other Bessel coefficients. The derivation below attempts to prove this principle.

The total E-field which is incident on the detector will be given by:

$$E_d(t) = E\left[e^{i(\omega t+\phi(t)+\beta\sin\Omega t)} + e^{i(\omega(t+\tau_o)+\phi(t+\tau_o)+\beta\sin\Omega(t+\tau_o)}\right] \quad (7\text{-}25)$$

In the above expression it can be seen that the amplitude modulation term has been ignored in order to simplifying the derivation. The photocurrent generated will be given by:

$$i_d(t) = E^2\left[2 + e^{i(\phi(t+\tau_o)-\phi(t)+\beta\sin\Omega(t+\tau_o)-\beta\sin\Omega t)} + e^{-i(\phi(t+\tau_o)-\phi(t)+\beta\sin\Omega(t+\tau_o)-\beta\sin\Omega t)}\right] \quad (7\text{-}26)$$

After considerable algebra the photocurrent autocorrelation will be given by

$$R(\tau) = E^4\left[4(1+e^{\frac{-\gamma\tau_o}{2}}) + 2(2e^{-\frac{\gamma\tau_o}{2}} + e^{-\gamma\tau_o})e^{i(\beta\sin\Omega\tau-\beta\sin\Omega\tau)} + 2e^{-\gamma\tau}e^{i(\beta\sin\Omega\tau-\beta\sin\Omega\tau)}\right]$$

(7-27)

This result confirms the understanding of the way this self-beating interferometer works and indeed all the sidebands do beat with each other. Introducing the Bessel Coefficients we obtain:

$$R(\tau) = E^4\left[4(1+e^{\frac{-\gamma\tau_o}{2}}) + 2(2e^{-\frac{\gamma\tau_o}{2}} + e^{-\gamma\tau_o})\sum_{n=-\infty}^{\infty}J_n(\beta)\cos(n\Omega\tau)\sum_{n=-\infty}^{\infty}J_n(\beta)\cos(n\Omega\tau)\right]$$

$$+ 2E^4e^{-\frac{\gamma\tau}{2}}\sum_{n=-\infty}^{\infty}J_n(\beta)\cos(n\Omega\tau)\sum_{n=-\infty}^{\infty}J_n(\beta)\cos(n\Omega\tau) \quad (7\text{-}28)$$

Again the spectrum at long optical delays will be given by the convolution of the sideband with the Lorentzian lineshape. The amplitude of each of the sidebands will depend on the combinations of Bessel coefficients from the other sidebands as dictated from the above expression.

$$R(\tau) = E^4\left[4(1+e^{\frac{-\gamma\tau_o}{2}}) + 2(2e^{-\frac{\gamma\tau_o}{2}} + e^{-\gamma\tau_o})\sum_{n=-\infty}^{\infty}J_n(\beta)\cos(n\Omega\tau)\sum_{n=-\infty}^{\infty}J_n(\beta)\cos(n\Omega\tau)\right]$$

$$+ 2E^4e^{-\frac{\gamma\tau}{2}}\sum_{n=-\infty}^{\infty}J_n(\beta)\cos(n\Omega\tau)\sum_{n=-\infty}^{\infty}J_n(\beta)\cos(n\Omega\tau) \quad (7\text{-}29)$$

Multiplying the terms out and equating to their respective sideband and restraining ourselves to the first three terms one obtains:

$$\left[(J_0^2 + 2J_1^2 + 2J_2^2 + 2J_3^2 + etc) + 4(J_0J_1 + J_1J_2 + J_2J_3)e^{i\Omega\tau} + (4(J_0J_2 + J_1J_3) + 2J_1^2)e^{i2\Omega\tau} + etc\right]$$

(7-30)

The trend can be clearly seen in the above result. However, due to the amplitude modulation it was seen earlier that the amplitude of the first two sidebands were given by:

$$\text{Carrier frequency} \quad J_0^2 = J_o^{\,2}(\beta) + J_1^{\,2}(\beta)m^2 \tag{7-31}$$

$$\text{First sideband} \quad J_1^2 = J_1^{\,2}(\beta) + [\frac{J_o(\beta)m}{4} - \frac{J_2(\beta)m}{4}]^2 \tag{7-32}$$

Substituting these amplitudes into the above expression the overall amplitude for the zero order sideband (A) will be given by

$$A = \left[J_0^2(\beta)(8+m^2) + J_1^2(\beta)(8m+16) + J_2^2(m^2) - 2J_0(\beta)J_2(\beta)m^2\right] \tag{7-33}$$

The amplitude of this zero order sideband is plotted as a function of modulation level (see Figure 7-6). It can be seen that in this case that this sideband goes through minimum at a point when M = 3.8 and this is different to the gated technique. It remains to be seen if this approach can be used to determine the chirp of the laser.

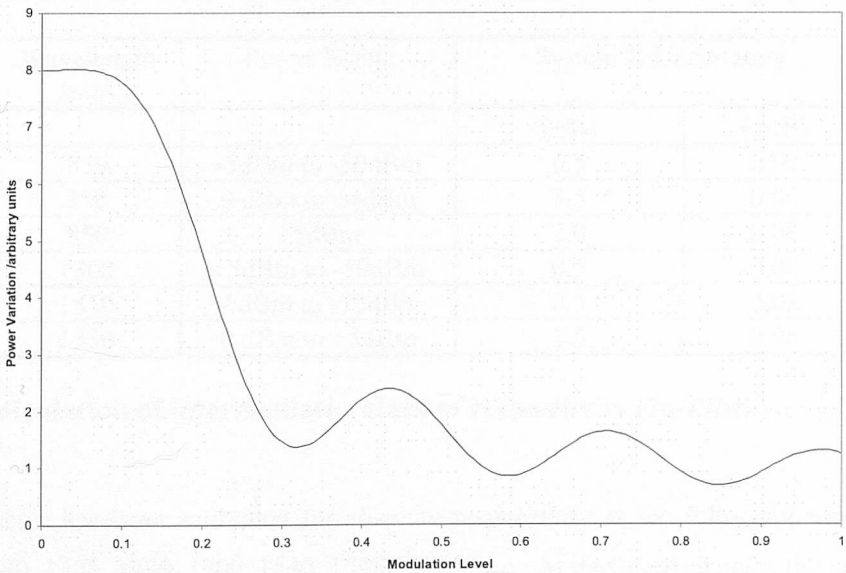

Figure 7-6: Zero Sideband as a Function of the RF Modulation Level.

One of the important conclusions from these last few sections is that for low modulation depths (so that essentially only one sideband is evident) the un-modulated linewidth of the laser can be determined. Low modulation levels are necessary because the Lorentzian tails of the neighbouring sidebands must have no effect on the sideband of interest.

8 Appendix B – Photodiode Uncertainties

NPL state the following uncertainties for the in-fibre calibration of the detector:

System 1: Comprising of Ge detector serial N° . 802043

Table 8-1: Responsivity of the Germanium reference detector (Note : 1% ≈ 0.04dB)

Wavelength(nm)	System 1. Uncertainty	
	(±%)	(±dB)
1280	0.5	0.02
1290	0.5	0.02
1305	0.5	0.02
1480	0.5	0.02
1500	0.5	0.02
1540	0.5	0.02
1548.5	0.5	0.02
1557	0.5	0.02

Table 8-2: Linearity of the Germanium reference detector

Wavelength (nm)	Power Range	System 1. Uncertainty	
		(±%)	(±dB)
850	-5dBm to -50dBm	0.5	0.02
850	0 dBm to +4dBm	1.5	0.06
850	+5dBm	2.0	0.08
1300	+5dBm to -50dBm	0.5	0.02
1550	-5dBm to -50dBm	0.5	0.02
1550	0 dBm to +5dBm	1.5	0.06

8.1 Calculation of intermediate values of responsivity (In-Fibre)

The detector has been calibrated for absolute responsivity at the following wavelengths: 1280, 1290, 1305, 1480, 1500, 1540, 1548.5, 1557nm. At these wavelengths the uncertainty in the value of responsivity is 1.0%. The detector has also been calibrated for free-space relative responsivity over the wavelength range 800nm to 1600nm.

Figure 8-1 shows the values of in-fibre responsivity plotted on the same graph as the values of free-space relative responsivity. By normalising the in-fibre responsivity to the free-space responsivity at 1305nm it can be seen that the values of in-fibre absolute responsivity change in proportion to the values of free-space relative responsivity.

From the graph it can also be seen that the in-fibre responsivities measured are in three distinct bands, these are:

(1280, 1290, 1305nm), (1480, 1500nm), (1540, 1548.5, 1557nm)

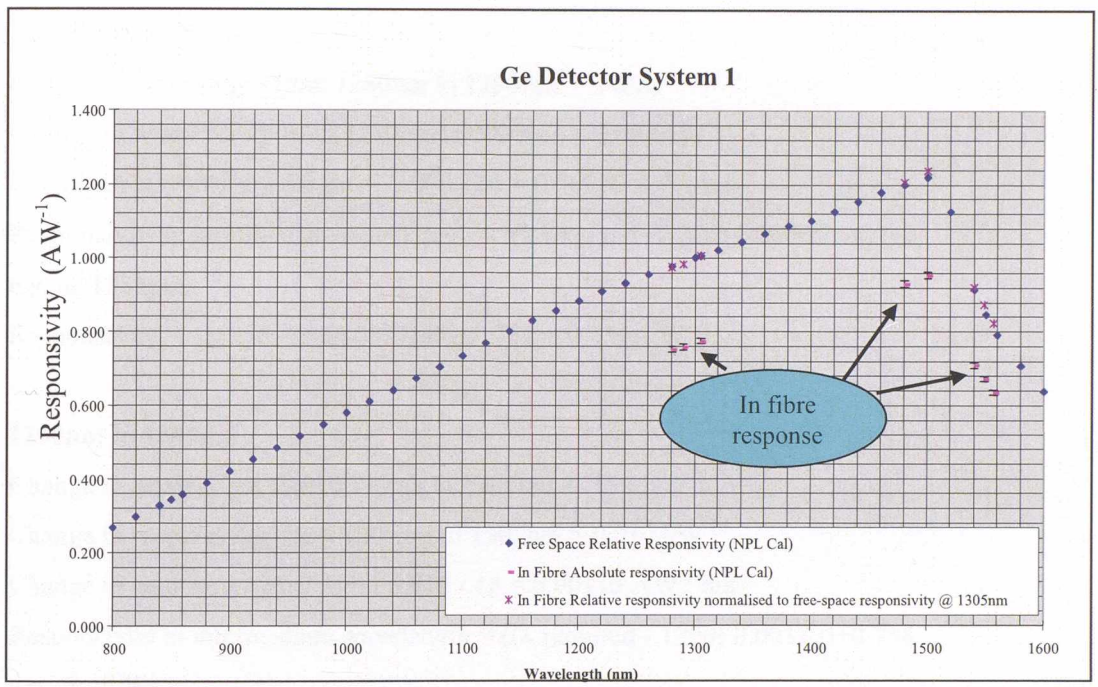

Figure 8-1: Ge Detector Responsivity.

To calculate the responsivity at intermediate points within each band, a straight line can be drawn through the points in each band. This will however give rise to an increase in the uncertainty of the value of responsivity at the intermediate wavelengths within each band. This additional uncertainty will be zero at the calibrated points but will increase as the wavelength increases from the calibrated point. As the wavelengths are a maximum of 20nm apart, the additional uncertainty caused by calculating values of intermediate responsivity can be considered to be negligible.

8.1.1 1280nm to 1305nm

This band consists of the following three wavelengths :

Table 8-3: 1280 to 1305nm Responsivity

Wavelength (nm)	Responsivity (AW^{-1})
1280	0.752
1290	0.758
1305	0.775

1280nm to 1290nm

Change in wavelength from 1280nm to 1290nm = 10nm

Change in responsivity from 1280nm to 1290nm = $0.006AW^{-1}$

Change in responsivity per nm = 0.006 / 10 = 0.00060 AW^{-1} nm^{-1}

Responsivity at intermediate wavelength = ((λ required - 1280) 0.00060)+0.752

e.g. @ 1285nm

Responsivity = ((1285-1280) 0.00060)+0.752 = $0.755A/W^{-1}$

1290nm to 1305nm

Change in wavelength from 1290nm to 1305nm = 15nm

Change in responsivity from 1290nm to 1305nm = $0.017AW^{-1}$

Change in responsivity per nm = 0.017 / 15 = 0.00113 AW^{-1} nm^{-1}

Responsivity at intermediate wavelength = ((λ required - 1290) 0.00113)+0.758

e.g. @ 1298nm

Responsivity = ((1298-1290).0.00113)+0.758 = $0.767AW^{-1}$

8.1.2 1480nm to 1500nm

This band consists of the following two wavelengths:

Table 8-4: 1480 to 1500nm Responsivity

Wavelength (nm)	Responsivity (AW^{-1})
1480	0.930
1500	0.954

1480nm to 1500nm

Change in wavelength from 1480nm to 1500nm = 20nm

Change in responsivity from 1480nm to 1500nm = $0.024AW^{-1}$

Change in responsivity per nm = 0.024 / 20 = 0.0012 AW^{-1} nm^{-1}

Responsivity at intermediate wavelength = ((λ required - 1480) 0.0012)+0.930

e.g. @ 1490nm

Responsivity = ((1490-1480).0.0012)+0.930 = $0.942AW^{-1}$

8.1.3 1540nm to 1557nm

This band consists of the following three wavelengths:

Table 8-5: 1540 to 1557nm Responsivity

Wavelength (nm)	Responsivity (AW^{-1})
1540	0.709
1548.5	0.673
1557	0.635

1540nm to 1548.5nm

Change in wavelength from 1540nm to 1548.5nm = 8.5nm

Change in responsivity from 1540nm to 1548.5nm = $-0.036AW^{-1}$

Change in responsivity per nm = -0.036 / 8.5 = -0.00424 AW^{-1} nm^{-1}

Responsivity at intermediate wavelength = ((λ required - 1540)x -0.00424)+0.709

e.g. @ 1544nm

Responsivity = ((1544-1540)x -0.00424)+0.709 = $0.692AW^{-1}$

1548.5nm to 1557nm

Change in wavelength from 1548.5nm to 1557nm = 8.5nm

Change in responsivity from 1548.5nm to 1557nm = $-0.038AW^{-1}$

Change in responsivity per nm = -0.038 / 8.5 = -0.00447 AW^{-1} nm^{-1}

Responsivity at intermediate wavelength = ((λ required - 1548.5)x -0.00447)+0.673

e.g. @ 1553nm

Responsivity = ((1553-1548.5)x -0.00447)+0.673 = $0.653AW^{-1}$

8.2 Uncertainty of the three bands

Using the methods shown above, the in-fibre responsivity can be calculated over the following wavelengths with negligible increase in the uncertainty quoted in the NPL calibration certificate (±1.0%)

(1280nm to 1305nm) (1480nm to 1500nm) (1540nm to 1557nm)

8.3 Calculation of intermediate values of responsivity outside the main In-fibre calibration bands

Values of responsivity can be calculated at wavelengths outside these bands, however the additional uncertainty of measurement will increase as the wavelength deviates from the band. At these other wavelengths the only way to calculate the absolute in-fibre responsivities will be to use the variations in the relative free-space responsivities as a multiplying factor.

8.3.1 1305nm to 1480nm

Table 8-6: 1305 to 1480nm Responsivity

Wavelength (nm)	Free-Space Relative Responsivity (AW^{-1})	Increase in Free-Space Relative Responsivity (%) from 1305nm	In-Fibre Absolute Responsivity (AW^{-1})	Increase in In-Fibre Absolute Responsivity (%) from 1305nm
1305	1.005	0	0.775	0
1480	1.200	19.403	0.930	20.000

It can be seen from Table 8-6 that the value of free-space responsivity has increased by 19.403% over the wavelength range 1305nm to 1480nm. The value of in-fibre responsivity has increased by 20.000% over the same wavelength range. If the value of in-fibre responsivity is increased in proportion to the free-space relative responsivity between the wavelength 1305nm to 1480nm, the calculated value of in-fibre responsivity will differ from the NPL quoted value by (20.000-19.403) = 0.6% (0.597%).

Using the calculation shown above, the maximum error in the calculation of the in-fibre responsivity is at 1480nm (0.6%). However, the value of in-fibre responsivity at this wavelength is stated in the calibration certificate, therefore there should be NO additional error at 1480nm.

If the wavelength is increased from 1305nm to a point mid-way between 1305 and 1480nm, and likewise the wavelength decreased from 1480nm to this mid-point, then the additional error will increase as the mid point is approached. The additional error being zero at 1305nm and 1480nm. This additional error should be less than 0.6% at the mid-point, however as it is not possible to calculate the degree by which the error is reduced, it will be left at 0.6%.

In summary, wavelength range 1305nm to 1480 nm should be split into two further ranges : 1305nm to 1390nm and 1395nm to 1480nm. The additional error will be zero at 1305nm and 1480nm, but will rise to 0.6% at 1390nm. This represents an additional error of :

For 1305nm to 1390nm :0.6 / (1390 - 1305) = 0.007% nm^{-1}

For 1480nm to 1395nm :0.6 / (1480 - 1390) = 0.007% nm^{-1}

8.3.2 Calculation of responsivity (1305nm to 1390nm)

Table 8-7: 1305 to 1390nm Responsivity

Wavelength (nm)	Free-Space Relative Responsivity (A/W)	Increase in Free-Space Relative Responsivity (%) from 1305nm	In-Fibre Absolute Responsivity (A/W) (Note 1)	Additional Error(%)
1305	1.005	0.000	0.775	0
1310	1.011	0.597	0.780	0
1315	1.016	1.095	0.783	0.1
1320	1.021	1.592	0.787	0.1
1325	1.026	2.090	0.791	0.1
1330	1.032	2.687	0.796	0.2
1335	1.037	3.184	0.800	0.2
1340	1.043	3.781	0.804	0.3
1345	1.049	4.378	0.809	0.3
1350	1.055	4.975	0.814	0.3
1355	1.06	5.473	0.817	0.4
1360	1.066	6.070	0.822	0.4
1365	1.072	6.667	0.827	0.4
1370	1.077	7.164	0.831	0.5
1375	1.082	7.662	0.834	0.5
1380	1.086	8.060	0.837	0.5
1385	1.09	8.458	0.841	0.6
1390	1.093	8.756	0.843	0.6

note 1: increased by same amount as Free-space relative responsivity

8.3.3 Calculation of responsivity (1390nm to 1480nm)

Table 8-8: 1390 to 1480nm Responsivity

Wavelength (nm)	Free-Space Relative Responsivity (A/W)	Increase in Free-Space Relative Responsivity (%) from 1305nm	In-Fibre Absolute Responsivity (A/W) (Note 1)	Additional Error(%)
1480	1.200	0.000	0.930	0.0
1475	1.194	-0.500	0.925	0.0
1470	1.188	-1.000	0.921	0.1
1465	1.184	-1.333	0.918	0.1
1460	1.179	-1.750	0.914	0.1
1455	1.173	-2.250	0.909	0.2
1450	1.167	-2.750	0.904	0.2
1445	1.160	-3.333	0.899	0.2
1440	1.153	-3.917	0.894	0.3
1435	1.146	-4.500	0.888	0.3
1430	1.139	-5.083	0.883	0.4
1425	1.132	-5.667	0.877	0.4
1420	1.125	-6.250	0.872	0.4
1415	1.118	-6.833	0.866	0.5
1410	1.112	-7.333	0.862	0.5
1405	1.106	-7.833	0.857	0.5
1400	1.101	-8.250	0.853	0.6
1395	1.097	-8.583	0.850	0.6

Using the method shown above, the in-fibre responsivity can be calculated over the wavelength range 1305nm to 1480nm with a maximum increase in uncertainty of 0.6%

note 1: increased by same amount as Free-space relative responsivity

8.3.4 Calculation of responsivity (1500nm to 1520nm)

The greatest uncertainty will be over the wavelength range 1500nm to 1520nm, as the detector responsivity roll off point is not known. As this point is not known it is not possible to calculate any values of responsivity over this range.

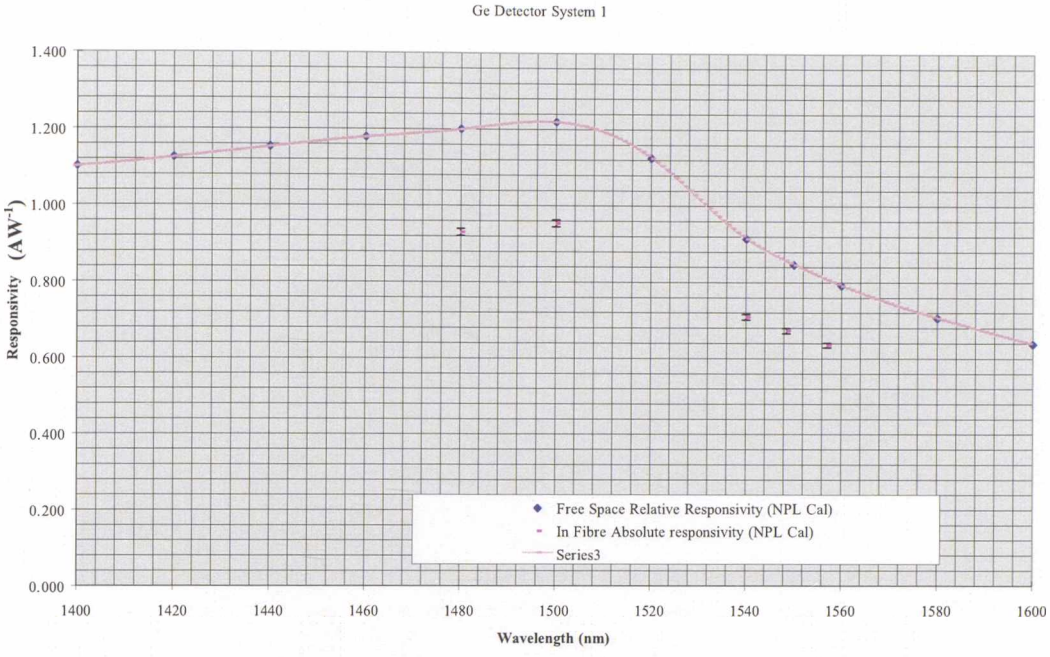

Figure 8-2: 1400 to 1600nm Responsivity.

8.3.5 Calculation of responsivity (1520nm to 1540nm)

Values of in-fibre responsivity can be calculated over this wavelength range by using the in-fibre responsivity at 1540nm and adjusting this value by the change in free-space relative responsivity down to a wavelength of 1520nm.

1520 nm to 1540nm

Table 8-9: 1520 to 1540nm Responsivity

Wavelength (nm)	Free-Space Relative Responsivity (A/W)	Increase in Free-Space Relative Responsivity (%) from 1305nm	In-Fibre Absolute Responsivity (A/W) (Note 1)
1540	0.914	0.000	0.709
1535	0.963	5.361	0.747
1530	1.018	11.379	0.790
1525	1.075	17.615	0.834
1520	1.125	23.085	0.873

note 1: increased by same amount as Free-space relative responsivity

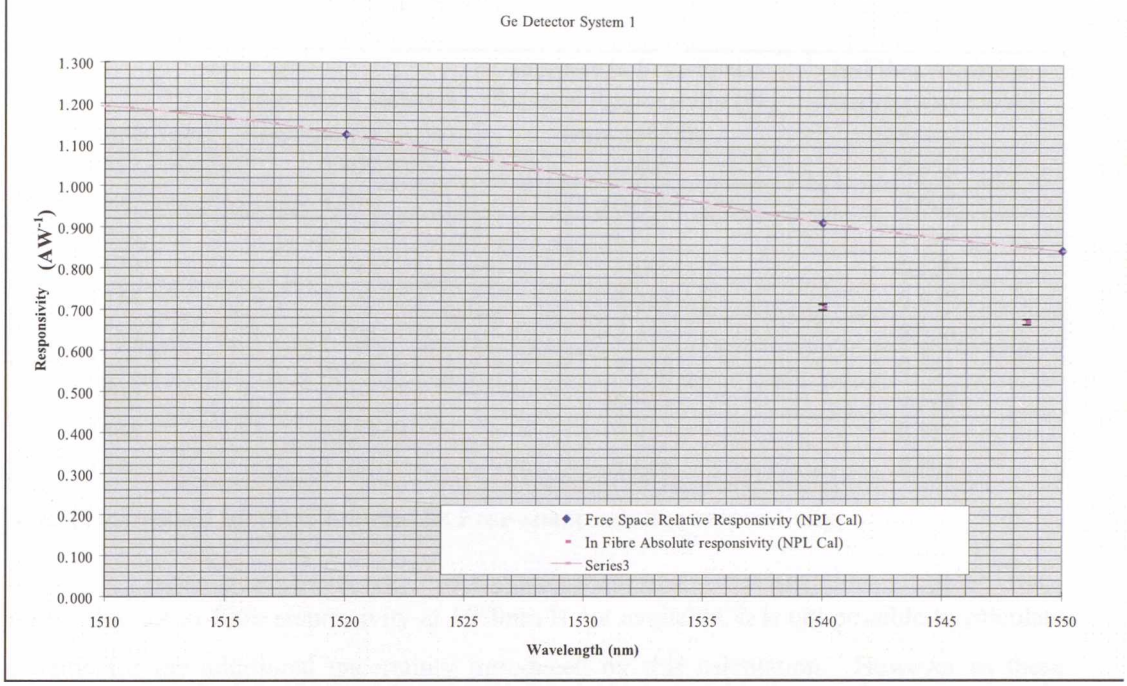

Figure 8-3: 1520 to 1540nm Responsivity.

As a value for in-fibre responsivity at 1520nm is not available, it is not possible to calculate a value for the additional uncertainty introduced by this calculation. However as these calculations have been conducted over a wavelength range of only 20nm, it is thought that the uncertainty will be less than 0.5%.

8.3.6 Calculation of responsivity (1557nm to 1600nm)

Values of in-fibre responsivity can be calculated over this wavelength range by using the in-fibre responsivity at 1557nm and adjusting this value by the change in free-space relative responsivity up to a wavelength of 1600nm.

1557 nm to 1600nm

Table 8-10: 1557 to 1600nm Responsivity

Wavelength (nm)	Free-Space Relative Responsivity (A/W)	Increase in Free-Space Relative Responsivity (%) from 1305nm	In-Fibre Absolute Responsivity (A/W) (Note 1)
1557	0.807	0.000	0.635
1560	0.791	-1.983	0.622
1565	0.767	-4.957	0.604
1570	0.745	-7.683	0.586
1575	0.725	-10.161	0.570
1580	0.706	-12.515	0.556
1585	0.688	-14.746	0.541
1590	0.671	-16.853	0.528
1595	0.654	-18.959	0.515
1600	0.637	-21.066	0.501

note 1: increased by same amount as Free-space relative responsivity

As a value for in-fibre responsivity at 1600nm is not available, it is not possible to calculate a value for the additional uncertainty introduced by this calculation. However as these calculations have been conducted over a wavelength range of only 43nm, it is thought that the uncertainty will be less than 0.5%.

8.3.7 Calculation of responsivity (800nm to 1280nm)

Values of in-fibre responsivity can be calculated over this wavelength range by using the in-fibre responsivity at 1280nm and adjusting this value by the change in free-space relative responsivity down to a wavelength of 800nm.

Table 8-11: 800 to 1280nm Responsivity

Wavelength (nm)	Free-Space Relative Responsivity (A/W)	Increase in Free-Space Relative Responsivity (%) from 1280nm	In-Fibre Absolute Responsivity (A/W) (Note 1)
1280	0.977	0.000	0.752
1270	0.966	-1.126	0.744
1260	0.955	-2.252	0.735
1250	0.943	-3.480	0.726
1240	0.931	-4.708	0.717
1230	0.920	-5.834	0.708
1220	0.908	-7.062	0.699
1210	0.896	-8.291	0.690
1200	0.883	-9.621	0.680
1190	0.870	-10.952	0.670
1180	0.857	-12.282	0.660
1170	0.844	-13.613	0.650
1160	0.830	-15.046	0.639
1150	0.816	-16.479	0.628
1140	0.801	-18.014	0.617
1130	0.785	-19.652	0.604
1120	0.768	-21.392	0.591
1110	0.751	-23.132	0.578
1100	0.743	-23.951	0.572
1090	0.718	-26.510	0.553
1080	0.703	-28.045	0.541
1070	0.688	-29.580	0.530
1060	0.672	-31.218	0.517
1050	0.656	-32.856	0.505
1040	0.640	-34.493	0.493
1030	0.624	-36.131	0.480
1020	0.609	-37.666	0.469
1010	0.594	-39.202	0.457
1000	0.578	-40.839	0.445
990	0.562	-42.477	0.433
980	0.546	-44.115	0.420
970	0.531	-45.650	0.409
960	0.515	-47.288	0.396
950	0.499	-48.925	0.384
940	0.483	-50.563	0.372
930	0.468	-52.098	0.360
920	0.452	-53.736	0.348
910	0.436	-55.374	0.336
900	0.420	-57.011	0.323
890	0.404	-58.649	0.311
880	0.388	-60.287	0.299
870	0.372	-61.924	0.286
860	0.357	-63.460	0.275
850	0.342	-64.995	0.263
840	0.326	-66.633	0.251
830	0.311	-68.168	0.239
820	0.296	-69.703	0.228
810	0.281	-71.238	0.216
800	0.266	-72.774	0.205

note 1: increased by same amount as Free-space relative responsivity

As a value for in-fibre responsivity at 800nm is not available, it is not possible to calculate a value for the additional uncertainty introduced by this calculation. However, it is thought that the uncertainty will be less than 1%.

8.3.8 Summary of additional uncertainty due to interpolation of responsivity values.

It can be seen from these calculations the following uncertainties will result from the interpolation of responsivity at various wavelengths:

Table 8-12: Fibre Power Uncertainty Summary

Wavelength range (nm)	Interpolation uncertainty	
	(%)	(dB)
1280 to 1305	0.0	0
1305 to 1480	0.6 maximum	0.024
1480 to 1500	0.0	0
1520 to 1540	0.5 maximum	0.02
1540 to 1557	0.0	0
1557 to 1600	0.5	0.02

9 Appendix C – Optical & RF Accuracy

This appendix summarises measurements performed on the Hewlett Packard Lightwave Analyser.

9.1 Optical Accuracy

Using the transfer detector (traceable to NPL), 1mW optical power was applied to the HP unit using the GEC laser diode and the lightwave 1319nm reference laser.

The HP unit provides a limited responsivity adjustment for source wavelengths, default being 1300nm and another for 1550nm. Three repeat measurements were performed over both operating modes (opt & elect) and the average results are shown below.

Table 9-1: Optical Accuracy as a function of wavelength

Applied	Wavelength	Popt	Pelect	Responsivity
1mW	1319nm	-0.1dBm	-16.6dBm	0.6614 AW^{-1}
1mW	1550nm	-0.1dBm	-16.6dBm	0.6614 AW^{-1}

Using the Popt-Pelect relationship below and assuming the detector load impedance is 50Ω the detector responsivity is obtained. As the Pelect for both wavelengths are the same this suggests the HP system lambda function performs satisfactorily.

$$Pelect = \beta^{2} x Popt^{2} x R \quad \therefore \quad \beta = \frac{\sqrt{\frac{Pelect}{R}}}{Popt} \tag{9-1}$$

The lower Popt measurements are probably the result of fibre coupling loss which typically is <0.3dB. The optical mode is referenced to the front panel and the electrical mode is at the output of the detector.

With the lambda setting set to 1300nm, measurements were taken to establish the responsivity of the HP detector at 1550nm, using the GEC laser diode as the source. The HP unit was initially set in the optical display mode. By adjusting the optical power incident on the HP unit to achieve 0dBm the unit was then switched over to the electrical mode resulting in an optical power of -15.8dBm.

Assuming the detector load impedance R is 50Ω the detector responsivity at 1550nm is 0.526 AW^{-1}.

The Popt measurement represents Pavg and is also used to derive the shot noise term, see equation. For example with Popt of -15.8dBm (elect mode) the RIN shot displayed was –153.54dB/Hz. This can be confirmed using;

$$RIN_{Shot} = \frac{2q}{i_{dc}} = \frac{2q}{\sqrt{\frac{Popt}{R}}} = -153.55dBm \qquad (9\text{-}2)$$

9.2 RF Accuracy

The remaining measurement terms required to calculate laser RIN are the thermal noise and system noise, both being rf. The rf marker is used to obtain these levels which similar to the dc optical power can be selected in terms of optical or electrical reference.

To achieve correct RIN calculations from the dc and rf measurements both dc and rf should be referenced to the same plane. This being the case the rf therefore should be at the output of the detector when in electrical mode, before amplifier impedance matching losses similar to the DERA system. Original literature suggests the reference point has in the past been at the input to the spectrum analyser module. HP confirmed that changes have been made during this product's life.

The two noise marker levels, Ntherm & Nsys are divided by the average optical power to obtain the respective RIN level displayed by the HP system. To ensure correct referencing of these terms back to the detector (say in the elect mode), aligning with the dc term, the offsets due to the amplifier gain, NF and impedance matching should be compensated for. It is not straight forward to confirm the rf accuracy, due to the low noise levels being considered and requirement of an optical reference signal.

The low noise reference source incorporated within the DERA RIN system has therefore been used in an attempt to establish the HP systems rf accuracy, see 5.2.3.1.

Due to the ratiometric relationship of the RIN measurements the 'opt' and 'elect' modes of the HP system should yield the same results. This has been confirmed from the following measurements taken using the GEC LD as a source at 1GHz.

Table 9-2: Comparison of 'opt' and 'elect' modes – HP System

	LW Opt Mode				LW Elect Mode			
Repeat No.	1	2	3	**Average**	1	2	3	**Average**
RIN Laser	-154.95	-155.13	-155.02	**-155.03**	-155.26	-155.26	-155.12	**-155.21**
RIN System	-146.42	-146.43	-146.43	**-146.43**	-146.45	-146.45	-146.43	**-146.44**
RIN Therm	-148.19	-148.17	-148.19	**-148.18**	-148.17	-148.17	-148.17	**-148.17**
RIN Shot	-153.54	-153.53	-153.54	**-153.54**	-153.54	-153.54	-153.53	**-153.54**

A number of soft key features are offered by the HP system, some of which are described below

INTERNAL OPTICAL ATTENUATOR - 0 to 30dB attenuation can be selected. Note the displayed optical power remains the same but the RIN shot will decrease (derived by i_{dc}) and the noise terms will increase to compensate, leaving the laser RIN unchanged.

SYSCOR - is an offset to the overall system amplitude typically used when two modules are calibrated together as in this case. This accounts for VSWR, input impedance and cable losses.

AMPCOR - similar to SYSCOR aimed more at the user to enable further level calibration errors to be compensated for.

9.3 Repeatability

The HP system was assessed for RIN repeatability. The GEC DFB laser diode (R21) was operated initially at 100mA and then 300mA, both attenuated to provide 1mW optical power incident on the HP system. To cover a wider range of laser noise an OTC DFB laser was also used providing 0.5mW.

The maximum variation observed was **1.36dB** over >500 measurements covering 100MHz to 20GHz, with RIN's ranging from -133dBHz^{-1} to -148dBHz^{-1} for the OTC laser and -143dBHz^{-1} to -155dBHz^{-1} for the GEC device. Typical repeatability was approximately 0.6dB

During this assessment the sensitivity limit of the HP system, denoted by a '+' symbol before the Laser RIN value, was observed occasionally. It is thought that these resulted from spurious data and have not been included in data averaging.

10 Appendix D – Relative Intensity Noise Measurement Procedure

The procedure for RIN measurement is shown below with the associated noise power components of each scan given. Measurement uncertainty is dependant on this procedure being followed.

Note:

1. All terms are linear values unless otherwise stated
2. Equipment used is to be listed and calibrated
3. Temperature controlled laboratory is used for all tests, 21±2°

- Equipment and the device under test (DUT) are turned on and allowed to warm up, 2hrs minimum.
- Equipment calibration is performed, ie zero'ing etc.
- Software, developed using QuickBasic, allows measurement parameter information and measurement results to be controlled by the user via a PC. The spectrum analyser is operated with resolution and video bandwidths of 10MHz and 100Hz respectively and RF input attenuation set at 0dB. The software also provides user instructions.
- Initially the DUT is fibre optically coupled, via the HP optical attenuator and appropriate in-fibre isolator to the Optical Digital Multimeter (DMM) to determine the wavelength of the DUT
- Then the DUT fibre is then decoupled from the Optical DMM and coupled to the transfer detector and the optical power adjusted by the optical attenuator to obtain the required test condition.
- The DUT fibre is then decoupled from the transfer detector and then applied to the ultra fast detector
- The spectrum analyser reference level and display range are adjusted to obtain a trace spanning the top third of the screen.
- The optical light is then blocked, using the attenuator disable, and the spectrum analyser reference level adjusted to enable the dark signal trace to be located on the screen at the lowest dut trace position (third from top of screen).
- The photodiode resistance is then measured using the Digital Multimeter (DMM), nominally 50Ω.
- With no light applied to the ultra fast detector the first noise level scan (N_{drk}) is recorded.

$$(N_{drk}) = \text{Syscal}(N_{th}) \quad Watts \tag{1}$$

- On completion of the scan the spectrum analyser reference level is reset to the level selected for the DUT trace.
- After enabling the optical attenuator and checking the optical power via the transfer standard, a second noise level scan is recorded, being the DUT (N_{dut}). During this scan the dc photocurrent is monitored automatically via the computer to obtain photocurrent drift.

$$(N_{dut}) = \text{Syscal}(N_{th}) + \text{Syscal}(N_q) + \text{Syscal}(N_L) \quad Watts \tag{2}$$

- The DUT is then uncoupled from the HP attenuator and the reference laser then coupled, via the HP optical attenuator and appropriate in-fibre isolator, to the Optical DMM to determine the wavelength.
- The reference laser is then coupled to the ultra fast detector (ensuring optical power is < 5mW).
- By adjusting the HP attenuator level the dc photocurrent, via the electrical DMM is **matched** to the DUT photocurrent previously recorded by the computer (ie. Shot noise matched).
- The spectrum analyser reference level is then adjusted to obtain a trace at the same screen position as the N_{drk} scan, to minimise Log Scale Fidelity errors.
- After coupling to the transfer detector to allow the optical power to be recorded the reference laser is re-coupled to the ultra fast detector (ensuring photocurrent match is maintained)
- The third noise level scan (N_{ref}) is recorded.

$$(N_{ref}) = \text{Syscal}(N_{th}) + \text{Syscal}(N_q) \quad Watts \tag{3}$$

Note: Syscal - System Calibration Factor

As with the DUT scan the dc photocurrent is monitored and recorded via the computer to obtain photocurrent drift and also mismatch between the Reference and DUT signals during the scan.

Note: During all of these scans the spectrum analyser set-up, e.g. resolution bandwidth, video bandwidth, RF input attenuation etc. must remain unchanged.

- By transferring the data of each scan into a spreadsheet or dedicated software program the required system calibration (Syscal), shot noise, thermal noise & RIN information can be derived for each measurement point across the frequency range (scan).
- This measurement procedure is repeated five times and the mean value for each laser RIN frequency point derived (see below) is quoted as the Laser spontaneous noise present at the input of the ultra fast photodetector. Five repeat measurements provide a suitable balance between measurement time and obtaining repeatability confidence.

Derivation

The RIN calculation process is as follows. Firstly the Dark scan is used as the base line measurement. By subtracting the Dark scan from the Reference scan the system calibration factor and the shot noise terms will remain.

$$(N_{ref}) - (N_{drk}) = Syscal(N_{th}) + Syscal(N_q) - Syscal(N_{th}) = Syscal(N_q)\ Watts \quad (4)$$

As the reference laser operates at a fixed wavelength and the DUT could operate anywhere in the telecommunications windows an adjustment factor needs to be incorporated to take into account detector responsivity differences. This will enable the system calibration factor to be corrected for the wavelength of the DUT.

$$\text{Responsivity Factor} = \frac{\beta_{dut}^2}{\beta_{ref}^2} \quad (5)$$

The responsivity (β) of the detectors at the wavelengths of interest can be derived from the measured optical power ($Pavg_{opt}$) at the input of the ultra fast detector and the recorded photocurrent i_{dc} as follows:

$$\beta = \frac{i_{dc}}{Pavg_{opt}} \text{ A/W} \quad (6)$$

Using this photocurrent the equivalent shot noise power (N_q) can be calculated to derive the system calibration factor for the wavelength of the DUT.

$$\text{Syscal} = \frac{\beta_{dut}^{2}}{\beta_{ref}^{2}} \frac{(N_{ref}) - (N_{drk})}{2qi_{dc}R} \tag{7}$$

This System calibration factor will account for system frequency responsivity, gain, noise figure, resolution bandwidth, impedance mismatch etc., of the system across the whole measurement range.

Next the (N_{ref}) scan is subtracted from the (N_{dut}) scan. As the photocurrents for both measurements have been matched the resultant shot noise can be cancelled along with the thermal noise hence leaving the spontaneous noise power of the DUT and the system calibration factor.

$$(N_{dut})-(N_{ref}) = \text{Syscal}(N_{th}) + \text{Syscal}(N_q) + \text{Syscal}(N_L) - \text{Syscal}(N_{th}) + \text{Syscal}(N_q)$$

$$= \text{Syscal}(N_L) \quad Watts \tag{8}$$

As we have already derived the system calibration factor Eq. (7) for the wavelength of interest we can now derive the laser spontaneous noise (N_L).

$$N_L = \frac{(N_{dut}) - (N_{ref})}{\text{Syscal}} \quad Watts \tag{9}$$

The remaining noise power (N_L) is divided by the average electrical power to obtain the spontaneous RIN level of the dut at each frequency point.

$$\text{RIN}_{\text{Laser}} = 10\,\text{Log}_{10}\frac{N_L}{i_{dc}^{2}R}\ dB/Hz \tag{10}$$

This measurement procedure is repeated five times and the mean value quoted as the Laser spontaneous noise present at the input of the photo-detector.

11 References

1 Bell A. G., 1880, 'Selenium and the photphone', *The Electrician,* pp124-125, pp220-221.

2 Hondros D., Debye P., 1910, 'Elektromagnetische Wellen an dielektrischen Drahten', *Ann Phys*, Vol.32, pp465-476.

3 Kapany N.S. 1967, *Fibre optics: Principles and applications*, Academic Press, New York.

4 Maiman T.H., 1960, 'Stimulated optical radiation in ruby', *Nature*, Lond., 187, pp493-494.

5 Kao K.C., Hockham G.A., 1966, 'Dielectric fibre surface waveguides for optical frequencies', *Proc. IEE*, 113(7), pp1151-1158.

6 Werts A., 1966, 'Propoagation de la lumiere coherente dans les fibres optiques', *L'Onde Electrique*, 46, pp967-980.

7 Long A., Buck J., Powell R., 2002 'Design of an Opto-Electronic Modulator Driver Amplifier for 40Gb/s Data Rate Systems', *J. of lightwave tech.*, Dec, Vol 20, No.12.

8 Dutta A., Takechi M., Virk R., 2002, '40Gb/s Postamplifier and PIN/Preamplifier Modules for Next Generation Optical Front-End Systems', *J. Lightwave Tech*, Dec, Vol.20, No.12.

9 Cunningham D.G., Nowell M., 1997, 'The IEEE 802.3z Worst Case Link Model for Optical Physical Media Dependent Specification Development', *Hewlett-Packard Laboratories*, White Paper, March.

10 Weiner T., 2003, 'Fibre Channel Fundamentals', *Spectra Logic Corporation*, White Paper, April.

11 Department of Trade & Industry / National System Policy Unit, 1994, *Project 24:Temporal & Frequency Response of Optoelectronic Devices*, 11 August.

12 Communications week International, 1996, *A sea of activity on world's fibre optic highways*, CMP Publications, Inc. March.

13 Vaezi-Nejad S.M., 1996, 'Optoelectronic lecture notes', *University of Greenwich.*

14 Mochida Y., 2002, 'Technology-Oriented Review and Vision of 40Gb/s-Based Optical Transport Networks', *J. Lightwave Tech*, Dec, Vol.20, No.12.

15 DeSalvo R., 2002, 'Advanced Components and Sub-System Solutions for 40Gb/s Transmission', *J. Lightwave Tech.* Dec, Vol.20, No12.

16 McOmber V., 1992, *Signal Analysis Forum - Noise & Modulation Distortion Measurements with the Lightwave Signal Analyzer*, Hewlett Packard, Santa Rosa.

17 Cancellieri G., 1993, *Single-Mode Optical Fiber Measurements*, Artech House, ISBN 0-89006-602-7, pp234-238, p222.

18 Hewlett Packard, Product Note 71400-1, 1991, *Lightwave Signal Analysers Measurement Relative Intensity Noise*, Hewlett Packard, Santa Rosa.

19 Hewlett Packard, 1990, 'Signal Analysis to measure characteristics of lasers and lightwave systems', *J. Lightwave*, February.

20 Hentschel C., 1989, *Fiber Optics Handbook*, Hewlett Packard, Santa Rosa.

21 Tsang W.T., Wang S., 1976, 'GaAs-AlGaAs double-heterostructure injection laser with distributed Bragg reflector', *Applied Phy. Lett.*, 28, p596.

22 Scifres D.R., Burham R.D., Streifer W., 1974, 'Distributed feedback single heterojunction diode laser', *Applied Phys. Lett.*, 25, p203.

23 Ogawa K., 1982, 'Analysis of mode partition noise in laser transmission systems', *IEEE J. Quantum Electronics*, QE18, pp849-855.

24 Jones G., 1992, 'Assessment of relative intensity noise and modulation bandwidth of quantum well DFB lasers', MSC Project, University College London.

25 Miller C.M., 1991, 'Intensity Modulation and Noise Characterisation of High-Speed Semiconductor Lasers', *IEEE Lett.*, May.

26 Joindot I., 1992, 'Measurements of relative intensity noise (RIN) in semiconductor lasers', *J. Phys. III,* France 2, pp1591-1603.

27 Linke R.A., 1985, 'Modulation induced transient chirping in single frequency lasers', *IEEE J. Quantum Electronics*, pp593-597.

28 Petermann K., 1991, *Laser Diode Modulation and Noise*, Kluwer Academic Publishers.

29 Cartledge J.C., Burley G.S., 1989, 'The effect of laser chirping on lightwave system performance', *J. Lightwave Technology*, 7(3), pp568-573.

30 Baney D., Sorin W., 1995, 'Broadband Frequency Characterisation of Optical Receivers Using Intensity Noise', *Hewlett Packard Journal*, Feb.

31 Senior M., 1992, *Optical Fiber Communications Principles and Practice*, Prentice Hall, p427.

32 Hewlett Packard, Application Note 150, 1989, *Spectrum Analysis Basics*, Hewlett Packard, November.
33 Hewlett Packard, Application Note 150-7, *Spectrum Analysis....Signal Enhancement*, Hewlett Packard, June.
34 Gambini P., Puleo M., Vezzoni E., 1990, 'Characterisation of laser diode intensity noise at microwave frequencies with high sensitivity', *CSELT Technical reports*, Vol. XVIII, No.5, October.
35 Hall M.M., Carlsten J.L., 1996, *Low-frequency intensity noise In semiconductor lasers*, Applied Optics, Vol 35, No.33, 20th November.
36 Harder C., Vahala K., Yariv A., 1983, 'Measurement of the linewidth enhancement factor α of semiconductor lasers', *Appl. Phys. Lett.*, Vol 42, pp328-330, Feb.
37 Kitamura M., Yamaguchi M., Murata S., Mito I., Kobayashi K., 1984, 'Low-threshold and high temperature single-longitudinal-mode operation of 1.55um-band DFB-DC-PBH LD's', *Electron. Lett.*, Vol 20, pp595-596, July.
38 Henry C.H., 1986, 'Phase Noise in Semiconductor Lasers', *J. of Lightwave Technology,* Vol. LT-4 No.3, March.
39 Gowar J., 1984, *Optical communications systems*, Prentice Hall Int., London.
40 Gallion F.B., Debarge G., 1984, 'Quantum phase noise and field correlation in single frequency semiconductor laser systems', *IEEE J. Quantum Electron.*, Vol QE-20, pp343-349.
41 Richter L.E., Mandelberg H.I., Kruger M.S., McGrath P.A., 1986, 'Linewidth determination from self-heterodyne measurements with subcoherence delay times', *IEEE J. Quantum Electron.,* QE-22, p2070.
42 Okoshi T., Kikuchi K., Nakayama A., 1980, 'Novel method for high resolution measurement of laser output spectrum', *IEEE Electronic Lett.*, Vol. 16, No. 16, pp630-631, 31 July.
43 Tkach R.W., Chraplyvy A.R., 1986, 'Phase noise and linewidth in an InGaAsP DFB laser', *J. Lightwave Technology*, Vol LT-4, No.11, p1711, Nov.
44 Ryu S., Yamamoto S., 1986, 'Measurement of direct frequency modulation characteristics of DFB-LD by delayed self-homodyne technique', *IEEE Electronic Lett.*, Vol.22, No.20, pp1052-1054, 25 Sept.
45 Esman R.D., Goldberg L., 1988, 'Simple measurement of laser diode spectral linewidth using modulation sidebands', *IEEE Electronic Lett.*, Vol. 24, No.22, pp1393-1395, 27 Oct.
46 Baney D.M., Sorin W.V., 1988, 'Measurement of a modulated DFB laser spectrum using gated delayed self-homodyne technique', *IEEE Electronics Lett*, Vol.24, No.11, 26 May.
47 Baney D.M., Sorin W.V., 1990, 'Linewidth and power spectral measurements of single frequency lasers', *Hewlett Packard Journal,* Feb.
48 Steele T.R., 1993, *Introduction to diode-pumped solid-state lasers*, Lightwave Electronics Corp., USA.
49 Martinelli M.A., 1989, 'Universal Compensator For Polarisation Changes By Birefringence On A Retracing Beam', *Optical Communications*, 72, pp341.
50 Electrostatics, 2001, *Protection of electronic devices from electrostatic phenomena, General requirements*, EN61340-5-1:2001, ISBN 058032346 3.
51 Chaimowicz J.C.A, 1989, *Lightwave Technology an Introduction*, Butterworths.
52 Helfrick A.D., 1991, *Electrical Spectrum & Network Analysers*, Academic Press.
53 Hewlett Packard, 1991, 'Receiver Design for Accurate Lightwave Measurements', *RF, Microwave & Lightwave Measurements Symposium and Exhibition.*
54 McOmber V., Miller C.M., Stokes L., 1992, 'Noise and Modulation Distortion Measurements with the Lightwave Signal Analyzer', *HP Lightwave Forum.*
55 Miller C.M., 1991, 'Intensity Modulation and Noise Characterization of High-Speed Semiconductor Lasers', *IEEE Lett.*, May.
56 Rowe H.E., 1965, *Signals & Noise In Communications Systems,* D. Van Nostrand Company, Priceton.
57 Yariv A., 1975, *Quantum Electronics*, Wiley, New York, pp311-313.
58 Nortel Networks, 2001, 'Marketing Presentation', Optical Fiber Communications Conference, Feb.